Inaugural dissertation

for

obtaining the doctoral degree

of the

Combined Faculty of Mathematics, Engineering and Natural Sciences

of the

Ruprecht - Karls - University

Heidelberg

Presented by

M.Sc. Kristina Žuža

born in: Zadar, Croatia

Oral examination: 10th October 2022

Characterization of mouse preoptic area cellular populations involved in thermoregulation

Referees:

Prof.Dr. Valery Grinevich
Prof.Dr. Jan Siemens
Prof.Dr. Hilmar Bading
Prof.Dr. Michaela Frye

Acknowledgements

I would like to thank to everyone who has been a part of my PhD journey:

Firstly, I would like to give my appreciation to Prof.Dr. Jan Erik Siemens, my PhD supervisor. The main part of my gratitude comes from giving me the opportunity to start my PhD in his lab. This was for sure not an easy decision, as back then I was a student with a minimum of laboratory experience, and with zero knowledge in neuroscience. I am thankful for all the support, and the trust that I was given by Jan. It helped me grow more confident in my capabilities as a scientist. I will cherish it always. I am also grateful for the input and the corrections in the writing of this thesis.

I wish to give my gratitude to my PhD co-supervisor, Dr. Gretel Kamm. Dr. Kamm has been an immense motivator, and most importantly, a great educator during my PhD time. She thought me many things in the lab and provided knowledge that goes way above the practical one, as to be critical of the scientific work of others, but of my work as well. She thought me that the beauty of working in science is to constantly question and try to provide the answers in the best and the most honest way possible we can and to keep high standards in scientific practice. I am also grateful for the input and the corrections in the writing of this thesis.

I want to acknowledge my thesis advisory committee members, Prof. Dr. Valery Grinevich and Dr. Vladimir Benes, for providing their time, support, and encouragement during my PhD thesis development.

In addition, I wish to thank my thesis defense committee, Prof. Dr. Valery Grinevich, Prof. Hilmar Bading, and Prof. Michaela Frye, for their time to read and evaluate this thesis.

I would like to acknowledge and express my gratitude to all of my collaborators:

Dr. Juan Boffi for supporting the idea of Patch-seq at its beginnings, for the help with the electrophysiology data analysis, moreover for the kindness you give to people around you.

Dr. Sergio Triana has shown me how to do the scRNA-seq integration analysis and has included me in the projects of spatial RNA sequencing.

Dr. Silvia Calderazzo has helped me with the statistical analysis of the RNA-seq data. She has invested hours in explaining to me the statistics behind the analysis, and she was interested to listen about the biology behind the experiment.

Dr. Gerald Quon and Dr. Nelson Johansen, Dr. Shrejoy Tripathy, and Dr. Sonny Chen, for all the discussion and their efforts to analyze in detail the Patch-seq data we obtained and for sharing their knowledge with me.

I especially want to thank the GeneCore EMBL team for welcoming me to their lab for all the RNAseq library preparations and teaching me how to do that. To Dinko Pavlinić, Laura

Villacorta, Jan Provaznik, Jonathan Landry, Rajna Hercog, Jelena Pistolić, Nayara Trevisan, Feris Jung, Anya Telzerow. I always felt comfortable and happy coming up to GeneCore and working with you.

My gratitude goes especially to Dr. Vladimir Benes, the head of the GeneCore team. Thank you for all the advice you have given me regarding my projects, the time you have spared for conversation any time I needed, and for your calm approach to any occurring issue. I will always keep in mind the way you treated everyone, including me, who was coming to you to ask for advice and help. It is worth admiring and striving to become the same.

Many thanks to Dr. Sara Kathrin Goetz and Dr. Katrin Schrenk-Siemens for translating the summary from English to German.

Special thanks go to my lab mates in AG Siemens:

To Dr. Katrin Schrenk-Siemens, a teacher and a role model. Katrin welcomed me to the lab when I started working at AG Siemens. She has thought me about everything that has to do with cell culture. Katrin was a support to the whole lab and me in the most challenging moments in the last 5 years.

To Dr. Moad Abd El Hay, thank you for the hours of laughs during our time in the AG Siemens and the best parties. Thank you for all the help in the calcium imaging experiments, teaching me how to analyze the data. Mostly, thank you for pushing me above my limits and not giving me an easy way out. *Sorry for the Seurat though*...

To Dr. Carolina Araujo Sousa, my dear colleague, and a *wise* friend. I want to thank her for being a person I could talk to about everything and anything, for listening and never being without a piece of advice, even when times were challenging for her as well. Anything is easier to persevere with friends at your side.

To Sebastian Marty Lombardi, my *beautiful* friend with a heart that knows no bitterness and no anger. I will cherish forever the teasing, gossiping, and laughs we had.

To Daniela Pimonov the joy of this lab. People like Daniela make every day at work easier and more beautiful. Thank you for all your help in the lab.

To Lisa Vierbaum, for teaching me how to mount free-floating sections on a glass slide with such patience, and understanding. For being a good colleague and a friend.

To Lisa Weiler, for being strict with safety measures in the lab, and for teaching me a lot about those I did not know before. Thank you for your support and help.

To Dr. Sara Nencini, for showing me how to be determined in achieving your aims. For being a nice colleague to work with. I will remember our Ephys times always with a smile.

To Kaya Baumert, a master's student in the lab who has provided me with a great experience of being a mentor to someone. I have learned a lot.

To Amandine Cavaroc, for your devoted work and all the help you provide with a calm approach worth everyone’s admiration.

To Daria Kocherhina, a student in the lab who has shown me that no matter the circumstances in this life, we must prevail by being kind and modest.

To Mrs. Ulrike Baur-Finck, for her assistance with the inevitable bureaucracy that follows science as any other job. Thank you for all the work you did for the lab, for all the patience, and for your kindness.

To Dr. Jörg Pohle for teaching me electrophysiology.

To Dr. Wojciech Ambroziak for collaborating on the Patch-seq experiments.

To Dr. Nencini, Dr. Pohle, and Dr. Wojceich Ambroziak for sharing data and figures to help clarify the work presented in this thesis and for collaborating on the acclimation project.

Finally, I want to thank all the current and previous members of AG Siemens, who have left their mark on my work and the knowledge I possess now: Kritika Mittal, Mildred Alejandra Gutierez Herrera, Manoj Yadav, Daniel Erdelyi, Osmond Aruna, Burçe Kabaoglu, Dr. Hagen Wende, Christina Steienmeyer-Stanek, and Annika von Seggern.

Further, I want to thank people who have made my life richer in the last 5 years:

I wish to thank Dr. Mariana Alves and Dr. Rafael Galupa, for their kindness and for introducing me to the Native Scientist organization. I also wish to thank Dr. Joana Moscoso for keeping Native Scientist alive and giving science back to the young ones in the community.

I want to thank Dr. Flavia-Bianca Cristian for giving me the opportunity to participate in the Pint of Science and the Feminism (in science) book club. I enjoyed participating in both very much. Your energy for the things you believe in is contagious and I wish you to keep up the great work you are doing.

I want to express my deep gratitude to my friends, and my Heidelberg crew. I will always be grateful for everything I learned from each one of you during the time we spent in Heidelberg together, for all the nice meals we shared, laughter, games, dance and music, hikes, and many beautiful moments. Thank you, Carol, Erica, Raj, Virginia, Veronika, Matteo, Sara, Alpi, Mariana, Sergio, Seba and Betsi, Bianca, Lisa, and Kritika.
My gratitude goes to my friends Dima and Vale for the beautiful Sundays spent together.

I am always grateful to my anchors back at home:
Marina, Edi, Gita, Šime, Iva, Ante, cimi Matea, Ane - Klarica i Jozić - sa Lukama i malenim velikim prijateljima- Hvala vam!

To Stanislav, Vesna, Andrea, and Zorba, for accepting me as their daughter, sister, and aunt. Who were always keen on listening about my work, asking questions, and being curious.

Finally, I want to express my gratitude to my family:

My brother Stipe, who has always understood the challenges I am facing, and with whom I could share the joy and the burden of this work,
My sister Antonia and my nieces Leona and Korina for the role of aunt that has made me so happy,

My grandparents Blaženka, Bartul, Šime and Kata for paving the way for all of us,

My husband Ivan, without whom this journey would have been much more difficult. I am grateful for all the support, kindness, and understanding. Hvala ti za ljubav!

My mother Gordana and father Dragan have given everything in their power for the well-being of my sister, my brother, and me. They raised me to be kind and thought me not to give up in difficult times. This thesis I dedicate to them.

“To što brodi ne mogu da prevale čovjek umije.”

Branimir Štulić

Summary

Thermoregulation is a dynamic homeostatic process, tightly regulated by the autonomic nervous system. How the brain coordinates maintenance of the body temperature within a narrow range of 37˚C, a condition that is needed for the survival of most of the species, remains unclear. Among the brain regions implicated in thermoregulation is the anterior portion of the hypothalamus, the preoptic area (POA). In this region neurons that respond to direct temperature stimuli and to the skin and spinal cord warming were found, suggesting that these warm-sensitive neurons (WSNs), are the cells that detect deep brain temperature and integrate it with temperature information from the periphery. The limiting factor in studying the WSNs of the POA and their role in thermoregulation is the lack of specific molecular markers that identify them.

Therefore, the goal of this thesis work was to characterize WSNs of the POA at the molecular level and to find their genetic marker(s). To achieve this goal I used a primary POA cell culture and performed calcium imaging while applying a temperature stimulus of 45˚C in the presence and the absence of the TRPM2 antagonist, 2-Aminoethoxydiphenyl borate (2-APB). I identified and hand-picked temperature responding cells and temperature non-responding cells for the single-cell RNA-sequencing (scRNA-seq). Analysis of the scRNA-seq data pointed to the limitations of the P9 cell culture used. The majority of the temperature non-responding cells expressed glial marker genes together with neuronal markers, a combination not found *in vivo*. I concluded that the genetic heterogeneity of the sequenced cells was too large and putative WSNs' molecular markers identified from cultured neurons would be ambiguous. In addition, to find markers of WNSs one has to take another approach, such as Patch-seq to analyze these neurons in more natural conditions.

One of the POA neuronal populations activated by a change in ambient temperature is expressing leptin receptor (POA^{LepR}). These neurons also exhibit an increase in action potential firing frequency (AP FF) during the process of chronic heat exposure to 36˚C that also leads to an increased heat endurance (at 39˚C). in mice. This intrinsic property of neurons (not affected by synaptic blockers), seems to be needed for a mouse to endure heat, as the animals in which the firing of POA^{LepR} is abolished fail to do so.

To learn more about the role of the POA^{LepR} neurons in the heat acclimation process I used FACS (Fluorescence Activated Cell Sorting) to isolate the POA^{LepR} neurons from POA of non-acclimated and acclimated (5 and 30 days at 36 ˚C) LeprCreHTB mice and performed RNA sequencing. I identified three genes *Kcnq2*, *Kcnn2*, and *Kcnh2*, all three coding for potassium ion channels, whose expression level changed with the course of heat acclimation. I have tested the functionality of these ion channels in AP

firing of the POA^{LepR} neurons, by employing electrophysiology and pharmacology in acute POA slices. Ion channels $K_v7.2$ and $K_v11.1$, coded by *Kcnq2*, and *Kcnh2,* respectively, exhibited a role in shaping the AP firing of POA^{LepR} neurons. Applying the antagonist of $K_v7.2$ disrupted harmonious AP firing of POA^{LepR} neurons coming from acclimated mice, rendering their membrane potential unsteady and their firing bursty. In addition, the application of the $K_v11.1$ antagonist increased the AP FF of POA^{LepR} neurons even further in the long-term acclimated condition.

Heat acclimation is a naturally occurring process happening across mammalian species, including humans. It is important for enduring physical burdens in hotter climates as it leads to the improved function of the thermoregulatory system. It is forthright to hypothesize that the POA, the central regulator of temperature homeostasis, plays a role in heat acclimation. However, knowledge about it is scarce. Knowing which molecules change in POA^{LepR} neurons transcriptome to increase firing, and to which other thermoregulatory relays these neurons project will help us understand their role and the role of POA in heat acclimation.

Zusammenfassung

Thermoregulation ist ein dynamischer homöostatischer Prozess, der durch das autonome Nervensystem streng reguliert wird. Eine Körpertemperatur im Bereich von 37˚C ist für die normale Funktion aller enzymatischen Reaktionen und zellulären Prozesse erforderlich. Wie das Gehirn die Aufrechterhaltung der Körpertemperatur koordiniert ist bisher jedoch noch unklar. Zu den Hirnregionen, die an der Thermoregulation beteiligt sind, gehört der Hypothalamus, genauer gesagt sein anteriorer Teil, der präoptische Bereich (POA). In dieser Region wurden Neuronen gefunden, die auf direkte Temperaturreize und auf die Erwärmung von Haut und Rückenmark reagieren, was darauf hindeutet, dass diese wärmeempfindlichen Neuronen (WSN) die Zellen sind, die die Temperatur in der Tiefe des Gehirns erkennen und sie mit den Temperaturinformationen aus der Peripherie integrieren. Der limitierende Faktor bei der Untersuchung der WSN des POA und ihrer Rolle bei der Thermoregulation ist das Fehlen spezifischer molekularer Marker, um diese zu identifizieren.

Daher war es das Ziel dieser Arbeit, die WSN des POA auf molekularer Ebene zu charakterisieren und ihre genetischen Marker zu finden. Um dieses Ziel zu erreichen, habe ich Kalzium-Imaging Experimente mit primären POA-Zellkulturen durchgeführt. Die Zellen wurden während eines Temperaturreizes von 45˚C in Gegenwart und Abwesenheit des TRPM2-Antagonisten 2-Aminoethoxydiphenylborat (2-APB) vermessen. Des Weiteren, identifizierte und selektierte ich Zellen mittels Einzelzell-RNA-Sequenzierung (scRNA-seq), welche auf die Temperatur reagierten und Zellen, die nicht auf die Temperatur reagierten. Die Analyse der scRNA-seq-Daten zeigten jedoch die Grenze der verwendeten P9-Zellkultur auf. Die Mehrzahl der sequenzierten Zellen, die nicht auf den Temperaturstimulus reagierten, exprimierten Glia-Markergene zusammen mit neuronalen Markern, eine Kombination, die *in vivo* nicht vorkommt. Ich kam daher zu dem Schluss, dass die genetische Heterogenität der sequenzierten Zellen zu groß war und dass die molekularen Marker der mutmaßlichen WSN, die aus den kultivierten Neuronen identifiziert würden, mehrdeutig sein würden.

Um Marker für WNS zu finden, muss man außerdem einen anderen Ansatz wählen, z. B. Patch-seq, der Elektrophysiologie und Transkriptomik kombiniert, um diese Neuronen unter natürlicheren Bedingungen zu analysieren.

Eine der POA-Neuronenpopulationen, die durch eine Veränderung der Umgebungstemperatur aktiviert wird, exprimiert den Leptinrezeptor (POALepR). Diese Neuronen zeigen auch einen Anstieg der Aktionspotenzial-Feuerungsfrequenz (AP FF) während einer chronischen Hitzeexposition bei 36˚C, was bei Mäusen auch zu einer erhöhten Ausdauer führt. Diese intrinsische Eigenschaft der Neuronen scheint

notwendig zu sein, damit Mäuse Hitze aushalten können, da die Tiere, bei denen das Feuern von POALepR abgeschaltet ist, dies nicht tun.

Um mehr über die Rolle der POALepR-Neuronen im Prozess der Hitzeakklimatisierung zu erfahren, habe ich mittels FACS (Fluoreszenz-aktivierte Zellsortierung) die POALepR-Neuronen aus POA von nicht akklimatisierten und akklimatisierten (5 und 30 Tage bei 36 ˚C) LeprCreHTB-Mäusen isoliert und eine RNA-Sequenzierung durchgeführt. Ich habe drei Gene Kcnq2, Kcnn2 und Kcnh2 identifiziert, die alle drei für Kalium-Ionenkanäle kodieren und deren Expressionsniveau sich im Verlauf der Wärmeakklimatisierung verändert. Ich habe die Funktionalität dieser Ionenkanäle beim AP-Feuerns der POALepR-Neuronen mit Hilfe der Elektrophysiologie und Pharmakologie in akuten POA-Schnitten getestet. Die Ionenkanäle Kv7.2 und Kv11.1, die von Kcnq2 bzw. Kcnh2 kodiert werden, spielten eine Rolle bei der Gestaltung des AP-Feuerns von POALepR-Neuronen. Die Anwendung des Antagonisten von Kv7.2 störte das harmonische AP-Feuern von POALepR-Neuronen aus akklimatisierten Mäusen, wodurch ihr Membranpotenzial unstetig und ihr Feuern unbeständig statt fand. Darüber hinaus erhöhte die Anwendung des Kv11.1-Antagonisten die AP –Feuerns der POALepR-Neuronen unter den Bedingungen der Langzeitakklimatisierung sogar noch weiter.

Die Wärmeakklimatisierung ist ein natürlicher Prozess, der bei allen Säugetierarten, einschließlich des Menschen, vorkommt. Sie ist wichtig, um körperliche Belastungen in wärmeren Klimazonen zu ertragen, da sie zu einer verbesserten Funktion des Thermoregulationssystems führt. Es liegt die Hypothese nahe, dass der POA, der zentrale Regulator der Temperaturhomöostase, eine Rolle bei der Hitzeakklimatisierung spielt. Es gibt jedoch keine direkten Beweise, die dies bestätigen. Wenn wir wissen, welche Moleküle sich im Transkriptom der POALepR-Neuronen verändern, um die Feuerkraft zu erhöhen, und auf welche anderen Thermoregulationsrelais diese Neuronen projizieren, können wir ihre Rolle und die Rolle des POA bei der Hitzeakklimatisierung in Zukunft besser verstehen.

Table of Content

List of Figures

List of Tables

Abbreviations

2-APB 2-Aminoethoxydiphenylborane

5-HT serotonin receptor

ac anterior commissure

ACSF artificial cerebrospinal fluid

AgRP agouti-related peptide

AHP afterhyperpolarization

AP action potential

AP FF action potential firing frequency

ATP adenosine triphosphate

AVPe anteroventral periventricular nucleus

B19 G rabies virus envelope glycoprotein

BAT brown adipose tissue

Bdnf brain-derived neurotrophic factor

BrdU bromodeoxyuridine

BRS3 bombesin-like receptor 3

Chr2 channelrhodopsin 2

CMV cytomegalovirus

CNO clozapine N-oxide

CNQX cyanquixaline (6-Cyano-7-nitroquinoxaline-2,3-dione)

CSNs cold sensitive neurons

CV (ISI) coefficient of variation of interspike interval

CVC cutaneous vasoconstriction

FF firing frequency

fgsea fast geneset enrichment analysis

FSC forward scatter

D-AP5 D-2-amino-5-phosphonovalerate

DE differential expression

DEGs differentially expressed genes

DH dorsal horn

DH dorsomedial hypothalamus

DMD dorsomedial hypothalamus

DMH dorsomedial hypothalamic nucleus

DNA deoxyribonucleic acid

DREADD designer Receptors Exclusively Activated by Designer Drugs

DRG dorsal root ganglia

E-4031 N-[4-[[1-[2-(6-Methyl-2-pyridinyl)ethyl]-4piperidinyl]carbonyl]phenyl]methanesulfonamide dihydrochloride

EE energy expenditure

EP3R prostaglandin EP3 receptor

eYFP enhanced yellow fluorescent protein

FACS fluorescencee activated cell sorting

FDR false discovery rate

Gad1 glutamate decarboxylase 1

Gad2 glutamate decarboxylase 2

GFAP glial fibrillary acidic protein

GFP green fluorescent protein

GSEA gene set enrichment analysis

HEK 293 human embryonic kidney–293 cells

HIF1 – α hypoxia-inducible factor 1-α

HSE heat shock responsive element

HSF1 heat shock factor

HTB histone-2B-tag

IHC Immunohistochemistry

ICV intracerebroventricular

IP intraperitoneal

IQR inter-quartile range

JAK2 janus kinase 2

KCa2.2 potassium calcium-activated channel subfamily n member 2

KNDy kisspeptin-neurokinin b dynorphin-expressing

Kv11.1 potassium Voltage-Gated Channel, Subfamily H (Eag-Related), Member 2

Kv7.2 potassium voltage-gated channel subfamily q member 2

Lepr leptin receptor

LepRb/Ob-Rb leptin receptor long form

LHA lateral hypothalamic area

LPB lateral parabrachial nucleus

LPBd dorsal division of

LPBel lateral external portion of LPB

LPS lipopolysaccharide

LTA long-term heat acclimation

mAHP medium afterhyperpolarization

Mapt microtubule Associated Protein Tau

Mbp myelin basic protein

ML252 ((S)-2-Phenyl-N-(2-(pyrrolidine-1-yl)phenyl) butanamide

MnPOA median proeptic nucleus

Mobp myelin-associated oligodendrocyte basic protein

MPA medial Preoptic Area

MPO medial Preoptic Nucleus

mRNA messenger ribonucleic acid

NA non-acclimated

NeuN neuronal nucleus protein

NK3R neurokinin 3 receptor

NOS1 nitric oxide synthase

NPY neuropeptide Y

NS-1643 N,N'-Bis[2-hydroxy-5-(trifluoromethyl)phenyl]urea),

ob/ob leptin deficient

Olig1 oligodendrocyte transcription factor 1

Olig2 oligodendrocyte transcription factor 2

Opn5 opsin 5

ORF open reading frame

OVLT organum vasculosum laminae terminalis

PACAP pituitary adenylate cyclase polypeptide

PaPy parapyramidal area

Patch-seq patch-sequencing

PCA principal component analysis

PCR polymerase chain reaction

PGD2 prostaglandin D2 synthase

PGE2 prostaglandin E2

PI propidium-iodide

pS6 phosphorylated ribosomal protein S6

pSTAT3 phosphorylated signal

STA short-term heat acclimation

STAT 3 signal transducer and transcription activator 3

STAT 5 signal transducer and transcription activator 5

Syn1 synapsin1

PRV pseudorabies virus

Ptger3 prostaglandin E receptor 3

QC quality control

qPCR quantitative polymerase chain reaction

QRFP neuropeptide pyroglutamylated RFamide peptide

RIN RNA integrity number

RMP resting membrane potential

RNA ribonucleic acid

RNA-seq ribonucleic acid sequencing

ROS active oxygen species

rRPa rostral raphe pallidus

RT room temperature

RVNM rostral ventromedial medulla

scRNA-seq single-cell RNA sequencing

SK slow-conductance calcium-activated ion channel)

SNN shared nearest neighbor

SSC side scatter

Syn2 synapsin 2

Syt1 synaptotagmin 1

Tacr3 tachykinin Receptor 3

Tcore body temperature

tE average endurance time

TeTxLC tetanus toxin light chain

t-SNE t-distributed stochastic neighbor embedding

Tubb3 tubulin Beta 3 Class III

TVA the avian tumor virus receptor A

UCP1 uncoupling protein 1

UV ultraviolet light

Vgat Vesicular GABA transporter

Vglut2 vesicular glutamate transporter 2

Vglut3 vesicular glutamate transporter 3

vLPO ventrolateral preoptic area

VMH ventromedial hypothalamic nucleus

WANs warm-activated neurons

WSNs warm sensitive neurons

WT wild type

CHAPTER 1

Molecular characterization of POA warm-sensitive neurons

1. INTRODUCTION

Thermoregulation is a homeostatic mechanism crucial for every animal's survival as it is involved in all biological functions from basic enzymatic to higher-level ones such as energy production(S. Morrison F. & Nakamura, K, 2011). It is tightly coordinated by a central nervous system (CNS) through temperature inputs arriving from peripheral thermoreceptors via the spinal cord to the brain, which processes information and gives out the command to thermoeffector organs to execute the orders to keep the body temperature (T_{core}) in check (Madden & Morrison, 2019). Key thermoeffector organs are cutaneous blood vessels, salivary (in rodents) and sweat glands (larger mammals and humans), skeletal muscle shivering and brown adipose tissue (BAT) thermogenesis.

1.1. POA IN THERMOREGULATION

1.1.1. A historical overview of POA in thermoregulation

More than a century ago, the work of researchers such as Aronsohn and Sachs revealed that damaging the corpus striatum, the base of the brains of rabbits, guinea pigs, and dogs, causes malfunction of temperature regulation in these animals (Aronsohn & Sachs, 1885; Isaac Ott, 1887). Further on, Barbour did work on rabbits, where he showed that introducing hot water-conducting metallic cannula to the hypothalamus activated body cooling (Barbour, 1912). Bazet followed the work of others by implementing brain lesions and showed that damaging the hypothalamus in cats causes an increase in body temperature (Bazett et al., 1933). Moreover, in 1938 Magoun used a slightly more sophisticated diathermic device that used current to create heat (Magoun et al., 1938). By inserting this device in the cats' brains, the part of the brain, which reacts the most to the heating, has been evaluated; heating an area ventral to the optic chiasm, and dorsal to the anterior commissure, caused panting in cats and the appearance of the sweat on the paws. Magoun pointed out that the preoptic area and suprachiasmatic region of the hypothalamus are more responsive to heating than the posterior hypothalamic regions. Following the work of Magoun, Hemingway measured effector mechanisms such as panting, vasodilation, and vasoconstriction, by warming up the hypothalamus of dogs (Hemingway et al., 1940). Animals were kept in a cold room and they exhibited shivering and ear blood vessels vasoconstriction, but after brain warming, shivering ceased, and constricted blood vessels dilated. Therefore, it was concluded that the heating „center" in the brain lies within the anterior hypothalamus, above the optic chiasm, the region known today as the preoptic area of the hypothalamus (POA). Twenty years later Hammel and colleagues corroborated the finding by

cooling the hypothalamus of the dogs which caused an increase in body temperature by exerting vasoconstriction and shivering (Hammel et al., 1960).

1.1.2. Thermosensitive units within the POA

With the thermoregulatory brain center identified, researchers have been able to continue characterizing this region more precisely. Classical experiments by Nakayama and colleagues have defined temperature-responsive neurons within the POA (Nakayama et al., 1961, 1963). These warm sensitive neuronal units exhibited a Q_{10} (a measure of temperature sensitivity) between 5 and 15. Q10 is a t

Temperature coefficient extracted from the Arrhenius equation, which describes the dependency of the rates of chemical reactions on temperature, e.g. if a neuron's discharge rate doubles upon a 10 ˚C temperature change then the Q_{10} for this neuron equals 2. Another measure for neuronal thermosensitivity is based on the thermal coefficient – a slope of the change in neurons' firing rate during the temperature change. If this slope gets ≥0.8 AP/s/˚C then the neuron is considered to be warm sensitive (Boulant, 2011). In addition to warm-sensitive neurons, cold-sensitive ones have been found within the POA (Hardy et al., 1964). These neurons respond with an increase of the AP firing upon cooling of the POA, with the slopes ranging between -0.4 to -3.5 AP/sec/ ˚C. An extensive review of the studies performed *in vivo* and *ex vivo* slices of the POA showed that around 30% of neurons within the POA are warm-sensitive (WSNs), 5-10% are cold-sensitive (CSNs), and the rest (60-70%) is temperature insensitive (Boulant, 2000; Boulant & Dean, 1986). This proportion is slightly lower in the POA cultured neurons, with 26% being WSNs, 7% CSNs, and the rest temperature insensitive. However, the POA is not the only temperature-sensitive region within the brain, as electrophysiological studies have shown that other regions in the rat's diencephalon contain similar proportions of all three temperature-defined neuronal categories (Dean & Boulant, 1989).

Already in 1963, Hammel proposed the set point theory as a principle for the thermoregulatory center in the brain based on this cellular POA architecture (WSN, CSNs, and ISNs) (Hammel et al., 1963). He postulated that thermoregulatory homeostasis is achieved via the balance of synaptic outputs of WSNs (neurons that get activated by temperature) and temperature-insensitive neurons. In brief, when the hypothalamic set point temperature (37˚C) gets challenged by the environmental temperature change, and the temperature increases above 37˚C, temperature-sensitive neurons in the POA get active and synaptically excite the neurons projecting to the effector mechanisms to increase the heat loss (Boulant, 2006). These effector neurons are otherwise synaptically inhibited by temperature-insensitive neurons. Therefore, at the temperature of 37˚C, excitatory outputs of WSNs and inhibitory outputs of temperature-

insensitive neurons, counterbalance each other and keep the set point temperature steady. This feature of neurons within the POA gives it a role of an integrator of temperature information, the one that senses the peripheral changes, and has tools to regulate the response to these changes.

Other theories on thermoregulation have been postulated as well. One of those is disputing the role of a central temperature information integrator, as Hammel was proposing for the POA, and suggests that thermoregulation is attained via temperature-sensitive neurons in the periphery sending outputs to the effector cells which activate effector response. Here, the decision of whether a heat loss, for example, will be activated does not depend on the set point comparator but merely on the summation of the sensory temperature-sensitive neurons' activation and their predisposition to activate an effector response (Kobayashi, 1989). In addition, the POA role in thermoregulation is challenged by another view, suggesting that thermoeffectors are working independently of each other, each activated by a different set point temperature, but working to contribute to the thermal balance (Romanovsky, 2004, 2007).

Despite the above-mentioned counterpoints to the theory of central brain thermoregulation, it seems that only the integrity of the POA influences precise body temperature regulation as shown by the earlier-mentioned lesion and warming studies. In addition, although other brain regions contain temperature-sensitive neurons, it has been shown that POA WSNs respond to the skin and spinal cord warming (Boulant & Hardy, 1974). This finding has made POA WSNs prime candidates for integrating peripheral and central information on temperature. Moreover, the facts that cooling the POA elicits brown adipose tissue (BAT) and shivering thermogenesis, and that warming activates heat defense mechanisms point to the central role of the POA in thermoregulation (Hammel et al., 1960; Imai-Matsumura et al., 1984; Kanosue et al., 1990).

1.1.3. Synaptic dependency of WSNs and CSNs

Initial studies suggested that synaptic input dependency is different for WSNs and CSNs. These studies showed that neuronal warm sensitivity persists during synaptic input blockade, while cold sensitivity turned out to be largely dependent on synaptic inputs (Kelso & Boulant, 1982). It is worth noting that the blockade of synaptic inputs in those experiments was achieved via balancing the composition of different ions (such as calcium and magnesium) to prevent synaptic activity and not by specific blockers of excitatory and inhibitory transmitters. This has raised the hypothesis that the cold-sensitive neurons receive inhibitory input from WSNs, which is decreased during the cold stimulus, and therefore their firing increases. In addition, the physiological relevance of cold-sensitive neurons has not been found and it has remained unclear whether they have a role in activating effector mechanisms for thermoregulation

(Kanosue, Yanase-Fujiwara, et al., 1994; Kanosue, Zhang, et al., 1994). However, some cold neurons were identified in the primary dissociated neurons from rat hypothalamus and recently a gene CNGA3 has been identified as a cold sensor in mouse POA dissociated neurons (Abe et al., 2003; Feketa et al., 2020).

1.2. MECHANISMS OF WSNs' WARM SENSITIVITY

Although discovered a century ago, the mechanism behind the temperature sensitivity of the POA WSNs is still not clear. Two different views of mechanisms behind this POA neuronal characteristic were observed and discussed among the researchers (Griffin et al., 1996; Hori et al., 1999; Kobayashi et al., 2006). First, Kobayashi and colleagues measured the resting membrane potential (RMP) of POA WSNs and found that the RMP gets more depolarized in the WSNs upon warming in comparison to the temperature-insensitive neurons (Kobayashi & Takahashi, 1993). In addition to this, some studies have identified inward sodium current to be temperature sensitive in POA dissociated neurons, speculating that this current shows increased Na^+ permeability upon warming and is followed by increased depolarization and neuronal firing rate (Kiyohara et al., 1990).

On the other hand, Boulant and colleagues have proposed that the resting membrane potential of WSNs is not affected by temperature but that it is the depolarizing pacemaking prepotentials that are increased in WSNs during warming, leading to a decreased interval between each action potential and faster firing (Curras et al., 1991; Griffin & Boulant, 1995). The depolarization prepotentials are assumed to be run by temperature-sensitive hyperpolarizing potassium current (A-type potassium current) (Griffin et al., 1996). It is important to highlight that the recordings which have led to these two different findings were done under different conditions; Kobayashi's group recognized WSNs while applying synaptic blockade and by applying the temperature sensitivity criterium of 0.5 AP/s/˚C, as Boulant's group did not use synaptic blockers and used criterium of 0.8 AP/s/˚C.

In addition, researchers have tried to model the ionic conductances dependent on the temperature and have found that changes in the expression levels of certain ion channels can contribute to the neuron warm sensitivity (Wechselberger et al., 2006). Ion channels such as pacemaking HCN (Hyperpolarization-activated cyclic nucleotide-gated cation channel), TREK1 (potassium two pore domain channel subfamily K member 2)/TRAAK (TWIK-Related Arachidonic Acid-Stimulated Potassium Channel), and TASK-1 (potassium two pore domain channel subfamily K member 2) all showed to possibly mediate neurons' warm sensitivity.

This has suggested that it is most likely not the case that only one ion channel modulates the neuronal warm-sensitivity but that it is probably a consortium of different molecules and the levels of their

expression that determines it. Additionally, more recently, a view on synaptic mechanisms behind warm sensitivity has changed, as it was found that WSN activity does after all depend on synaptic inputs mediated by activation of cation channel TRPM2 (Kamm et al., 2021). This finding gives a novel perspective on the mechanism of WSNs' warm sensitivity as it points out that searching for the molecules mediating the intrinsic thermal sensation in the brain might not lie within the WNSs themselves but as well within their local circuitry.

1.3. AFFERENT AND EFFERENT THERMAL PATHWAYS

The change in ambient temperature is sensed by the Aδ and C nerve fibers containing temperature receptors such as TRP (transient receptor potential) ion channels. Myelinated A-delta afferent fibers are sensing cold in primates and humans (Hensel & Iggo, 1971), as primarily unmyelinated C-fibers sense cold and warmth in humans, rodents, and other mammals (Duclaux & Kenshalo DR, 1980; Iriuchijima & Zotterman, 1960). These primary somatosensory neurons that sense temperature has their somas in dorsal root ganglia (DRG) located next to the spinal cord and are innervating the whole body, or in trigeminal ganglia (TG) situated close to the brain which is innervating the head and face, as their axons extend on two sides (Vriens et al., 2014). One side extends to the periphery (skin, mucosa, internal organs) to collect information about the temperature, and the other to pass on this information, toward second-order neurons in the spinal cord dorsal horn. In addition, these neurons are capable of temperature detection themselves, as their somas are equipped with temperature-sensing ion channels (Ran et al., 2016).

The afferent fibers containing the cold detector, TRPM8 (transient receptor potential melastatin 8) ion channel, sense cold and are the main provider of cold information toward the dorsal horn (Ran et al., 2016). On the other hand, the fibers expressing the TRPV1 (transient receptor potential vanilloid 1) ion channel, bring information about warmth (Mishra et al., 2011). TRPV1 ion channel has been found as a heat-sensitive TRP channel, and the ablation of neurons containing TRPV1 leads to a lack of thermoregulatory responses to heat (Pogorzala et al., 2013). Since ablation of the TRPV1 ion channel does not completely abolish heat sensitivity; the effort was put to investigate other potential ion channels contributing to this function of peripheral nerve fibers (Vriens et al., 2014). Additional TRP channels were found to be temperature sensitive and involved in peripheral temperature sensation; a recent work from Vandewauw et al. has found a TRP channel trio: TRPM3, TRPV1, and TRPA1, to be important in perceiving noxious heat stimuli (Vandewauw et al., 2018). Interestingly, knocking out all three channels at the same time has caused almost a complete deficiency in heat sensitivity of Aδ and C nerve fibers.

The spinal dorsal horn (DH), located in the spinal cord, receives input from the DRG and projects toward the thalamus (Hylden et al., 1986; J. Li et al., 2006) and lateral parabrachial nucleus (LPB) (Cechetto et al., 1985; Nakamura & Morrison, 2008). The projections from DH to the thalamus end up in the cortex and serve for temperature perception. However, this spinothalamic pathway is required for neither autonomic nor behavioral responses to changes in cutaneous temperature (Nakamura & Morrison, 2010; Yahiro et al., 2017). On the other hand, the projections from DH to LPB, integrating information from cutaneous and deep body temperature sensors of the DRGs and TGs, are essential for the activation of thermoregulatory responses to the change in skin temperature (Nakamura & Morrison, 2008, 2010). The LPB itself contains neurons that are activated by skin cooling and warming. The lateral external portion of LPB (LPBel) is activated by cold exposure (4˚C) and is required for activating the cold defense mechanisms by projecting to the preoptic area, in particular to the MnPO (Nakamura & Morrison, 2008). Parallel to that, the dorsal division of LPB (LPBd) contains neurons activated by warmth (36˚C), projecting to the MnPO. It was found that the LPBd is needed to decrease cutaneous vasoconstriction and inhibit BAT thermogenesis, two effector mechanisms for getting rid of the excess heat (Nakamura & Morrison, 2010). In addition, in mice, about 83% of the heat-activated LPB POA projecting neurons are genetically marked by pre-prodynorphin but the function of that peptide in thermoregulation is not known (Geerling et al., 2016).

1.3.1. Thermoeffector mechanisms in thermoregulation

The finding that the POA contains warm sensitive units, which as well respond to skin and spinal cord heating placed the neurons of that hypothalamic nucleus in the core of thermoregulation by giving it a bridging role between the thermosensory afferents and thermoeffector efferents (Boulant & Hardy, 1974; Guieu & Hardy, 1970). The key thermoeffector organs are cutaneous blood vessels, salivary (in rodents) and sweat glands (larger mammals and humans), skeletal muscles, and brown adipose tissue (BAT) responsible for shivering and non-shivering thermogenesis, respectively (Madden & Morrison, 2019) (Figure 1.1). Thermogenic effector mechanisms such as BAT adipose tissue thermogenesis and skeletal muscle shivering produce heat via excess ATP uncoupling from the mitochondria. Vasoconstriction keeps the warm blood within the animal's body and serves as a heat-conserving mechanism. Cutaneous Vasodilatation on the other hand serves as a heat dissipation mechanism as the surface area through which warmth from the blood can be dissipated is increased. In addition, salivation in rodents or sweating in humans and some other mammals is helping to cool the skin down and helps to lower the body

temperature. In particular in combination with vasodilation, sweating is among the most effective cooling systems in the animal kingdom

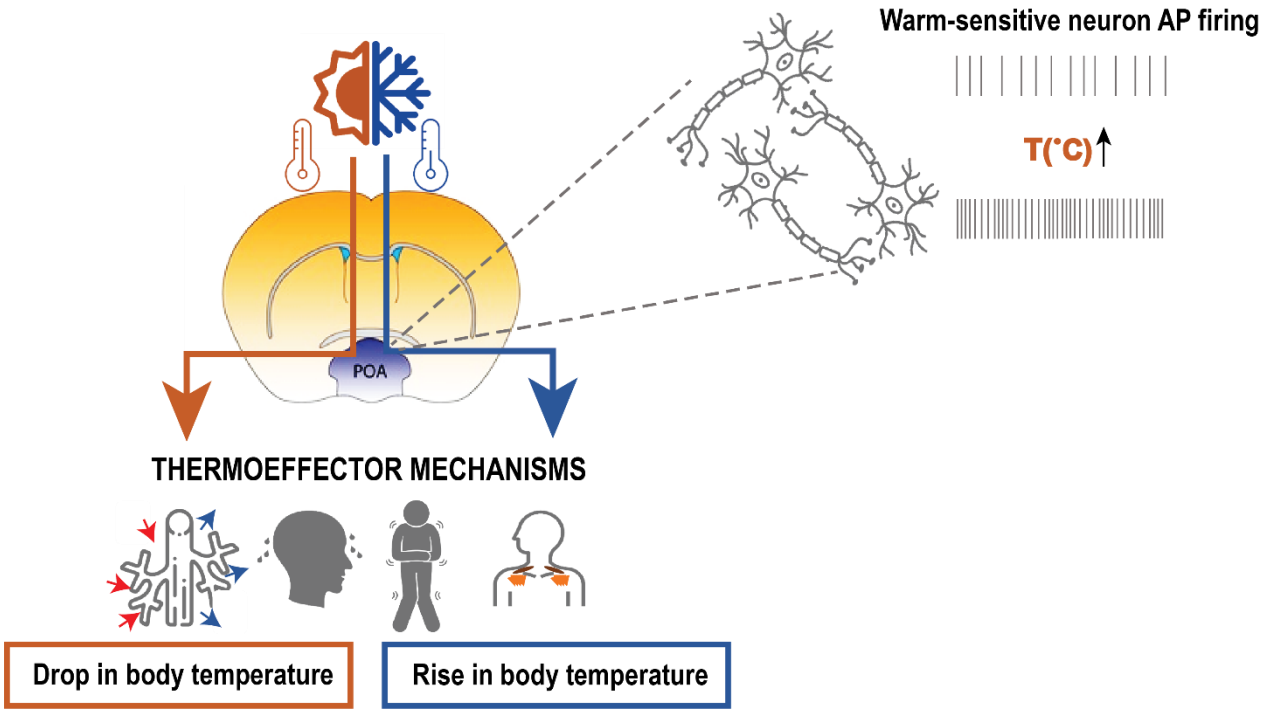

Figure 1.1. Activation of thermoeffector mechanisms by heating or cooling the POA
POA neurons contain warm sensitive neurons that respond to POA warming with i+the increase in action potential firing frequency. Heating or cooling the POA activates thermoeffector mechanisms such as cutaneous blood vessels vasodilation/vasoconstriction, sweating, skeletal muscle shivering, and BAT (Brown adipose tissue) thermogenesis, which in turn cause a drop in body temperature and rise in body temperature, respectively.

1.3.1.1. Cutaneous vasodilation and vasoconstriction

In mice, it has been found that inhibiting MnPO neurons induces tail vasoconstriction by increasing CVC sympathetic nerve activity (SNA) (Abbott et al., 2016). On the contrary, the activation of the same neurons showed to induce tail vasodilatation(M. Tanaka et al., 2009). POA neuron activation by skin warming induces inhibition of cutaneous vasoconstriction (CVC) thereby promoting vasodilation. Rostral Raphe pallidus (rRPA), rostral ventromedial medulla (RVNM), and Parapyramidal area in the medulla oblongata (PaPy) contain sympathetic premotor neurons which project to the preganglionic neurons in thoracolumbar spinal cord mediating CVC, these in turn project to paravertebral sympathetic ganglion cells innervating cutaneous blood vessels (Nakamura, 2004; Smith et al., 1998; Tóth et al., 2006). Inhibiting $GABA_A$ receptors in rRPA neurons was found to prevent the POA-warming-evoked tail vasodilatation in

rats (M. Tanaka et al., 2002). On the contrary, if glutamate receptors are blocked cold-activated vasoconstriction perishes (M. Tanaka et al., 2011). Both of these findings suggest that inhibitory connections from WSNs in the POA to rRPa are controlling cutaneous blood flow thermoregulation (Ootsuka & Tanaka, 2015).

Active vasodilation does not exist in rodents, as it depends on inhibition of the pathways for the CVC. However, it has been established that cutaneous sympathetic nerves exist in humans, and that activation of those leads to vasodilatation (Johnson et al., 2014).

1.3.1.2. BAT and skeletal muscle thermogenesis

The largest brown adipose tissue depot in rodents is the interscapular BAT which serves as a thermogenic organ owing to the UCP1 (uncoupling protein 1, thermogenin) protein in the mitochondrial membranes which allows proton turnover back to the mitochondria during the oxidative phosphorylation creating extra ATP energy (Shabalina et al., 2013). BAT thermogenesis highly depends on β3-adrenergic receptors expressed on brown adipocytes and sympathetic norepinephrine release, which binds β3-adrenergic receptors leading to the activation of the UCP1 protein (Cannon & Nedergaard, 2004). Moreover, although previously thought to be functional only in newborns, the BAT was found to be present and functionally active in adult humans (Cypess et al., 2009). In addition, based on more recent emerged literature, it is debated whether BAT activity is driven by β3 or by β2-adrenergic receptors(Blondin et al., 2020).

The MnPO neurons get activated by cool sensing afferents arriving from the LPBel, it is believed that these CSNs inhibit MPA neurons, by which disinhibition of the BAT sympathoexcitatory neurons in the dorsomedial hypothalamic nucleus (DMH) occurs (S. F. Morrison & Madden, 2014). Rostral ventromedial medulla (RVMM), rostral raphe pallidus (rRPAa), and parapyramidal area (PaPy) contain BAT sympathetic premotor neurons, and DMH projects to these regions to elicit BAT thermogenesis (Kataoka et al., 2014; Y. Zhang et al., 2011). Finally, it seems that serotonergic and glutamatergic neurons in rRPA and PaPy are responsible for the final activation of BAT thermogenesis, as the inhibition of either spinal Vglut-3 (vesicular glutamate transporter 3) or 5-HT (serotonin receptor) receptors inhibits rRP- activation-evoked and cold-evoked BAT thermogenesis, respectively (Madden & Morrison, 2010; Nakamura, 2004).

1.3.1.3. Skeletal muscle shivering

Skeletal muscle shivering during cold results in excessive ATP production which serves as a fuel for thermogenesis (S. Morrison F. & Nakamura, K, 2011). Shivering thermogenesis is centrally controlled via a

similar pathway as BAT thermogenesis, as it was shown that blocking rRPa and PaPy prevents cold-initiated shivering (Nakamura & Morrison, 2011). Here, DMH provides excitatory inputs to rRPa somatic muscle premotor neurons, which act on α, and γ motor neurons of the ventral horn in the spinal cord. It seems that vLPO neurons are important for regulating muscle shivering thermogenesis by providing direct or indirect inhibitory drive onto rRPA which was shown by abolishing cold-evoked shivering once the vLPO neurons were activated (Conceição et al., 2019).

1.3.1.4. Evaporative cooling

Evaporative heat loss is achieved by sweating in humans, and by salivation and saliva spreading in rodents, whereas some mammals such as dogs employ panting to dissipate the heat. The mechanisms behind these different effector mechanisms serving the same purpose are not completely elucidated, although it is quite clear that warming of the anterior hypothalamus induces panting in dogs, salivary secretion in rats, and paw sweating in cats (Hemingway et al., 1940; Kanosue et al., 1990; Magoun et al., 1938). Heating the anterior hypothalamus evokes salivation, most probably by projection towards the superior salivary nucleus projecting to salivary glands, whereas heating of the posterior hypothalamus evoked grooming and saliva spreading, a thermoregulatory behavior observed in rodents(Madden & Morrison, 2019; H. Tanaka et al., 1986). Although it is not fully investigated, it seems that paraventricular and lateral POA might be connected to the salivatory submandibular and sublingual glands, as it was shown by pseudorabies virus tracing (Hübschle et al., 1998). Therefore, these POA regions might function as an important relay in heat-evoked salivation

1.4. POA IN FEVER

Fever is a naturally occurring increase in the body temperature serving as an immune response to infections (Kluger, 1991). It is well established that prostaglandins, more specifically the one of type E2, are responsible for fever mediation (Engblom et al., 2003; S. Li et al., 1999). Prostaglandin E2 is synthesized by brain endothelial cells and by peripheral tissues in response to pyrogens such as lipopolysaccharide (LPS), a membranous component of gram-negative bacteria (Matsumura et al., 1998; Steiner et al., 2006). It has been established that the MnPO area plays a critical role in fever by expression of EP3 prostaglandin receptor (EP3R) without which fever response to LPS is significantly attenuated (Lazarus et al., 2007). Moreover, it was recently shown that EP3R expressing MnPO neurons, important for fever development, are glutamatergic and innervate RPa (Machado et al., 2020). It is thought that activation of EP3R with PGE2 attenuates the neuronal activity, as it was shown that the majority of WSNs in the POA are inhibited by

prostaglandins (Ranels & Griffin, 2003). From the thermal set point of view, inhibiting the WSNs changes the set point of the POA, and therefore, since the body temperature now appears lower than the set point one, POA elicits a range of effector mechanisms to conserve heat such as skeletal muscle shivering and cutaneous vasoconstriction (Flier et al., 1994; Hammel et al., 1963).

Unlike the increase of the body temperature in fever, the hyperthermia observed outside of inflammatory reactions is usually a sign of failure of effector mechanisms to dissipate heat but without offsetting the POA temperature set point. For example, EP3R deficient mice fail to develop fever, but hyperthermia evoked by the stress of handling the animal persists (Machado et al., 2020). Additionally, it has been shown that hyperthermia caused by psychological stress in rats also involves BAT thermogenesis, meaning that it shares, at least partially, some effector mechanisms as the fever and body temperature defense in cold (Shibata & Nagasaka, 1984). Moreover, it was confirmed that chronic hyperthermia evoked by chronic stress, or psychogenic fever, is mediated by emotion-related forebrain regions mediating the effect through the DMH towards BAT (Kataoka et al., 2020).

1.5. POA NEURON POPULATIONS INVOLVED IN THERMOREGULATION

The question of how exactly the preoptic area warm-sensitive neurons (WSNs) detect temperature, remains unanswered by the present day, and this is mainly due to the lack of molecular markers of these neurons. However, WSNs are included in the thermoregulatory models as the integrators of the local brain and peripheral temperature (S. F. Morrison & Nakamura, 2019; S. Morrison F. & Nakamura, K, 2011). The lack of molecular markers of the POA WSNs, and the possible other POA neurons involved in thermoregulation prevents the advancement of the research on the role the WSNs might have in thermoregulation. Therefore, researchers have tried to investigate the specific cellular populations involved in intrinsic temperature sensing of the POA neurons, as well as the POA area cellular populations activated by exposure to ambient temperature change. The current knowledge of the populations in the POA involved in thermoregulation is summarized in Table 1. (in Appendix page number158).

Song and colleagues have identified the TRPM2 (transient receptor potential cation channel subfamily M, type 2) ion channel as a somatic heat sensor in POA primary neuronal cultures from 2 days old mice (Song et al., 2016). The POA cultured neurons from the TRPM2 knock-out (KO) animals have exhibited complete abolishment of temperature sensitivity, whereas the calcium imaging in POA slices from adult KO animals has shown that some warm-sensitive neurons persist. This has pointed out the fact that POA neurons in adulthood must contain other molecules sensing intrinsic temperature. In addition, activation of TRPM2 expressing POA neurons using chemogenetically activated G-protein coupled

receptors (Designer Receptors Exclusively Activated by Designer Drugs (DREADDs)) has induced hypothermia while inhibiting the same neurons has led to mouse hyperthermia. Moreover, the activation of the glutamatergic population of the POA neurons recapitulated TRPM2-driven hypothermia and not that of the inhibitory population. This finding was opposite to the models of thermoregulation that involved only inhibitory WSNs to be mediating the temperature information to the downstream targets. Moreover, the prostaglandin E2 (PGE2) injection known to induce fever by acting on the EP3 receptor in POA, has caused significantly higher body temperature in the TRPM2 KO animals than in the WT controls. Summing up these results, TRPM2 was the first ion channel shown to be functionally relevant for the POA temperature detection, found to limit fever and drive hypothermia in mice.

Further on, Wang and colleagues found that WSNs of the POA are enriched with prostaglandin D2 (PGD2) synthase (T. A. Wang et al., 2019). Knockdown of *Ptgds* gene coding for PGD2 exhibited a lethal effect on mice that were not able to sustain their body temperature and eventually died. The expression of *Ptgds* in POA was also present in CSNs and temperature insensitive neurons. Nevertheless, its effect on thermoregulatory homeostasis is assigned to the WSNs of the POA, at least in hyperthermic conditions, due to the low activity of temperature-insensitive and CSNs neurons in these temperature ranges.

The work of Abbott and colleagues has identified the POA neuronal population that as well induces profound hypothermia in mice when activated (Abbott & Saper, 2017). In this work, glutamatergic neurons of the median preoptic area (MnPO) were activated directly via optogenetic manipulation of channelrhodopsin 2 (Chr2) expressing glutamatergic neurons (Vglut2). This activation has led to hypothermia achieved via observed cutaneous vasodilatation. This finding has confirmed partially the finding of Song and colleagues that Vglut2 neurons of POA participate in thermoregulation. In some instances, the activation of these neurons by Chr2 has also inhibited drinking in mice, since this was not occurring in each activation attempt, it was concluded that MnPO glutamatergic neurons consist of subpopulations of cells involved in thermoregulation and water consumption but that these two are not fully overlapping. The precise mapping of Chr2 injection and optic fiber implantation sites has revealed that the strongest hypothermia was occurring when the anterior part of the POA containing OVLT (organum vasculosum laminae terminalis) and MnPO was targeted. This work has insinuated that indeed POA might be quite a heterogeneous region containing different nuclei containing cell types devoted to diverse and/or overlapping functionalities.

Apart from the paradigm in which researchers have tried to look into the POA intrinsic WSNs by activating them with direct warming, they have also looked for POA neurons that get activated by

peripheral changes in temperature. Several markers of POA thermoregulatory neurons have been identified in this way (Tan et al., 2016; Yu et al., 2016; Zhao et al., 2017)

Tan and colleagues have identified the population of neurons within the POA activated by peripheral (37˚C) warming (Tan et al., 2016). They have captured these neurons by immunoprecipitation via phosphorylated ribosomal protein S6 (pS6), a technique named phosphoTRAP. Capturing the ribosomes allowed capturing of mRNAs translated to proteins during the neuronal activating stimulus. Analysis of the mRNAs has revealed that pituitary adenylate cyclase-activating polypeptide (*Adcyap1*, also known as PACAP), and brain-derived neurotrophic factor (*Bdnf*) are enriched in these WSNs. Calcium imaging of neurons in freely moving mice, while applying peripheral warming, showed increased activity of PACAP and *Bdnf* POA neurons. Moreover, activation-induced hypothermia is achieved via tail vasodilation and suppression of BAT thermogenesis. The term WSNs used for PACAP/*Bdnf* neurons, however, is a bit confusing, as it was shown that these neurons are not intrinsically warm-sensitive. It was proposed by others in the field to name these neurons “warmth-activated neurons” (WANs) (Siemens & Kamm, 2018), and more recently “warm-responsive neurons” (WRNs) term has been used for the same cell population (Machado & Saper, 2022; Upton et al., 2021). Nevertheless, PACAP/Bdnf genes are marking the population of neurons receiving the information about the thermal input from peripheral skin receptors, whose activation induces autonomic (BAT thermogenesis, tail vasodilatation) and behavioral (preference for the cooler environment) heat loss mechanisms, making these neurons part of the thermoregulatory circuit (Tan et al., 2016).

Another population found to be activated by peripheral warmth, and suggested to receive input from the peripheral temperature sensors, is the MnPO leptin receptor (LepR) expressing neurons (Yu et al., 2016). Activation of these neurons also led to a decrease in the $T_{core,}$ inhibition of energy expenditure via BAT thermogenesis, and promoted body extension, a behavior observed in animals exposed to high ambient temperatures. The activation of these neurons caused a decrease in body weight by a decrease in food consumption. The POA LepR neurons described in that work were assumed to be glutamatergic as 60% of the phosphorylated signal transducer and activator of transcription 3 (pSTAT3), a marker of LepR activity, expressing neurons co-localized with *Vglut2*, and only 19% with *Vgat* neurons. Additionally, the activation of glutamatergic, and not of GABAergic POA neurons, reproduced similar thermoregulatory effects (decreased T core, energy consumption, body extension) as activation of POA LepR neurons.

However, the work of Zhao and colleagues has revealed GABAergic neuronal population in the ventrolateral preoptic area (vLPO) and medial preoptic area (MPO), activated by the peripheral thermal challenge (Zhao et al., 2017). The activation and inhibition of vLPO *Vgat* expressing neurons, induced

hypothermia, and hyperthermia, respectively. This effect was achieved via vLPOA connection to the dorsomedial hypothalamus (DMD). The connection was described as vLPO neurons inhibiting thermogenic DMD neurons, leading to hypothermia.

An additional population of GABAergic POA neurons inducing hypothermia was one of the vLPO-expressing galanin neurons (Kroeger et al., 2018). Apart from hypothermia, activating those neurons by Chr2 photoactivation caused an increase in NREM sleep and the ablation of these neurons caused elevated baseline T_{core}.

Another glutamatergic population within the MnPOA activated by peripheral warming (32˚C) causing hypothermia when chemogenetically activated was that one expressing NOS1 (nitric oxide synthase) (Harding et al., 2018). Activating these neurons in mice caused hypothermia and induced sleep, connecting again two different functionalities such as thermoregulation and sleep in one relatively small nucleus as is the MnPOA. On the other hand, activating the GABAergic population of warm activated neurons in the POA did not cause hypothermia.

Unlike previously mentioned neuronal POA populations, bombesin-like receptor 3 (BRS3), an orphan G-protein coupled receptor, expressing POA and DMH neurons shown to be activated by peripheral cold, and to be involved in thermoregulation (Piñol et al., 2018, 2021). Optogenetic activation of the Brs3 expressing neurons via Chr2 in POA has caused hyperthermia, an increase in T_{core}, blood pressure, and heart rate in mice. The same effect in body temperature increase was observed when the neuronal projections from POA BRS3 to DMH were activated, and the Tcore increase was assigned to the increase in BAT thermogenesis, as the BAT temperature showed to increase during the POA BRS3-DMH activation.

Additional interesting findings connecting POA and thermoregulation came from work related to the investigation of hibernation and torpor in mice. First, Takahashi and colleagues have found neurons residing in the anteroventral periventricular nucleus (AVPe), medial preoptic area (MPA), and periventricular nucleus, expressing neuropeptide pyroglutamylated RFamide peptide (QRFP) activation of which caused profound hypothermia (<30˚C) in the duration of 48 hours (Takahashi et al., 2020). It was found that these neurons from AVPe ad MPA project densely to the DMH and that these projections are a key to hibernation induction. QRFP expressing neurons were in majority glutamatergic (78%). In addition, these neurons showed to be a subpopulation of PACAP/BDNF neurons found by Tan and colleagues (Tan et al., 2016). This again pointed to the possibility of large cellular diversity within the POA and distinct subtypes of neurons within one region.

Next, Hrvatin and colleagues followed the cellular populations activated by torpor in the mouse brain (Hrvatin et al., 2020). They implemented targeted recombination in active populations (TRAP)-a technique where tamoxifen-inducible Cre recombinase is driven from the immediate early gene *Fos* locus, in which neuronal activity drives the cFos and Cre expression, and if tamoxifen is injected Cre protein is brought to the nucleus and recombines any flox-ed sequence. Here they TRAP-ed neurons by torpor (mice were exposed to 24h of food restriction and housed at 22˚C). They crossed the TRAP mouse line with the mice having Cre-dependent GqDREADD allele, and therefore the expression of Cre during tamoxifen injection allowed Cre recombination and expression of GqDREADD in torpor TRAP-ed neurons, allowing for their later re-activation. This reactivation has led to reduced metabolism and locomotor activity and lowered body temperature similar to in a torpor state. Analysis of brain regions activated by torpor revealed anterior and ventral portions of medial and lateral preoptic areas as key regions for torpor. Single nucleus RNA sequencing (snRNA-seq) analysis of torpor TRAPed neurons revealed that *Vglut2*$^{+}$ *Adcyap*$^{+}$ (PACAP) neurons were making 46% of TRAPed cells, activation of which has phenocopied reactivation of TRAPed neurons but as well decrease in body temperature and activity observed during natural torpor. Interestingly these POA torpor-activated PACAP neurons were not warmth-activated ones as described in previous work of Tan and colleagues, as these were reactive to cold and not heating. This showed that PACAP POA neurons consist of a functionally diverse population of neurons.

The large single-cell RNA sequencing (scRNA-seq) atlas of the preoptic area helped to characterize this large nucleus (Moffitt et al., 2018). This data set has revealed 43 inhibitory and 23 excitatory neuronal clusters in the POA and researchers have provided spatial mapping of these genetic populations *in situ* based on their scRNAseq markers and previously known markers of major cell classes. This work has revealed 14 PACAP/BDNF enriched neuronal clusters within the POA, the majority of which were excitatory neurons. One of these clusters, cluster E3/e13, displayed anatomical position of PACAP/BDNF warmth-activated neurons, it was marked by *Sncg* gene coding for γ-synuclein, estrogen-signaling modulator, and expressed high levels of cFos when the mouse was challenged with 37˚C.

In silico analysis has revealed that the *e10* cluster from Hrvatin et al. torpor populations, and the *e13* cluster from Moffit et al. POA scRNA-seq, represent the same cellular population in the POA (Upton et al., 2021). The analysis of the transcriptome of this joint cluster resulted in revealing its genetic markers: *Qrfp* (Pyroglutamylated RFamide Peptide), *Ptger3* (prostaglandin E receptor 3), *Lepr* (leptin receptor), *Opn5* (opsin 5) and *Tacr3* (Tachykinin Receptor 3), therefore, it was named QPLOT.

PTGER3 receptor expressed in MnPO glutamatergic neurons is found responsible for mediating LPS-induced fever (Machado et al., 2020). As mentioned before, a *Vglut2* expressing POA neurons causes

hypothermia when activated by GqDREADD (Abbott & Saper, 2017). In addition, ablating these neurons caused hyperthermia during heat exposure corroborating their role in activating heat loss mechanisms.

The *Opn5* gene codes for G-protein coupled receptor and violet light detector, and, apart from skin and retina, is expressed in the POA of mice (K. X. Zhang et al., 2020). In particular, it was found expressed in glutamatergic POA neurons expressing also *Adcyap1* and *Bdnf* genes. The chemogenetic activation of Opn5 expressing POA neurons has suppressed BAT thermogenesis and T_{core}, its inhibition has increased BAT thermogenesis and T_{core}, and mice lacking this protein exhibited elevated T_{core}, increased BAT hyperactivity, and caused an increase in energy expenditure.

Additionally, the gene found enriched in Hrvatin and Moffit clusters was *Tacr3* gene coding for neurokinin 3 receptor (NK3R) responsible for neurokinin B signaling (Padilla et al., 2018). Activation of the of Kisspeptin-Neurokinin B Dynorphin-expressing (KNDy) neurons of the arcuate nucleus projection to the POA decreases body temperature via vasodilatation and induces cFos in POA. Therefore, it might be that QPLOT neurons in the POA expressing *Tacr3* are mediating also this effect.

POA neurons were already shown to express Esr1 gene coding for ERα (estrogen receptor alpha) and some of these neurons were also temperature-sensitive (Silva & Boulant, 1986). The activation of MPA (medial preoptic area) neurons expressing ERα induced hypothermia and the expression of ERα was found induced during the bouts of torpor in mice. Moreover, their ablation prevented mice from entering the full torpor (Z. Zhang et al., 2020). Interestingly, the Esr1 receptor is also one of the genes found expressed in the cluster of QPLOT neurons.

The QPLOT joint cluster coming from two independent data sets of the POA transcriptome has revealed POA neuronal cluster involved in temperature detection, fever mediation, hormonal balance, energy expenditure, and thermogenesis. Nevertheless, it pointed out the genetic and functional diversity of the cellular populations residing within this region. All the above-presented work evolved in less than a past decade revolves around finding the molecular niche of the thermoregulation within the POA. However, the task seems daunting, as several neuronal populations seem to be somehow involved in the thermoregulatory homeostasis. scRNA-seq data joined with anatomical mapping together with chemogenetics, optogenetics, viral tracing, and TRAPing of the POA cellular populations have helped in elucidating the molecular makeup behind the neurons involved in thermoregulation, however, it has also pointed out that several markers need to be used at the same time to define this population. In addition, a piece of knowledge about the markers of intrinsic WSNs remains scarce, and It seems as if these neurons are difficult to tackle. The possible reason might be the recent finding that the temperature sensitivity of WSNs is synaptically modulated as this raises the question of whether the warm sensitivity is indeed an

intrinsic property of the WSNs, or is it depending largely on synaptic inputs of neighboring and remote cells (Kamm et al., 2021). Questions remain: How much do the WANs/WRNs overlap with WSNs? Is the role of intrinsic WSNs important at all in thermoregulation? The latter question is as old as the finding of the WSNs in the POA, as the primary responses that rise to defend the body temperature get activated immediately after the ambient temperature are changed without enough time to change internal body temperature, and therefore not yet activating the intrinsic WSNs (Siemens & Kamm, 2018). However, even after the ablation of peripheral thermoreceptors neurons, body temperature remains undisturbed, pointing out that other temperature sensors are enough to maintain stable thermoregulation (Mishra et al., 2011).

2. AIMS

For most of the mammalian species, maintaining core body temperature (T_{core}) around 37˚C requires coordination of different effector mechanisms in response to environmental and internal challenges, such as cold and hot external temperatures and systemic infection or inflammation which often leads to fever (S. F. Morrison & Nakamura, 2019). The key brain region responsible for orchestrating the T_{core} defense is the preoptic area (POA), positioned within the hypothalamus above the optic chiasm. One of the main findings supporting this claim is that direct warming or cooling of POA, by using diathermy or a thermode, elicits heat-dissipating or heat-conserving and heat-producing mechanisms, respectively (Hemingway et al., 1940; Magoun et al., 1938). These findings have led to the hypothesis that to activate the downstream thermoeffector mechanisms such as vasodilatation or vasoconstriction, sweating, shivering or brown adipose tissue thermogenesis, the POA must contain intrinsically temperature-sensitive cells which would convey the message of change in the brain temperature.

Several electrophysiological (Ephys) studies have shown that such warm sensitive neurons (WSNs) do reside within the POA and they can be recognized as neurons that increase their firing frequency upon local temperature increase (Boulant & Dean, 1986; Nakayama et al., 1961, 1963). Importantly, it has been shown that the WSNs of the POA are affected by spinal cord and skin warming, implying they are good candidates to integrate peripheral and central temperature information (Boulant & Hardy, 1974).

The current models of thermoregulation include the warm-sensitive neurons (WSNs) of POA in explaining the thermoregulatory processes, but we still know neither their exact role in thermoregulation nor the mechanism of their intrinsic warm sensitivity (S. F. Morrison & Nakamura, 2019; S. Morrison F. & Nakamura, K, 2011). One of the main reasons for this knowledge gap is the lack of specific molecular markers for WSNs. Previously, it was found in our lab that the ion channel TRPM2 (transient receptor potential cation channel subfamily M member 2) participates in the heat sensitivity of the hypothalamic preoptic area (POA) neurons (Song et al., 2016). In that work calcium (Ca^{2+}) imaging on POA neuronal cultures, obtained from neonatal (P2) mice, was performed during warming, and neurons responding to temperature were identified as WSNs. Ca^{2+}-imaging of TRPM2 knockout (KO) P2 animals showed abolished temperature response. On the other hand, Ca^{2+}-imaging in the acute slices of the TRPM2 KO adult animals showed that the cells responding to temperature persist, implying that other molecules apart from the TRPM2 are contributing to the temperature sensitivity of the more mature POA neurons.

Due to the lack of specific genetic markers, the investigation of POA WSNs is limited to Ephys studies in tissue slices based on the classically defined criteria for warm sensitivity (increase in AP firing

rate due to temperature by 0.8 AP/s/˚C). With these constraints, it is hard to study WSNs' connectivity to other brain regions and therefore almost impossible to investigate their role in thermoregulation.

Based on the scientific background elaborated above, the overall objective of this part of the thesis work was to characterize WSNs of the POA on their molecular level. Specifically, I aimed to:

1) Obtain mouse primary POA postnatal neural culture from mice of more mature age and test their warm-sensitivity via Ca^{2+} imaging.

2) Obtain transcriptome data of temperature-sensitive POA primary cultured neurons, serving as a proxy to the WSNs, by single-cell RNA sequencing approach (scRNA-seq).

3) Find genetic markers of POA WSNs.

3. RESULTS

3.1. Ca^{2+} IMAGING IN PRIMARY POA NEURONAL CULTURES

Since it has been shown that the TRPM2 KO adult animals still contain the cells responding to temperature within the POA unlike their 2-day-old counterparts (Song et al., 2016), I decided to work towards culturing POA neurons of more mature animals than P2 to investigate the transcriptome of temperature-sensitive cells via single-cell RNA sequencing (scRNA-seq). Culturing CNS neurons from adult animals is notoriously known to be difficult due to the limited regeneration capability of mature neurons (Gordon et al., 2013; Levin et al., 2016). However, some examples of successful primary neural cultures from CNS, mainly from early postnatal days of rodents, and structures such as retina (Kretz et al., 2007), pyramidal hippocampal, and cortical neurons are known (Beaudoin et al., 2012; Kaech et al., 2012; Petrović et al., 2021).

The most advanced postnatal time point from which I managed to obtain healthy primary POA cultures, by using the protocol established in the lab used for culturing POA neurons from P2 mice (Song et al., 2016), was postnatal day 9 (P9). I obtained neural cultures by dissecting the POA (Figure 1.2. A) from four C57BL/6 P9 pups within the same experiment. Cells were cultured for 3 days on glass coverslips immersed in the well of 24 well-plate and on the 3rd day Ca^{2+} imaging was performed (a more detailed description of cell culturing and Ca^{2+}-imaging can be found in the Materials and Methods section, Chapter 3). To visualize Ca^{2+} dynamics cells were loaded with CAL520- a synthetic fluorescent calcium indicator dye (Tada et al., 2014), and the coverslip was placed in a perfusion chamber and imaged while changing the temperature of the bath with a gravity-assisted perfusion system. Figure 1.2. C shows an example field of view of a coverslip with neural POA primary cells loaded with CAL520 and visualized in Metafluor (Molecular Devices) during and after each of the 3 stimuli presented to cells. The protocol of cell temperature stimulation consisted of 3 stimuli in which temperature was raised from 25 ˚C room temperature (RT) to 45 ˚C and lowered back to RT within 45 seconds (Figure 1.2. B). The 2nd stimulus was followed by perfusing cells with Ringer's solution containing a 2-APB drug (2-Aminoethoxydiphenylborane), a TRPM2 blocker (Togashi et al., 2008), to distinguish from cells that mediate the temperature response via TRPM2 and others that potentially respond to temperature via additional molecules. At the end of each protocol, Ringer's containing high potassium (hK^+) concentration was perfused to cells to visualize general neuronal excitability.

While recording Ca^{2+} dynamics of cells responding to temperature and 2-APB I identified 3 types of cells in the neural culture. I identified cells that did not respond to temperature (Non-responder; left

plot), cells responding 3 times to 45 ˚C degrees stimulus and their temperature response was not affected by the 2-APB (2-APB insensitive responders; middle panel), and cells that responded more strongly to 45 ˚C stimuli, but whose response was abolished by 2-APB (2-APB sensitive responders; lower panel). Example average traces of each category are plotted in Figure 1.2**.** D) ΔF/F values were calculated by subtracting the average baseline fluorescence($\Delta F = F - F_{(baseline)}$) before the 1st 45 ˚C- stimulus (first minute of the recording) from the fluorescence values and dividing it by the baseline ($\Delta F/F_{(baseline)}$).

The population analysis of the cell's response to the temperature is shown in Figure 1.2. E). The maximum amplitude of response to each stimulus (max(ΔF/F) is plotted. The blue dashed line represents the average of 3 standard deviations (SD) values of maximum response (Mean (3*SD(max(ΔF/F))) during the 2nd 45 ˚C stimuli with 2-APB of each coverslip in that experiment. From this, I could observe that some cells still respond to temperature with ΔF/F higher than 3 SDs of maximum responses during the 2nd 45˚C stimulus coupled with the 2-APB, concluding that 2-APB does not completely block all the cells responding to temperature. In this experiment, 15.7% of cells during the first, 1.8 % during the 2nd, and 7.6% during the third stimulus responded with ΔF/F higher than the cut-off value. Overall, in P9 POA cell culture, about 15% of cells were temperature-sensitive, and the temperature response of about 98% percent of those was blocked by TRPM2 antagonist 2-APB.

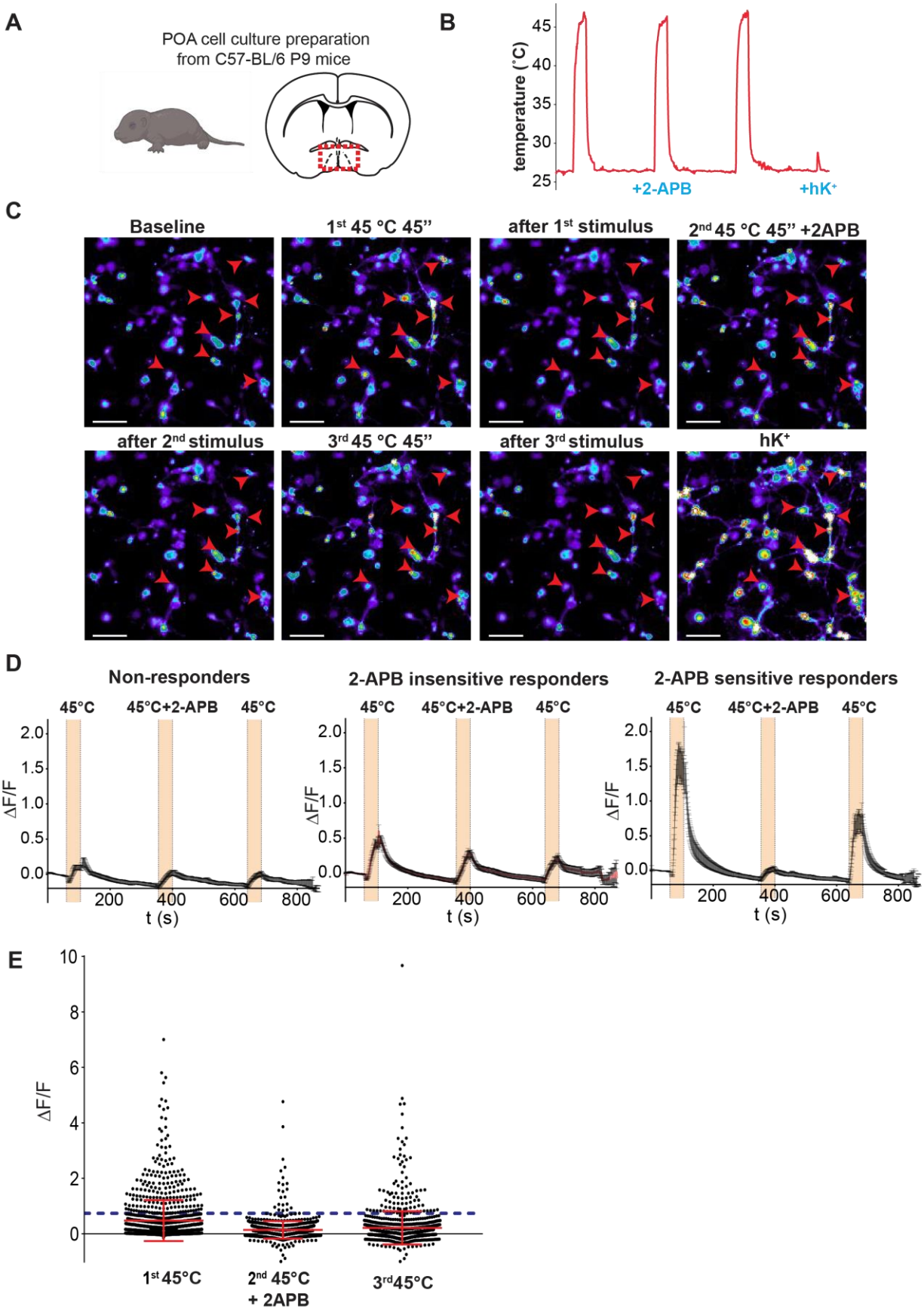
A
POA cell culture preparation
from C57-BL/6 P9 mice
B
temperature (°C)
45
40
35
30
25
+2-APB
+hK+
C
Baseline
1st 45 °C 45”
after 1st stimulus
2nd 45 °C 45” +2APB
after 2nd stimulus
3rd 45 °C 45”
after 3rd stimulus
hK+
D
Non-responders
2-APB insensitive responders
2-APB sensitive responders
45°C
45°C+2-APB
45°C
ΔF/F
t (s)
E
ΔF/F
1st 45°C
2nd 45°C
+ 2APB
3rd45°C

Figure 1.2. Ca^{2+} imaging on POA cultured neurons

(A) POA was dissected from 4 P9 C57BL6 mice and cells were cultured on glass coverslips for 3 days. (**B)** A temperature example trace is shown. Each temperature stimulus reached ≈45±1˚C and lasted for 45 seconds. During the 2nd temperature stimulus, 50 µM 2-APB containing Ringer's was perfused. At the end of the experiment high potassium Ringer's (100 mM, hK^+)was perfused into the cells. **(C)** A field of view (10x objective, zoomed in 1x) of a coverslip with POA neurons after 3 days of culturing at each of the steps from the stimulation explained above. Cells were loaded with Cal-520 to visualize calcium dynamics in a response to a temperature and hK^+ stimulus. Red arrows point to cells responding to 45˚C stimuli. The scale bar is 50 µm. **(D)** 3 categories of the cells in the POA culture were found by Ca^{2+} imaging. The upper panel represents an average trace (mean (ΔF/F) ± SEM, $n_{(cells)}$ =20) of cells not responding to temperature. The middle panel represents an average trace of the cells (mean ΔF/F ± SEM, $n_{(cells)}$ =34) responding to all 3 stimuli. The lower panel represents an average trace of cells (mean ΔF/F ± SEM, $n_{(cells)}$ =33,) responding to temperature stimuli that are blocked by the 2-APB drug. Orange-colored areas represent the time of the 45˚ C temperature stimulus. **(E)** Ca^{2+} response population analysis of primary POA neuronal cell culture. Plotted are the maximal amplitude values of individual cell responses to the 1st, 2nd, and 3rd 45˚C stimulus. 2nd stimulus was coupled with 2-APB perfusion. Each dot represents one individual cell. The dashed line represents an average value of 3x standard deviations of maximum response of cells to the 2nd 45˚ C stimulus with the 2-APB (mean (3*SD(max)=0.74). Error bars represent mean ±SD (1st 45˚ C: 0.48 ± 0.74; 2nd 45˚ C+ 2-APB: 0.14 ± 0.32; 3rd 45˚ C: 0.21 ± 0.60; n(cells)=1171, n(coverslips)=7).

3.2. SINGLE-CELL RNA SEQUENCING OF P9 POA CULTURED CELLS

After defining the type of neurons in the primary POA neural culture based on their temperature response to the 45˚C stimulation and TRPM2 blocker 2-APB (Figure 1.2. D) I went on to manually pick cells from each group for the scRNA-seq (Figure 1.3. A). The hypothesis is that their transcriptome will reveal genes that represent and are, ideally, specifically expressed in warm-sensitive cells, thereby revealing molecular markers and potentially even receptors and other molecules that are functionally required to convey their temperature sensitivity. Once I would identify cells responding to temperature by Ca^{2+}-activity, I aspirated cells with a glass pipette and transferred them to the PCR tube containing Smart-seq2 buffer for cDNA library preparation for the scRNA-seq (Picelli et al., 2014). I did the same for cells not responding to temperature. Therefore, the cells were visualized during the Ca^{2+}-imaging, collected according to the response to temperature stimulus, and their calcium traces were analyzed *post-hoc*.

I processed 125 samples collected in this way by the Smart-seq2 protocol (Picelli et al., 2014). 93 of these cells yielded a good quality pre-amplified cDNA library (Figure 1.3. B upper panel) where the distribution of DNA fragments at the Bioanalyzer electropherogram was peaking at ≈1.5-2kb with a small number of the fragments below the 500 bp (base pairs), and the final sequencing library with the

fragments size of ≈ 300-800 bp (Figure 1.3. B; lower panel). These 93 single cells were sequenced on the Illumina platform by NextSeq 500 System Mid output kit, at the Genomics Core facility (EMBL Heidelberg) reaching the read depth (number of counts) of 1.4 million on average per cell (Figure 1.3. C; middle panel). Out of these 93 cells, there were: a) 22 Non-responders; b) 37 2-APB insensitive responders; c) 34 2-APB sensitive responders.

After de-multiplexing the samples according to their unique barcodes, I did quality control (QC) of the sequenced reads with the FastQC tool (Steven W. Wingett & Simon Andrews, 2018). Reads were then aligned to the mouse transcriptome and quantified using Salmon (Patro et al., 2017). scRNA-seq data analysis was performed in R and R Studio by using R based tool Seurat (Butler et al., 2018; Stuart et al., 2019). The QC of the single-cell transcriptome in Seurat suggests removing cells from the sequencing data set that have >10% of mitochondrial counts and <2000 unique genes. A high percentage of reads coming from mitochondria can point toward cell death or loss of cytoplasmic mRNA due to perforated cell membrane(Ilicic et al., 2016). As for the number of unique genes, perforated low-quality cells will often have very few genes, but on the other hand, cell doublets may show deviant high gene count (Butler et al., 2018; Ilicic et al., 2016). The QC I performed in Seurat showed that all of the 93 cells had good quality with on average 7930 unique genes (minimum of 4427), 1.46 million counts (reads), and 2.4% of mitochondrial counts detected per cell (max = 7.2% <10%) (Figure 1.3. C). Therefore, I did not filter any cells out from the data set according to these quality metrics concluding that the samples were of good quality.

Next, to further inspect the transcriptome of the cells I performed non-linear dimensional reduction via t-distributed stochastic neighbor embedding (*t-SNE*) which places similar cells together in low-dimensional space according to clusters calculated in Seurat (Macosko et al., 2015). This cluster calculation is based on principal component analysis of the genes bringing the most variability to each cell category. Figure 1.3. D) shows the t-SNE plot of 93 cells clustered according to their transcriptome and colored according to their Ca^{2+}-imaging phenotype. From this graph, I concluded that the transcriptome of these cells does not completely recapitulate their physiological responses to temperature stimuli observed with Ca^{2+}-imaging. t-SNE graph clustering according to the principal component genes, did not find a clear separation between the groups of cells.

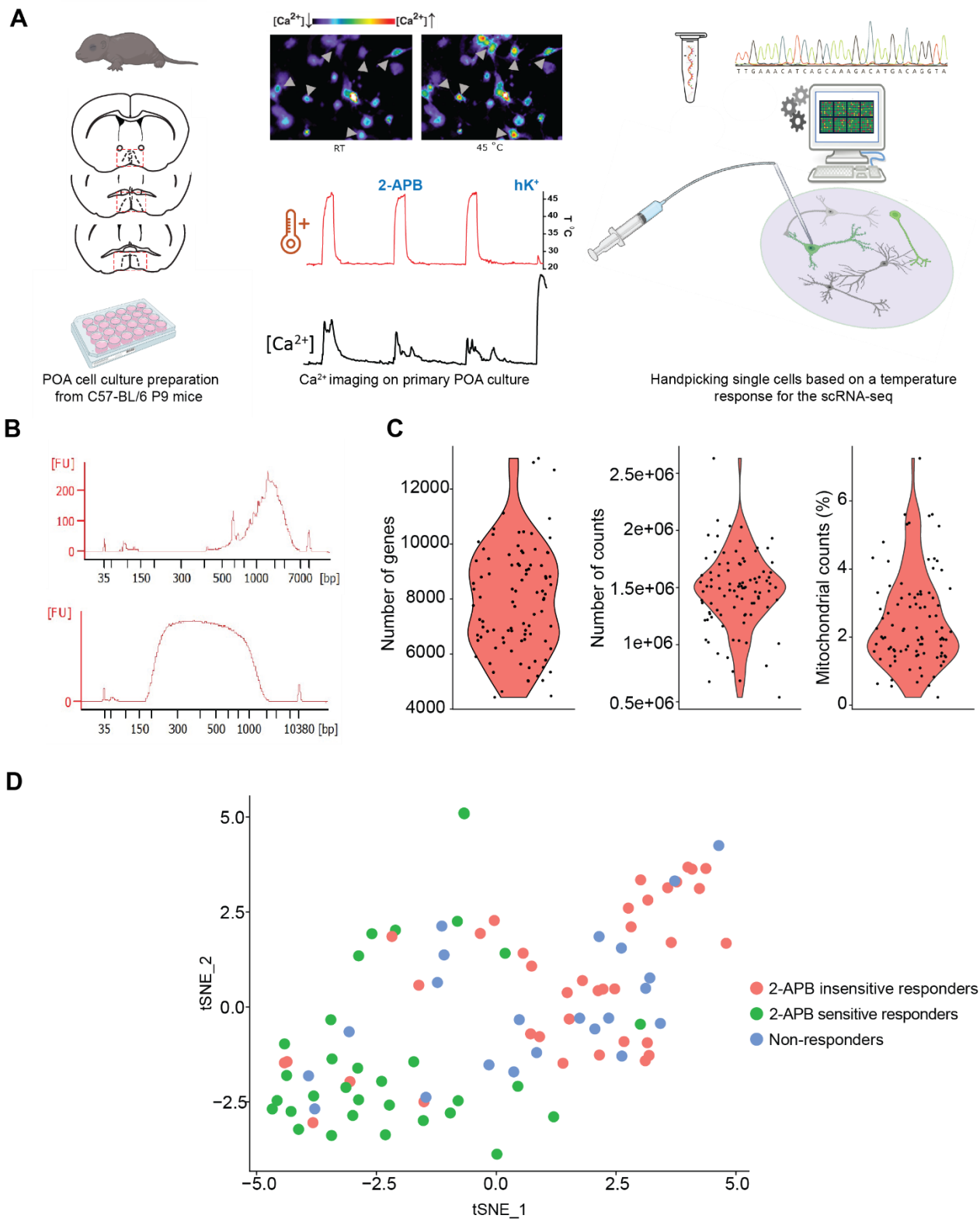

Figure 1.3. scRNA-seq of P9 POA neural culture

(A) Scheme of the experiment design: 3 POA sections were obtained from 4 P9 C57BL/6 pups each by vibratome sectioning. Cells were cultured on glass coverslips immersed in 24 well plates for 3 days. On the 3rd day, Ca^{2+}-imaging

was performed. Cells were single-picked under the microscope according to their response to a temperature stimulation by joystick driven mechanical manipulator and aspirated by applying pressure on a glass capillary, after which they were ejected into a tube containing buffer for Smart-seq2 single-cell RNA sequencing. **(B)** Example traces of cDNA library from electropherogram run on a Bioanalyzer. The upper panel shows a trace of a cDNA from 1 cell after the first PCR enrichment, and the lower panel shows a corresponding example of a final cDNA library. **(C)** Violin plots showing quality control (QC) metrics of sequenced cells: genes detected per cell (average=7931.05), number of reads per cell (average=1,4662.84), and percent of mitochondrial genes detected (average=2.4%) of all detected genes in a cell. Each dot represents one cell. **(D)** t-distributed stochastic neighbor embedding (*t-SNE*) plot of a transcriptome coming from sequenced POA neurons. Each dot on a graph represents one cell; color describes the Ca^{2+}-imaging category cell belonged to 2-APB insensitive responders: cells responding to temperature stimulus not affected by 2-APB; 2-APB sensitive responders: cells responding to temperature stimulus also affected by 2-APB; Non-responders: cells not responding to temperature stimulus.

I analyzed the transcriptome of the sequenced cells further and looked for specific genetic markers starting with the neuronal and glial genes (Figure 1.4.). As seen in Figure 1.4. A), the expression of neuronal markers *NeuN* (Neuronal nucleus protein), *Syt1* (synaptotagmin 1), *Tubb3* (β3-tubulin), *Syn2* (synapsin 2), *Vgat* (Vesicular GABA transporter), *Vglut2* (Vesicular glutamate transporter 2), Syn1 (synapsin1), *Gad1* (glutamate decarboxylase 1), *Gad2* (glutamate decarboxylase 2), and *Mapt* (Microtubule Associated Protein Tau) was detected in the transcriptome of sequenced cells. I observed the enrichment of neuronal genetic markers such as *Syt1, Vgat*, *Vglut2, Syn1, Gad1, and Gad2* in the cells belonging to the category of 2-APB sensitive responders in comparison to the other two categories. Figure 1.4. B) shows an expression of glia markers *Olig1* (Oligodendrocyte transcription factor1), *Olig2* (Oligodendrocyte transcription factor), *Mbp* (Myelin basic protein), and *GFAP* (Glial fibrillary acidic protein). I observed the enrichment of glial genetic markers in the categories of Non-responders and 2-APB insensitive responders in comparison to the category of 2-APB sensitive responders. In addition, the expression of *Trpm2* was quite low in all of the cells, and that can be due to several reasons. The scRNA-seq is a method prone to zero reads, and this is particularly biased towards the genes that are lowly expressed in the cells (Hicks et al., 2018). Indeed, Trpm2 was found to be expressed only at low levels in other scRNA-seq data as well (Moffitt et al., 2018).

From this unexpected result (Figure 1.4.) and t-SNE analysis (Figure 1.3. D), I concluded that the sequenced cells were not only neuronal but the same cells also displayed glial features and expressed glia genetic markers. The cells in the Ca^{2+}-imaging categories of Non-responders and 2-APB insensitive responders showed higher expression of glial markers and lower expression of certain neuronal markers. On the other hand, cells belonging to the category of 2-APB sensitive responders had higher expression of neuronal markers and a lower level of the glial ones.

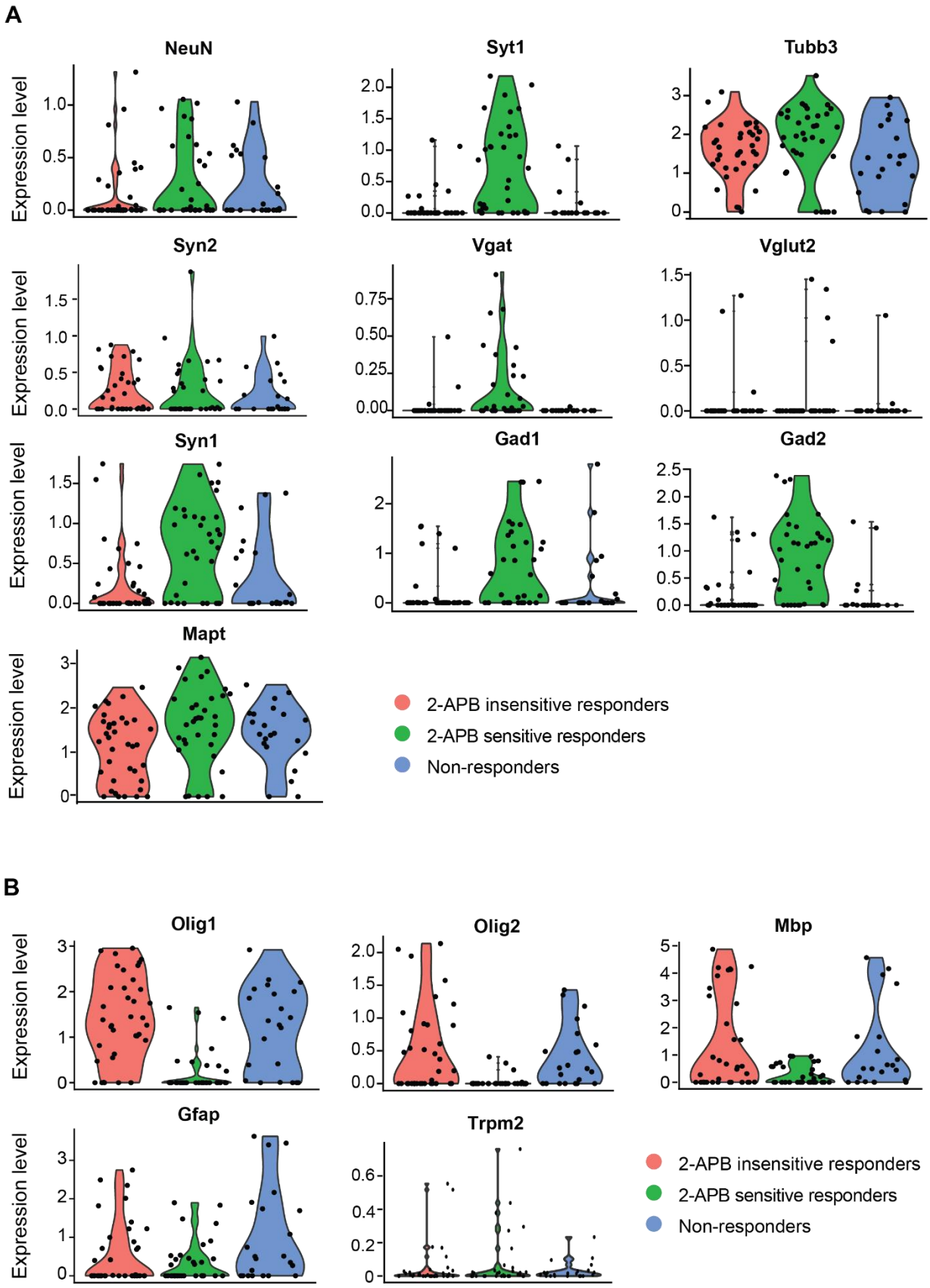
A
NeuN
Syt1
Tubb3
Syn2
Vgat
Vglut2
Syn1
Gad1
Gad2
Mapt
Expression level
2-APB insensitive responders
2-APB sensitive responders
Non-responders
B
Olig1
Olig2
Mbp
Gfap
Trpm2
Expression level
2-APB insensitive responders
2-APB sensitive responders
Non-responders

Figure 1.4. Expression of neuronal, glial markers, and Trpm2 in POA cultured P9 neurons revealed by scRNA-seq

(A) Expression of the neuronal markers *Neun* (Neuronal nuclear protein, *Rbfox3*), Syt1 (synaptotagmin 1), *Tubb3* (β3-tubulin), *Syn2* (synapsin 2), *Vgat* (Vesicular GABA transporter), *Vglut2* (Vesicular glutamate transporter 2), Syn1 (synapsin1), Gad1 (glutamate decarboxylase 1), Gad2 (glutamate decarboxylase 2), Mapt (Microtubule Associated Protein Tau). **(B)** Expression of the glial markers *Olig1* (Oligodendrocyte transcription factor1), *Olig2* (Oligodendrocyte transcription factor), *GFAP* (Glial fibrillary acidic protein), *Mbp* (Myelin basic protein); and *Trpm2* (Transient receptor potential cation channel, subfamily M, member). Y-axis depicts log2 scaled expression levels of the gene transcript. Each dot represents one single cell, and each violin plot on a single graph represents a group a cell belonged to in the Ca^{2+} imaging experiment. The legend shows color coding of the Ca^{2+} imaging groups: 2-APB insensitive responders: cells responding to temperature stimulus not affected by 2-APB; 2-APB sensitive responders: cells responding to temperature stimulus also affected by 2-APB; Non-responders: cells not responding to temperature stimulus.

To investigate this conclusion further and to assess whether culturing of neonatal POA cells resulted in a hybrid neuronal-glial phenotype, I did immunofluorescence staining in the primary cultures of P9 POA neurons prepared in the same manner as for the Ca^{2+}-imaging and scRNA-seq. I used antibodies raised against neuronal marker NeuN and oligodendrocyte marker OLIG2. Figure 1.5. A), shows an example field of view in one of the stained coverslips showing all 3 channels in grayscale and a merged image of 3 channels with DAPI in blue, NeuN in green, and OLIG2 in red. From the zoomed inset, one can appreciate that some cells co-express NeuN and OLIG2 simultaneously. Quantification of the proportion of the cells double-positive for NeuN and OLIG2 is shown in Figure 1.5. B). From 1084 cells that were positive for NeuN and DAPI, 484 cells (42.5 %) co-expressed NeuN and OLIG2 proteins. This result shows that 42.5% of the primary cultured cells, which express the neuronal marker NeuN, express oligodendrocyte (OLIG2) markers at the same time.

In addition, to assess whether native POA neurons at this stage of postnatal development also co-express neuronal and glial markers simultaneously, I did immunohistochemical staining against NeuN and OLIG2 in the POA tissue obtained from postnatal day 9 (P9) C57BL/6 mice. Figure 1.5. C) shows example stainings on frozen brain sections within the POA at bregma positions 0.26 mm and 0.14 mm according to the Paxions mouse brain atlas. From the merged images of DAPI in blue, NeuN in green, and Olig2 in red, one can appreciate that OLIG2 positive cells are found near the NeuN positive somas. The quantification of the overlap of the NeuN signal with the OLIG2 signal in tissue in Figure 1.5. D) showed that from 1361 quantified cells expressing NeuN and DAPI, 107 (14%) were also expressing the OLIG2 protein. However, the quantification very likely reflected technical limitations of the NIS elements software (NIKON) used for

the analysis. For cells that resided very close to each other, the software was unable to distinguish NeuN positive cells from olig2-positive neighboring cells that were thereby classified as double (Neun and Olig2) positive, while closer inspection by eye showed separation of the two fluorescent signals (Figure 1.5. C; 3x zoom in inset). Inspecting these cells quantified as double-positive led me to a conclusion that the overlapping cells for NeuN and OLIG2 were rare findings in the P9 POA tissue, very different from the POA cell cultures, where the most, if not all of the Olig2 signal overlapped with cells expressing NeuN.

From the immunofluorescence stainings, I concluded that the culturing of POA cells for 3 days induced artificial transcriptional changes, resulting in a hybrid glia-neuron phenotype which we captured by scRNA-seq. Although I expected to have some glial cells in the POA cultures, the existence of cells co-expressing both oligodendrocytes and NeuN is not a naturally occurring phenotype, as shown by staining in the tissue of the P9 C57BL/6 mice.

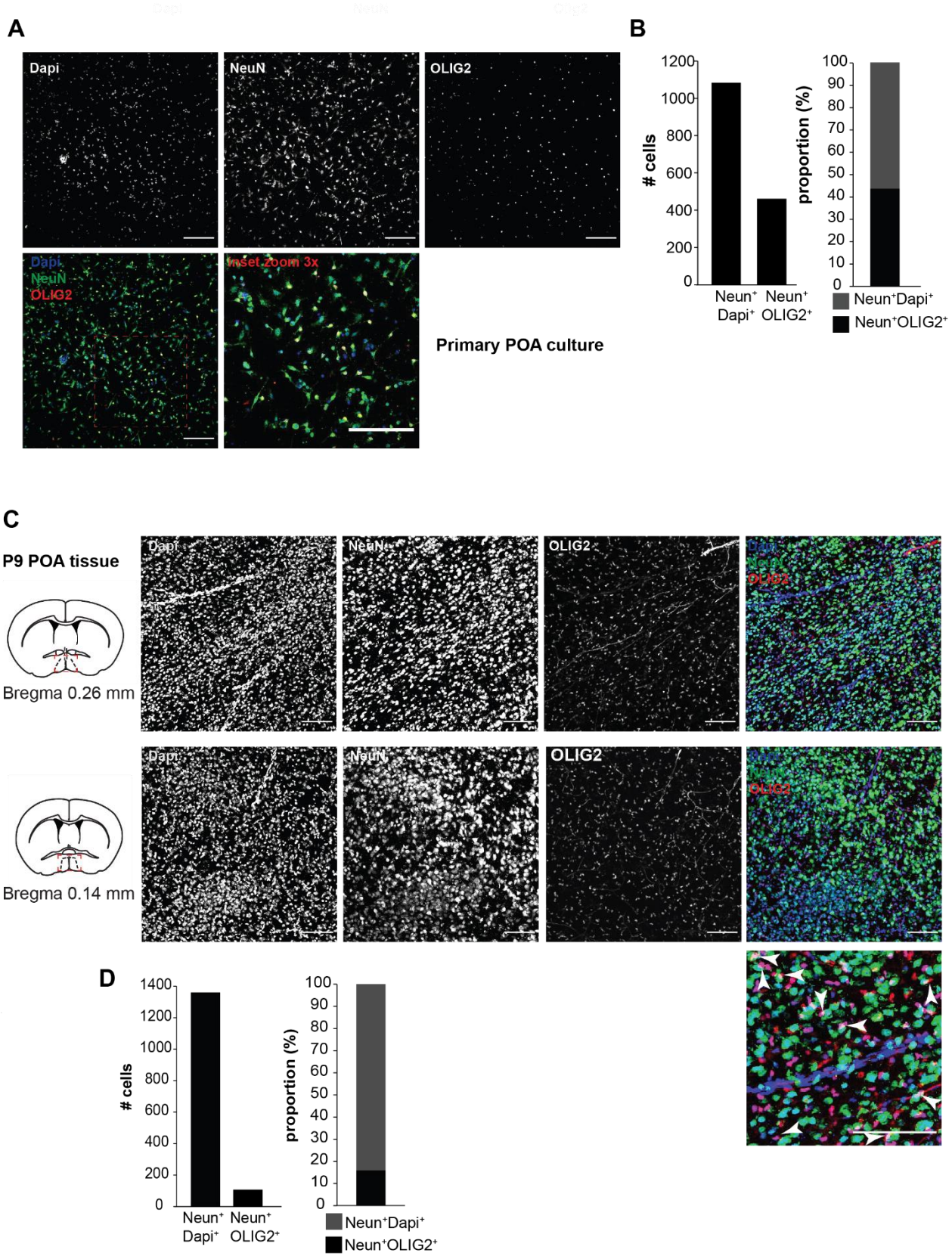
A
Dapi
NeuN
OLIG2
Dapi
NeuN
OLIG2
Inset zoom 3x
Primary POA culture
B
cells
1200
1000
800
600
400
200
0
Neun+ Dapi+
Neun+ OLIG2+
proportion (%)
100
90
80
70
60
50
40
30
20
10
0
Neun+Dapi+
Neun+OLIG2+
C
P9 POA tissue
Bregma 0.26 mm
Bregma 0.14 mm
Dapi
NeuN
OLIG2
D
cells
1400
1200
1000
800
600
400
200
0
Neun+ Dapi+
Neun+ OLIG2+
proportion (%)
100
90
80
70
60
50
40
30
20
10
0
Neun+Dapi+
Neun+OLIG2+

Figure 1.5. Immunofluorescence and immunohistochemistry against NeuN and Olig 2 in P9 primary cell culture and P9 POA tissue.

(A) An Immunofluorescence on the primary neuronal culture from POA of P9 pups. Images are an example of the field of view from one coverslip with cultured cells. Staining was done with antibodies raised against NeuN and OLIG2 and counterstained with Dapi. The upper panels show grayscale pictures of individual channels belonging to an example coverslip, taken with a 10x objective. In the lower panel is an image of all 3 channels merged; Dapi in blue, NeuN in green, and OLIG2 in red. The right panel represents a 3x zoom-in area of the same image (red square). The scale bar is 200 µm. **(B)** Quantification of Neun and OLIG2 double-positive cells ($NeuN^+$ $OLIG2^+$). On the left graph plotted are the total number of Neun cells (DAPIpositive) and the total number of $NeuN^+$ OLIG2 2^+ cells. On the right graph plotted are proportions of $NeuN^+$ $OLIG2^+$ of all Neun cells (dapi positive). **(C)** Immunohistochemistry of the POA sections from the P9 mice. Staining was done with antibodies raised against NeuN and $OLIG2^+$ and counterstained with Dapi. Both panels show an example of the IHC in two sections of the P9 mouse at the bregma positions 0.26 mm and 0.14 mm according to Paxinos mouse brain atlas as depicted in a cartoon containing POA (red dashed square on the section), where the following pictures are taken at. The images of each channel: Dapi, NeuN, and OLIG2, and a merged image of all 3 signals Dapi in blue, NeuN in green, and OLIG2 in red are shown. Images are taken with 20x objective. The scale bar represents 100 µm. The 3x zoom-inset is shown below to depict the cells which are quantified as NeuN and OLIG2 co-expressing arrowheads sharing that OLIG2 signals are in the vicinity of NeuN soma. **(D)** Quantification of Neun and OLIG2 double-positive cells ($NeuN^+$ $OLIG2^+$). On the left graph plotted are the total number of Neun cells (dapi positive) and a total number of $NeuN^+$ OLIG2 $^+$ cells. On the right graph plotted are proportions of $NeuN^+OLIG2^+$ of all Neun cells (dapi positive).

In 2018. Moffit and colleagues (Moffitt et al., 2018) performed scRNA-seq of more 30 000 adult mouse POA cells which identified about 70 neuronal populations according to their transcriptome and spatial organization. The broad categorization of this scRNA-seq POA atlas according to the genetic markers they expressed revealed groups of inhibitory and excitatory neurons, microglia, astrocytes, immature oligodendrocytes, and mature oligodendrocytes, ependymal cells, endothelial cells, fibroblasts, macrophages, and mural cells. In addition to the broad categorization, the subdivision of the inhibitory and excitatory neuronal clusters revealed 43 and 23 subgroups of neuronal cell types.

The availability of the molecular POA atlas motivated me to investigate if the cell types revealed by Moffit and colleagues could be used to help categorize the cultured POA cells for which I had obtained and analyzed the transcriptome. To do this within the Seurat software platform I performed integration of scRNA-seq data (Stuart et al., 2019)from our primary neural POA cultures with the Moffit scRNA-seq data set which allowed quantification of the cell types present in both data sets (Figure 1.6.). Figure 1.6. A) shows a visualization of the integration via t-SNE graphs: the left one shows the Moffit cell types to which the sequenced cells from POA primary cell culture were mapped, and the right plot shows the cell

categories based on Ca^{2+}- imaging. The broad Moffit groups to which sequenced cells mapped were newly formed oligodendrocytes, immature oligodendrocytes, inhibitory and excitatory neurons, ependymal cells, microglia, mural cells, fibroblasts, and macrophages. I quantified how many cells from each Ca^{2+}-imaging category mapped to each of the Moffit broad groups and as well to how many categories they mapped to (Figure 1.6. B). This quantification once again revealed the transcriptomic heterogeneity of the primary POA neural culture we used as it showed that the cells from each of the Ca^{2+}- imaging categories mapped to several different broad groups from the POA scRNA-seq atlas. For example, 37 2-APB-insensitive responders mapped to seven broad groups of which 12 cells mapped to immature oligodendrocytes, 10 cells to ependymal cell type**,** 8 to newly formed oligodendrocytes, 3 cells mapped to fibroblasts, and 1 to macrophages, as only 3 cells mapped to excitatory and inhibitory neuronal cell types. Seven of 22 temperature non-responders mapped to ependymal cells, 8 to immature oligodendrocytes, and only 2 cells to excitatory neurons, the rest were divided among newly formed oligodendrocytes, fibroblasts, macrophages, and mural cells. 2-APB sensitive responders, which were 34 in the scRNA-seq data set, mapped to 6 broad cell types from the Moffit data set with 3 cells mapped to excitatory neurons, 16 cells to inhibitory neurons, 3 cells mapped to fibroblasts, 5 cells mapped to immature oligodendrocytes, 3 to macrophages, and 4 cells to microglia. Once again, this analysis showed that the 2-APB sensitive responders are the category most likely closest to the neuronal cell type as the majority of the cells in the category were mapped to neuronal cell types (19/35).

Further on, mapping to Moffit subgroups (Figure 1.6. C) revealed that the mapping of the cells from the 2-APB sensitive responder category was divided into 3 excitatory and 4 inhibitory subgroups elucidating even further their transcriptome. From this analysis, I could learn about the identity of neuronal cell types in the POA of primary neural cultures from P9 such as that inhibitory neurons express galanin (*Gal*) and neuropeptide Y (*Npy*) as they map to inhibitory clusters i22 and i25 from Moffit data set.

The overarching goal of the project was to find molecular markers of the WSNs of the POA. I aimed to achieve this goal by scRNA-seq of 3 functional groups differentiated by Ca^{2+}-imaging of POA primary neural culture while stimulating them with a temperature of 45 ˚C and TRPM2 blocker 2-APB. These were the cells that do not respond to temperature (Non-responders), the cells that respond to temperature and whose response is not abolished by the 2-APB (2-APB insensitive responders), and cells that respond to temperature and whose sensitivity was abolished by 2-APB (2-APB sensitive responders). However, the primary cell culture from the POA, which I used to categorize POA neurons by temperature sensitivity, turned out to be a mixture of different cell types. The biggest problem here is that it turned out that 2-APB sensitive responders are in the majority of neurons, while the rest of the cells were, based on

transcriptional analysis, non-neuronal cells, which makes it difficult to compare their transcriptomic differences in terms of temperature sensitivity. Therefore, the differential gene expression analysis between 3 functional groups did not yield any neuronal molecular markers explaining the temperature sensitivity but merely cell type differences (data not shown). Although it was expected to have some glial cells in the culture I used, I hypothesize that culturing cells for 3 days induced additional transcriptional changes which I captured by scRNA-seq.

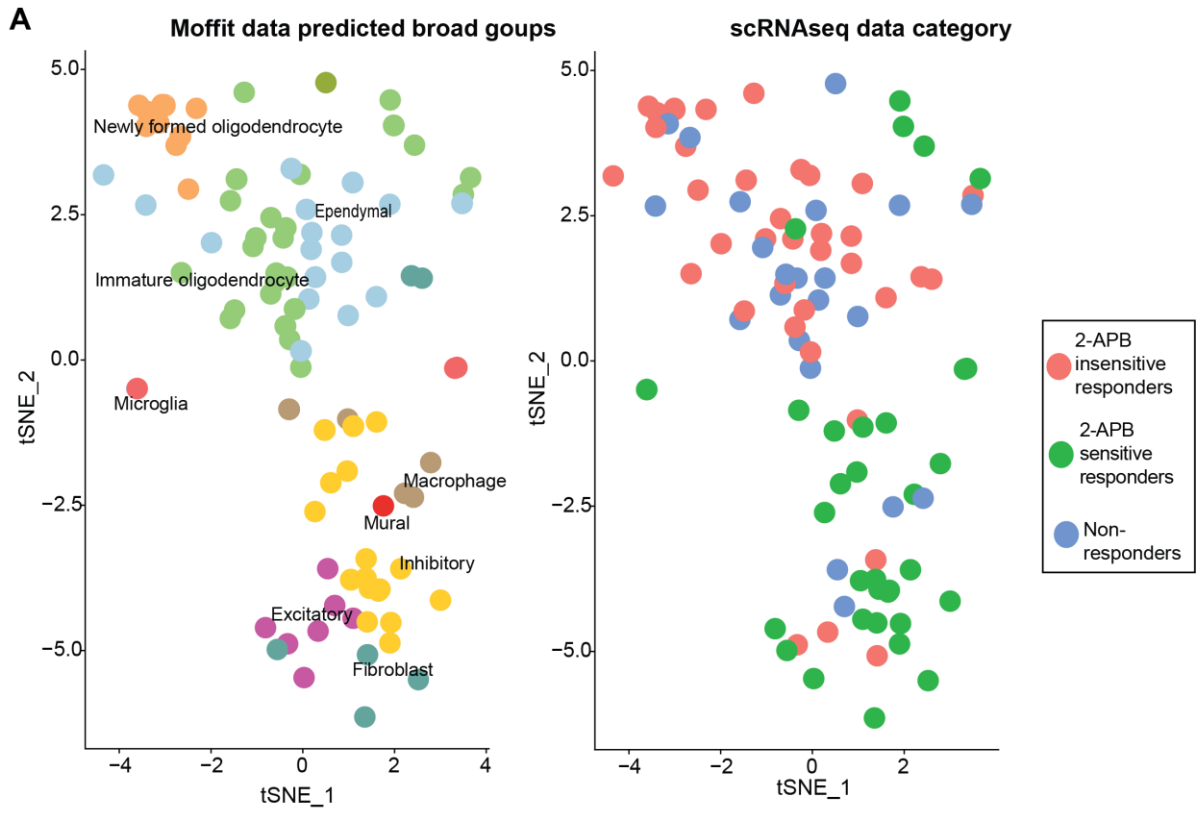
A
Moffit data predicted broad goups
scRNAseq data category
Newly formed oligodendrocyte
Ependymal
Immature oligodendrocyte
Microglia
Macrophage
Mural
Inhibitory
Excitatory
Fibroblast
tSNE_1
tSNE_2
2-APB insensitive responders
2-APB sensitive responders
Non-responders

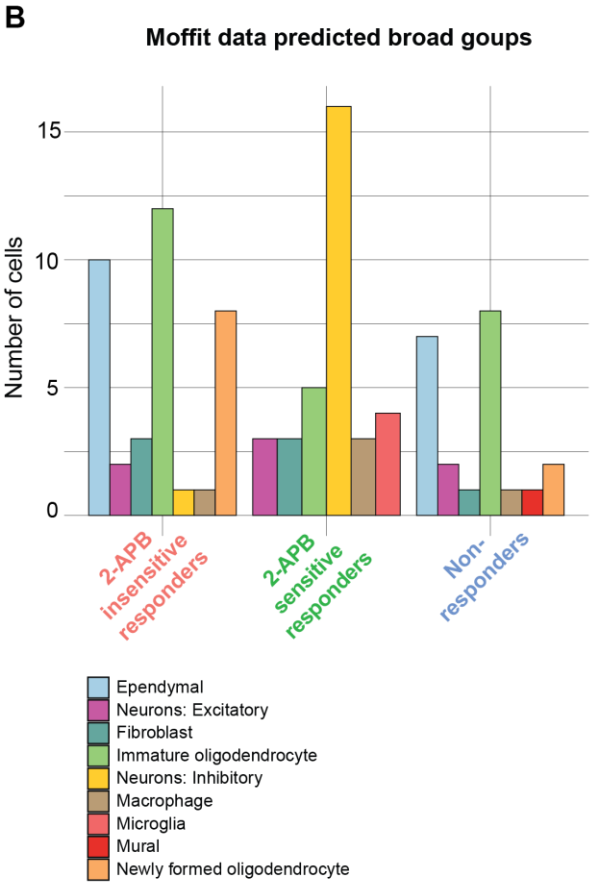
B
Moffit data predicted broad goups
Number of cells
2-APB insensitive responders
2-APB sensitive responders
Non-responders
Ependymal
Neurons: Excitatory
Fibroblast
Immature oligodendrocyte
Neurons: Inhibitory
Macrophage
Microglia
Mural
Newly formed oligodendrocyte

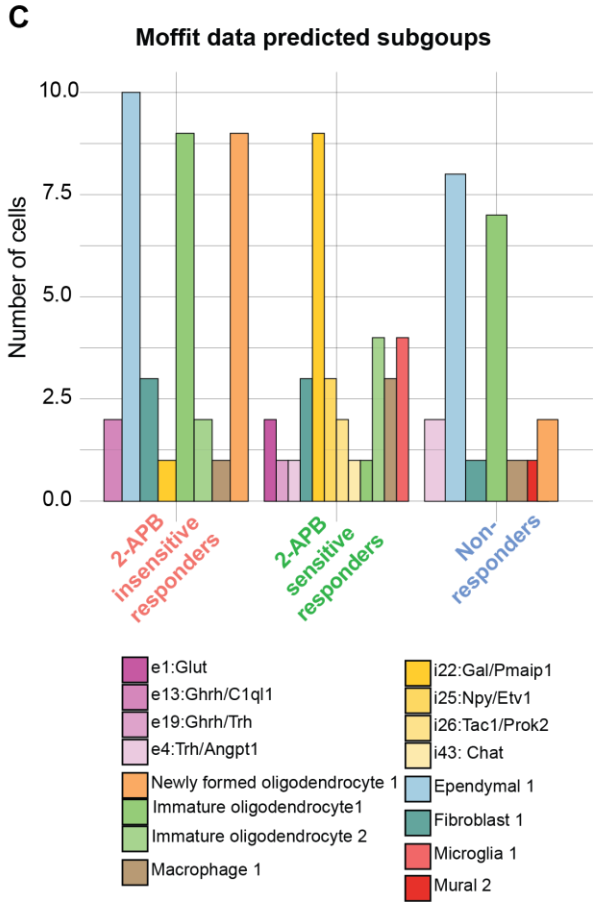
C
Moffit data predicted subgoups
Number of cells
2-APB insensitive responders
2-APB sensitive responders
Non-responders
e1:Glut
e13:Ghrh/C1ql1
e19:Ghrh/Trh
e4:Trh/Angpt1
Newly formed oligodendrocyte 1
Immature oligodendrocyte1
Immature oligodendrocyte 2
Macrophage 1
i22:Gal/Pmaip1
i25:Npy/Etv1
i26:Tac1/Prok2
i43: Chat
Ependymal 1
Fibroblast 1
Microglia 1
Mural 2

Figure 1.6. Cell type mapping of P9 POA primary cells to the scRNA-seq data of the adult POA from the Moffit data set.

(A) Cell type mapping was achieved through the integration (Butler et al., 2018) of the scRNA-seq data of P9 POA primary cell culture to the scRNA-seq data of the adult POA from Moffit et al. (Moffitt et al., 2018). Visualization is achieved with tSNE plots. The left tSNE plot shows broad cell types from Moffit et al. data to which P9 POA sequenced cells are mapped. The right graph presents a tSNE of cell groups in the Ca^{2+} imaging groups: 2-APB insensitive responders: cells responding to temperature stimulus not affected by 2-APB; 2-APB sensitive responders: cells responding to temperature stimulus also affected by 2-APB; Non-responders: cells not responding to temperature stimulus. The legend below the histogram shows the color-coding of the broad cell categories from the single-cell POA atlas. The bar graph in **(B)** presents quantification of the number of the cells from the scRNA-seq data set mapped to Moffit broad cell types, and the bar graph in **(C)** presents quantification of the number of the cells from the scRNA-seq data set mapped to Moffit subgroups cell types. The legend below the histogram shows the names and the main marker genes of the cell type subgroup from the single-cell POA atlas found by Moffit scRNA-seq data analysis.

3.3. PATCH-SEQ METHOD AS AN ALTERNATIVE TO THE PRIMARY NEURONAL CULTURE FOR THE SEARCH OF WSNs' GENETIC MARKERS

The recently emerged tool to access the cell population's transcriptome, potentially useful for the search for the markers of the WSNs, is the Patch-seq method which combines analysis of neurons' transcriptome and electrophysiology (Cadwell et al., 2016; Fuzik et al., 2016). The advantage of Patch-seq is the possibility to use acute brain slices of adult animals for the measurement of action potentials, and other electrophysiological parameters, while as well obtaining the material for the transcriptome of single cells. With this method, I could measure the warm-sensitivity of the neurons via classical criteria of AP firing frequency increase during warming (Boulant & Dean, 1986). I have decided to test if we could apply this method to our search for WSNs molecular markers. (Figure 1.7.).

This pilot Patch-seq experiment was a collaboration with a colleague in the lab Dr. Wojciech Ambroziak who performed ephys recordings and collection of the cell material, and I prepared the materials for the sequencing and cDNA libraries.

In the experiments we have used acute slices from Vgat-Cre/HTB mouse line where inhibitory neurons ($Vgat^+$) are marked by green fluorescent protein (GFP) fused with histone H2B (HTB). Both, $Vgat^+$ (GFP+) and the GFP^- cells were patched in the whole-cell mode, APs were recorded for ≈2 minutes, and cellular content was then collected with the recording electrode by applying negative pressure, and used for the Smart-seq2 (Picelli et al., 2014) preparation of the cDNA libraries for the scRNA-seq (Figure 1.7. A). We hypothesized that transcriptomic analysis would show enrichment for *Vgat* and other genetic markers

of inhibitory neurons in GFP^+ patched cells. Confirming this hypothesis would be proof of the principle that with the Patch-seq approach we could obtain genetic markers of WSNs. In addition to patched cells, the negative control should be collected in every patching experiment to account for possible contamination coming from guiding the recording pipette through the layers of cells in the tissue. The internal solution in the recording pipette for the negative control contained the same ingredients as for patched sample collection, the pipette is immersed into the tissue, retracted, and the internal solution ejected into the tube containing Smart-seq2 buffer. Two types of negative control were performed: one in which after immersion to tissue, pressure at the pipette tip was not released, and the other where pressure was released to mimic as close as possible the sample collection (Cadwell et al., 2017; B. R. Lee et al., 2021).

Finally, I processed the collected samples with the Smart-seq2 protocol (Picelli et al., 2014), 75% of which yielded good quality cDNA (Figure 1.7. B; upper panel) determined with a Bioanalyzer electropherogram (Agilent Technologies, 2009). 36 patched samples, which yielded good quality cDNA, were sequenced (16 fluorescent and 11 non-fluorescent and 9 negative controls) at the Genomics Core facility (EMBL Heidelberg) with the NextSeq Mid Illumina sequencer with single-end 150 bp readout, yielding > 2 million reads per sample. Negative controls, which yielded cDNA (roughly 10% of the total negative controls) (Figure 1.7. B; middle panel), were included because their transcriptome could serve as a readout of potential contamination in our patched samples. Negative controls not yielding any cDNA were the goal to which we strived, and were not included in the sequencing(Figure 1.7. B; bottom panel). After the first steps of QC of the sequencing reads, I did the cell QC (Figure 1.7. C) in Seurat (Butler et al., 2018; Stuart et al., 2019). Six cells did not pass the quality control according to the number of genes per cell (<2000), counts per cell, and percent of mitochondrial counts (>10%), all six were negative controls. To explore the transcriptome and see if the *Vgat*$^+$ (GFP^+) patched cells are enriched in *Vgat* transcripts as expected, I looked into the individual gene expression levels. In Figure 1.7. D) plotted is expression level of *Vgat* and *Vglut2* genes for which we hypothesized that would be showing enriched expression levels in GFP^+ (inhibitory) and GFP^- (excitatory) patch-clamp recorded cells, respectively. From the violin plots, one can see that detection of these broad neuronal markers is quite low, whereas on the other hand, *Gad1* and *Gad2* inhibitory neuronal markers, were expressed on a higher level in *Vgat*$^+$ than in *Vgat*$^-$ cells.

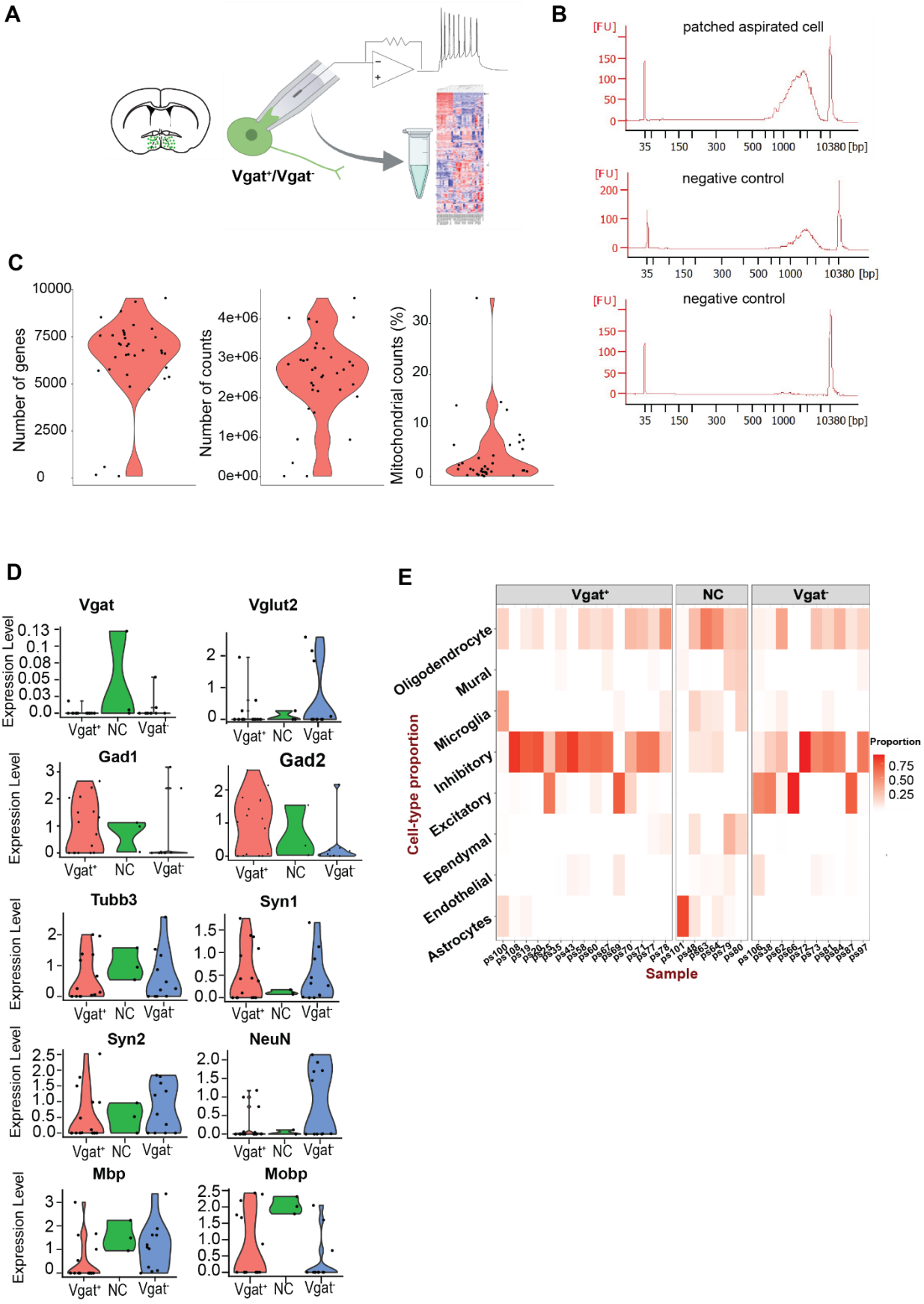
A
Vgat+/Vgat-
B
patched aspirated cell
negative control
negative control
[FU]
35 150 300 500 1000 10380 [bp]
C
Number of genes
Number of counts
Mitochondrial counts (%)
D
Vgat
Vglut2
Gad1
Gad2
Tubb3
Syn1
Syn2
NeuN
Mbp
Mobp
Expression Level
Vgat+ NC Vgat-
E
Vgat+
NC
Vgat-
Oligodendrocyte
Mural
Microglia
Inhibitory
Excitatory
Ependymal
Endothelial
Astrocytes
Cell-type proportion
Proportion
0.75
0.50
0.25
Sample

Figure 1.7. Patch-seq pilot experiment with the Vgat POA neurons.
(A) Scheme of the experiments: 3 acute brain slices were obtained and the patch-clamp recordings were performed in the Vgat^{+} (GFP expressing) neurons. After the recording of action potentials, cell content was aspirated into the recording pipette. The sample was ejected into the tube containing buffer for the Smart-seq2 single-cell RNA sequencing. **(B)** Example traces of cDNA library from electropherogram run on a Bioanalyzer. The upper panel shows a trace of a cDNA from 1 cell after the first PCR enrichment, the middle electropherogram shows an example of the negative control yielding cDNA, and the bottom electropherogram shows an example of the negative control not yielding the cDNA. Negative controls were obtained by immersing the recoding pipette into the acute brain slice without a cell recording or intentional aspiration of the material. **(C)** Violin plots showing quality control (QC) metrics of sequenced cells: genes detected per cell, number of counts per cell, percent of mitochondrial genes detected in a cell. **(D)** Violin plots showing the expression of neuronal markers *Slc32a1* (Vgat), *Slc17a6* (Vglut2), *Gad1* (Glutamate decarboxylase 1), *Gad2* (Glutamate decarboxylase 2), *Tubb3* (β3-tubulin), *Syn1* (synapsin1), *Syn2* (synapsin 2), Neun (Neuronal nuclear protein), and the expression of glial markers *Mbp* (Myelin basic protein) and *Mobp* (Myelin Associated Oligodendrocyte Basic Protein). Y-axis depicts log2 scaled expression levels of the gene transcript. Each dot represents one single cell, and each violin plot on a single graph represents a group a cell belonged to in the patch-seq experiment Vgat^{+}(GFP), NC (negative control), and Vgat^{-} cells. **(E)** The heatmap represents the proportions of the genes in each of the patch-seq samples corresponding to the genes in the Moffit data broad cell types. Columns present cells, and rows represent the Moffit broad cell type. The cell modeling presented in the heat map is work done in collaboration with Nelson Johansen, UCS Davis (Johansen & Quon, 2022).

The concern about contamination in patch-seq samples was confirmed by the expression level of glial genes in the transcriptome of patched neurons coming from other cell type's mRNAs, particularly the ones coming from oligodendrocytes such as myelin-associated oligodendrocyte basic protein (*Mobp*) and Myelin basic protein (*Mbp*) (Figure 1.7. D). I was motivated to assess further the level of contamination in the pilot Patch-seq data. Currently, the best way to address the amount of contamination in Patch-seq data is to have access to the RNAseq transcriptome cell atlas from the region from which the Patch-seq data is obtained. As described above, Moffit et al. have performed scRNA-seq from more than 30 000 POA cells recovering different cell types in the region (Moffitt et al., 2018). From this cell atlas, it is possible to model cell types in the region of interest by using genes recovered by scRNAseq (Johansen & Quon, 2022). The heatmap in Figure 1.7. E), shows the proportion by which each cell in our Patch-seq pilot data set is modeled by one of the cell types from POA scRNA-seq data (Oligodendrocyte, Mural, Microglia, Inhibitory neurons, Excitatory neurons, Ependymal, Endothelial cells, and Astrocytes). From this result, I conclude that most of the contamination in the obtained patch-seq pilot data set comes from the oligodendrocyte cell type. Quantification of the modeling showed that 25% of patch-clamp recorded cells should be

removed from further analysis because these express a larger proportion of transcripts coming from glial cell types than the transcripts coming from neurons.

4. DISCUSSION

4.1. RESEARCH BACKGROUND AND SUMMARY OF KEY FINDINGS

Body temperature is a dynamic homeostatic property, tightly regulated by the autonomic nervous system. How the brain coordinates the maintenance of the body temperature within a narrow range of 37 ˚C, a condition that is needed for all enzymatic reactions and cellular processes to function properly, remains unclear (Siemens & Kamm, 2018). It has been decades since the POA (preoptic area of the hypothalamus) is defined as a key CNS structure responsible for thermoregulation by lesion studies or direct heating and cooling of the region. Intrinsically temperature-sensitive neurons have been found in this brain region (Boulant & Dean, 1986; Nakayama et al., 1961, 1963). It has been shown that 30% of neurons recorded in acute brain slices are warm sensitive which is reflected in these neurons increasing AP firing frequency while direct warming is applied (Boulant, 2000; Griffin & Boulant, 1995; Kelso et al., 1982; Kelso & Boulant, 1982). These WSNs are activated by peripheral warming as well, which makes them plausible integrators of peripheral and central temperature information (Boulant & Hardy, 1974).

The lack of knowledge about the molecular composition of the POA warm-sensitive neurons presents a hurdle in elucidating how the POA acts as a body thermostat. Knowing molecules that identify them would make it possible to investigate further their connectivity to other brain regions involved in thermoregulatory processes. Therefore, the goal of this part of the thesis was to try to answer the questions of whether POA WSNs express specific genetic markers and which genes those are.

The approach I used to learn about the POA WSNs transcriptome was based on the work of Song et al. Similarly as in that work I used the primary POA cell culture but this time with a week older, 9 days old C57BL/6 N mice (P9), and performed calcium imaging while applying a temperature stimulus of 45 ˚C in the presence and the absence of the TRPM2 antagonist, 2-Aminoethoxydiphenyl borate (2-APB). I identified 3 types of cells according to their temperature sensitivity: temperature non-responding cells (Non-responders) temperature-sensitive cells (2-APB insensitive responders), and cells that responded more strongly to 45 ˚C stimuli but whose response was abolished by 2-APB (2-APB sensitive responders) (Figure 1.2. E).

Furthermore, I identified by Ca2+-imaging, hand-picked, and performed scRNA sequencing of Non-responder cells; (n=22), 2-APB insensitive responders (n=37), and 2-APB sensitive responders (n=34) to compare their transcriptome and find markers of WSNs. Analysis of the scRNA-seq data pointed to the limitations of the P9 cell culture used (Figure 1.4. and Figure 1.6.). The majority of the temperature Non-responders and 2-APB-insensitive temperature-sensitive cells sequenced expressed glial marker genes

together with neuronal markers, whereas 2-APB sensitive responders expressed more neuronal markers (Figure 1.4.). In-silico mapping of the POA neural culture transcriptome to the POA scRNA-seq atlas has confirmed that collected cells are a mixture of different cell types (Figure 1.6.) with 2-APB temperature-sensitive responders mapping to inhibitory neurons. In addition, immunofluorescence staining for neuronal (NeuN) and oligodendrocyte (OLIG2) markers showed that almost half of the cells in the POA neural culture co-express these markers on the protein levels as well (Figure 1.5. A and B). I did not find this combination of proteins expressed in the same proportion in the POA P9 brain sections used for the immunohistochemistry (Figure 1.5. C and D). Therefore, I concluded that the genetic heterogeneity of the sequenced cell categories was too large and that putative WSNs' molecular markers identified from cultured neurons would be ambiguous.

The recently emerging tool to access certain cell population transcriptome, the Patch-seq method, which combines analysis of neurons' transcriptome, electrophysiology, and morphology seemed like a feasible alternative to the cultured cells system for a search of markers of WSNs (Cadwell et al., 2016; Földy et al., 2016; Fuzik et al., 2016). Together with a colleague in the lab, I performed a pilot experiment using VgatCre/HTB mouse line in which my colleague patched and obtained cellular material from the GFP^+ (*Vgat*$^+$) and GFP^- (*Vgat*$^-$) cells, after which I processed the samples for the RNAseq and analyzed the data we obtained (Figure 1.7.). Patch-seq method turned to present its hurdles, such as higher drop-out rates of detected genes, as I also observed in the lack of reads for *Vgat* and *Vglut2* (Figure 1.7. D). Additionally, I detected the contamination of the samples with the mRNA from other cell types due to the leading of the recording electrode throughout the thick layer of tissue. Since we had access to the scRNA-seq atlas of the POA brain region (Moffitt et al., 2018), I could assess the contamination source and quantify it (Johansen & Quon, 2022). The 25% of the patched samples should be from the further analysis as they expressed reads from other cell types and not only neurons (Figure 1.7. E). This has made me question the feasibility of the patch-seq method for obtaining the transcriptome of WSNs from adult tissue.

4.2. HOW GOOD IS THE PRIMARY POA NEURONAL CULTURE FOR THE SEARCH FOR THE GENETIC MARKER OF POA WSNs?

The reason to use primary cultures from older animals, in comparison to the previous work in our lab, was the fact that the TRPM2 KO animals still had temperature-sensitive neurons present, as shown by Ca2+-imaging in adult POA acute slices (Song et al., 2016). The Ca2+-imaging results I obtained from the experiments with P9 POA cell culture (Figure 1.2.) have closely recapitulated the findings of Song et al. In that work the criteria for determining WSNs were set via calcium response of human embryonic kidney–

293 cells (HEK 293) loaded with the ratiometric fluorescent calcium indicator fura-2. If a cell responded above the 5-time standard deviation of mean HEK 293 cells response to 45˚C, it was considered warm sensitive. They found that about 16.3 % of cells in POA culture from P2 mice responded to 45˚C stimulus above this criterion. In my Ca2+-imaging recordings, I used a different calcium indicator, Cal520, which is unlike fura-2, a single-wavelength indicator (Tada et al., 2014). In P9 POA cell culture, about 15% of cells were temperature-sensitive, and the temperature response of about 98% percent of those was blocked by TRPM2 antagonist 2-APB. The cell was characterized as a WSN if it was above the cutoff value determined by the mean of maximum amplitude of cell response to 45˚C stimulus with 2-APB (mean(3*SD(max(ΔF/F (45˚C+2-APB))))) from all the coverslips in one experiment. The rest of the cells in the primary POA culture were temperature-insensitive (Figure 1.2. E). This finding was in concordance with that of Song and colleagues, but as well with the other studies using POA neural cultures (Tabarean et al., 2005) or dissociated POA neurons (Cai et al., 2012) to test temperature sensitivity.

In the Ca^{2+}-imaging I performed, I found as well cells responding to temperature but insensitive to 2-APB (Figure 1.2.D). These cells were not detected in the Ca2+ imaging performed on P2 cultures with the Fura2 calcium indicator, as the temperature response of all cells seems to be abolished by 2-APB (Song et al., 2016). The Cal-520 fluorescent indicator has higher dynamics and calcium sensitivity than the fura-2 indicator (Lock et al., 2015). Since APB-sensitive temperature responders respond to 45˚C temperature stimulus with lower calcium levels than the 2-APB-sensitive temperature responders (Figure 1.2. D), as projected from ΔF/F calculation, it could be that these cells went undetected in calcium imaging with Fura-2. However, it might as well be that this cell category was not present in the P2 POA primary cell cultures, and due to neuronal maturation, the cells in the P9 POA culture have started to express other ion channels sensitive to heat apart from TRPM2. There are many examples of increased expression of certain ion channels or enhancement of their functionalities during early postnatal development such as HCN channels and TRPM4 in mouse hippocampal pyramidal neurons or Kcnq2 in the hippocampus, which increase their expression during postnatal development (Riquelme et al., 2021; Vasilyev & Barish, 2002; Weber et al., 2006).

The goal of the project was to find markers of WSNs via scRNA-sequencing of temperature-sensitive neurons from the primary POA neural culture. I obtained the transcriptome data of 93 cells from which 22 Non-responders, 37 2-APB insensitive responders, and 34 2-APB sensitive responders. First, the t-SNE graph-based clustering analyzed according to the principal component genes, did not show a clear separation between the 3 groups of sequenced cells (Figure 1.2. D). There was however the inclination of 2-APB sensitive cells to separate from the rest. The detailed look into the expression of neuronal and glial-

specific genetic markers showed that these cells do express neuronal markers more strongly than the other 2 cell categories (Figure 1.4. A). On the contrary, Non-responders and, 2-APB insensitive responders have expressed glial markers in a higher manner than the 2-APB sensitive responders (Figure 1.4. B). This result has made me suspect the nature of the transcriptome coming from the primary neural POA culture as it seemed that many cells are expressing neuronal and glia markers at the same time. I confirmed this finding by immunofluorescence staining of oligodendrocyte and neuronal markers, OLIG2 and NeuN, in POA primary cultures (Figure 1.5. A). These markers colocalized in 42% of cultured cells, a finding three times less occurring in the P9 POA tissue (Figure 1.5. B). Looking more carefully into NeuN and OLIG2 overlapping cells in the P9 POA tissue, I observed some NeuN positive cells that had an OLIG2 expressing nucleus near their soma (Figure 1.5. C; 3x zoom-in inset). It was described in the work of others that oligodendrocytes from satellite, perineuronal cells near neuronal soma (Valério-Gomes et al., 2018). In the cell counting method I used in NIS elements software, it was difficult to segment the cells standing in close vicinity to one another. Therefore, I expect that the percentage of NeuN and OLIG2 double-positive cells (ones expressing both proteins) in the P9 tissue should be even less than 14%.

In addition, mapping of the POA neural culture transcriptome to the larger scRNA-seq data set of the POA (Moffitt et al., 2018), has revealed a more detailed transcriptomic identity of the cell categories I found with the Ca^{2+}-imaging (Figure 1.6.). It confirmed the finding that the cells presented mixed cell types with the 2-APB sensitive responders mainly mapping to inhibitory neurons and the other two categories to oligodendrocytes and ependymal cells.

Interestingly, although the cultured cells turned out to be a mix of cell types, the category that was most temperature-sensitive is recapitulating the literature knowledge on the nature of the WSNs. Some papers where WSNs were identified *in vitro*, defined them as GABAergic (Eberwine & Bartfai, 2011; Lundius et al., 2010), and in current models of thermoregulation their output towards heat conserving mechanisms are thought to be inhibitory (Madden & Morrison, 2019; S. Morrison F. & Nakamura, K, 2011). However, with novel literature, the thermoregulatory model is changing, as several populations residing in the POA and involved in thermoregulation are glutamatergic (Machado & Saper, 2022).

In addition, the comparison of two independent RNAseq data sets poses certain challenges, such as technical variabilities, animals, or cell lines that are used for the experiments. However, computation of the common “anchors” between two data sets has been possible with the Seurat tool (Stuart et al., 2019), where the anchors represent cell pairs in which the similarity between two cells is evaluated by the overlap in their local shared nearest neighbor (SNN).

To the best of my knowledge, the primary neural culture from the POA was until now never characterized in the detail on the transcriptome level. There are, however, few examples where comparisons have been made between the *in vitro* neuronal models used in research and the ex vivo tissue. For example, a transcriptomic analysis of the study of primary hippocampal cultures cells sequenced right after dissociation from the tissue showed about 1000 up or down-regulated genes between two conditions, and it revealed several changed biological pathways (King et al., 2021). Furthermore, it has been shown that even a standard procedure such as medium change can cause dramatic changes in the transcriptome profiles of the primary neurons by inducing up and down-regulation of thousands of genes (Rubiolo et al., 2016). Additionally, it has been shown that the space and volumes of the cell culturing devices, such as microfluidics chips, affect the cell transcriptome (Middelkamp et al., 2021). The human-induced pluripotent stem cell-derived neurons (hiPSCs) and other cell types were evaluated when cultured on microfluidic chips, and it has been found that those cells exhibit increased expression of genes related to cell adhesion, tissue migration, and activation of metabolic processes in comparison to cells cultured on the large cell-plates. Another interesting example of culturing conditions affecting the cell transcriptome is the presence of oligodendrocytes within the hippocampal neuronal culture which was found to affect the neuronal activity of GABAergic neurons such as synaptic activity and action potential firing (Mazuir et al., 2021). Processes linked to these changes included synapse assembly, action potential generation, and transmembrane ion transport.

All the above-mentioned provide examples of how culturing conditions can impact the native transcriptome of the cultured cell types. In my literature review, I was not able to find concrete examples where co-expression of NeuN and Olig2 is measured in postnatal neuronal cultures, and thus I was not able to relate my 3-day POA culture results to any finding reported in the literature. It could very well be that this went undetected in other rodents' postnatal cells. Some papers, however, have found Olig2 to co-localize with NeuN in the brains of a human fetus (Jakovcevski, 2005), and others have found Olig2 expression in immature neuronal and glial progenitors of the embryonic spinal cord which give rise to motor neurons (Takebayashi et al., 2000). Moreover, it was found that Olig2+ cells give rise to inhibitory and excitatory neurons (reviewed in (Szu et al., 2021). This leads me to the conclusion the Olig2 transcription factor is participating in the definition of neural cell type in early embryonic development.

In addition, the trituration of the brain tissue can be less favorable for the neurons' survival than for the glial cells' survival, since neuronal neurites are damaged during dissociation. In addition, glial cells keep their proliferative potentials, as neurons do not. Therefore, some researchers use antimitotic drugs to prevent glial cell proliferation in the culture systems (Mao & Wang, 2001; Seibenhener & Wooten,

2012). Since glial cells preserve their proliferative potential, it could be that the culturing conditions I used led to their proliferation and differentiation to a mixed cell type.

Furthermore, it could be that coexpression of NeuN and OLIG2 was observed by others, but it did not prove to be physiologically relevant. For example, no matter that cultured POA primary neurons probably express Olig2, and other glial markers, the number of cells responding to temperature we got matched the number of others performing similar quantification of WSNs in the primary POA cultures (Tabarean et al. 2005), and the work established in our lab (Song et al., 2016). On the other hand, transcriptomic analysis of the cultured cells was the experiment that led me to the finding that it might be ambiguous to find the marker of the WSNs. This is not because these cells do not express genes that code for ion channels and molecules responsible for their temperature-sensitivity, since they show a clear response to 45˚C stimulation. However, it might be that the readout of these genes, especially if these are expressed at a low level in the cell, might be overwritten by the expression of more prominent cell-type markers, and was not captured by our scRNA-seq approach (Sims et al., 2014). This is because scRNA-seq is a method prone to zero reads, a characteristic that is biased against the lowly expressed genes due to overamplification of highly abundant genes (Hicks et al., 2018). For example, functional Trpm2 expression, an ion channel whose activity I measured by highly sensitive calcium imaging, was found to be quite lowly expressed by scRNA analysis in all of the cells and not only 2-APB sensitive functionally confirmed Trpm2-expressing cells (Figure 1.4. B). It can be that the depth of the sequencing method I used is not enough to detect low-expressed genes. However the Smart-seq2, the method I used, is one of the most sensitive methods for gene detection, and the average number of reads per cell achieved in this experiment was 1.4 million, more than it is considered necessary to reach the plateau in the number of genes detected (Haque et al., 2017; Ziegenhain et al., 2017).

Importantly, Kamm and colleagues in our lab, have further investigated the role of the TRPM2 ion channel in heat detection in the POA (Kamm et al., 2021). In this work, the TRPM2 was found not to be a somatic heat sensor in WSNs, but instead, it was found at the local neuron synapses from where it modulates the firing of neighboring WSNs. In addition, the warming from 33-36 ˚C was enough of a stimulus to activate TRPM2 in the synapses, a temperature which is more close to the physiological state, unlike 42˚C at which one can observe somatic responses of cultured POA neurons. Equally important, this work re-assessed the previously established and widely accepted knowledge that the warm-sensitivity of POA neurons is an intrinsic property and not synaptically driven (Kelso & Boulant, 1982; Madden & Morrison, 2019; S. F. Morrison & Nakamura, 2019; Tan & Knight, 2018). The proportion of the warm-sensitive POA neurons remained the same in the slices of adult mice when blockers of the fast synaptic

transmission were applied. However, the recording of the temperature sensitivity before and after the application of the synaptic blockers showed that almost every WSN changed its thermal coefficient with synaptic blocker application and became warm-insensitive (Kamm et al., 2021).

Together, these findings have confirmed the doubt that the early postnatal cultures might not be reliable for a search of the genetic markers of the WSNs in the POA, since it is very likely that some of the proteins responsible for the heat sensation and its modulation are not in the mature form as in the intact tissue. However, the molecular mapping of the temperature-responsive cells blocked by 2-APB to inhibitory neuronal population, as is expected from the literature on WSNs, points out that the cultured cells still might have kept a certain transcriptomic repertoire to reveal WSNs' molecular background. However, since the temperature-insensitive cells identified in the Ca2+-imaging were not neuronal, I lost the ability to compare these neurons directly to extract the potential markers of WSNs. Moreover, the warm sensitivity, after all, is modulated by synaptic inputs, which POA cultures are devoid of, and therefore from the cell culture model, I would not be able to grasp a complete picture of WSNs. The questions that rose from this finding relevant for this study are: If the synaptic input defines whether a neuron will be warm-sensitive or not, depending on the constellation of synaptic inputs it receives, how does one approach the search of WSNs? Should one, therefore, use synaptic blockers to identify the WSNs, or would that even further tamper with the *in vivo* occurring WSNs? How many WSNs are intrinsically warm-sensitive and in how many of WSNs is that property synaptically driven? Would a neuron still need to be equipped with a certain molecular armor to be warm sensitive although this sensitivity is synaptically modulated?

4.3. PATCH-SEQ AS AN ALTERNATIVE METHOD TO SEARCH FOR MARKERS OF WSNs

The patch sequencing (Patch-seq) method offers an alternative to the immature cultured neurons for investigating the electrophysiological, morphological, and transcriptomic cell-type composition of the brain's regions (Cadwell et al., 2020; Muñoz-Manchado et al., 2018; Scala et al., 2019, 2021). It employs a collection of the cellular content with a recording pipette after Ephys measurement. One of the main pitfalls of the Patch-seq method is the contamination coming from mRNAs of other cell types surrounding the cell of interest. Tripathy et al. have observed a significant increase of unwanted cell type contamination in publicly available Patch-seq, compared to scRNA-seq data sets in which cells were obtained by tissue dissociation and droplet-based RNA sequencing methods (Tripathy et al., 2018). The main issue pointed out was that samples with greater contamination indices express markers of their cell type at lower levels. In our pilot-Patch-seq experiment, we also experienced the problem of contamination coming from non-

patched cells, especially oligodendrocytes (Figure 1.7. E). In addition to the problem of contamination, Patch-seq is facing the problem of a low abundance of mRNA starting material. This is because in this method we are not obtaining the whole cell but aspirating a portion of the intracellular content after patch-clamp recording. Therefore, it is expected to have a higher drop-out rate of detected genes with Patch-seq than with scRNA-seq data sets obtained by other methods. Indeed I also observed this dropout in the pilot data set by the low abundance of certain expected genes such as Vgat (Figure 1.7. D). This could represent a problem in particular in our case where we want to find the transcriptomic differences between cells that exert subtle physiological differences, such as temperature sensitivity. However, the availability of large scRNA-seq data sets from the region of interest provides the opportunity to analyze the transcriptome obtained via Patch-seq post-hoc, quantify the contamination, and remove the contaminated cells from further analysis (Johansen & Quon, 2022; Sicherman et al., 2021). Moreover, certain improvements have been implemented in Patch-seq on the technical level such as aspiration of the cell nucleus together with the cytoplasm which should also increase the amount of starting mRNA material and therefore the number of genes detected by RNA-seq should increase as well (Cadwell et al., 2017).

Patch-seq is growingly applied in neuroscience, especially when the goal is to correlate differences at the level of gene expression with the ones at the level of cell electrophysiology. One should also not forget the power of combinatorial data that is gathered by Patch-seq, as electrophysiological and morphological data together with the transcriptome obtained, could give more information about the cell types than each alone (Lipovsek et al., 2021). Patch-seq has been used to reveal the transcriptomic, morphological, and electrophysiological profile of the cell-type differences in mouse cortex (Gouwens et al., 2020; Scala et al., 2021). In that work, it was shown useful to map Patch-seq samples to the larger single-cell atlas of the region to facilitate the correlation of electrophysiology to the transcriptome obtained by Patch-seq due to the drop-out of the reads that Patch-seq is facing. However, in both of these papers, the numbers of cells patched and sequenced are in the thousands, numbers not easily feasible for smaller laboratories. In my case, where I aim to search for markers of WSNs, there is a specific hurdle with the numbers of cells one needs to analyze to expect telling results achieved with Patch-seq. The occurrence of WSNs in mouse brain slices in which the warm sensitivity is assessed was in a range of 21-27% (Kamm et al., 2021). On top of that, from the pilot-patch seq experiment, I have learned that about 25% of cells exhibited contamination coming from other cell types, and I would have to remove these from further analysis (Figure 1.7. E). Furthermore, the cDNA library preparation had a similar number of dropouts in both scRNA-seq experiments presented in this thesis work, which was also about 25%. That means, if one

would like to have 100 WSNs for Patch-seq analysis, oI would have to patch and record 700 cells and collect about 175 WSNs to account for dropouts after cDNA library preparation and the cell contamination. This illustrates why Patch-seq is challenging, as being low throughput, hand-laborious, and interdisciplinary-demanding (Lipovsek et al., 2021).

Moreover, attempts have been made in terms of WSN marker identification by implementing Ephys recordings and scRNA-seq (T. A. Wang et al., 2019). In this paper, the authors propose that the gene Ptgds is a marker of POA WSNs. Ptgds codes for lipocalin-type prostaglandin-D-synthase (L-PGDS) which generates prostaglandin D2 (PGD2). The authors of the work have found that PGD2 lowers mice Tcore when challenged with hyperthermic stimuli such as injection of prostaglandin E2 (PGE2). In addition, Ptgds knockdown turned out to be lethal as mice could no longer maintain their body temperature. However, the expression of Ptgds transcript in the POA was not found to be specific for WSNs but also to reside in cold-sensitive and temperature-insensitive neurons, discrediting the specificity of this gene as a marker of WSNs. Moreover, the expression of Ptgds in the POA scRNA-seq data from Moffit and colleagues was found in each of the POA cell types, and it was larger in oligodendrocytes than in the neuronal cell types (Figure 1.8.).

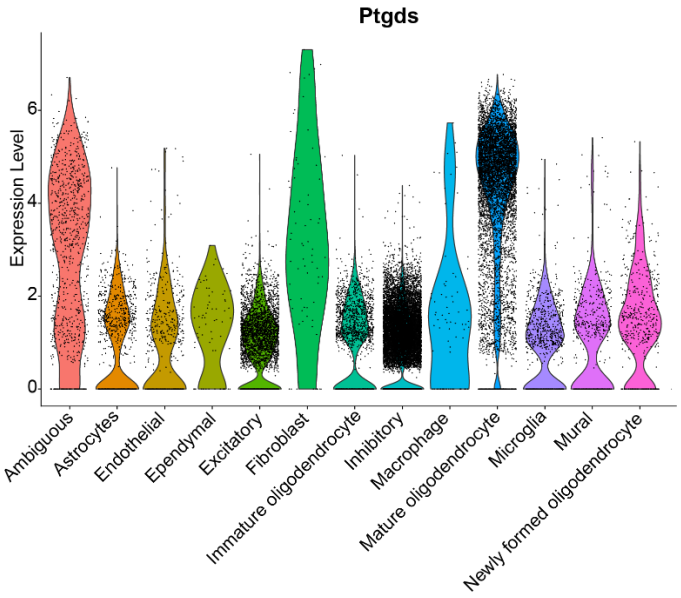

Figure 1.8. Expression of Ptdgs in broad cell Moffit et al.categories revealed by scRNA-seq of the POA.
Violin plots of the expression levels (Y-axis presents log2 scale on the) of Ptdgs transcript in the broad cell populations from the POA scRNA-seq atlas (Moffitt et al., 2018). Ambiguous cells were characterized by co-expression of *Vglut2* and *Vgat2*. Note that Ptdgds appear to be broadly expressed in many cell types.

Overall, I learned from this pilot experiment that Patch-seq might provide a powerful tool to collect data on WSNs transcriptome, electrophysiological properties, and morphology when coupled with the larger scRNA-seq data sets from the brain region of interest. On the other hand, I learned that it is a laborious, low throughput method, prone to contamination from unwanted cell types, and one should carefully inspect the feasibility of this method implementation depending on the prior knowledge of physiology and transcriptome (e.g. large scRNA-seq atlases of the region) of the cells of interest.

4.4. STUDY IMPLEMENTATION AND FUTURE RESEARCH

In this thesis work, I tried to find markers of WSNs, by using primary neural culture from POA of 9 days old mice. I have found that in terms of the transcriptome, this primary neural culture insufficiently recapitulates the state of adult POA neurons, and exhibits too heterogeneous transcriptome at the single-cell level, and therefore I concluded that it is not sufficient for the search for genetic markers of WSNs. Although I did not reach the aim of this study to find the markers of WSNs, others as well might want to use a similar approach to learn about POA cell types that exert certain kinds of physiology. With the scRNA-seq, I learned about the limitations of the primary POA culture when it comes to studying neuronal physiological properties we want to transfer to *in vivo* conditions. Moreover, novel findings of my colleagues and myself have shed a light on the central thermoregulation, by re-defining the role of the TRPM2 ion channel in POA warm sensitivity as a synaptic and not somatic driver of WSNs activity, and interestingly found that WSNs activity is highly modulated by synaptic inputs (Kamm et al., 2021). Both of these findings could not be achieved on the primary cell culture. Therefore, further research of WSNs demands investigation of these cells in their native environment.

A potentially useful tool to do this is Patch-seq which allows for measuring the electrophysiological properties of a neuron, in this case, it would be the thermal coefficient (AP/s/˚C) while increasing the temperature, capturing its transcriptome, and morphology (Cadwell et al., 2016; Földy et al., 2016; Fuzik et al., 2016). Not without its flaws, this method which was put to a test also in this thesis still offers a powerful tool to analyze the physiologically defined cell type. This is especially promising if one has an access to the large single-cell data sets of the transcriptome of the region where neurons of interest are residing (Cadwell et al., 2020; Gouwens et al., 2020; Muñoz-Manchado et al., 2018; Scala et al., 2019, 2021).

Previously, we thought that temperature sensitivity was a WSN intrinsic property, now we learned that this is not the entire story (Kamm et al., 2021). Therefore, and in light of our data, the concept of neuronal warm-sensitivity has changed and the approaches for searching markers of WSNs have to be re-

evaluated. When further investigating the characteristics of WSNs, one should consider implementing the blockers of synaptic inputs to look for intrinsically temperature-sensitive neurons or to first assess how many of WSNs is truly intrinsic and how many are modulated by synaptic inputs. In addition, other Ephys properties should be gathered and analyzed with the hope of finding an additional unique characteristic of these neurons. Perhaps Patch-seq offers a manner by which Ephys data can be collected while simultaneously transcriptionally profiling the neurons to define WSNs of POA in greater detail.

5. MATERIALS AND METHODS

5.1. ANIMALS

Animals used in this part of the thesis were postnatal day 9 C57BL/6JRj and VgatCreHTB line for which VgatCre (Slc32a1tm2(cre)Lowl/J, The Jackson Laboratory strain number 016962) was crossed with Rosa26Lox-stop-LoxHTB (The Salk Institute for Biological Studies). For obtaining P9 C57BL/6JRj pregnant female mice were ordered from Janvier company. The females arrived at our animal room at the 13th week of pregnancy and were housed at room temperature (23 ± 1°C; unless specified otherwise) with a standard 12-h light/dark cycle and with ad libitum access to food and water. The pups were kept with their after birth mothers until day 9. All experiments employed a mixture of male and female mice and were per the local ethics committee and governing body (Regierungspräsidium Karlsruhe, Germany) and were approved under protocol numbers: T-01/17, T-05/19.

5.2. POA P9 NEURAL CULTURE

5.2.1. Glas coverslip preparation

Glass coverslips of 5mm diameter (11888372, Menzel Fischer Scientific) were cleaned by leaving them in 1M HCL overnight, and on the next day, they were incubated for several hours in 70% ethanol and rinsed well with H_2O. Coverslips would then be left to dry for 1h under the cell culture hood with the UV light on, and stored in a clean petri dish until use. 20 µl of poly-D-lysin (P7886 Sigma) (1:100 in H_2O) was added to each dry coverslip and left to incubate overnight at 37 ˚C in the home-made humidity chamber (petri dish lid of 10 cm diameter covered with parafilm, placed inside of a petri dish of 20 cm diameter, surrounded with ca lean paper towel wetted with 1xPBS). On the next day, poly-D-lysin was removed, coverslips were washed with 3x 1xPBS, and 20 µl of laminin (L2020 Sigma, 1:10 in H_2O) was placed on each coverslip instead, and incubated for a minimum of 2h at 37 ˚C in the home-made humidity chamber.

5.2.2. POA neural cell suspension preparation and culturing

Four C57 BL/6 mice were sacrificed by a quick decapitation. Brains were removed from the skull and immersed in ice-cold ACSF. Before slicing in the same ACSF, brains were glued to the cutting stage of a Vibratome (HM650V, Thermo Scientific, USA) together with an agar block (3%) which supported the brains against the vibratome pushing. The ACSF (in mM; 125 NaCl, 2.5 KCl, 2.5 $NaHCO_3$, 1.25 NaH_2PO_4X $2H_20$, 1 $MgCl_2$, 2 $CaCl_2$), and it was constantly bubbled with carbogen (95% O_2, 5%CO_2). Brains were sliced at frequency 50, speed 9, thickness 300 µm, and amplitude 1. 2-3 slices containing the whole POA were

collected and placed in a petri dish containing ice-cold HBSS (-) solution (in mM; 10 D-glucose, Hepes in 1x HBSS medium). POA was dissected in HBSS (-) under a dissection microscope. POA tissue was then cut into 4 smaller pieces which were transferred to the clean 1.5 ml tube and 1ml of PK solution (30 mg/ml Proteinase K (P6556 Sigma), 20 µl of 50x B-27 supplement, in 1ml of HBSS(+) (in mM; 10 D-glucose, 10 HEPES, 1.2CaCl2, 0.8 MgCl2, in 1xHBSS medium (14175-083, ThermoFisher Scientific, Gibco)). The tissue was incubated for 5 minutes at 30˚C. PK solution was then removed from the issue without disturbing it (tissue stayed at the bottom of the tube), and rinsed with 1x HBSS(-). 1ml of papain solution (0.5 mg/ml papain (Sigma P4762-25mg), 20 µl of 50x B-27 supplement (Invitrogen 17504-044), 5mM L-Cysteine (Calbioquem) in HBSS(-)) was added to the tissue, incubated 30 minutes at 37 ˚C with inverting a tube every 5 minutes to mix well. After 30 minutes, papain solution was removed, and tissue was rinsed 1x with HBSS(-). 1ml of a warm (37˚) cell culture media (10%FBS, 0.5 ml of 100x Glutamax (ThermoFisher Scientific, Gibco), 1ml of B27 50x supplement, 0.5 ml of PenStrepC 100x in 50ml of Neurobasal medium (21103049, ThermoFisher Scientific, Gibco)) was added. The tissue was triturated with a 1ml pipette tip, for about 5-10 x, while avoiding creating bubbles. The supernatant was collected, avoiding bigger chunks of tissue, transferred to a new tube, and centrifuged for 4 minutes, at 4 ˚C, and 250 rpm. The supernatant was discarded and cells were resuspended in 20 µl/coverslip of cell culture media, e.g. for 5 coverslips 100 µl of media was used. Laminin was aspirated away from the coverslips, coverslips were left to dry for about 10 minutes, and 20 µl of cell suspension was added to the glass coverslip. The cell suspension was left to incubate on the coverslips at a cell incubator (37 ˚C, 5%CO2) in a homemade humidity chamber. After 2h coverslips containing cells were transferred to a well of 24 well-plate each and filled with 1ml of pre-warmed (37 ˚C) culture media and left in a cell culture incubator (37 ˚C, 5%CO_2). On the following day, the cell media was exchanged for a fresh one, and cells were left to recover for 2 additional days. On the 3rd day, calcium imaging was performed.

5.3. CALCIUM IMAGING DATA ACQUISITION AND ANALYSIS

Coverslips containing cells were transferred back to a humidity chamber (described in 3.1.1). Cells were washed with 50µl 1xRinger solution (in mM; 140NaCl, 5.0KCl, 2 $MgCl_2$ x6 H_2O, 2 $CaCl_2$ x2H_2O, 10 Glucose, 10 HEPES, adjusted to pH 7.4), and then covered with 50µl 1x Ringer's containing 10 µM Cal520AM (21130, AAT Bioquest) and 0.05% pluronic acid F-127 (P6866, Invitrogen). Cells were left to incubate with calcium dye for 1h in a dark in a homemade humidity chamber at 37˚C before the calcium imaging.

The cell containing coverslips were placed in the perfusion chamber (RC-22, Warner Instruments) while perfusing through it Ringer's solution constantly at room temperature (23-25˚C) by a gravity-driven perfusion system (ValveBank II Automate Scientific) at a rate of max 2.5ml/minute, and a vacuum pump (Ecovac, Schuett Biotech). The thermocouple probe (IT 18, Physitemp) was placed as close as possible to the coverslip and connected to the BAT-12 digital thermometer (Physitemp) by which the temperature was read. CoolSnapHQ2 camera was used for recording, connected to an AxioObserver D1 microscope (Zeiss) with ET470/40x excitation and ET525/50m emission filters (Chroma). Images were taken at 1Hz in MetaFluor software (Molecular Devices), at 20ms exposure time, binning 2. The stimulus of 45˚C was achieved by connecting a perfusion system running the Ringer's with the homemade glass coils connected to a heated circulating water bath (Multitemp III, Pharmacia Biotech).

Each stimulus lasted 45 seconds, between each stimulus 4 minutes were allowed for cells to recover. During the 2nd stimulus, Ringer's containing 30 µM 2-APB was perfused to cells. 4 minutes after the 3rd stimulus high K^+ solution was perfused on cells (in mM; 45 NaCl, 100KCl, 2 $MgCl_2$ x6 H_2O, 2 $CaCl_2$ x2H_2O 10 glucose, 10 HEPES) to observe maximum depolarization of the cells. The total procedure of recording with 1 coverslip lasted for about 13 minutes.

Calcium imaging analysis was performed using FIJI (Fiji is Just ImageJ 2.1.0) (Schindelin et al., 2012). Motion correction was done by the *moco* plugin (Dubbs et al., 2016), and cells were detected by thresholding and setting the size of particles at 15 pixels^2. The average fluorescence (F) of a cell was measured in FIJI by the mean gray value. Measurements were exported to Excel, where ΔF/F values were calculated by subtracting the average baseline fluorescence ($\Delta F = F - F_{(baseline)}$) before the 1st 45 ˚C stimuli (first minute of the recording) from the fluorescence values and dividing it by the baseline ($\Delta F/F_{(baseline)}$).

5.4. CELL COLLECTION AND SINGLE-CELL RNA SEQUENCING

All the surfaces where buffers for cell collection were prepared were sprayed with RNseZAP (Ambion). Calcium imaging video was played from the beginning immediately after the recording, and regions of interest were placed around the cells identified as 2-APB insensitive temperature responders (3x responding to 45˚C), 2 –APB 2-APB sensitive temperature responders (response to a 2nd 45˚C blocked by 2-APB), or non-responders (no visual fluorescence increase during 45˚C stimulus). Cells of interest were then found under the microscope. I aimed to collect one cell from each of the categories per coverslip, meaning 3 cells per coverslip. A glass capillary connected to a 50ml syringe pressure system was navigated to the cells with an MM3A-LS micromanipulator (Kleindiek) while observing the approaching under a

microscope. Cells were aspirated with an application of a negative pressure until one could not observe the cell at the coverslip anymore.

Glass capillary was loaded with 1µl of a Ringer's with RNAse inhibitor (1µl of RNAse inhibitor (40U/µl, Promega N2515) diluted in 40 µl of sterile-filtered Ringer's). After aspiration cell was ejected with a syringe-applied pressure to a 0.2 ml PCR tube containing 4µl of the Smartseq2 buffer (2µl of lysis buffer (19µl 0.2% Triton-X-100 mixed with 1µl of RNase inhibitor), 1µl of dNTP mix, and 1µl of oligo-dT primers). Sometimes the glass was broken to ensure that the cell was ejected to a 4µl buffer. After ejection of a cell into the 0.2 ml tube, the sample was snap-frozen in liquid nitrogen.

5.4.1. cDNA library preparation

cDNA library preparation from single-cell samples was done at GeneCore (EMBL, Heidelberg) by following Picelli et al protocol (Picelli et al., 2014). I will highlight here the differences in that protocol. Firstly, all the samples were processed in batches of a maximum of 21 samples as I recognized this is the number of samples I could handle without jeopardizing the quality. Reverse transcription was done according to the published protocol with SuperScript Transcriptase IV (ThermoFisher Scientific, cat.no. 18090010) but without the IS PCR primers. The first amplification was done by 21 cycles at the PCR cycler. The cleanup by SPRI magnetic beads was done with a ratio of 0.6:1 (beads: sample) with skipping the ethanol washes. If primer dimers were present after the 1st clean-up, 2nd cleanup was repeated with a ratio of 1:1. After the purification, the cDNA quality control step was performed by running all the samples on a Bioanalyzer Agilent high-sensitivity DNA chip. Samples that were selected for further processing were never below a concentration of 120 pg/µl, and the library devoided the small fragments with a peak between 1.5 and 2kb.

cDNA library tagmentation was done by in-house GeneCore (EMBL, Heidelberg) adapted protocol and the Tn5 enzyme was produced in the Protein Expression and Purification *Core* Facility (EMBL, Heidelberg). 1.25 µl of 100-200 pg/µl cDNA was used for the tagmentation reaction after which 12 cycle PCR enrichment was performed by adding a unique combination of adapter index primers to each sample. Finally, SPRI bead cleanup was performed by skipping the ethanol washes. Library quality was again verified at Bioanalyzer High Sensitivity DNA chip and the concentration of each sample was measured on Qubit as well. By these two measurements molarity of each sample was calculated, 93 samples were pooled equimolar (80nM) and pipetted to one tube. The final pool was cleaned up with SPRI beads 1:1, and this time 80% ethanol wash was included. Sequencing was performed on the Illumina NGS platform with the NextSeq mid 500.

5.4.2. scRNA-seq analysis

First, trimming of the adapter sequences was done with the fast tool (S. Chen et al., 2018) run by a Linux command line. Next, I did the quality control of the reads by using FASTQC (Steven W. Wingett & Simon Andrews, 2018). To quantify the transcripts detected in scRNA-seq data, I used the Salmon tool (Patro et al., 2017) to align the obtained reads to the mouse transcriptome (GRCm38.p6, release M20). Next, I proceeded with the analysis in R-based packages. I used the resulting transcripts quantification files from *Salmon* to associate them with gene IDs for gene-level summarization and creation of the count matrix with the Bioconductor *tximport* package (Soneson et al., 2016). Next, I used *Seurat (V3)* (Stuart et al., 2019) for further analysis by following the *Seurat-Guided Clustering* tutorial for basic scRNA-seq analysis, and the *Integration and Label Transfer* tutorial for integration of obtained data set to a scRNA-seq POA atlas (Moffitt et al., 2018).

5.5. IMMUNOFLUORESCENCE STAINING IN P9 POA NEURAL CELL CULTURE

Cells were prepared in the same manner as described above in (5.2.2 (page 51)) and on the 3rd day of culturing I stained the cells with the antibodies raised against OLIG2 and NeuN. Antibodies used were mouse Olig2 (MABN50, Merck) and rabbit anti-NeuN (D4G4O, Cell Signaling). Briefly, cells on the coverslips were washed 1x with PBS1x, fixed with 4% PFA (paraformaldehyde) in PBS1x, for 10 minutes at RT. Next, cells were washed 1x with 1xPBS and blocked for 1h at RT n 10%NGS in 1xPBS. Primary antibodies against OLIG2 and NeuN were diluted in blocking solution (3%NGS, 0.1% Triton-X-100in 1XPBS) at 1:500 and 1:1000 respectively, and cells were incubated in the primary antibody solution overnight at 4 ˚C. On the following day, cells were washed 3x with 1xPBS. The secondary antibodies anti-mouse IgG Alexa 647 and anti-mouse IgG Alexa 488 were diluted at 1:750 in a blocking solution (3%NGS, 0.1% Triton-X-100 in 1XPBS) together with DAPI. Cells were incubated for 2h at RT with the secondary antibody solution after which they were washed 3x with 1xPBS and 1x with H_2O. Coverslips were mounted on the glass slides with Immu-Mount (Epredia, Fisher Scientific). Pictures were taken at the Nikon imaging center at Heidelberg University, with the Nikon A1R confocal microscope under Nikon Plan Apo λ 10x NA 0.45 (working distance 4mm, the field of view 1.27 x 1.27mm) objective. Immunofluorescence images were processed in FIJI (Schindelin et al., 2012) and cell counting was plotted in Microsoft Excel 2016.

5.6. IMMUNOHISTOCHEMISTRY STAINING IN P9 POA BRAIN SECTIONS

Brains from C57BL/6j were obtained and incubated overnight in 4% PFA at 4 ˚C. On the next day, brains were incubated for 3 h in 10%sucrose, at 4˚C followed by incubation in 30% sucrose at 4 ˚C

overnight. Brains were cut at 50 µm thickness on a microtome and kept in a cryoprotectant solution (150 g of sucrose, 200ml of ethylene glycol, and 0.1 M PBS until 500ml) in the 24 well plates until staining was performed. Briefly, POA sections were permeabilized by 0.2% Triton-X-100in 1XPBS (PBST) at 4 ˚C overnight. On the 2nd day sections were blocked in 10% goat serum (GS) in 0.2%PBST, 2h at RT. Primary antibodies mouse Olig2 (MABN50, Merck) and rabbit anti-NeuN (D4G4O, Cell Signaling) were diluted at 1:100 and 1:1500, respectively, in 1%GS in 0.2%PBST. 200 µl of staining solution as used per well/section. Sections were incubated in the primary staining solution at 4 ˚C for 3 days. On the 5th day, sections were washed with 0.2%PBST, 4x10 minutes at RT. Secondary antibody solution (anti-mouse IgG Alexa 647 and anti-mouse IgG Alexa 488 were diluted 1:750 in a blocking solution 1%GS in 0.2%PBST) containing DAPI was applied on sections and were left incubating at 4 ˚C overnight. Sections were washed 4x for 5 minutes with 1xPBS, mounted on glass slides, and covered with Immu-Mount (Epredia, Fisher Scientific) and a glass coverslip. Pictures were taken at the Nikon imaging center at Heidelberg University, with the Nikon A1R confocal microscope under Nikon Plan Apo λ 20x NA 0.75 (working distance 1mm, a field of view 0.64 x 0.64mm) objective. Immunohistochemistry images were processed in FIJI (Schindelin et al., 2012) and cell counting was plotted in Microsoft Excel 2016.

5.7. PATCH SEQUENCING

For the Patch-seq electrophysiology, 8 to 12-week-old VgatCreHTB mice were anesthetized using a Ketamine/Xylazine cocktail (ketamine: 220 mg/kg, Ketavet; Zoetis, USA and Xylazine 16 mg/kg, Rompun; Bayer, Germany). Under the deep anesthesia validated by the non-responsive movement of limbs to the pinching of the skin, mice were quickly decapitated, and brains were dissected out to the ice-cold oxygenated (95% O2, 5% CO2) slicing ACSF (in Mm; 1.2 $NaH_2PO_4xH_2O$, 2.5 KCl, 20HEPES, 25 glucose; 30 $NaHCO_3$, 93 NMDG (n-methyl-glucamine), 5 Na-Ascorbate, 3 Na-pyruvate, 12 N-acetylcysteine, 10 $MgSO_4x7H_2O$, 0.5 $CaCl_2$). Coronal (250 µm thick) POA slices were obtained with a vibratome (Leica VT1200S) in the same slicing solution. Slices were then transferred to and incubated at 32 °C in a bath containing oxygenated holding ACSF (in mM; 118 NaCl, 2.5KCl, 7 glucose, 1.2 $NaH_2PO_4xH_2O$, 24 $NaHCO_3$, 5 HEPES, 7 Glucose, 4 Ascorbic acids (sodium-L-ascorbate), 2.4 Na-pyruvate, 2 N-acetylcysteine (NAC), 1 $MgSo_4*7H_2O$; 2 $CaCl_2$). After a recovery period of 30 minutes, individual slices were transferred to the recording chamber where they were continuously perfused with oxygenated recording ACSF (in mM; 125 NaCl, 2.5 KCl, 7 glucose, 1.2 $NaH_2PO_4xH_2O$, 24$NaHCO_3$, 5 HEPES, 8 Glucose, 1 $MgSO_4*7H_2O$, 2 $CaCl_2$), at ≈2 ml/min. Electrophysiological recordings of the cells were acquired using a MultiClamp 700B amplifier (Molecular Devices, USA), Axon Digidata 1550B digitizer (Molecular Devices, USA), and Clampex 11.0.3

software (Molecular Devices, USA). Cells were visualized using a SliceScope upright microscope (Scientifica, UK) equipped with a 40X water immersion objective (U-TV1X-2, Olympus, Japan). Images were acquired by a digital CCD camera (ORCA-R2 C10600-10B, Hamamatsu Photonics K.K., Japan) using MicroManager 1.4 software (Vale's lab, UCSF, USA). Borosilicate glass micropipettes (O.D. 1.5 mm, I.D. 0.86 mm, Sutter Instrument, BF150-86-7.5) were pulled with the micropipette puller (P-97, Sutter Instrument, USA). The open pipette resistance was between 2-4MΩ. Recording pipettes were filled with 0.4 to 0.8 µl of the internal solution adjusted for Patch-seq containing in mM (120 potassium gluconate, 2 KCl, 5 NaCl, 10 HEPES, 10 EGTA, 1 MgATP, 1 $CaCl_2$) with 20 µg/ml glycogen, and 0.25 U/µl recombinant RNase inhibitor (40U/µl, Promega N2515). After obtaining the Giga seal, the cell action potentials were recorded in the whole-cell mode for ≈2.5minutes to simulate the potential recording of a WSN neuron. After the recording cells' internal content was aspirated by application of the negative pressure. 27 samples were obtained in this manner for the scRNA-seq. In addition, 9 negative controls were obtained by immersing a recording pipette into the tissue and applying negative pressure.

Samples obtained were processed by Smartseq2 protocol for scRNA-seq as described in 5.4.1 (page 54) and data analyzed as in 5.4.2.

5.8. GENOTYPING PCR PROTOCOLS

VgatCre**:** forward primer CCGGCTTCGTGCATTCACTC, rewerse primer ACACCGGCCTTATTCCAAG. PCR cycler procedure: 94 ˚C 3 min; 40 x: 94˚C 30 sec, 58 ˚C 30 sec, 72 ˚C 1min; 72 ˚C 5min, 16 ˚C hold.PCR reaction/1 sample: 2xbuffer 13 µl (36.4% sucrose, 3.5mM MgCl2, 11mM (NH4)2SO4, 0.005% cresole red, 1:1000 β-mercaptoethanol), dNTPs 10mM, Fwd primer 10mM (1µl), Rew primer 10mM (1µl), taq polymerase 5U/µl (0.125 µl), H_2O (3µl), DNA sample 1 µl.

CHAPTER 2

Molecular characterization of POA^{LepR} neurons involved in heat acclimation

1. INTRODUCTION

1.1. HEAT ACCLIMATION

1.1.1. Motivation to investigate heat acclimation

Mammals, such as humans and rodents, are endotherms and can maintain autonomously their body temperature (T_{core}) within a narrow range. Because of this homeostatic response, mammals can prevail and be active in a broader range of environmental temperatures, unlike ectotherms whose T_{core} depends directly on the environment (Asarian et al., 2012). The ability to defend the T_{core} despite external changes is extremely important to maintain a stable internal-cellular milieu once it is usurped by a dynamic external environment (Taylor, 2014). Due to global climate warming researchers are more and more interested in investigating the process behind adaptation and acclimation to a warmer environment and the potential evolutionary means by which these are being achieved in different species (Cavicchi, Sandro, 1995; McCarthy & Intergovernmental Panel on Climate Change, 2001).

For further reading, it is important to distinguish three terms; *acclimatization*, *acclimation*, and term *adaptation*. *Acclimatization* refers to the changes happening to the organism due to two or several changing variables in its natural environment, for example, increased temperature and reduced oxygen supply, and it is a more common natural occurrence as it is rare to have only one environmental factor changing at once (Hutchison & Maness, 1979). The term *acclimation* refers to the changes that happen due to one variable, most often in a controlled experimental environment, for example, increased environmental temperature (Hutchison & Maness, 1979). It is also important not to confuse the term *adaptation* with *acclimation* or *acclimatization*. Adaptation refers to evolutionary response and genetic change in a population happening over the course of generations to adapt to environmental change which is causing stress to the organism (Collier et al., 2019). Unlike acclimation or acclimatization adaptation is irreversible, even when the environmental stressor is removed the achieved change in the organism persists (Collier et al., 2019). Importantly, acclimation and acclimatization allow for the development of a new physiologic condition through coordinated metabolic changes to help survive the current challenging environment (Bauman & Bruce Currie, 1980).

While meeting the challenge of heat stress or chronic heat exposure organism responds with changes achieved via a process called heat acclimation (Horowitz, 2002). At its core, heat acclimation is a joint term for physiological changes that develop over a prolonged period and help to increase heat endurance or better prevalence in a novel hotter environment. Hallmarks of it are lowered skin and body

temperature, lowered heart rate, and increased cutaneous blood flow and sweat rate (Sawka, Michael N. et al., 2011). Collectively, these alterations allow the organism to cope with higher environmental temperatures.

The acclimated state is characterized by a decreased T_{core} threshold for activation of the heat dissipation mechanism and an increased T_{core} threshold for heat stress injury (Horowitz, 2016). Analysis of different acclimation protocols has shown that acclimation homeostasis is achieved through a bi-phasic process of short-term heat acclimation (STA) and long-term heat acclimation (LTA). The differences between these two phases are reflected in the responses of the effector organs to inputs from the autonomic nervous system, which is inefficient in STA and becomes efficient in LTA (Horowitz, 2002). A summary of the changes happening in both phases of heat acclimation is presented in Figure 2.1.

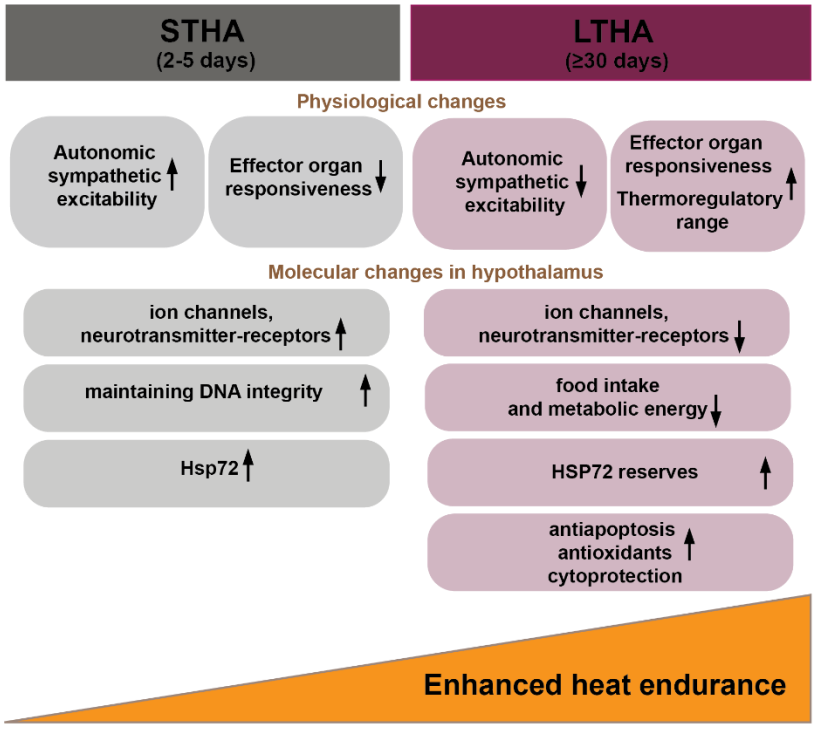

Figure 2.1. Heat acclimation is a biphasic process

At the onset of heat acclimation in STA (short-term heat acclimation, 2 days at heat) there is increased autonomic nervous system excitability. During STA there is a marked lowered effector organ responsiveness or in other words, reduced organ functionality in concordance to the demands of a new environment. LTA (long-term heat acclimation, from 2/5 to ≥30 days) is marked by a decrease in sympathetic nervous system excitability due to achieved acclimatory homeostasis. Molecular changes at the level of the hypothalamus during STA show an increase in the expression level of ion channel and neurotransmitter receptors coding genes showing increased cellular signaling. A decrease in the expression of genes related to food intake and metabolic energy production might play a role in the decrease in heat

production. Transcripts related to maintenance of DNA integrity indicate induced DNA damage. Hsp72 increased production shows increased heat stress levels and higher reserves upon achieved acclimation in LTA. On the other hand, hypothalamic transcriptome from LTA mice shows a decrease in the level of ion channel coding genes and neurotransmitter receptors showing decreased excitability and signaling. Decreases in transcripts related to maintenance of DNA integrity show reduced DNA damage. An increase in apoptosis, antioxidative, and cytoprotection-related genes lead to the potential production of cell-protective molecules. All these molecular changes together bring up better heat endurance. Adapted from: *Heat acclimation and cross-tolerance against novel stressors: genomic–physiological linkage* (Horowitz, 2007)

Heat acclimation in humans has been investigated in terms of military and occupational settings, and athletic performance. The adaptations to novel hotter environments observed in humans include improved sweating, improved skin blood flow, lowered body temperatures, reduced cardiovascular strain, improved fluid balance, altered metabolism, and enhanced cellular protection (Périard et al., 2015). It is not yet fully investigated how exactly these adaptations are achieved.

1.1.2. Cellular and molecular changes behind heat acclimation

Heat acclimation impacts animals on several levels, starting from changes on the transcriptional level to the ones at the level of organ function (Horowitz, 2014). In this part, I will provide several examples of these changes observed after applying different heat acclimation protocols in rats. For example, in the most important evaporative organ of rats, a submaxillary salivary gland, muscarinic receptors activate calcium signaling to induce secretion and therefore cool the animal (Horowitz & Meiri, 1985). The secretory efficiency in the submaxillary gland was diminished during the STA (rats spent 2 to 10 days at 34˚C) because of the increased number of receptors at the cellular membrane leading to receptor desensitization and consequentially to reduced Ca^{2+} induced secretion (Kloog et al., 1985). This effect of receptor density persisted in LTA (20 to 60 days at 34˚C) but it was followed by an increased secretion efficiency, which shows that acclimation-induced cellular changes are biphasic. The first phase of acclimation (STA), when organ function is perturbed marks a transition phase toward the condition when organ function is efficient and stable (LTA) (Horowitz, 2014). Another interesting example of cellular changes resulting in physiological adaptation achieved during heat acclimation is the increased NO (nitrogen oxide) production in the blood plasma of heat acclimated rats (G. H. Li et al., 2008). Here, heat acclimation consisted of either constant exposure to 32 ˚C or the same temperature exposure only during the last half of a dark phase, during a period of 10 days. An increase in NO plasma levels decreased the sensitivity of the thoracic aorta to noradrenaline making it more dilated which could lead to increased heat dissipation. This is a possible explanation for increased splanchnic blood flow in acclimated animals

exposed to heat stress despite having the same vasoconstriction effect as the non-acclimated animals (Haddad & Horowitz, 1999).

Due to the cellular and organ changes one might hypothesize that certain molecular changes have to occur during the course of acclimation. Among several other findings, the level of heat shock protein 72 (Hsp72) was found to be increased in the heart tissue of rats during acclimation (Horowitz et al., 1997). In the response to cellular stress, such as heat, transcription of Hsp genes accelerates and these proteins pile up in the cellular milieu (Amorim et al., 2015). The most heat-sensitive of all heat shock proteins, the Hsp72 is found to stabilize denatured proteins by which it structures cytoskeleton and restores cellular function to enhance cell survival. Hsp-72 has been indirectly implicated in modulating the T_{core} threshold for activation of the heat dissipation mechanism and increasing the T_{core} threshold for heat stress injury (Horowitz, 2007; Maloyan & Horowitz, 2002). It is not proven, however, that an increased level of HSP-72 is essential for developing an acclimation phenotype because full heat acclimation can be achieved although its levels are not elevated in humans (Hom et al., 2012). Interestingly, the heat shock factor (HSF1), necessary for transcription of all heat shock genes by binding the heat shock responsive element (HSE), has been found to increase with acclimation to different temperature ranges in *Drosophila* (Garbuz et al., 2003). In addition, acetylation of histone 4 at HSE of Hsp72 and Hsp90 was observed at the onset of STA in rats, indicating possible increased activity of HSF1 binding to HSE of these HSP genes (Tetievsky & Horowitz, 2010).

Further on, the acclimation effect on mitochondrial metabolism was shown as well by decreased oxygen consumption and reactive oxygen species (ROS) production in LTA rat myocardiocytes after ischemia or heat stress (Assayag et al., 2012). Additionally, mitochondrial metabolism was changed by an improved function of the cytochrome oxidase chain due to hypoxia-inducible factor 1-α (HIF1 – α) remodeling (Mreisat et al. 2020); Assayag et al. 2012).

1.1.3. Central modulation of heat acclimation and its genetic background

The hallmark of achieved heat acclimation is a reduced temperature threshold for activating heat-dissipating mechanisms, e.g. increased sweat rate during exercise after daily heat exposures in humans (Brück & Zeisberger, 1987; Fox et al., 1963). This has been recently confirmed in heat acclimated humans by finding that skin sympathetic nerve activity, which activates heat loss mechanisms, is increased following heat acclimation (7 consecutive days of heat acclimation to 40-41˚C) (Barry et al., 2020). Such a coordinated shift in temperature thresholds for thermoregulatory effectors once heat acclimation has been achieved argues for central modulation of heat adaptation (Horowitz et al., 1999). This is suggested

to happen through altered sensitivity and discharge rates of hypothalamic temperature-sensitive neurons based on a model of adjusted set point proposed by Hammel (Hammel et al., 1960, 1963). In his model, Hammel suggests an antagonistic effect of temperature-sensitive and insensitive neurons, where temperature-sensitive neurons excite heat loss effector neurons and inhibit heat production dependent on the organisms' environment demands (Boulant, 2006). Pierrau et al. have tested the ratio of intrinsically temperature-sensitive neurons residing within the preoptic area of the rat hypothalamus (POA) upon warm acclimation. They found that 2 weeks of exposure to warm temperature decreases the number of these warm sensitive neurons (WSNs) in the POA (Pierau et al., 1998). To my best knowledge, this finding has not been corroborated until now, nor has its biological importance been further verified. Moreover, an additive increase of c-Fos expression due to both hypohydration stress and stress caused by acclimation in MnPOA (median preoptic nucleus) of the hypothalamus according to (Patronas et al., 1998) suggests the involvement of POA in both processes. Additionally, it has been shown that hypohydration might interfere with the acclimation process by abolishing the heat endurance during the course of heat acclimation and increasing the T_{core} thresholds for activating heat dissipation mechanisms (Schwimmer et al., 2004). Therefore, the interference of hypohydration with acclimation phenotype might take place in the POA. This additionally points to the role of central thermoregulation in heat acclimation.

To look for the changes that happen on the genetic level of the hypothalamus, including nowadays established central controller of thermoregulation, the POA, Schwimmer et al. performed the analysis of RNA of the whole hypothalamus obtained from rats by cDNA Atlas array (Schwimmer et al., 2006). The goal was to find genes that could modulate the bi-phasic process of heat acclimation such as a shift of higher to lower T_{core} thresholds for activation of effector mechanisms to dissipate the heat after the full acclimation has been achieved. Analysis of transcripts changed in hypothalamic tissue obtained at STA were showing the upregulation of voltage-gated ion channels, ion pumps and transporters, neurotransmitters, and hormone receptors, pointing out increased excitability (Horowitz & Meiri, 1985). On the other hand, LTA transcriptomic profile was showing downregulation of genes coding for mitochondrial energy metabolism and cellular maintenance processes. Therefore, the hypothalamic gene expression pattern was recapitulating the biphasic physiology of heat acclimation.

To conclude, thermoregulation is an important neural process connecting changes in temperature of external and internal environments with the peripheral and central nervous system allowing for a systemic response to the change in temperature (S. F. Morrison & Nakamura, 2019). Heat acclimation is a homeostatic process of prevailing the environmental challenges and improving animal fitness in a novel environment which is achieved through a plethora of metabolic changes (Bauman & Bruce Currie, 1980;

Collier & Gebremedhin, 2015). How exactly are these processes connected in the central nervous system, and which cell types are they mediated by are questions that I seek to answer in this thesis work.

1.2. LEPTIN HORMONE AND LEPTIN RECEPTOR

1.2.1. Genetic and molecular mapping of mutations causing ob/ob and db/db phenotypes

In 1949, a spontaneous mutation was observed in Jackson Laboratories which caused mice to excessively eat and gain weight (Ingalls AM et al., 1950). Apart from being obese these mice had other physiological problems such as infertility, increased corticosterone levels, hypothermic, and diabetic (J. Friedman, 2014). The place of the mutation was mapped to *Ob* (obese) gene on chromosome 6 (J. M. Friedman, Leibel, & Bahary, 1991; J. M. Friedman, Leibel, Siegel, et al., 1991).

Within the time from 1959 and 1966, two new obese phenotypes were observed in mice, with genes carrying mutations named “adipose” (*ad*) and “diabetic” (*db*) (Falconer & Isaacson, 1959; Hummel K.P. et al., 1966).

In 1978, Coleman and colleagues performed parabiosis experiments where they stitched together living *ob/ob* mice to wild-type (WT) or *db/db* mice (Coleman, 1978). The observation was that *ob/ob* mice, when paired to *db/db* or normal mice, ate less and lost weight. On the other hand, wild-type mice paired with *db/db* mice eventually stopped eating and died. From these observations, Coleman and colleagues suggested the existence of a blood circulating factor that reduces the food intake and body weight but must be lacking in *ob/ob* mice. According to Coleman, the same blood circulating factor was acting through its receptor that must be lacking in *db/db* mice which were compensating for the lack of blood factor function with its overproduction.

Later on, the *Ob* gene was cloned and showed to code for 167 amino acid-long protein, with a mutation in the 105th amino acid resulting in a dysfunctional form of the novel blood circulating factor (hormone) in *ob/ob* mice (Y. Zhang et al., 1994). Due to its ability to reduce body weight when supplemented with mice, this hormone was named leptin (from Greek *leptos*, “thin”) (J.L. Halaas, 1995).

Finally, the *Db* gene has been mapped to chromosome 4 and its cloning led to the discovery that it codes for a leptin receptor protein (OB-R) (Tartaglia et al., 1995). Interestingly, the expression of newly cloned leptin receptors was higher in the hypothalamus in relation to other tissues (G.-H. Lee et al., 1996). In addition, it has been found that different splicing variants of Ob-r result in proteins with cytoplasmic portions variable in length (G.-H. Lee et al., 1996). Moreover, a long-form of a receptor Ob-Rb- in db/db mice were shown to have guanine to thymine mutation at the splicing sites rendering the receptor dysfunctional by causing premature termination of the receptor signaling.

1.2.2. Leptin to leptin receptor signaling

Leptin is a hormone primarily produced by white adipose tissue and later on found to be produced by the stomach and placenta (Bado et al., 1998; Masuzaki M. et al., 1997; Y. Zhang et al., 1994). The leptin production increase is positively correlated to energy levels stored in adipose tissue and levels of leptin in plasma are higher as total body fat is increased (Ahima et al., 2000; Hamann et al., 1995). Leptin has a plethora of physiological functions such as decreasing food intake, increasing satiety, and affecting many other neuroendocrine and autonomic systems including the increase in the metabolism rate and energy expenditure (EE) (Ahima et al., 1996). Fasting decreases leptin levels in blood circulation and intraperitoneal injection of leptin during fasting has shown to prevent a delay in ovulation of female mice caused by starvation, showing that leptin directly affects the mouse estrous cycle (Ahima et al., 1996). This discovery was in line with the finding that *ob/ob* mice (lacking leptin) are infertile (Ingalls AM et al., 1950). Overall, leptin has an important role in energy homeostasis, as normal levels of leptin signal energy storage in fat cells to avoid hunger and prepare for high energy demands, whereas a low level of leptin signals a lack of stored energy, therefore promoting food-seeking and diminishes EE (Myers MG, & Leibel RL, 2015). Leptin acts through its receptor LepR (Ob-r) primarily found in the hypothalamus (H. Chen et al., 1996; Tartaglia et al., 1995).

Db/db mice which have the same phenotype as *ob/ob* mice lack the long form of leptin receptor - LepRb (Ob-Rb)- showing that this particular splicing variant is a key receptor for leptin function (H. Chen et al., 1996; G.-H. Lee et al., 1996). LepRb is an IL-6 receptor family type I receptor and its activation promotes phosphorylation of transcription factor family signal transducers and activators of transcription (STATs) (Baumann et al., 1996). STAT3 plays a predominant role in leptin to LepRb signal transduction whereas STAT5 and STAT1 are dispensable for leptin signaling (Bates et al., 2003). The binding of leptin to the LepRb isoform leads to the formation of Janus kinase 2 (JAK2) and the LepRb complex (Figure 2.2). JAK2 phosphorylates tyrosine 985, 1077, and 1138. STAT3 and STAT 5 bind to phosphorylated tyrosines on LepRb and get phosphorylated as well converting them to their active form and that translocate to the nucleus where they initiate transcription of genes targeted by leptin (Park and Ahima 2014).

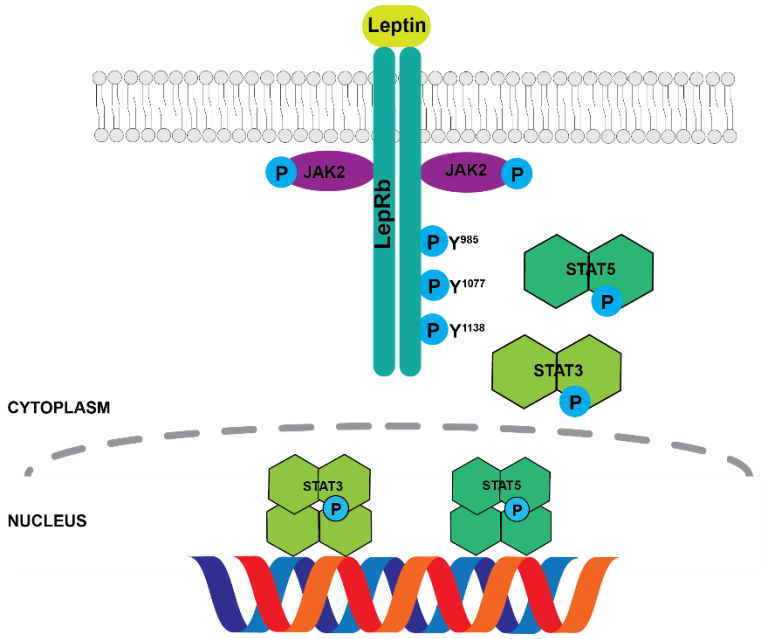

Figure 2.2. Leptin signaling through the long form of leptin receptor (LepRb).
When leptin binds to its receptor this leads to the formation of the Janus kinase 2 (JAK2)/lLepRb complex. JAK 2 phosphorylates itself and as well tyrosine amino acids at positions 985, 1077, and 1138 of the LepRb. Signal transducer and transcription activator 3 and 5 (STAT 3 and STAT5) bind to phosphorylated tyrosines. The phosphorylation of STAT3 and STAT5 makes them active and enter the nucleus where they initiate the transcription of their target genes involved in leptin signaling. Adapted from: *Leptin signaling*, Park and Ahima, Faculty of 1000 reports, 2014 (Park & Ahima, 2014).

LepRb is mostly expressed in the brain and if its expression in LepRb null mice (*db/db*) is rescued by a CNS (central nervous system) neuron-specific LEPR transgene, the physiology of *db/db* mice returns to one of the wild-type (WT) mice (de Luca et al., 2005). When LepRb is knocked down in hypothalamic neurons specifically, the phenotype of mice resembles that of *db/db* and *ob/ob* mice although it stabilizes when the mouse reaches mature age (Ring & Zeltser, 2010). Moreover, the ablation of LepRb in Vgat (vesicular GABA transporter) or NOS1 (nitric oxide synthase-1) neurons, both hypothalamic neuron subpopulations, show a phenotype similar to that observed in *db/db* mice pointing out that the hypothalamus might be the key brain region for leptin signaling (Leshan et al., 2012; Vong et al., 2011). On the other hand, ablation of LepRb in hypothalamic cell populations, such as arcuate nucleus POMC (proopiomelanocortin), AgRP (agouti-related peptide), and NPY (neuropeptide Y) expressing neurons has only a mild effect on body weight and food intake(Balthasar et al., 2004; van de Wall et al., 2008). That suggests that other hypothalamic cell populations might play a more indispensable role in obesity caused by a lack of LepRb. Additionally, leptin exerts a distinct function via these two arcuate hypothalamus

cellular populations by increasing the activity of satiety-promoting (anorexigenic) POMC neurons and decreasing the activity of feeding-promoting (orexigenic) NPY neurons (Elias et al., 1999). This suggests the potential diverse role of leptin signaling depending on LepRb expressing neuronal population specificity.

1.2.3. Thermoregulation of ob/ob and db/db phenotypes

One of the characteristics of ob/ob mice is a lower body temperature in comparison to lean mice and the fatal inability to defend the body temperature when acutely exposed to a cold environment (Mayer J. & Barnett R.J., 1953). On the other hand, acclimating *ob/ob* mice to a milder but still cool environment of 12 ˚C for 2 weeks enables them to better endure cold (Trayhurn & James, 1978). Due to decreased $T_{core,}$ one could hypothesize that *ob/ob* mice have a lower T_{core} "set point" in comparison to WT mice and therefore would choose the colder environment over the thermoneutral temperature (30˚) to defend that set point (Fischer et al., 2020). In the temperature preference test, when mice are given the freedom to explore a range of temperatures and to choose their preferred temperature, *ob/ob* mice still choose thermoneutrality as so do their WT counterparts (Carlisle & Dubuc, 1984; Fischer et al., 2016). This has led to a conclusion that it is not the "set point" that is changed in *ob/ob* mice but that the threshold for activation of certain thermoeffectors mechanisms is lowered in absence of leptin (Fischer et al., 2020). Therefore, the mechanisms of heat preservation are activated at higher temperatures than in WT mice. At subthermoneutral temperatures such as 27˚C *ob/ob* mice do have lower body temperature than WT mice, meaning they appear hypothermic (Fischer et al., 2016). Yet, at that temperature *ob/ob* mice successfully defend their body temperature and keep it stable by increasing metabolism levels which shows that leptin has an effect on the central control of T_{core} and that *ob/ob* mice are anapyrexic (exert lower T_{core}) through reduction of threshold to activate thermoeffector mechanisms. In concordance, it has been shown that inability to adapt to cold observed in *ob/ob* mice is not due to defects in heat conserving mechanisms but due to lowered heat production capacity because of flawed thermogenesis (Davis & Mayer, 1954). Moreover, the investigation of brown adipose tissue (BAT) thermogenesis has not shown a crucial difference between *ob/ob* and WT mice. However, there is an indication that white-adipose tissue lipolysis, a provider of the fuel for muscle shivering thermogenesis, is reduced in *ob/ob* mice in comparison to WTs (Dehaye et al., 1977).

The *db/db* mice also exert severe hypothermia when exposed to the cold and lowered body temperature, similar to that observed in *ob/ob* mice (Trayhurn, 1979). Unlike in the *ob/ob* phenotype, BAT

seems to be less functional than the one in WT mice shown by reduced reactivity to norepinephrine injection which is known to activate sympathetic BAT thermogenesis.

1.2.4. Leptin effect on thermoregulation

The lack of leptin in *ob/ob* mice is thought to be the cause of decreased body temperature, and indeed leptin treatment increases T_{core} of *ob/ob* mice by acute (hours), semi acute (two days), and chronic supplementation (Fischer et al., 2016; Harris et al., 1998). It has been shown that leptin does that via reducing the heat loss via tail vasoconstriction and not by increasing EE or activating thermogenesis in BAT. When food is scarce or when environmental conditions are too harsh for foraging, small mammals such as rodents are capable to enter a hibernation-like state called torpor (Geiser, 2020). Injection of leptin in *ob/ob* mice that did not receive enough food at a cold environment of 21˚C prevented torpor bouts seen in *ob/ob* pair-fed mice that did not receive leptin (Fischer et al., 2016). Therefore, leptin via its pyretic effect activated T_{core} defense without decreasing the metabolic rate. Interestingly, although intraperitoneal IP administration of leptin did not cause an increase in EE or BAT thermogenesis, the intracerebroventricular (ICV) injection of leptin did increase EE in *ob/ob* and food-deprived lean mice, and it did activate BAT in WT mice (Mistry et al., 1997; Rodríguez-Rodríguez et al., 2019). It is not known why is there a discrepancy among experiments when leptin is administered peripherally or centrally but it could be that concentrations achieved via ICV injections are much higher than the physiological ones (Fischer et al., 2020).

1.3. HYPOTHALAMIC LEPTIN RECEPTOR EXPRESSING NEURONS

1.3.1. Hypothalamic leptin receptor-expressing neurons in thermoregulation

The mRNA coding for LepRb was found expressed throughout the different brain regions such as the hypothalamus, midbrain, and brainstem (Scott et al., 2009). The strongest labeling in the hypothalamus was found in the medial preoptic area (MPA), ventromedial hypothalamic nucleus (VMH), lateral hypothalamic area (LHA), and dorsomedial hypothalamic nucleus (DMH). In addition, Zhang et al. have verified the anatomical distribution of LepRb in DMH and dorsomedial hypothalamus (DH) and the POA (Y. Zhang et al., 2011). To investigate whether LepRb expressing DMH/DHA and median preoptic area (referring to the median preoptic nucleus (MnPO) and medial preoptic area (MPA)) neurons might be involved in thermoregulation, they traced BAT projections with pseudorabies virus (PRV) and found that 34% and 33% of total PRV^+ neurons expressed LepRb in DMH/DHA and mPOA, respectively. They also showed that cold exposure of mice activates cFos expression in DMH/DHA neurons but not in mPOA.

Additionally, they found that mPOA and DMH/DH neurons project to rostral raphe pallidus (rRPa) and that mPOA Leprb neurons project directly to DMH/DHA, both of which are known thermoregulatory regions (S. F. Morrison & Nakamura, 2019). This finding suggests that LepRb expressing neurons are involved in different neuronal populations and act at different levels of thermoregulatory circuits. Another finding coming from the same laboratory showed that chemogenetic activation of LepRb neurons in MnPO promotes hypothermia by decreasing the T_{core}, energy expenditure, BAT thermogenesis, and feeding (Yu et al., 2016). Activation of these neurons also induced body extension, a thermoregulatory behavior observed in mice exposed to high environmental temperatures. In concordance with the work of Zhang et al., the authors showed that LepRb expressing MnPO neurons are activated by ambient warmth (30˚C) and not by cold, showing that these POA neurons receive information about environmental temperature. Interestingly, immunostaining against pSTAT3 (phosphorylated signal transducer and activator of transcription 3) revealed neurons in the POA activated by i.p. injection of leptin. Of those pSTAT3 positive POA neurons, 58% were expressing vesicular glutamate transporter (*Vglut2*), while only 19% were expressing *Vgat*. Moreover, activation of *Vglut2*, but not of *Vgat* expressing neurons, recapitulated the hypothermia phenotype observed when activating LepRb POA neurons, suggesting that the glutamatergic fraction of LepRb POA neurons mediates this response. Although these two papers point to the thermoregulatory role of POA neurons expressing LepRb (POA^{LepRr}), the role of leptin in modulating the activity of that that cell population in thermoregulation is not proven. Therefore Yu et al. have invested effort to research leptin signaling in POA directly and have shown that leptin has diverse effects on POA^{LepR} neurons when measured in brain slices with a whole-cell patch-clamp (Yu et al., 2018). The majority of POA^{LepR} neurons were depolarized by leptin puff or bath perfusion, as others were hyperpolarized or unaffected. Delivering leptin *in vivo* to POA locally, activated phosphorylation of STAT3 in the POA and transiently decreased feeding in mice. However, leptin delivery did not interfere with energy expenditure nor food intake at different ambient temperatures (cold, room temperature, and warmth) suggesting that leptin signaling in POA affects food intake independently of thermoregulation. Interestingly, POA-specific knockdown of LepRb did not affect body weight homeostasis and metabolic adaptations dependent on different ambient temperatures. On the contrary, LepRb knockdown did affect body weight homeostasis only during negative and positive energy balance, fasting, and high fed diet, respectively, but without affecting food intake (Yu et al., 2018).

To conclude, POA^{LepR} neurons seem to play an important role in thermoregulation by receiving peripheral input from the periphery and defending T_{core} by inhibiting BAT thermogenesis and promoting

thermoregulatory behavior to dissipate the heat but leptin signaling itself seems to primarily play a role in body weight homeostasis (Yu et al., 2016, 2018; Y. Zhang et al., 2011).

1.3.2. Action potential firing of POA^{LepR} neurons during the heat acclimation and mouse heat tolerance

In our lab, Dr. Jorg Pohle evaluated LepRb expressing neurons in POA (POA^{LepR}) neurons and their role in the heat acclimation process. By crossing the Lepr ^{Cre} line with the $^{Rosa26Lox\text{-}stop\text{-}LoxHTB}$ (HTB: H, histone-2B-tag GFP; T, TVA; B, rabies glycoprotein B19 G) he obtained the LeprCreHTB mouse line where Lepr^{+} neurons are labeled by GFP, which enabled visualization of Lepr expressing neurons (Leshan et al., 2006; Y. Li et al., 2013) (Figure 2.3.). This allowed recording of the action potential (AP) firing of POA^{LepR} neurons (Figure 2.4. A). He has found that POA^{LepR} neurons of heat acclimated mice – the ones that spend a minimum of 4 days up to 4 weeks at the constant ambient temperature of 36 ˚C - significantly increase AP firing frequency (AP FF) in comparison to POA^{LepR} neurons from mice that spent the whole time at standard housing conditions (room temperature of 23 ˚C) or only 24 hours at 36 ˚C (Figure 2.4. B). The firing of these neurons before and after acclimation was intrinsic and not affected by blocking GABA-ergic and glutamatergic synaptic transmission (Figure 2.4. E) with Gabazine (Ueno et al., 1997), CNQX, and D-AP5 (X.-H. Li et al., 2017). Following these findings, Dr. Sara Nencini did an *in vivo* heat endurance assay where she challenged mice from 4 different heat acclimation conditions by placing them at a hot temperature of 39 ˚C (Figure 2.4. C). She found that mice that have spent a longer time acclimating at 36 ˚C were better at defending their body temperature when challenged with a hot 39˚C environmental temperature (Figure 2.4. D left panel). The longer the animal spent time acclimating the longer it took for its body temperature to reach the lethal threshold of 41.5 ˚C (Figure 2.4. D right panel).

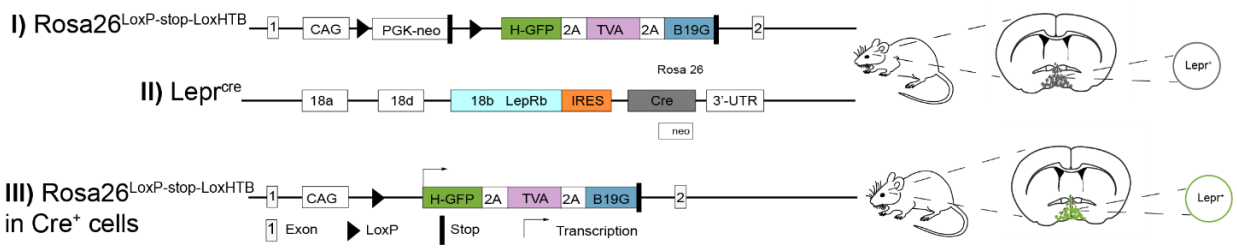

Figure 2.3. LeprCre mouse line crossed to HTB line enables visualization of Lepr expressing cells

Panel I): Coding sequences for hGFP (histone-tagged GFP to label the nuclei of recombined cells), the TVA receptor (the avian tumor sarcoma leucosis virus receptor A to allow infection with the EnvA pseudotyped rabies glycoprotein (RG)-deleted rabies virus), and the B19 G rabies glycoprotein (RG, to trans-synaptically and retrogradely spread the virus to presynaptic neurons) are joined by 2A cleavage peptide and a LoxP flanked stop cassette was placed in front

of them. This mouse line was originally designed for transsynaptic tracing of the neural circuits; TVA, the avian tumor virus receptor A to allow infection with the pseudotyped RG-deleted rabies virus envelope glycoprotein EnvA. **Panel II):** Coding sequences for Cre recombinase were placed into the 3'UTR region of the *LRb* exon, rendering Cre expression under the control of the mRNA encoding *LRb*. **Panel III)**: In the presence of Cre recombinase, transcription of the open reading frame (ORF) is enabled and hGFP, the TVA receptor, and the B19 G rabies glycoprotein are expressed. Adapted from: *Leptin Receptor Signaling and Action in the Central Nervous System Leshan et al.Obesity, 2006, and from Molecular layer perforant path-associated cells contribute to feed-forward inhibition in the adult dentate gyrus*, Li et al. 2013, PNAS (Leshan et al., 2006; Y. Li et al., 2013).

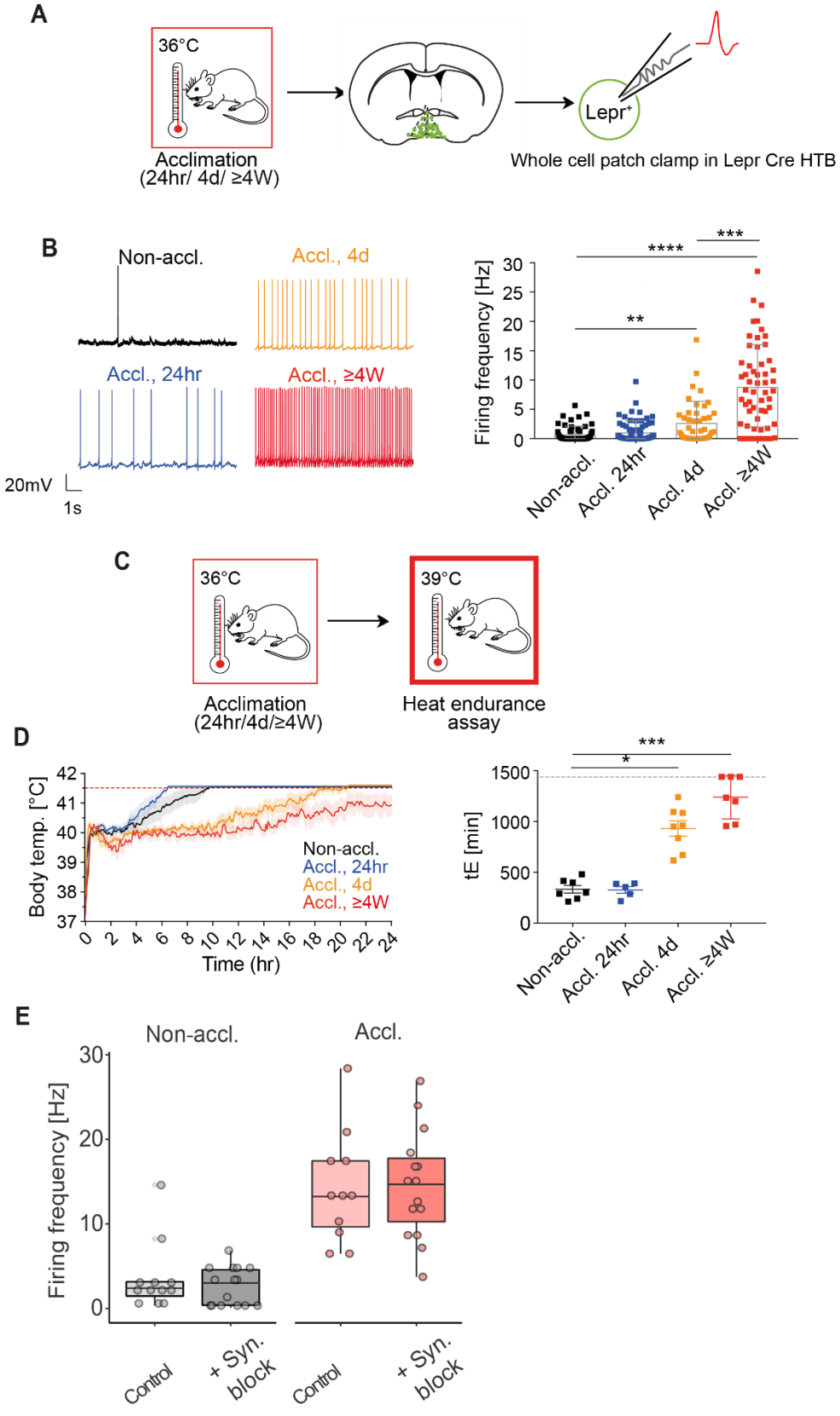
A
36°C
Acclimation
(24hr/ 4d/ ≥4W)
Lepr+
Whole cell patch clamp in Lepr Cre HTB
B
Non-accl.
Accl., 4d
Accl., 24hr
Accl., ≥4W
20mV
1s
Firing frequency [Hz]
Non-accl.
Accl. 24hr
Accl. 4d
Accl. ≥4W
C
36°C
39°C
Acclimation
(24hr/4d/≥4W)
Heat endurance
assay
D
Body temp. [°C]
Time (hr)
Non-accl.
Accl., 24hr
Accl., 4d
Accl., ≥4W
tE [min]
E
Non-accl.
Accl.
Firing frequency [Hz]
Control
+ Syn. block

Figure 2.4. AP firing frequency of POA^{LepR} neurons during the heat acclimation and mice heat tolerance
(A) Cartoon depicting the acclimation procedure of LeprCreHTB mice to heat (36 ˚C). Acute brain slices from LeprCreHTB mice acclimated and non-acclimated to heat (mice housed at room temperature) were used for whole-cell patch-clamp electrophysiology for action potential firing frequency (AP FF) recording. **(B)** Example traces from AP recordings belonging to 4 different conditions: Non_accl. = room temperature mice (black); Accl. 4d (Acclimated 4 days at 36˚C; orange), Accl. 24h (Acclimated 24 hours at 36˚C; blue) temperature) and Accl. ≥4W (Acclimated ≥4 weeks at 36˚C; red). The right panel shows the firing frequency of cells responding to each condition. (n= 42/5: 42 neurons from 5 mice) per group. Kruskal-Wallis test, P <0.0001; Dunn's multiple comparisons test; P=0.0062 (Non-acclimated : Accl.4d), P<0.0001 (Non-accl. : Accl. ≥ 4 weeks/full acclimation), P=0.0005 (Accl. 4d : Accl.≥ 4 weeks). Brain slices were recorded at 33°C bath temperature. **(C)** After heat acclimation mice were subjected to the heat endurance assay. **(D)** Left panel: Average body temperature of non-acclimated (black, n=7), 24 hr (blue; n=5), 4 days (orange; n=8) and 4-5 weeks (red; n=7) acclimated animals in the heat endurance assay monitored for a maximum of 24 hr or until the animal reached the cut-off temperature of 41.5°C (dashed red line). Right panel: Average endurance time (t_E, min) of mice shown on the left. Cut-off time: 24 hr (dashed grey line). Kruskal-Wallis test, P<0.0001; Dunn's multiple comparisons test; P=0.0262 (Non-accl. : Accl. 4d), P=0.0006 (Non-accl. : Accl. ≥ 4 weeks). Data represent mean ± S.E.M. **(E)** Fast synaptic transmission blockers (CNQX 10 µM, D-APV 50 µM, and Gabazine 5 µM) do not affect AP firing rates in non-acclimated and acclimated POA^{LepR} neurons in *ex vivo* brain slices. Data obtained by Dr. Sara Nencini (data in panel B and C), Dr. Jörg Pohle (data in panel B) and Dr. Wojciech Ambroziak (data in panel E). The figure was made by Dr. Sara Nencini (panels A-D) and Dr. Wojciech Ambroziak (panel E) and it is a part of a manuscript that is currently under revision process.

In addition, my colleagues wanted to verify if the acclimation-induced AP firing increase in the POA^{LepR} is needed for heat endurance developed after heat acclimation. They used a neuronal silencing technique via virally delivered Cre-dependent tetanus toxin light chain (TeTxLC) (Sweeney et al., 1995) to the POA of LepR-Cre mice before heat acclimation (Figure 2.5.). TeTxLC-silenced animals performed worse in the heat acclimation process (Figure 2.5. B) as several animals reached a lethal 41.5 ˚C during the first 2 days of the 36 ˚C acclimation protocol. Other TeTxLC-silenced animals failed earlier in the endurance assay test in comparison to control virus-injected animals (Figure 2.5. C-E). Although this experiment pointed out the importance of POA^{LepR} neurons output activity in mouse heat acclimation and heat endurance performance, it did not directly show that action potential firing of POA^{LepR} is strictly necessary for better heat endurance developed after heat acclimation. Therefore, my colleagues performed another set of experiments using chemogenetic interference with POA^{LepR} firing. For this, they injected virus-containing Cre-dependent inhibitory G-protein coupled Designer Receptors Exclusively Activated by Designer Drugs (Gi-DREADD) into the POA of LepR-Cre mice. After the Cre-dependent recombination, POA^{LepR} neurons express Gi-DREADD which can be activated by delivery of exogenous ligand clozapine N-oxide (CNO)and

will consequentially decrease the firing of neurons (Miao et al., 2015). CNO was delivered during the 39˚C heat endurance assay due to which LepR-Cre animals failed to maintain stable T_{core} and endure the heat challenge. (Figure 2.5. F-H). This led to the conclusion that AP firing of POA^{LepR} neurons is needed for heat endurance developed after heat acclimation.

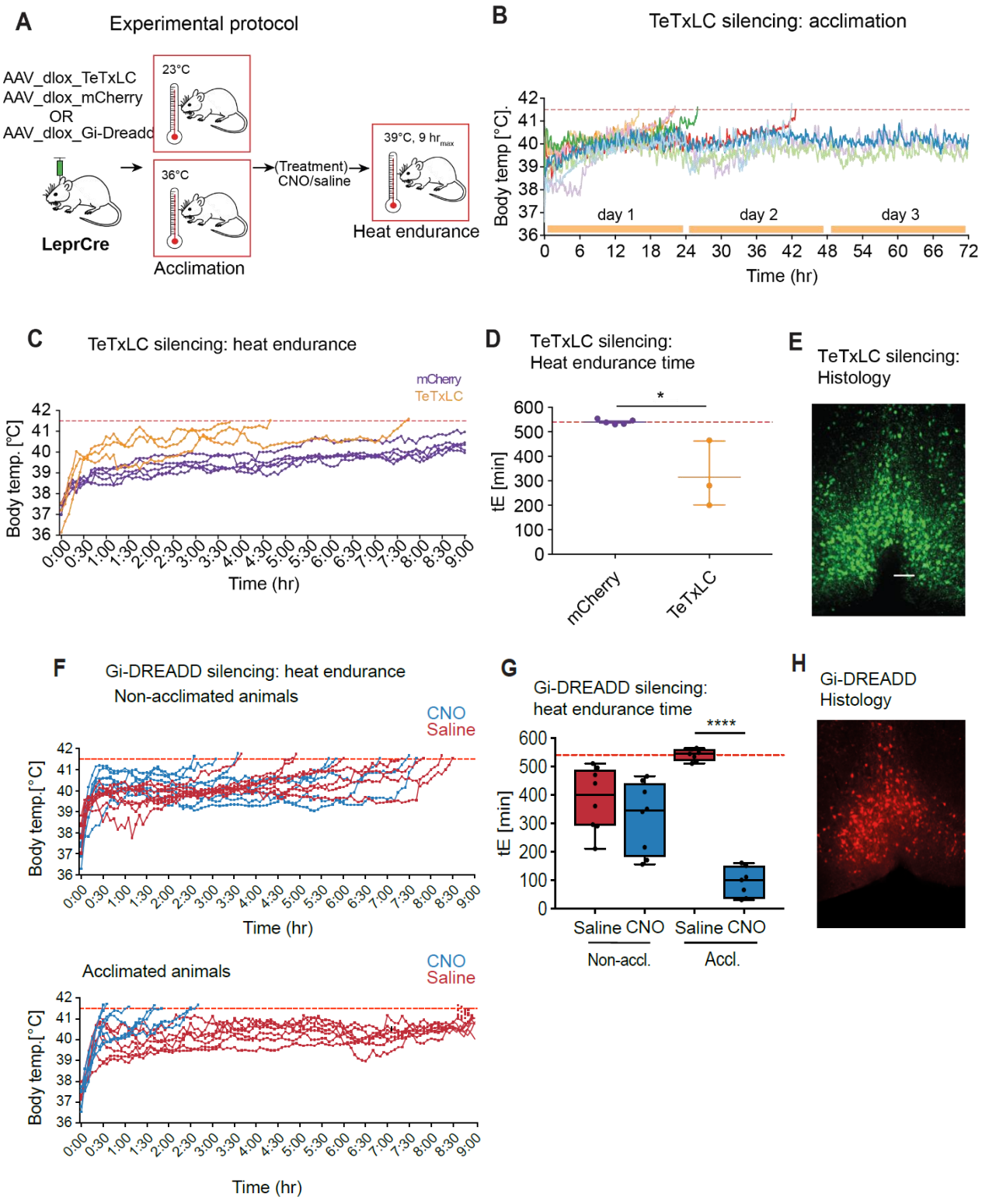

Figure 2.5. Silencing of POA^{LepR} activity impairs acclimation and prevents heat tolerance

(A), Schematic showing the two different experimental approaches to interfere with POA^{LepR} activity. LepR-Cre animals were injected in the POA with Cre-dependent TeTxLC- or Gi-DREADD viral particles to permanently eliminate

synaptic output from POA^{LepR} neurons or to temporarily silence POA^{LepR} activity, respectively. **(B)** Body temperature traces of individual animals injected with TeTxLC are shown during the first 3 days of heat acclimation (36°C). 6 out of 9 animals with silenced POA^{LepR} outputs failed during the first two days of acclimation and reached the T_{core} cut-off of 41.5°C (demarcated by the dashed red line). **(C)**, TeTxLC silenced animals that completed the 30-day heat acclimation (36°C) (n=3) were tested together with heat acclimated mCherry virus-injected control animals (n=5) in the heat endurance assay (39˚). **(D)**, Average endurance time (tE, min) for the two groups shown. Mann Whitney test; P=0.0262 (mCherry : TeTxLC). Endurance assay was terminated after 9 hours. **(E)**, Representative image of POA^{LepR} neurons labeled with mCherry that is co-expressed together with TeTxLC. Scale bar size: 250 µm. **(F)**, Heat endurance assay of Gi-DREADD infected mice. Non-acclimated (top panel) or acclimated (bottom panel) animals were injected either with CNO (0.3 mg/kg i.p.) or saline 10 min before the assay and the body temperature was continuously monitored. Non-acclimated animals did not endure the heat challenge assay, independently of whether they received CNO or vehicle (saline). In acclimated mice, CNO injection (but not saline injection) eliminated acquired heat tolerance and the animals quickly reached the cut-off temperature (41.5°C). **(G)**, Average endurance time (tE) for the groups shown on the left. Kruskal-Wallis test, P<0.0001; Dunn's multiple comparisons test; P<0.0001 (Accl. Saline: CNO); n= 8 animals for Non-acclimated groups and n=7 for Acclimated groups. **(H)**, Representative image of POA^{LepR} neurons labeled with eYFP (enhanced yellow fluorescent protein) that is co-expressed together with Gi-DREADDs; scale bar: 250 µm. Boxplots show median and interquartile range. Data was obtained by Dr. Sara Nencini and Dr. Jörg Pohle. The figure was done by Dr. Sara Nencini and it is part of a manuscript that is currently under revision process.

2. AIMS

Acclimation is a phenotypic adaptation, which, unlike other immediate physiological reactions of the nervous system to the changes in the environment, takes more time to develop (Khlebovich 2017). In other words, acclimation is a biological trait of adaptation to changes in the environment that persist longer e.g. temperature, humidity, and food availability, and it is achieved through a change in gene activity. Heat acclimation, however, is a process of phenotypic adaptation to a temperature change in the environment resulting in the achievement of a thermo-tolerant phenotype marked by lowered thresholds for activation of the heat dissipation mechanism (Horowitz, 2007). Development of this phenotype is achieved through the variety of changes at a molecular, cellular, and organ level of the organism. The preoptic area of the hypothalamus (POA) is considered to be the key brain region in orchestrating the T_{core} defense and body temperature homeostasis (S. F. Morrison & Nakamura, 2019; S. Morrison F. & Nakamura, K, 2011). Being the thermoregulatory center, POA is believed to play an important role in regulating the heat acclimation process (Pierau et al., 1998; Schwimmer et al., 2006).

My colleagues found that, after mice spend 4 days up to 4 weeks at a constant temperature of 36 ˚C, they become better at enduring heat challenges (usually lethal 39 ˚C), and POA leptin receptor-expressing neurons (POA^{LepR}) exhibit increased action potential firing frequency (AP FF) (Figure 2.4). This led to the hypothesis that the increase in firing frequency of POA^{LepR} neurons could be facilitating heat acclimation and therefore enabling mice to a better heat endurance *(Nencini S., Ambrozak W., Pohle J., et al. Unpublished Manuscript)*. Moreover, during the silencing of POA^{LepR} firing by Gi-DREADD expression in POA^{LepR} neurons mice failed to endure heat during the challenge of 39˚C (Figure 2.5 F-H). This result further strengthened the hypothesis that increased AP FF of POA^{LepR} after heat acclimation is necessary to develop improved heat endurance following heat acclimation.

Moreover, I hypothesized that the molecular changes in the POA^{LepR} neurons are the cause of increased firing frequency in POA^{LepR} neurons during heat acclimation. The encouragement to this hypothesis was the result that the application of synaptic blockers does not affect the firing of these neurons, neither before nor after heat acclimation. Therefore, investigating those changes would shed light on the mechanism of why LepR expressing POA neurons seem to be necessary for heat acclimation and more generally elucidate the general role of POA in this homeostatic process.

Therefore, I decided to investigate the transcriptional changes happening in the POA^{LepR} neurons during the heat acclimation process. In order to accomplish this, I took advantage of the LeprCreHTB line (Figure 2.3) for fluorescence-activated cell sorting (FACS) of POA^{LepR} cells followed by RNA sequencing.

The specific questions I wanted to address with this approach were:

1) Which transcriptional changes happen in the POA^{LepR} neurons during the heat acclimation?

2) Do any molecules found differentially expressed before and after acclimation modulate POA^{LepR} neurons' action potential firing frequency?

3) Can I deduct the function that POA might have in heat acclimation from molecular changes found?

3. RESULTS

3.1. ANATOMICAL DISTRIBUTION OF LEPR NEURONS IN THE POA

It has been shown by others before that heat acclimation induces neuronal proliferation in rat hypothalamus already after 5 days of heat acclimation of 32˚C (Matsuzaki et al., 2009). After 33 days of heat acclimation, the novel cells have been shown to differentiate into mature neurons by co-staining a marker of proliferating cells bromodeoxyuridine (BrdU) and marker of mature neurons NeuN. Since the protocol of heat acclimation I used in my experiments had an even higher temperature and lasted for almost 30 days, I wondered if the number of neurons in the POA of mice also increases due to heat acclimation and if the number of LepR neurons is changed. For that reason, I wanted to quantify specifically the number of neurons expressing both LeprR and NeuN. In addition, we knew from the work of others how the LepR neurons anatomically distribute in the POA (Scott et al., 2009; Yu et al., 2016; Y. Zhang et al., 2011) but I wanted to verify if the LeprCre line crossed with HTB truthfully recapitulates previous findings. Since POA^{LepR} neurons change the AP firing frequency most drastically after ≥4 weeks at 36 ˚C heat acclimation, I compared IHC staining in POA sections of acclimated to the non-acclimated mice, to verify that the anatomical pattern and the number of LepR neurons within the POA remain the same after heat acclimation.

To re-evaluate the anatomical distribution of Lepr$^+$ neurons in POA I collected brain tissue from non-acclimated (housed at standard housing conditions, room temperature ≈23 ˚C) and acclimated (housed for ≥4 weeks at 36 ˚C) LeprCreHTB adult animals and did immunohistochemistry (IHC) on free-floating POA sections. Sections that I collected for representation of the POA region were spanning the area starting with position Bregma 0.5 mm and ending with Bregma 0.10 mm going from anterior to posterior brain axis according to Paxinos mouse brain atlas (Figure 2.6. A)**.** For this IHC I collected 30 µm thick sections, corresponding to anatomical bregma positions described above and I incubated them with primary antibodies raised against GFP and neuronal marker NeuN.

Figure 2.6. B) shows an example expression pattern in the POA of a mouse that was housed at room temperature (Non-acclimated) and that was housed for ≥30 days at 36˚C (long-term acclimated). From these examples and other processed tissue, I concluded that the anatomical distribution of LepR$^+$ neurons in the POA appeared to remain the same after heat acclimation. In addition, I quantified the overlap of LepR (GFP) and NeuN in both conditions (Number (Lepr$^+$NeuN$^+$) = mean±SEM=81,35 ± 3,006 and 82,64 ± 2,303 in Non-acclimated and Acclimated conditions, respectively, two-tailed t-test p=0.9473).

The percent of double-positive LEPR^{+}NeuN^{+} neurons remained unchanged after ≥4 weeks of 36 ˚C heat acclimation (Figure 2.6. C).

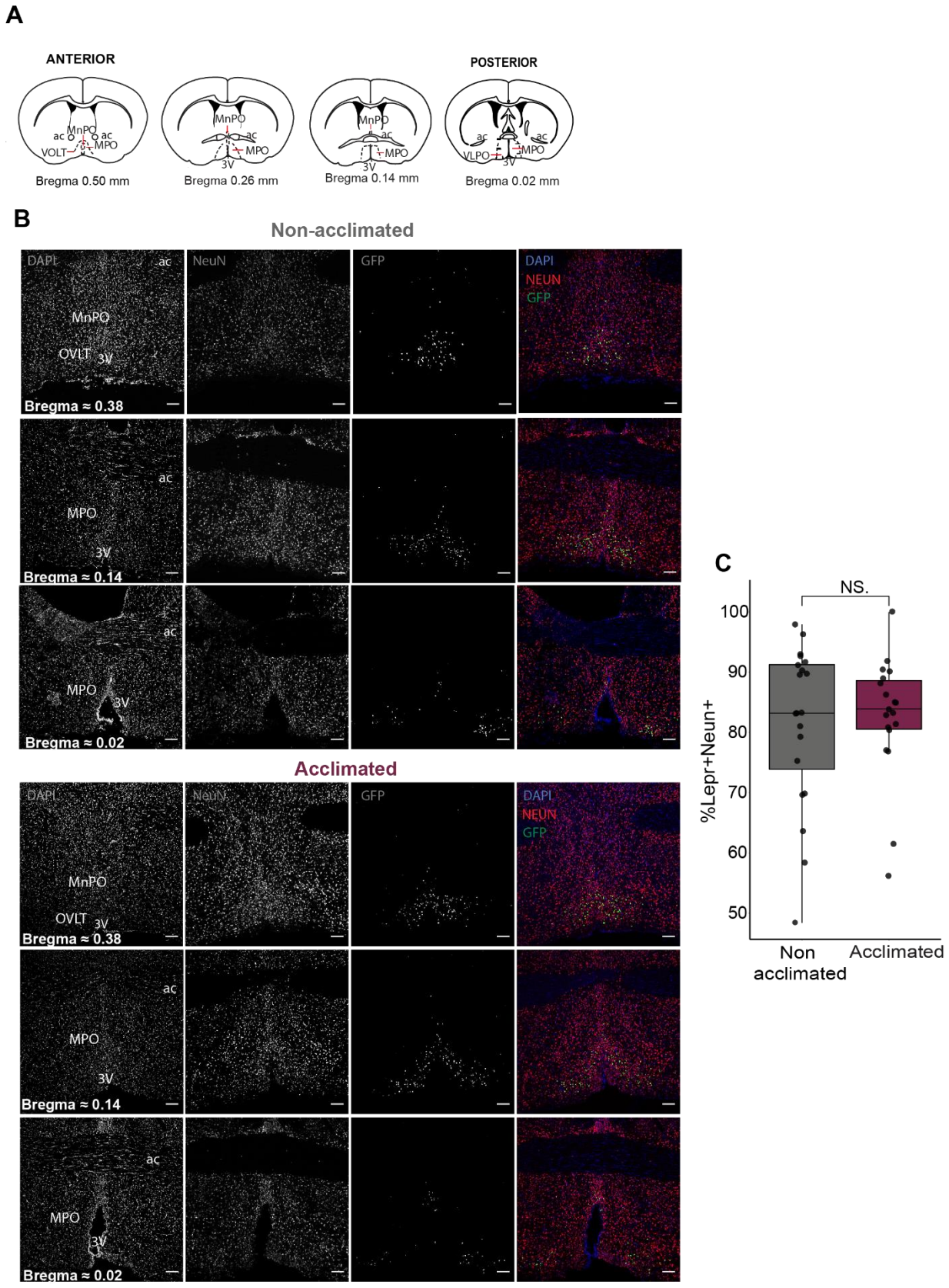
A
ANTERIOR
POSTERIOR
MnPO
ac
MPO
VOLT
3V
VLPO
Bregma 0.50 mm
Bregma 0.26 mm
Bregma 0.14 mm
Bregma 0.02 mm
B
Non-acclimated
DAPI
NeuN
GFP
NEUN
OVLT
Bregma ≈ 0.38
Bregma ≈ 0.14
Bregma ≈ 0.02
Acclimated
C
NS.
%Lepr+Neun+
100
90
80
70
60
50
Non acclimated
Acclimated

Figure 2.6. Number of POA^{LepR} in the POA before and after heat acclimation

(A) Map of POA region adapted from Paxinos brain atlas (Anterior to posterior). **(B)** Representative images of IHC staining (top to bottom=anterior to posterior) of POA sections were obtained from non-acclimated and acclimated (>4 weeks at 36 ˚C) LeprCreHTB mice stained against DAPI, GFP (LepR), and NeuN. Scale bar represents 100 µm, images taken with 10x objective at a confocal microscope. **(C)** Quantification of double-positive LEPR$^+$NeuN$^+$ cells by each obtained section (n=20 vs n=19, non-acclimated vs acclimated condition respectively (N=3 vs N=3 mice) plotted as a % of double-positive LEPR$^+$NeuN$^+$ of all LEPR$^+$ cells. Statistical significance is calculated by unpaired, two-tailed t-test; NS p=0.9473 (mean± SEM =81,35 ± 3,006 and 82,64 ± 2,303 in Non-acclimated and Acclimated conditions, respectively). Each dot on a boxplot represents a quantified section, the upper and lower hinge of a box represent the first and third quartiles (the 25th and 75th percentiles) and a middle hinge represents the median. The upper and lower whisker extend from their respective hinges to the largest and lowest value no further than 1.5 x IQR (inter-quartile range). Data beyond the end of the whiskers are representing the outlying points. ac Anterior commissure; MnPOA Median preoptic nucleus; MPO Medial Preoptic Nucleus; IHC Immunohistochemistry.

3.2. FACS SORTING AND BULK RNA SEQUENCING OF POA^{LEPR} NEURONS FROM NON-ACCLIMATED AND ACCLIMATED MICE

To gain insight into transcriptional changes that happen in the POA^{LepR} neurons during heat acclimation, I decided to use the FACS sorting technique to obtain bulks of POA^{LepR} cells and isolate their mRNA for sequencing. I could visualize POA^{LepR} neurons via GFP expression in the LeprCreHTB line where LepR neurons are labeled by histone-2B-GFP (described in Figure 2.3).

In the adult brain, perineuronal nets made of chondroitin sulfate proteoglycans engulf neurons somas, and dendrites (Horii-Hayashi et al., 2015). Therefore, cell trituration and dispersion from the adult mouse brain tissue can result in a low neuronal survival rate. To increase the neuronal survival rate for fluorescence-activated cell sorting (FACS) I applied a protocol for neuronal dissociation which employs enzymes to digest extracellular matrix glycoproteins resulting in an increased cell survival rate (Moffitt et al., 2018).

For each sorting round, I collected brains from a total of 3 LeprCreHTB male and/or female mice, dissected the POA, triturated the tissue to dissociate the cells, and did FACS sorting of GFP$^+$ and GFP$^-$ cells. I repeated the procedure with the POA tissue obtained from mice under 3 different conditions: non-acclimated (NA, RT 23˚C), short-term acclimated (STA; 4-5 days at 36˚C), long-term acclimated (LTA, ≥4 weeks at 36˚C). Later on, I used FACS-sorted samples for the RNA sequencing (Figure 2.7. A). In order to distinguish between living and dead cells during the cell sorting, I used propidium-iodide (PI) which enters the cell if it has a compromised plasma membrane. After that, PI intercalates with the double-stranded

DNA and stains the cell (Riccardi & Nicoletti, 2006). The cell survival rate in the POA dissociated samples was ranging from 60%-90% and did not differ among the 3 acclimation conditions (Figure 2.7. B).

Gating for the GFP$^+$ cell population was determined based on GFP and PI fluorescence intensity (Figure 2.7. C). GFP$^+$ population was spreading towards higher values of fluorescent intensity on the GFP scale looking at samples coming from NA to LTA conditions (Figure 2.7. C; top to bottom). Indeed, flow cytometry analysis showed that GFP intensity was significantly different between samples obtained from non-acclimated LeprCreHTB animals, where it was the lowest (Mean ±STD = 3.6 ±0.13), to samples obtained from long-term acclimated animals, where it was the highest (Mean ±STD= 6.5 ±0.68). (Figure 2.7. D; left-most panel). The same trend was observed and was statistically significant for forward scatter (FSC, parameter determining the cell size) and side scatters (SSC, parameter determining the cell granularity) parameters of the analyzed GFP$^+$ population (Figure 2.7. D; middle panels).

Interestingly, although all of the samples were prepared as reproducibly as possible, the percent of GFP$^+$ cells from all the surviving (PI$^-$) cells was significantly lower in the STA condition in comparison to the NA and LA conditions among which there was no statistically significant difference observed (Figure 2.7. D; right-most panel). This suggested the potential technical problems occurring while obtaining neurons from STA-treated mice, or, since the approach to obtain neurons was held consistent among the preparations, more likely the biological differences (see the discussion section).

By neuronal dissociation followed by the FACS sorting, I obtained 5 samples from NA and LTA conditions and 8 samples from the STA condition. Each sample was sorted into a GFP$^+$ and GFP$^-$ population. This resulted in 36 samples in total for RNA sequencing.

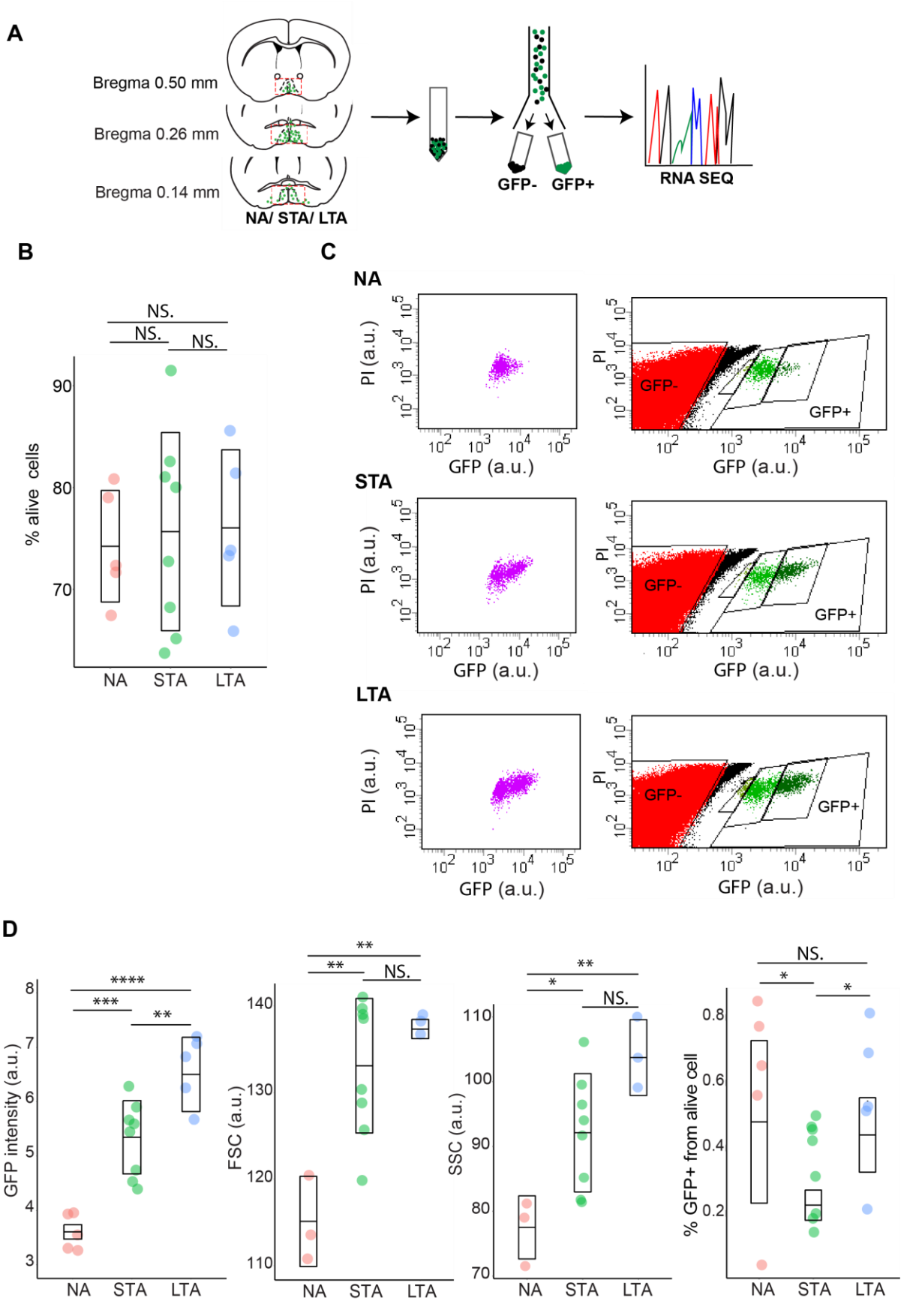
A
Bregma 0.50 mm
Bregma 0.26 mm
Bregma 0.14 mm
NA/ STA/ LTA
GFP-
GFP+
RNA SEQ
B
% alive cells
NS.
NS.
NS.
NA
STA
LTA
C
NA
STA
LTA
PI (a.u.)
GFP (a.u.)
GFP-
GFP+
D
GFP intensity (a.u.)
FSC (a.u.)
SSC (a.u.)
% GFP+ from alive cell
****
***
**
NS.
*

Figure 2.7. Fluorescence-activated cell sorting (FACS) of LepR neurons for RNA sequencing

(A) Scheme of the FACS sorting procedure**:** 3 depicted brain sections were collected in each FACS sorting round from 3 LeprCreHTB mice that were or non-acclimated (NA), short-term acclimated (STA) or long-term acclimated (LTA). POA (red square) containing LEPR$^+$ cells (green dots) was dissected and triturated. Cells were sorted according to GFP fluorescence into GFP positive (GFP$^+$) and GFP negative (GFP$^-$) bulk cell samples used for RNA sequencing. **(B)** Flow cytometry evaluation of % of live cells - propidium iodide negative (PI$^-$) - from all events in each dissociated cells sample. Statistical significance was calculated with way ANOVA followed by Tukey's multiple comparisons; NA: STA NS. p=0.950, NA: LTA NS. p=0.9366, STA: LTA NS. p=0.9967. Box represents the mean (middle line) and ± standard deviation of the mean (upper /lower hinge. NA (mean ± SD =74.24 ± 5.477, N=5); STA (mean ± SD = 75.68±9.73, N=8); LTA (mean ± SD = 76.04 ± 7.67, N=5). **(C) Left panel,** flow cytometry example dot-plots of PI$^-$ and GFP$^+$ population of cells coming from non-acclimated NA, STA, and LTA LeprCreHTB mice. Purple dots represent the GFP$^+$ population selected for sorting (PI$^-$ and GFP$^+$ events). **(C) Right panel,** flow cytometry example dot-plots of PI$^-$ and GFP$^+$ (green dots) and GFP$^-$ (red dots) population selected for cell sorting, corresponding to the dot-plots in the left panel. Black dots represent events left out from sorting as a measure of precaution to avoid false positive and false negative events. Regions within the GFP$^+$ box present the division of the GFP$^+$ population into cells with lower and higher GFP fluorescence intensity. **(D)** Flow cytometry parameters measured for NA, STA, and LTA of GFP$^+$ sorted samples used for RNA sequencing. Statistical significance is calculated by One way ANOVA followed by Tukey's multiple comparisons. Box represents the mean (middle line) and ± standard deviation of the mean (upper /lower hinge). Each point represents a sample for which quantification has been done. **GFP intensity:** NA:STA ***p=0.0003, NA:LTA ****p < 0.0001, STA:LTA **p=0.0091; NA (mean ± SD =3.606 ± 0.1316, N=5); STA (mean ± SD =5.346 ± 0.6733, N=8); LTA (mean ± SD =6.5 ± 0.6828, N=5); **FSC (Forward Scatter)**: NA:STA **p=0.0052, NA:LTA **p=0.0044, STA:LTA NS.p=0.6231; NA (mean ± SD=115.1 ± 5.212, N=3); STA (mean ± SD =133.1 ± 7.774, N=8); LTA (mean ± SD =137.3 ± 1.111; N=3); **SSC (Side Scatter)**: NA:STA *p=0.0497, NA:LTA **p=0.0052, STA:LTA NS.p=0.1250; NA (mean=77.5 ± 4.874; N=3; STA (mean ± SD = 92.1 ± 9.129; N=8; LTA (mean ± SD =103.7±5.856; N=3), **%GFP$^+$ from alive cells**: NA:STA *p=0.0194, NA:LTA NS.p=0.901, STA:LTA *p=0.0495; NA mean ± SD =0.48 ± 0.249; N=5; STA (mean ± SD =0.225 ± 0.046; N=8); LTA (mean ± SD =0.44 ± 0.114; N=5). a.u.= arbitrary units

Next, I isolated the RNA from each sample by using the Qiagen microRNA kit (described in the methods section). I first assessed the RNA quality and quantity of the isolated RNA via the RIN algorithm (RNA integrity number) using Bioanalyzer Eukaryote Total RNA Pico chip (Masotti & Preckel, 2006). at the Gene Core facility at EMBL, Heidelberg (Figure 2.8.). RIN algorithm is a standardized way to calculate the RNA integrity from the electropherogram (Imbeaud, 2005). It calculates the ratio of the area under the 28S and 18S ribosomal RNA peaks to the whole area under the graph (Figure 2.8. A); the higher RIN number represents less RNA degradation. The samples which had low RIN numbers (Figure 2.8. B), in the range from RIN= 0 (non-determined) to RIN=1.25, were 4/8 samples belonging to the STA condition. These were

later included in sequencing because they still yielded a good cDNA library as shown by Bioanalyzer High Sensitivity DNA Assay (Agilent Technologies, 2009) (Figure 2.8. A).

After determining the RNA quality of the samples I prepared a cDNA library (examples in Figure 2.8. C) for each of the 36 samples and pooled the cDNA in 2 batches for RNA sequencing (Figure 2.8. D). Sequencing was performed by the Gene Core staff on Illumina NGS sequencing platform; Next-seq High on 2 flowcells with 75 base pair, single end readout.

After obtaining the results of RNA sequencing I did quality control of RNA sequencing reads with the FastQC tool (Steven W. Wingett & Simon Andrews, 2018) and transcriptome indexing followed by transcripts quantification using the Salmon package (Patro et al., 2017). Next, I assessed the counts of the *Egfp* and *Lepr* gene transcripts in each sample and according to each sorted pair of GFP$^-$ and GFP$^+$ cell populations (Figure 2.8. E). Detected levels of both *Egfp* and *Lepr* genes were higher in samples sorted as GFP$^+$ than in the ones sorted as GFP$^-$ with average normalized counts for *Egfp* being 92.63 and 622.05 and for *Lepr* 54.06 and 1226.30 in samples sorted as GFP$^-$ and in samples sorted as GFP$^+$, respectively. When comparing the counts in each sample from each acclimation condition according to GFP fluorescence only expression levels of *Lepr* gene in the NA condition were not significantly different between GFP$^-$ and GFP$^+$ samples. This might be due to one GFP$^-$ sample in NA condition (grey circled symbol) which had high expression of *Lepr* gene. Nevertheless, the GFP$^+$ sample pair corresponding to the questionable NA GFP$^-$ sample still showed higher expression of the *Lepr* gene (green circled symbol).

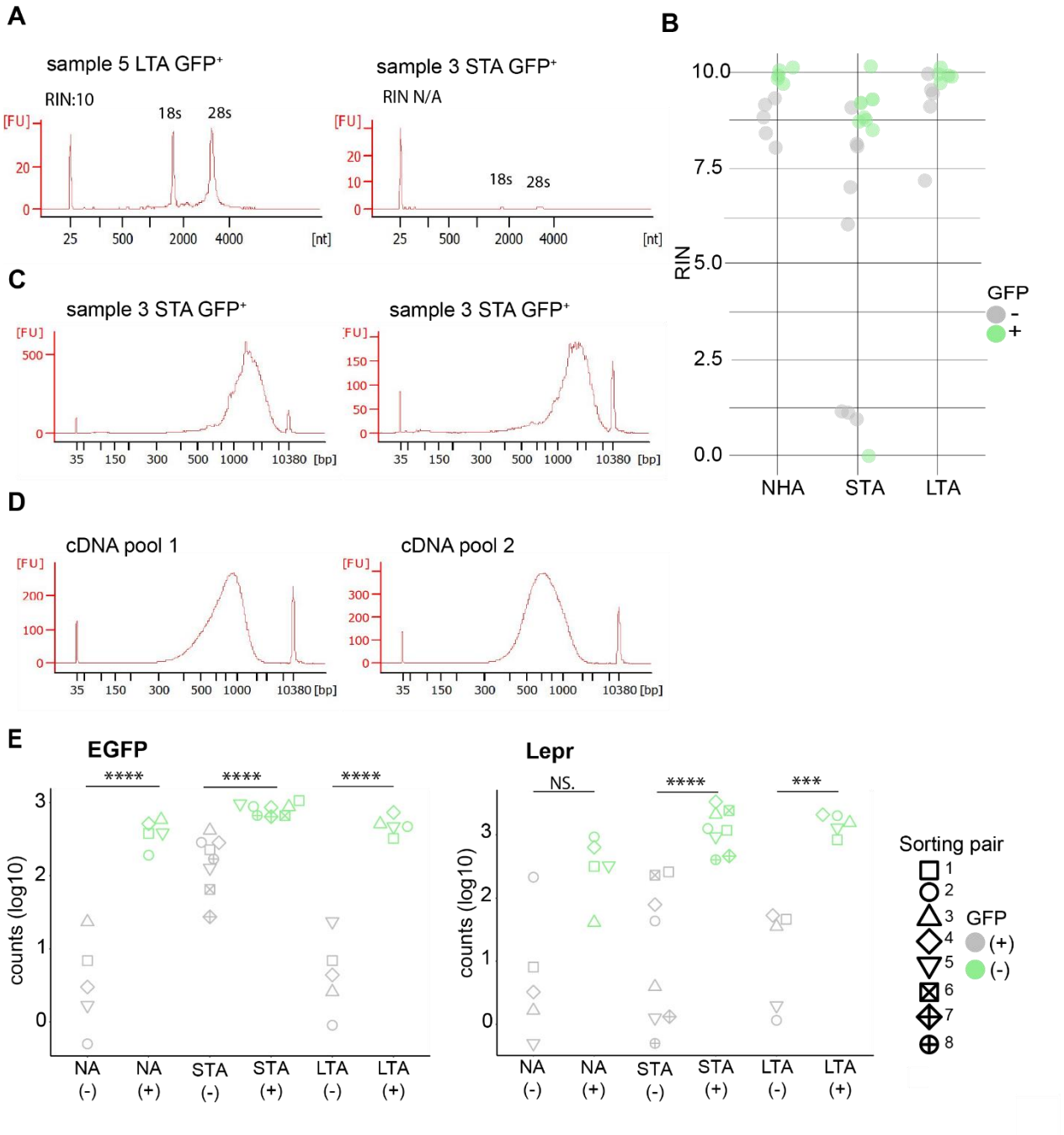

Figure 2.8. Quality control of RNA samples and RNA sequencing data set

(A) Example of Bioanalyzer RNA pico chip trace (left) and RIN level of all the samples per condition (right). **(B)** RIN numbers were determined via Bioanalyzer Eukaryote Total RNA Pico chip of each sorted sample. **(C)** Example of Bioanalyzer High Sensitivity DNA Assay traces from 2 STHA cDNA samples with low RIN numbers. **(D)** Bioanalyzer High Sensitivity DNA Assay traces of final pooled cDNA used for sequencing. **(E)** mRNA expression levels (log10 counts) of *Egfp* (left panel) and *Lepr* (right panel) in GFP$^+$ vs GFP$^-$ FACS-sorted, RNA-sequenced samples. Each symbol represents one sorted pair; GFP$^+$ and GFP$^-$ samples coming from the same bulk of cells (prepared from the same tissue). Green and gray colors represent GFP$^+$ and GFP$^-$ samples, respectively. NA (Non-acclimated), STA (short-term acclimated),

LTA (Long.-term acclimated). Statistics was calculated using On-way ANOVA with Sidak's multiple comparison test: EGFP counts; NA (GFP-):NA (GFP+) ****, p<0,0001, STA (GFP-):STA (GFP+) ****, p<0,0001, LTA (GFP-):LTA (GFP+) ****, p<0,0001; Lepr counts; NA (GFP-):NA (GFP+) NS., p=0.58, STA (GFP-):STA (GFP+) ****, p<0,0001, LTA (GFP-):LTA (GFP+) ***, p=0,0004.

3.2.1. Differential expression and gene set enrichment analysis of RNA sequencing data

Next, I performed a principal component analysis on the RNA sequencing data by using a function from R based package DESeq2 (Love et al., 2014). The PCA plot in Figure 2.9. A) showed that two principal components in the obtained RNA seq data set are the GFP phenotype and the acclimation. For example, it shows that all the GFP$^+$ samples are grouped to the right side of the PCA plot, and then these are further separated to the bottom and top of the plot depending if samples are coming from non-acclimated or acclimated mice, respectively.

To look at the differential gene expression between samples coming from NA, STA, and LTA samples I performed a differential gene expression analysis with the help of Dr. Silvia Calderazzo (DKFZ) who designed the statistical approach for the analysis. I wanted to extract from the obtained data the differences between NA, STA, and LTA conditions, taking into account the GFP + and - phenotype. The DE analysis done in DESeq2 (Love et al., 2014) resulted in 386 significant (p-adjusted value ≤ 0.1) differentially expressed genes (DEGs) among NA and LTA conditions, 562 DEGs between NA and STA conditions, and 96 DEGs between STA and LTA.

The heatmap in Figure 2.8. B) represents the expression of 150 significant DEGs (in rows; top 50 according to p-adjusted value from 3 comparisons NA:LTA; NA:STA; STA:LTA) in each of 36 samples (columns) from 3 conditions (top 50 DEGs from3 comparisons are listed in Table 2 (in Appendix, page 161). The samples cluster primarily according to the GFP phenotype, followed by clustering of GFP$^+$ samples according to acclimation treatment. Moreover, the major differences between GFP$^+$ samples (the POA^{Lepr} neurons) seem to be coming from 3 different acclimation conditions. Whereas the majority of the genes increase their expression levels from NA towards STA and to LTA (upper part of the heatmap in GFP$^+$ samples), others decrease the expression level from NA to STA and LTA (middle part of the heatmap in GFP$^+$ samples).

The additional step of the precaution in the analysis was to check whether there are certain confounding effects brought to the data set by experimental design- the so-called batch effect (Liu & Markatou, 2016). The variables that can cause the batch effects in the RNA sequencing experiments, such as cDNA library processing groups, pools of the cDNA samples, and the number of sorted cells per sample seemed not to be affecting the sample clustering on the heatmap with the most significant DEGs.

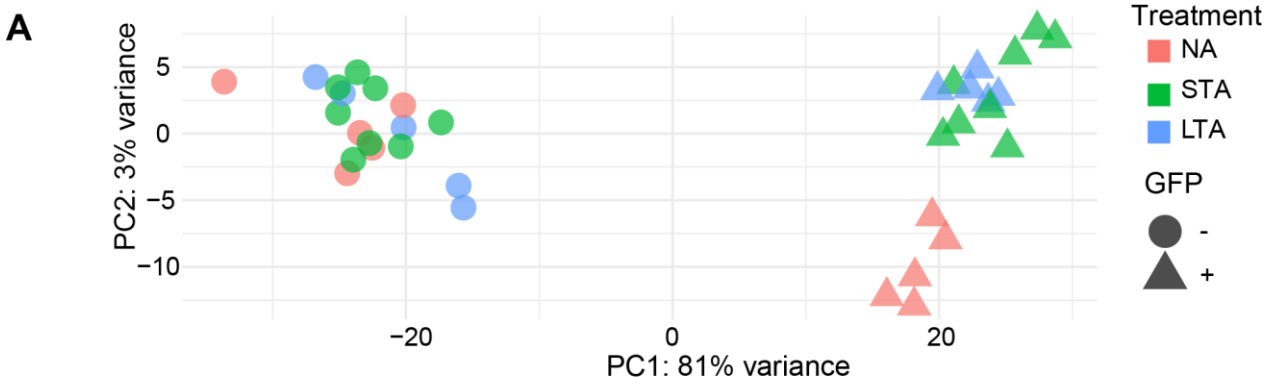
A
PC2: 3% variance
5
0
−5
−10
−20
0
20
PC1: 81% variance
Treatment
NA
STA
LTA
GFP
-
+

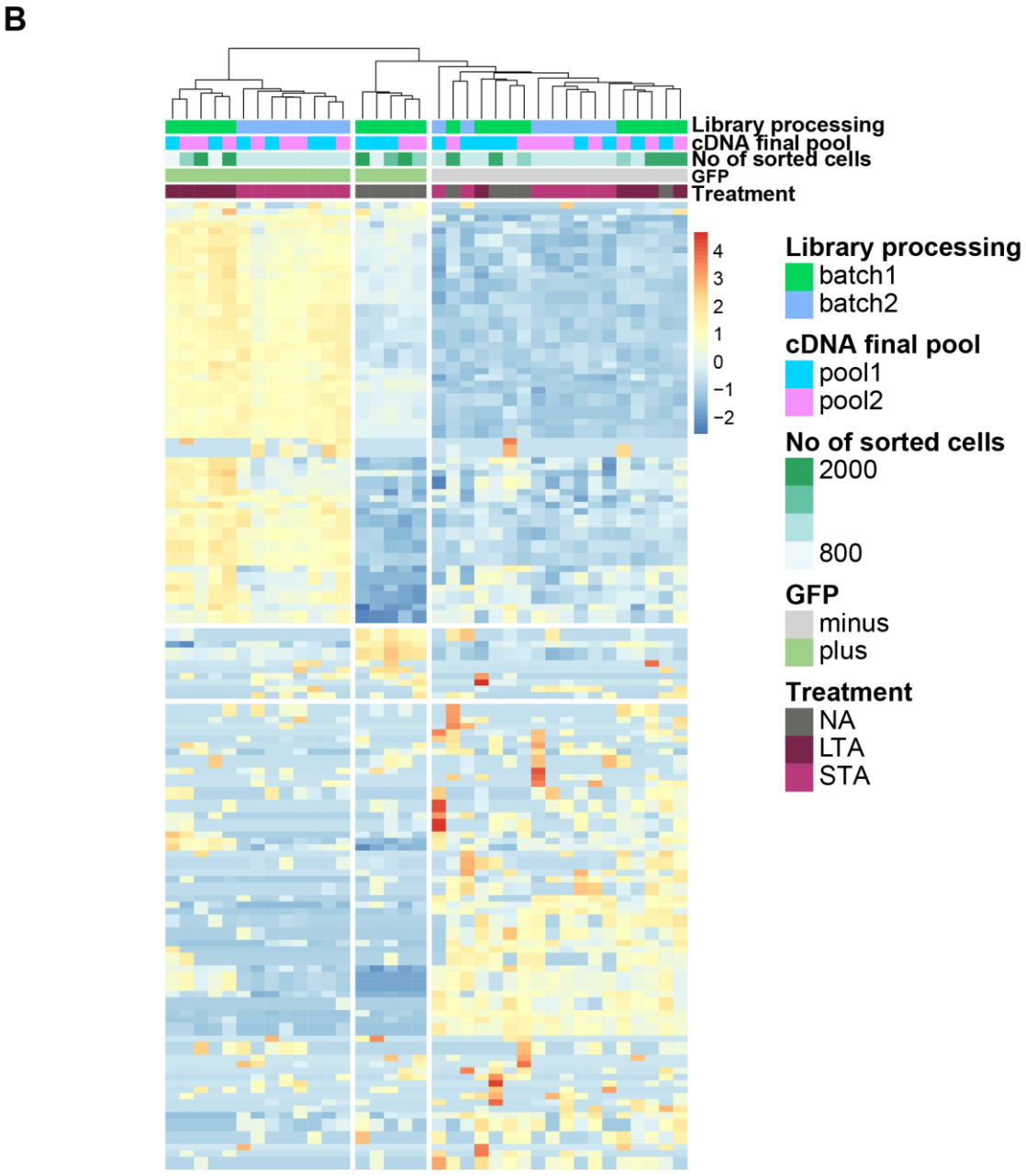
B
Library processing
cDNA final pool
No of sorted cells
GFP
Treatment
4
3
2
1
0
−1
−2
Library processing
batch1
batch2
cDNA final pool
pool1
pool2
No of sorted cells
2000
800
GFP
minus
plus
Treatment
NA
LTA
STA

Figure 2.9. Differential gene expression analysis of RNA sequencing data of POA^{LepR} neurons
(A) Principle component analysis (PCA) of the RNA sequencing data set based on the top 500 genes with the highest variance. **(B)** Heatmap of top 50 differentially expressed genes (DEGs, sorted according to p-adjusted value) from NA:STA, NA:LTA, and STA:LTA comparisons (total number of plotted genes is 150). Columns represent sequenced samples and rows represent genes. The color scale represents the calculated z-score of the counts. Apart from the treatment (acclimation condition) and GFP variables, potential batch-effect variables such as Library processing, final cDNA pool, and the number of sorted cells are added above each sample. DESeq2 package (Love et al., 2014) was used for differential expression analysis with Wald test for the significance testing of the p-value and Benjamini-Hochberg for calculating the false discovery rate (FDR, adjusted p-value).

Additionally, to begin to analyze the functional consequences of heat acclimation at the cellular level, and to get the first insight into the transcriptional changes associated with it, I performed gene set enrichment analysis (GSEA) by using an R package *fgsea* (Fast GeneSet Enrichment Analysis) (Korotkevich et al., 2016; Sergushichev, 2016). I applied GSEA by looking at the hallmark gene sets in one of the Molecular Signature Data Base annotated gene collections (Liberzon et al., 2015). Hallmark gene sets represent specific biological states or processes and display the expression of coherent gene groups. Figure 2.10. A) and B) show *fgsea* normalized enrichment scores for each pathway and if a pathway is significantly enriched in the DEG data set (annotated with turquoise or red color if significant or not, respectively). When using DEG from NA:STA comparison (Figure 2.10. A) 28 hallmark pathways in total were changed. Out of those 27 were up-regulated and 1 was down-regulated. When feeding *fgsea* with DEG from NA:LTA comparison (Figure 2.10. B) 33 hallmark pathways in total were changed. Out of those 28 were up-regulated and 5 were down-regulated according to *fgsea* NES values. The majority of the pathways were shared among the two DEG data sets resulting from NA:STA and NA:LTA differential expression analysis (Table 3. and Table 4.; marked in blue color (in Appendix, pages 163-164); e.g. hypoxia gene set was enriched and up-regulated in both DEGs sets. On the other hand, several pathways were specifically enriched in each of the comparisons (Table 3 and Table 4.; marked in red color) (in Appendix, pages 163-164); e.g. protein secretion pathway was only enriched among DEG when comparing NA:STA and IL6 JAK-STAT3 signaling and interferon-γ pathways were found enriched only in DEG set from NA:LTA differential analysis. The only common down-regulated enriched gene set was oxidative phosphorylation, whereas other common pathways were up-regulated.

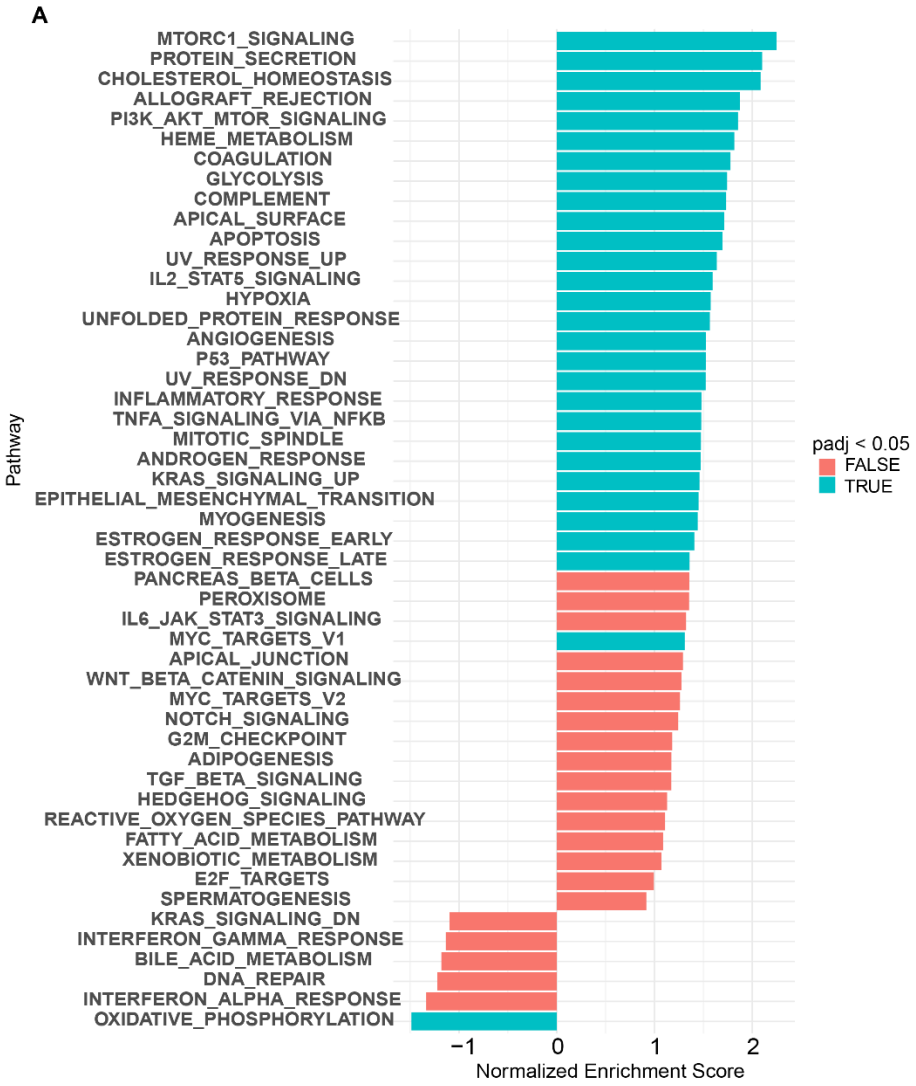

[Figure continues on the next page]

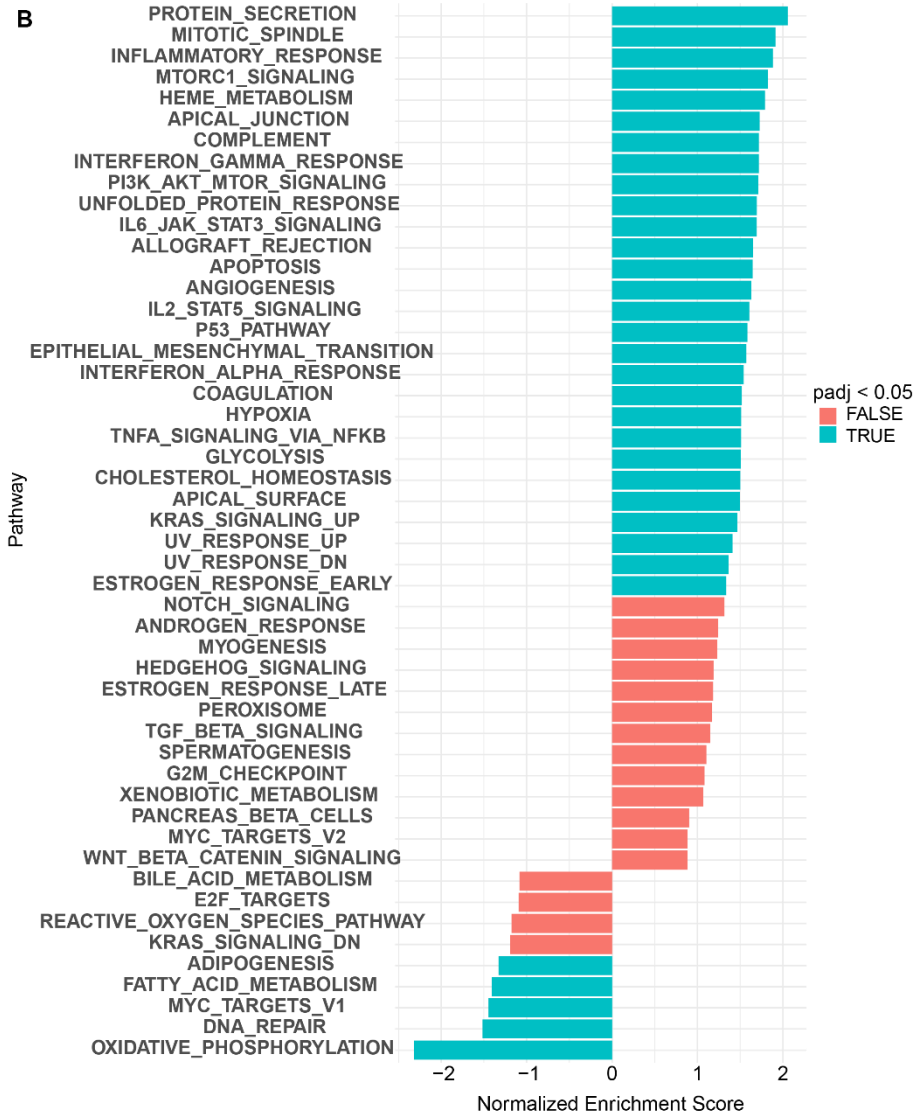

Figure 2.10. Gene set enrichment analysis of DEGs in the RNA sequencing data

(A) GSEA analysis of DEGs coming from the comparison of NA to STA conditions presented through normalized enrichment scores. **(B)** GSEA analysis of DEGs coming from the comparison of STA to LTA conditions presented through normalized enrichment scores. Gene pathways are presented and their corresponding enrichment scores are calculated in the *fgsea* R package. Pathways colored in blue are the ones significantly up-or down-regulated in the DEGs coming from each comparison in A and B.

Next, I hypothesized that proteins that participate in the observed increase in neuron firing properties (Figure 2.4. B) could be expected among the group of ion channels that could be either up-or down-regulated during heat acclimation. Data from our lab that supports this hypothesis is the finding that the firing of the acclimated POA^{LepR} neurons persists even after the application of synaptic blockers, and therefore is an intrinsic property of these neurons (Figure 2.4. E). Therefore, I decided to look for genes

coding for ion channels in the obtained RNAseq data and to analyze if any of those belong to the group of DEGs. To investigate all known ion channels as a reference I used the website tool Channelpedia (EPFL, Blue Brain Project https://channelpedia.epfl.ch/), a repository that collects data on all known ion channels and their families While investigating different families of ion channels I found *Kcnq2* (Potassium Voltage-Gated Channel Subfamily Q Member 2, $K_v7.2$) ion channel to be significantly up-regulated (p-adjusted value < 0.1) during the course of acclimation (Figure 2.11. A). Two other potassium ion channels; *Kcnn2* (Potassium Calcium-Activated Channel Subfamily N Member 2, $K_{Ca}2.2$) and *Kcnh2* (Potassium Voltage-Gated Channel Subfamily H Member 2, $K_v11.1$) (Figure 2.11. B and C). I found it to be borderline significant between non-acclimated and long-term acclimated conditions only (p-adjusted value = 0.13 and 0.15, respectively)

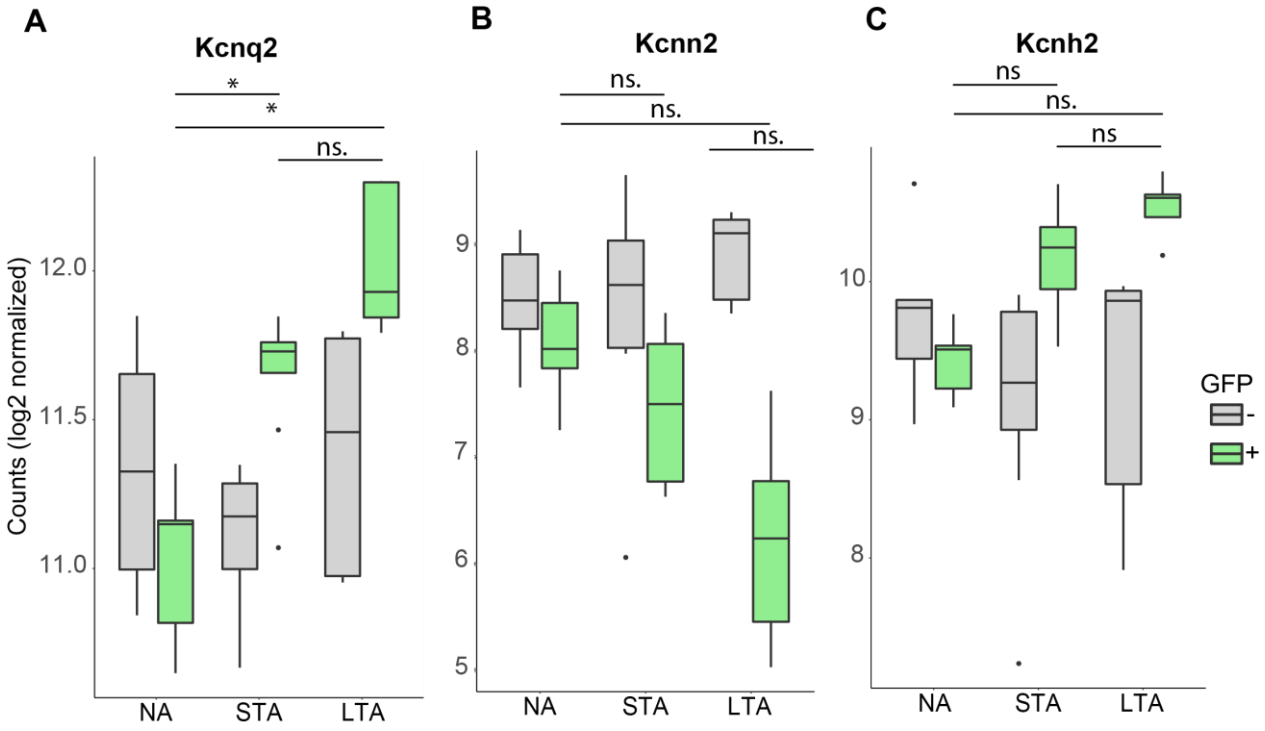

Figure 2.11. The expression level of potassium channels in GFP$^+$ (Lepr$^+$) and GFP$^-$ (Lepr$^-$) samples from NA, STA, and LTA conditions

(A) Expression level (log2 normalized counts) of *Kcnq2* (Kv7.2, Potassium Voltage-Gated Channel Subfamily Q Member 2) mRNA in GFP$^+$ and GFP$^-$ samples of each of the acclimation conditions. NA:LTA *padj. = 0.05408426; NA:STA (GFP+) * padj.= 0.03605393; STA:LA NS.padj. = 1. **(B)** Expression level (log2 normalized counts) of *Kcnn2* ($K_{Ca2.2}$, Potassium Calcium-Activated Channel Subfamily N Member 2) mRNA in GFP$^+$ and GFP$^-$ samples of each of the acclimation conditions. NA:LTA NS. padj. = 0.1310168; NS. padj. = 0.7813248; STA:LA NS. padj. = 0.71727. (C) Expression level (log2 normalized counts) of *Kcnh2* (Kv11.1, Potassium Voltage-Gated Channel Subfamily H Member 2) mRNA in GFP$^+$ and GFP$^-$ samples of each of the acclimation conditions. NA:LTA NS. padj. = 0.1515015; NA:STA NS.

padj.= 0.130829; STA:LA NS. padj.1. Expression levels are calculated by the DESeq2 package (Love et al., 2014) with the Wald test for the significance testing of the p-value and Benjamini-Hochberg for calculating the false discovery rate (FDR or adjusted p-value). Differential expression results are calculated for the difference between GFP^{+} samples and statistical analysis behind it is taking into account expression changes that happen in GFP^{-} samples in each acclimation condition as well. The upper and lower hinge of a box represent the first and third quartiles (the 25th and 75th percentiles) and a middle hinge represents the median. The upper and lower whisker extend from their respective hinges to the largest and lowest value no further than 1.5 x IQR (inter-quartile range). Data beyond the end of the whiskers are called "outlying" points. NA Non-acclimated, STA short-term acclimated, LTA Long.-term acclimated.

3.3. PHARMACOLOGY OF POTASSIUM ION CHANNELS IN POA ^{LEPR} NEURONS

Since 3 potassium ion channel genes were the only ones from genes coding for ion channels that are up-or down-regulated in the course of the acclimation process, I wanted to look further if these channels have a role in the AP firing of POA^{LepR} neurons. To do that I used whole-cell patch-clamp electrophysiology (Ephys) in the acute mouse brain slices and recorded AP firing while applying different ion channel blockers or activators by bath application in ACSF. Before endeavoring in collecting this data I first wanted to make sure that the data on the change of firing frequency (Figure 2.4 B) with the course of acclimation holds when I perform the Ephys recordings. Therefore, I recorded the AP firing frequency of POA^{LepR} neurons in the acute brain slices from LeprCreHTB which spent 0 days at 36˚C (NA), 5 days at 36˚C (STA), and ≥4 weeks at 36 ˚C (LTA). Like my colleagues before, I also observed a significant difference in AP firing frequency between NA and STA and LTA conditions, but no significant difference in AP firing frequency (AP FF) of POA^{Lepr} between STA and LTA conditions (Figure 2.12. A). Other than AP FF, I extracted information on pseudo resting membrane potential (pseudoRMP). PseudoRMP is the average value of the neuron membrane potential obtained by averaging membrane voltage values recorded in Clampfit (Molecular Devices, San Jose, CA 95134). The pseudoRMP was significantly different from NA and STA and LTA conditions, but similarly to AP FF not significantly different between the STA and the LTA condition (Figure 2.12. B). In addition, I calculated the coefficient of variation of the interspike interval (CV (ISI)), which is a parameter that allows assessing how regular the firing of APs is (Figure 2.12. C) (Taube, 2010). Firing regularity or CV (ISI) (standard deviation of the ISI divided by mean ISI) was significantly different between POA^{LepR} neurons harvested from mice subjected to NA and LTA conditions showing that the firing pattern changed from a slow and irregular pattern in the NA condition to a fast and regular one in the LTA condition. Figure 2.12. D shows example AP traces from each condition.

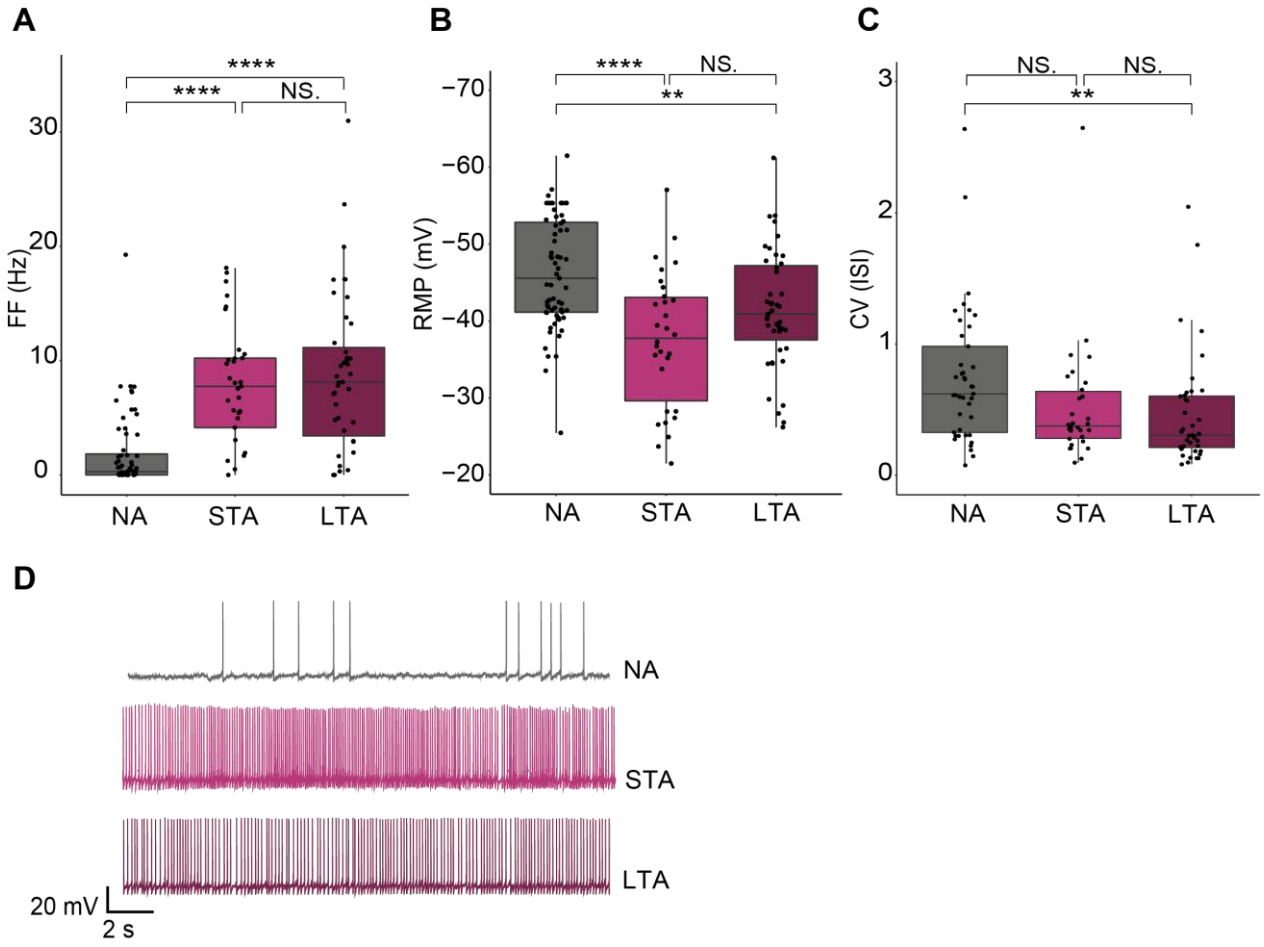

Figure 2.12. POA^{LepR} neurons electrophysiological properties during the acclimation process

(A) Firing frequency (FF(Hz)) of Lepr^{+} (HTB) neurons measured by the whole-cell current-clamp in acute brain/POA slices obtained from NA (Non-acclimated), STA (Short-term acclimated), LTA (Long-term acclimated) LeprCreHTB mice. Statistics are calculated with 1 way ANOVA non-parametric Kruskal-Wallis, Dunn's multiple comparisons test. NA:STA ****p<0.0001, NA:LTA ****p<0.0001, STA:LTA NS. p>0.9990. NA (mean±SD= 1.859 ± 3.284, N=7, n=64), STA (mean ± SD= 7.78 ± 5.3, N=3, n=33), LTA (mean ± SD=8.713 ± 6.861, N=3, n=43). **(B)** Pseudo resting membrane potential (mV) corresponding to cells in (A). Statistics is calculated with 1way ANOVA, parametric, Tukey's multiple comparisons test NA:STA ****p<0.0001; NA:LTA **p=0.0059; STA:LTA NS.p=0.0851. NA (mean ± SD= -46.25 ± 7.2, N=7, n=63), STA (mean ± SD= -37.52 ± 8.773, N=3, n=30), LTA (mean ± SD= -41.46± 7.701, N=3, n=43). **(C)** Coefficient of variation of interspike interval (CV (ISI)) corresponding to cells in (A). Statistics are calculated with 1 way ANOVA non-parametric Kruskal-Wallis, Dunn's multiple comparisons test. NA:STA NS.p=0.1213; NA:LTA **p=0.0018; STA:LTA NS.p=0.7811. NA (mean ± SD= 0.7414 ± 0.5193, N=7, n=41), STA (mean ± SD= 0.5205 ± 0.4701, N=3, n=30), LTA (mean ± SD= 0.4631 ± 0.4266, N=3, n=40). Each dot on a boxplot represents a cell, the upper and lower hinge of a box represent the first and third quartiles (the 25th and 75th percentiles) and a middle hinge represents the median. The upper and lower whisker extend from their respective hinges to the largest and lowest value no further than 1.5 x

IQR (inter-quartile range). Data beyond the end of the whiskers are "outlying" points. **(D)** Example traces of action potential firing from 3 conditions.

Finally, I went on further by testing the possible importance of 3 candidate potassium channels in the AP firing of POA^{Lepr} neurons.

3.3.1. K_v7.2 (Kcnq2)

In order to test the importance of K_v7.2 (*Kcnq2*) in regulating AP firing of the POA^{LepR} neurons, I used ML252 ((*S*)-2-Phenyl-*N*-(2-(pyrrolidine-1-yl)phenyl) butanamide), a selective blocker of K_v7.2 channel (Cheung et al., 2012). The application of 10 µM ML252 drug in ACSF (artificial cerebrospinal fluid) bath solution did not cause the difference in AP FF of non-acclimated LepR$^+$ neurons (Figure 2.13. A and D). However, the drug caused a dramatic change in the firing pattern of neurons obtained from long-term acclimated mice: In many neurons (14 of 32 recorded neurons), the highly regular firing pattern observed in acclimated LepR neurons was transformed into a pattern of bursts with long intervals of no firing (Figure Figure 2.13. D and E). Including the CV (ISI) in this analysis was therefore essential to demonstrate and quantify the drug-induced change in AP firing (Figure 2.13. C).

Additionally, the K_v7.2 channel antagonist decreased the pseudoRMP in neurons coming from the LTA condition (Figure 2.13. B) (K. Li et al., 2021). In summary, although blocking the K_v7.2 did not reduce AP firing frequency in POA^{LepR} neurons after heat acclimation, it significantly changed the pattern of firing of 43% of these neurons and specifically in heat acclimated conditions.

The K_v7.2 has been previously implicated in the control of neuronal firing regularity and its mRNA levels have been found to increase after induced neuronal hyper-excitability (Carver et al., 2020; Greene & Hoshi, 2017). I hypothesize that the up-regulation of K_v7.2 modulates AP firing of POA^{LepR} neurons to become more regular during the heat acclimation and to serve as a break to otherwise potentially exaggerated firing.

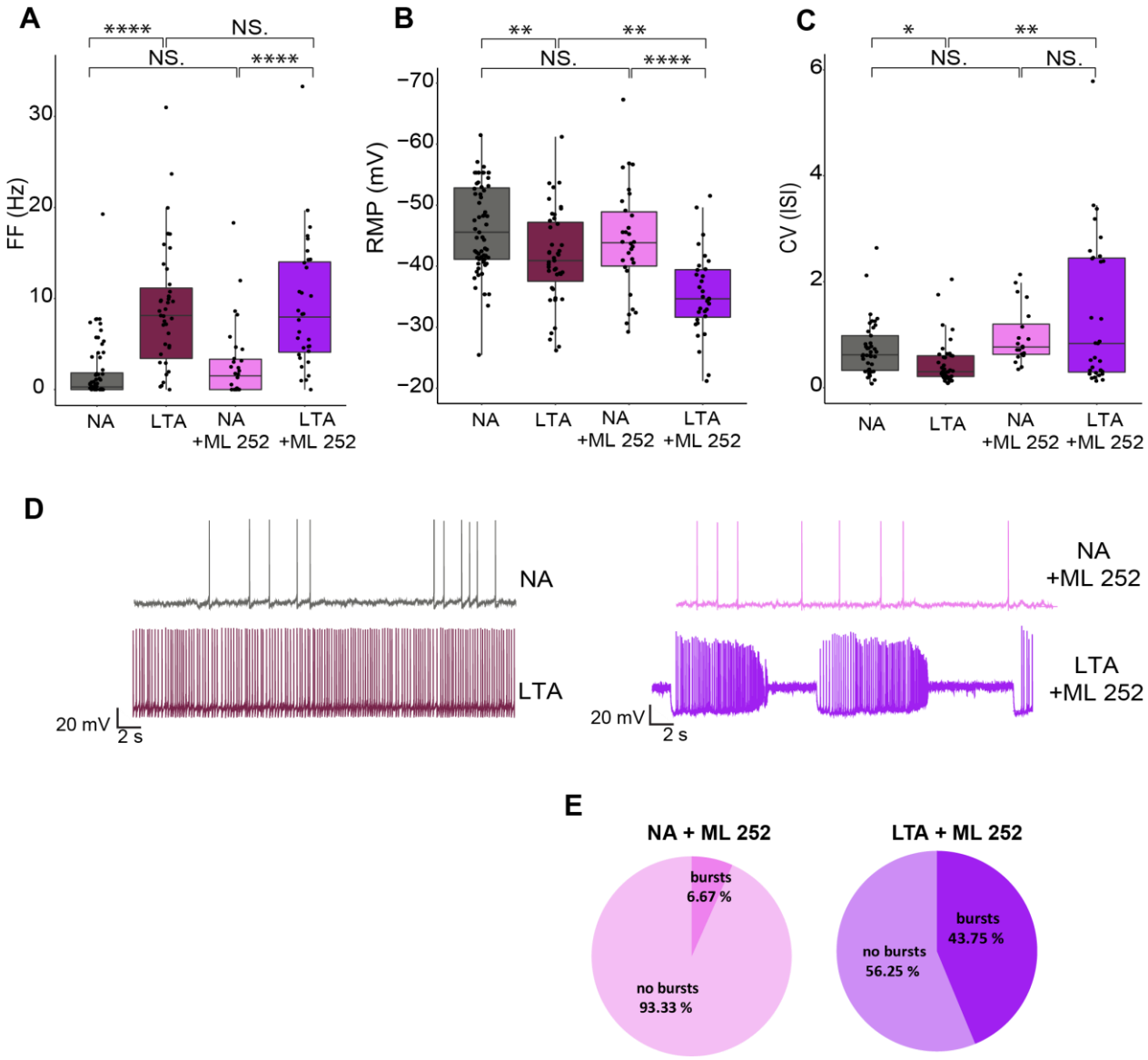

Figure 2.13. Kv7.2 (*Kcnq2*) ion channel pharmacology in POA^{LepR} neurons

(A) Effect of 10 µM ML252- Kv7.2 (*Kcnq2*) channel blocker on firing frequency (FF (Hz)) of Lepr^{+} (HTB) neurons measured by whole cell current clamp in acute brain/POA slices obtained from NA STA (Short-term acclimated), LTA (Long-term acclimated) LeprCreHTB mice. Statistics is calculated with 1 way ANOVA non-parametric Kruskal-Wallis, Dunn's multiple comparisons test. NA:LTA ****p<0.0001; NA:NA+ML252 NS. p>0.9999; LTA:LTA+ML252 NS. p>0.999; NA+ML252:LTA+ML252 **** p<0.0001. NA (mean±SD= 1.859 ± 3.284, N=7, n=64), LTA (mean ± SD=8.713 ± 6.861, N=3, n=43), NA+ML252 (mean ± SD=2.806 ± 4,212, N=3, N=30), LTA+ML252 (mean ± SD=9.129 ± 7.091, N=3, n=32). **(B)** Effect of ML252- Kv7.2 (Kcnq2) channel blocker on pseudo resting membrane potential of Lepr^{+} (HTB) corresponding to cells in (A). Statistics is calculated with 1way ANOVA, parametric, Tukey multiple comparisons test: NA:LTA **p=0.0064; NA:NA+ML252 NS.p=0.6428; LTA:LTA+ML252 **p=0.0030; NA+ML252:LTA+ML252 ****

p<0.0001. NA (mean ± SD= -46.25 ± 7.2, N=7, n=64), LTA (mean ± SD= -41.46± 7.701, N=3, n=43), NA+ML252 (mean ± SD= -44.22± 8.704, N=3, N=30), LTA+ML252 (mean ± SD= -35.41 ± 6.816, N=3, n=32). **(C)** Effect of ML252- Kv7.2 (Kcnq2) channel blocker on coefficient of variation of interspike interval (CV (isi)) of Lepr^{+} (HTB) neurons corresponding to cells in (A). Statistics is calculated with 1 way ANOVA non-parametric Kruskal-Wallis, Dunn's multiple comparisons test: NA:LTA *p=0.0105; NA:NA+ML252 NS.p=0.4148; LTA:LTA+ML252 **p=0.0015; NA+ML252:LTA+ML252 NS. p>0.9999. NA (mean ± SD= 0.7414 ± 0.5193, N=7, n=41), LTA (mean ± SD= 0.4631 ± 0.4266, N=3, n=40), NA+ ML252 (mean ± SD= 0.9739 ± 0.5386, N=3, N=20), LTA+ ML252 (mean ± SD= 1.391 ± 1.395, N=3, n=31). Each dot on a boxplot represents a cell, the upper and lower hinge of a box represent the first and third quartiles (the 25th and 75th percentiles) and a middle hinge represents median. The upper and lower whisker extend from their respective hinges to the largest and lowest value no further than 1.5 x IQR (inter-quartile range). Data beyond the end of the whiskers are "outlying" points. **(D)** Example traces of action potential firing from 4 conditions. **(E)** Pie-charts with quantification of bursty AP firing and RMP oscillations occurrence in Lepr+ neurons recorded with ML 252 drug.

3.3.2. K_{Ca}2.2 (Kcnn2)

Next, I tested the possible role of the K_{Ca}2.2 ion channel, a member of SK (small conductance calcium-activated potassium channels) in POA^{LepR} neurons AP firing known to participate in medium afterhyperpolarization (mAHP) of an action potential (Pedarzani et al., 2001). Afterhyperpolarization (AHP) plays an important role in neuronal excitability and firing pattern (Storm, 1990). For example, activating SK channels in hippocampal pyramidal neurons reduces neuronal excitability due to increased mAHP amplitude (Pedarzani et al., 2001, 2005). In the POA^{LepR} RNA sequencing, we see a decrease of SK2 mRNA with a log2-fold change of -2.03 between NA and LTA conditions (Figure 2.11**.**). I hypothesized that decreased mRNA levels of this ion channel might serve as a mechanism to increase neuronal firing. To test this hypothesis, I applied the CYPPA (10µM) activator (*N*-Cyclohexyl-*N*-[2-(3,5-dimethyl-pyrazole-1-yl)-6-methyl-4-pyrimidinamine) of K_{Ca}2.2 to see if opening this channel has an effect on AP firing frequency, pseudoRMP and CV (ISI) of POA^{LepR} neurons in non-acclimated and long-term acclimated condition(Hougaard et al., 2007).

Application of the SK2 channel activator CYPPA has reduced the firing frequency of POA^{LepR} neurons in LTA conditions (Figure 2.14. A) whereas it did not affect pseudoRMP and CV (ISI) (Figure 2.14. B and C). The reduction of AP FF of acclimated POA^{LepR} neurons due to the application of CYPPA SK2 activator goes along with the hypothesis that the more of the channel is open the higher the mAHP amplitude and therefore the span between each subsequent AP is larger. However, the effect of the activator can solely confirm the the presence of K_{Ca}2.2 channel in these neurons and cannot prove the

specific role of the channel. Figure 2.14. D shows example AP traces from each condition with and without CYPPA. On the other hand, the application of general SK2 blocker-apamin (Bond, 2004) did not have any effect on AP FF, pseudoRMP nor CV (ISI) (Figure 2.14. E), F), and G)). Apamin acts a non-specific SK channel family blocker. The lack of its observed effect might be due to technical reasons, such as the drug concentration being too low to reach the neurons and therefore not exerting the effect. On the other hand, it can be that $K_{Ca}2.2$ has no significant role in modulating AP firing of POA^{LepR} neurons neither before nor after the heat acclimation and that the reduction of SK2 mRNA during the heat acclimation is redundant.

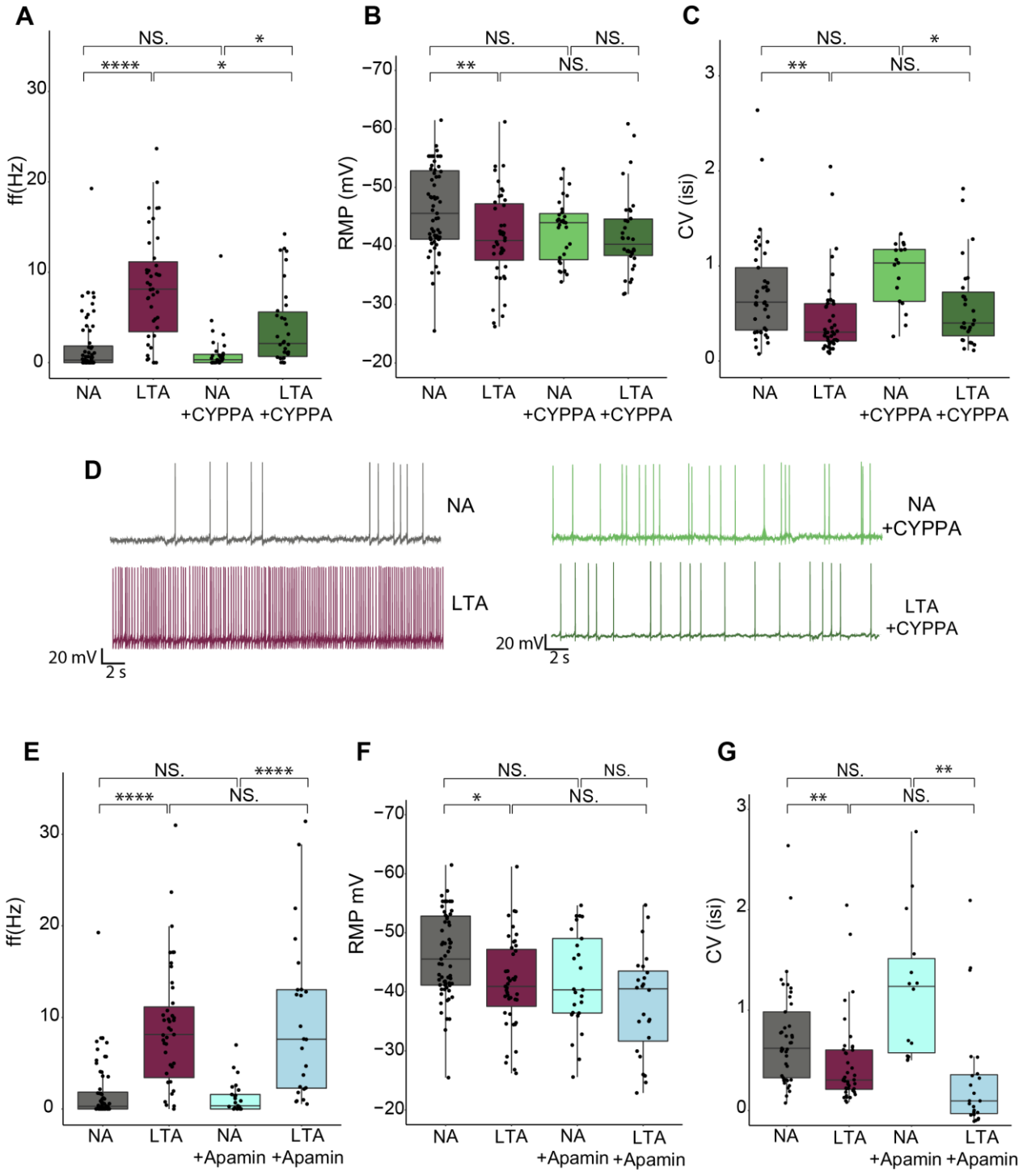

Figure 2.14. $K_{Ca2.2}$ (SK2, *Kcnn2*) ion channel pharmacology in POA^{LepR} neurons

(A) Effect of 10 µM CYPPA $K_{Ca2.2}$ activator on firing frequency (FF (Hz)) of Lepr^{+} (HTB) neurons measured by whole cell current clamp in acute brain/POA slices obtained from NA (Non-acclimated), STA (Short-term acclimated), LTA (Long-term acclimated) LeprCreHTB mice. Statistics is calculated with 1 way ANOVA non-parametric Kruskal-Wallis, Dunn's multiple comparisons test. NA:LTA ****p<0.0001; NA:CYPPA+NA NS.p>0.9999; LTA:LTA+ CYPPA *p=0.0421,

NA+CYPPA:LTA+CYPPA *p=0.0120. NA (mean±SD= 1.859 ± 3.284, N=7, n=64), LTA (mean ± SD=8.713 ± 6.861, N=3, n=43), NA+CYPPA (mean±SD= 1.137 ± 2.291, N=3, N=31), LTA+ CYPPA (mean±SD= 3.953 ± 4.35, N=3, n=34). **(B)** Effect of CYPPA $K_{Ca2.2}$ activator on pseudo resting membrane potential (mV) of Lepr^{+} (HTB) neurons corresponding to cells in (A). Statistics is calculated with 1way ANOVA, parametric, Tukey multiple comparisons test: NA:LTA **p=0.0026; NA:NA+CYPPA NS. p=0.0689; NA:LTA+CYPPA * p= 0.0176; LTA:LTA+CYPPA NS.p=0.9987; NA+ CYPPA:LTA+CYPPA NS. p=0.9876. NA (mean ± SD= -46.25 ± 7.2, N=7, n=63), LTA (mean ± SD= -41.46 ± 7.701, N=3, n=43), NA+ CYPPA (mean ± SD= -42.59 ± 5.309, N=3, N=31), LTA+ CYPPA (mean ± SD= -41.84± 6.859, N=3, n=34). **(C)** Effect of CYPPA $K_{Ca2.2}$ activator on coefficient of variation of interspike interval (CV (ISI)) of Lepr^{+} (HTB) neurons corresponding to cells in (A). Statistics is calculated with 1 way ANOVA non-parametric Kruskal-Wallis, Dunn's multiple comparisons test: NA:LTA **p=0.0053; NA:CYPPA+NA NS.p=0.1874; LTA:LTA+CYPPA NS.p=0.5925; NA+CYPPA:LTA+CYPPA *p=0.0104. NA (mean ± SD= 0.7414 ± 0.5193, N=7, n=41), LTA (mean ± SD= 0.4631 ± 0.4266, N=3, n=40), NA+ CYPPA (mean ± SD= 1.206 ± 1.265, N=3, N=18), LTA+ CYPPA (mean ± SD= 0.581 ± 0.4526, N=3, n=27). **(D)** Example traces of action potential firing from 4 conditions. **(E)** Effect of apamin- SK2 channel blocker on firing frequency (FF (Hz)) of Lepr^{+} (HTB) neurons measured by whole cell current clamp in acute brain/POA slices obtained from NA, STA and LTA LeprCreHTB mice. Statistics is calculated with 1 way ANOVA non-parametric Kruskal-Wallis, Dunn's multiple comparisons test. NA:LTA ****p<0.0001, NA:NA+apamin NS. p>0.9999; LTA:LTA+apamin NS.p>0.999; NA+apamin:LTA+apamin **** p<0.0001. NA (mean±SD= 1.859 ± 3.284, N=7, n=64), LTA (mean ± SD=8.713 ± 6.861, N=3, n=43), NA+apamin (mean ± SD=1.231 ± 1.754, N=3, N=25), LTA+apamin (mean ± SD=9.654 ± 8.787, N=3, n=24). **(F)** Effect of apamin- SK2 channel blocker on pseudo resting membrane potential of Lepr^{+} (HTB) neurons corresponding to cells in (A). Statistics is calculated with 1way ANOVA, parametric, Tukey multiple comparisons test: NA:LTA *p=0.0117, NA:NA+apamin NS.p=0.0892; LTA:LTA+apamin NS. p=0.3339; NA+apamin: LTA+apamin NS. p=0.3234. NA (mean ± SD= -46.25 ± 7.2, N=7, n=63), LTA (mean ± SD= -41.46± 7.701, N=3, n=43), NA+apamin (mean ± SD= -41.91 ± 8.284, N=3, N=25), LTA+apamin (mean ± SD= -38.11 ± 8.803, N=3, n=24). **(G)** Effect of apamin- SK2 channel blocker on coefficient of variation of interspike interval (CV (isi)) of Lepr^{+} (HTB) neurons corresponding to cells in (A). Statistics is calculated with 1 way ANOVA non-parametric Kruskal-Wallis, Dunn's multiple comparisons test: NA:LTA **p=0.0096; NA:NA+apamin NS. p=0.1804; LTA:LTA+apamin NS. p>0.9999, NA+apamin: LTA+apamin ** p=0.0011. NA (mean ± SD= 0.7414 ± 0.5193, N=7, n=41), LTA (mean ± SD= 0.4631 ± 0.4266, N=3, n=40), NA+apamin (mean ± SD= 1.413 ± 1.006, N=3, N=15), LTA+apamin (mean ± SD= 0.5519 ± 0.5706, N=3, n=23).Each dot on a boxplot represents a cell, the upper and lower hinge of a box represent the first and third quartiles (the 25th and 75th percentiles) and a middle hinge represents median. The upper and lower whisker extend from their respective hinges to the largest and lowest value no further than 1.5 x IQR (inter-quartile range). Data beyond the end of the whiskers are "outlying" points.

3.3.3. K_v11.1 (Kcnh2)

To verify a role of a third channel candidate, K_v11.1 (Potassium Voltage-Gated Channel Subfamily H Member 2; Ether à go-go-related gene; *erg*), in the AP firing of the POA^{Lepr} neurons, I used a blocker of K_v11.1 E4031(Cui & Strowbridge, 2018). The application of 10 µM E-4031 in ACSF bath solution significantly increased POA^{Lepr} AP FF even further in the LTA condition (Figure 2.15. A). This effect was not observed when the same drug concentration was applied while recording non-acclimated POA^{LepR} neurons (Figure 2.15. A). E-4031 affected pseudoRMP of the POA^{LepR} neurons by decreasing it significantly in both NA and LTA conditions (Figure 2.15. B). Interestingly, this reduction was not enough to induce AP FF in both conditions. The drug did not affect the CV (ISI) of POA^{LepR} neurons (Figure 2.15. C), unlike bursts and oscillations observed when blocking the K_v7.2 channel (Figure 2.13). Figure 2.15. D) shows example AP traces from each condition with and without E-4031. The increase in AP FF after blocking K_v11.1 could point to the role of this ion channel in AP FF of POA^{LepR} neurons during heat acclimation. Similar to the one of K_v7.2, it could serve as a break to the exaggerated firing of POA^{LepR} neurons during heat acclimation. Although, it seems the mechanism by which this channel is participating in shaping the anatomy of AP is different as it does not usurp the regularity of AP firing but it affects the frequency by other means.

Further on, I also tested the effect of NS-1643 (*N*,*N*'- *Bis*[2- hydroxy- 5- (trifluoromethyl)phenyl]urea), a K_v11.1 opener (Elmedyb et al., 2007), on firing frequency, RMP, and CV (ISI) of POA^{Lepr} neurons in LTA condition (Figure 2.15. E), F), G). The drug did not affect any of the analyzed electrophysiological variables of POA^{LepR} neurons in the LTA condition. I did not test its effects in the NA condition. Figure 2.15. H) shows example AP traces from each tested condition with and without NS1643. Again, the lack of the observed effect of an activator might be due to technical reasons such as the concentration being too low to achieve the effect or because the additional opening of the drug does not affect POA^{LepR} neurons.

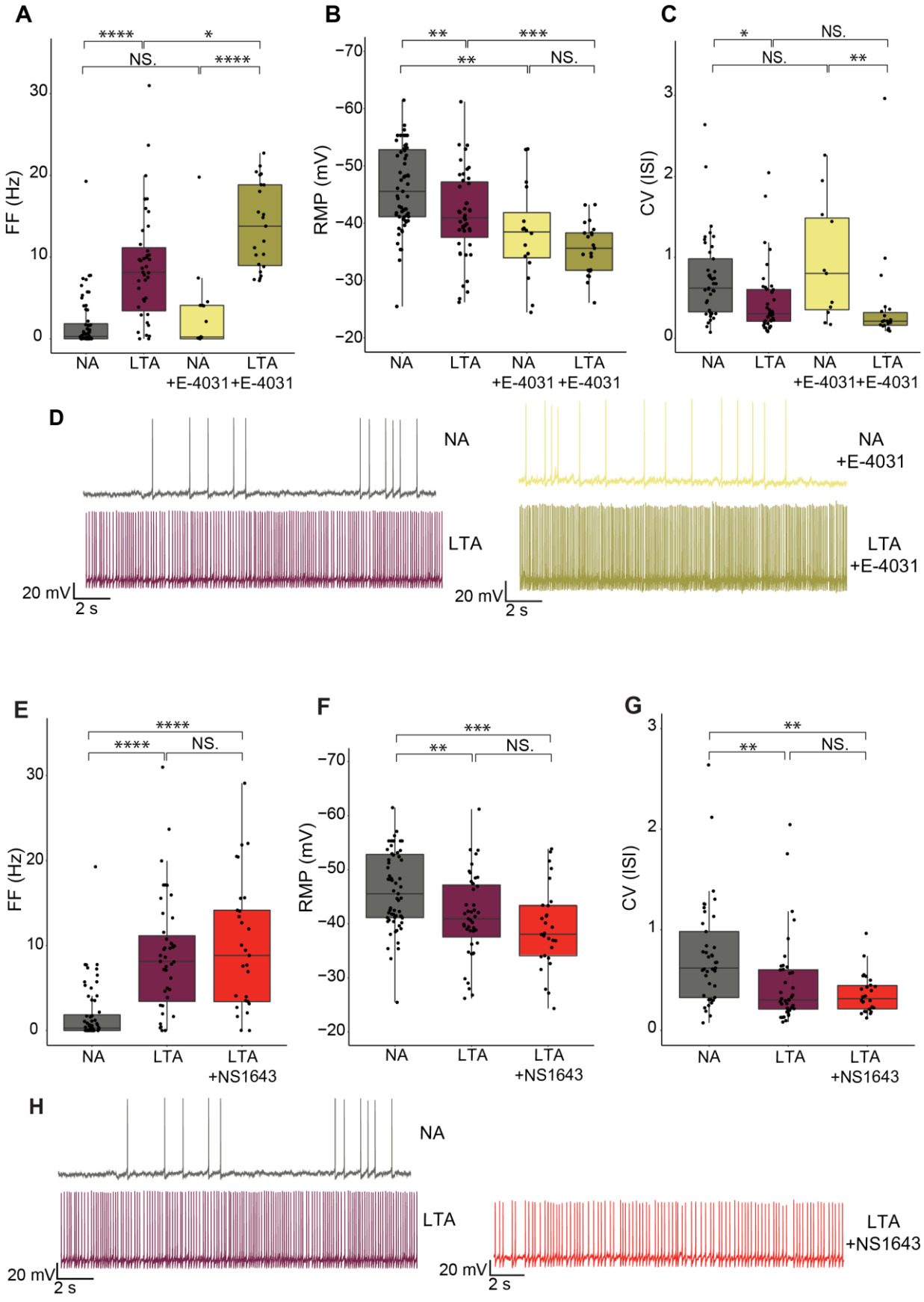
A
B
C
D
E
F
G
H
FF (Hz)
RMP (mV)
CV (ISI)
NA
LTA
NA +E-4031
LTA +E-4031
LTA +NS1643
NS.
20 mV
2 s

Figure 2.15. K_v11.1 (Kcnh2) ion channel pharmacology in POA^{LepR} neurons

(A) Effect of 10 μM E4031- K_v11.1 (Kcnh2) channel blocker on firing frequency (FF (Hz)) of Lepr$^+$ (HTB) neurons measured by whole cell current clamp in acute brain/POA slices obtained from NA (Non-acclimated), STA (Short-term acclimated), LTA (Long-term acclimated) LeprCreHTB mice. Statistics is calculated with 1 way ANOVA non-parametric Kruskal-Wallis, Dunn's multiple comparisons test. NA:LTA ****p<0.0001, NA:NA+ E4031 NS. p>0.9999, NA:LTA+E4031 ****p<0.0001, LTA:NA+E4031 **0.0059; LTA:LTA+ E4031 * p>0.0357; NA+ E4031:LTA+ E4031 **** p<0.0001. NA (mean±SD= 1.859 ± 3.284, N=7, n=64), LTA (mean ± SD=8.713 ± 6.861, N=3, n=43), NA+E4031 (mean ± SD=2.918 ± 5.068, N=2, N=16), LTA+ E4031 (mean ± SD=13.86 ± 5.273, N=3, n=23). **(B)** Effect of E4031 – K_v11.1 (Kcnh2) channel blocker on pseudo resting membrane potential of Lepr$^+$ (HTB) neurons corresponding to cells in (A). Statistics is calculated with 1way ANOVA, parametric, Tukey multiple comparisons test: NA:LTA **p=0.0067, NA:NA+E4031 **p=0.0010, NA:LTA+E4031 **** p<0.0001, LTA:LTA+E4031 *** p=0.0008, NA+ E4031:LTA+ E4031 NS. p=0.3202. NA (mean ± SD= -46.25 ± 7.2, N=7, n=64), LTA (mean ± SD= -41.46± 7.701, N=3, n=43), NA+ E4031 (mean ± SD= -38.34± 8.374, N=2, N=16), LTA+ E4031 (mean ± SD= -34 ± 6.674, N=3, n=23). **(C)** Effect of E4031 – K_v11.1 (KcnH2) channel blocker on coefficient of variation of interspike interval (CV (isi)) of Lepr$^+$ (HTB) neurons corresponding to cells in (A). Statistics is calculated with 1 way ANOVA non-parametric Kruskal-Wallis, Dunn's multiple comparisons test: NA:LTA *p=0.0111, NA:NA+E4031 NS. p>0.9999, NA:LTA+E4031 ***p=0.0002, LTA:LTA+ E4031 NS p=0.5568, NA+ E4031: LTA+ E4031 ** p=0.0061. NA (mean ± SD= 0.7414 ± 0.5193, N=7, n=41), LTA (mean ± SD= 0.4631 ± 0.4266, N=3, n=40), NA+ E4031 (mean ± SD= 0.939 ± 0.7404, N=2, N=11), LTA+ E4031 (mean ± SD= 0.3928 ± 0.6133, N=3, n=22). **(D)** Example traces of action potential firing from 4 conditions above. **(E)** Effect of 10 μM NS1643- Kv11.1 (Kcnh2) channel activator on firing frequency (FF (Hz)) of Lepr$^+$ (HTB) neurons measured by whole cell current clamp in acute brain/POA slices obtained from NA (Non-acclimated), STA (Short-term acclimated), LTA (Long-term acclimated) LeprCreHTB mice. Statistics is calculated with 1 way ANOVA non-parametric Kruskal-Wallis, Dunn's multiple comparisons test. NA:LTA ****p<0.0001; NA:LTA+NS1643 ****p<0.0001; LTA:LTA+NS1643 NS. p>0.9999. NA (mean±SD= 1.859 ± 3.284, N=7, n=64), LTA (mean ± SD=8.713 ± 6.861, N=3, n=43), LTA+ NS1643 (mean ± SD=9.874 ± 7.786, N=3, n=29). **(F)** Effect of 10 μM NS1643– K_v11.1 (Kcnh2) channel activator on pseudo resting membrane potential of Lepr$^+$ (HTB) neurons corresponding to cells in (E). Statistics is calculated with 1way ANOVA, parametric, Tukey multiple comparisons test: NA:LTA **p=0.0040; NA:LTA+NS1643 *** p=0.0001; LTA:LTA+NS1643 NS. p=0.4076. NA (mean ± SD= -46.25 ± 7.2, N=7, n=64), LTA (mean ± SD= -41.46± 7.701, N=3, n=43), LTA+ NS1643 (mean ± SD= -39.17 ± 7.465, N=3, n=29). **(G)** Effect of 10 μM NS1643– Kv11.1 (Kcnh2) channel activator on coefficient of variation of interspike interval (CV (isi)) of Lepr$^+$ (HTB) neurons corresponding to cells in (E). Statistics is calculated with 1 way ANOVA non-parametric Kruskal-Wallis, Dunn's multiple comparisons test: NA:LTA **p=0.0014; NA:LTA+ NS1643 **p=0.0012, LTA:LTA+ NS1643 NS p>0.9999. NA (mean ± SD= 0.7414 ± 0.5193, N=7, n=41), LTA (mean ± SD= 0.4631 ± 0.4266, N=3, n=40), LTA+ NS1643 (mean ± SD= 0.3638 ± 0.1952, N=3, n=26). **(H)** Example traces of action potential firing from 3 conditions. Each dot on a boxplot represents a cell, the upper and lower hinge of a box represent the first and third quartiles (the 25th and 75th percentiles) and a middle hinge represents the median. The

upper and lower whisker extend from their respective hinges to the largest and lowest value no further than 1.5 x IQR (inter-quartile range). Data beyond the end of the whiskers are "outlying" points.

3.4. POA^{LepR} NEURONS ARE A PART OF WARM-ACTIVATED POA NEURONS

Two genes, that have been proposed earlier as markers of POA neurons activated by peripheral warmth; warm-activated neurons (WANs), brain-derived neurotrophic factor (*Bdnf*), and pituitary adenylate cyclase polypeptide (*Adcyap1* or PACAP) were both significantly upregulated with acclimation process (Figure 2.16. A) (Moffitt et al., 2018; Tan et al., 2016). In addition, in 2018, Moffit et al. showed that the Lepr gene is expressed in PACAP/Bdnf cluster anatomically overlapping with WANs. To investigate therefore if POA^{LepR} neurons are part of the WANs population I did the IHC on the POA of LeprCreHTB mice challenged with peripheral heat for 4h at 36˚C, and stained with the antibody raised against cFos- an immediate early gene produced by active neurons (Morgan et al., 1987) together with an antibody raised against the GFP. The heat challenge resulted in an earlier established pattern of cFos immunostaining in POA (Scammell et al., 1993; Yoshida et al., 2005; Yu et al., 2016; Y. Zhang et al., 2011; Zhao et al., 2017) which was not present in room temperature control mice (Figure 2.16. B; left panel). In addition, quantification of GFP (LepR) and cFos overlap after a heat challenge doubled from an average of 30% in room temperature control animals to an average of 60% in peripherally warmed animals (Figure 2.16. B; right panel), confirming the previous finding of Yu et al. (Yu et al., 2016). Therefore, from these results and the knowledge in the literature, I conclude that the POA^{LepR} neurons are activated by peripheral warmth. In addition, POA^{LepR} neurons up-regulate during heat acclimation genes coding for PACAP and Bdnf. The role of these neuropeptides is not described in heat acclimation nor is the mechanism by which they modulate WANs activity investigated in detail.

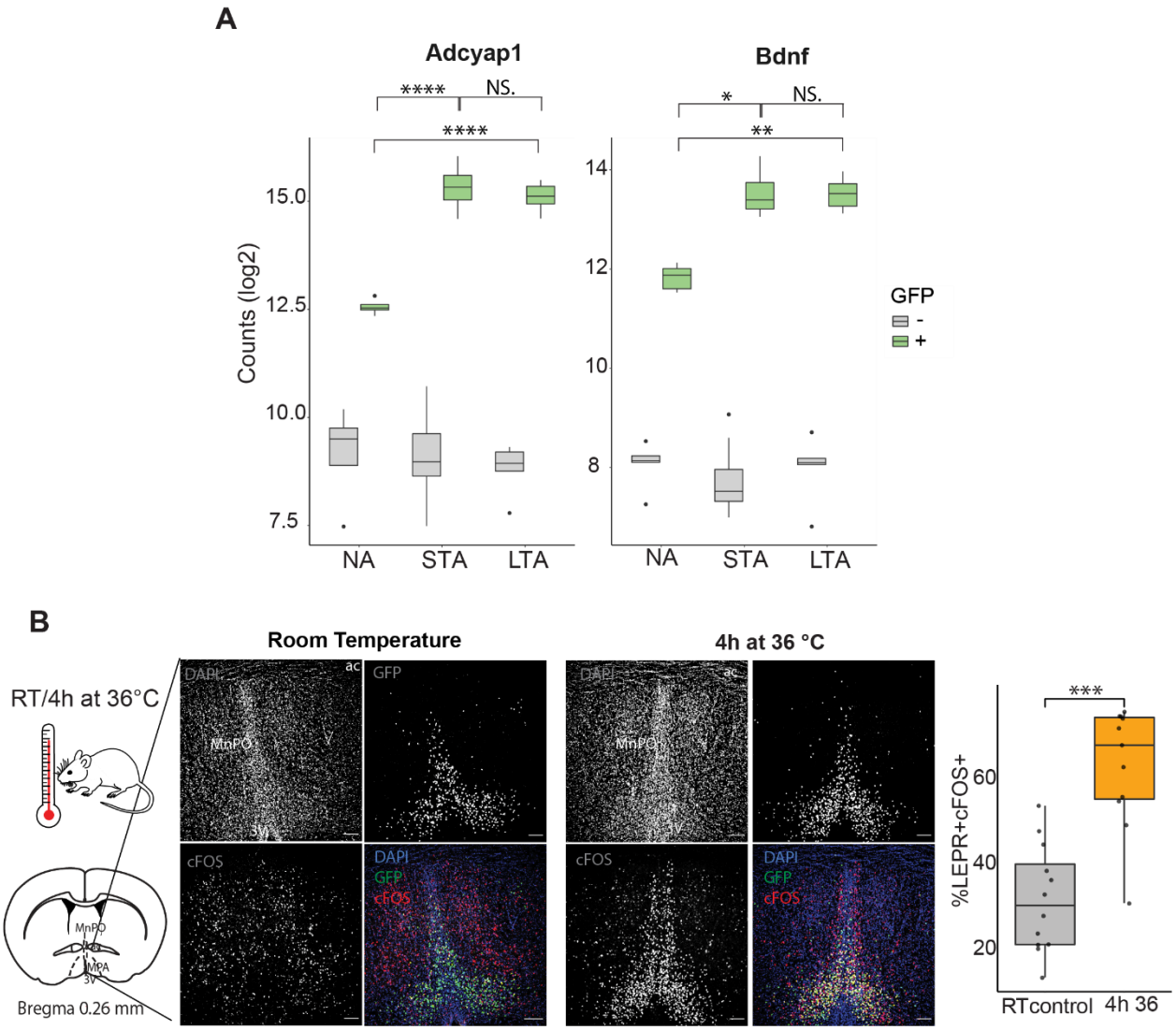

Figure 2.16. Warming challenge increased % of POA^{LepR} expressing immediate early gene *cFos*

(A) mRNA expression of Adcyap1 (PACAP) and Bdnf neuropeptides in FACS-sorted and sequenced Lepr^{+} (GFP^{+}) and Lepr^{-}(GFP^{-}) cells. Expression is presented as log2 normalized counts. Statistics were calculated with the DESeq2 package, Wald test was used for calculating the p-value and Benjamini-Hochberg was used for calculation of FDR (false discovery rate)/p-adjusted value; ***Adcyap1***: NA:LTA ****padj. = 9.902491e-05; NA:STA **** padj=3.937078e-05; STA:LTA NS. padj=1; ***Bdnf***: NA:LTA * padj= 0.02859663; NA:STA p= **padj=0.001344327; STA:LTA p= NS. padj=1. Differential expression results are calculated for the difference between GFP^{+} samples but statistical analysis behind it is taking into account expression changes that happen in GFP^{-} samples in each of the acclimation conditions as well. The upper and lower hinge of a box represent the first and third quartiles (the 25th and 75th percentiles) and a middle hinge represents the median. The upper and lower whisker extend from their respective hinges to the largest and lowest value no further than 1.5 x IQR (inter-quartile range). Data beyond the end of the whiskers are called "outlying" points. **(B) (left panel)** Immunohistochemical staining on POA sections obtained from LeprCreHTB mice

that were kept at RT only vs. mice that were exposed to 36˚C for 4 h (N=2 vs. N=2) stained against DAPI, GFP, and cFos. Images were taken with a confocal microscope, under a 10x objective. Scale bar represents 100 µm .**(right panel)** Quantification of double-positive LEPR (GFP^+) neurons co-labeled with cFOS normalized to all LEPR (GFP^+) cells per section (RT control; n=12, mean±SEM=30,77 ± 3,453 vs 4h at 36˚C n=11, mean±SEM=60,36 ± 4,057). Statistical difference between two conditions is calculated by a non-paired, two-tailed T-test **** $p<0.0001$. Each dot on a boxplot represents a quantified section, the upper and lower hinge of a box represent the first and third quartiles (the 25th and 75th percentiles) and a middle hinge represents the median. The upper and lower whisker extend from their respective hinges to the largest and lowest value no further than 1.5 x IQR (inter-quartile range).

4. DISCUSSION

4.1. RESEARCH BACKGROUND AND SUMMARY OF KEY FINDINGS

Heat Acclimation is a homeostatic process of adaptation to a novel warmer climate achieved by changes in metabolism and cellular signaling (Horowitz 2014). Although the POA is the thermoregulatory center in mammals, it is not clear which role it plays in the process of heat acclimation resulting in increased heat endurance. My colleagues found that the mice develop larger heat endurance after acclimation to 36˚C which also leads to an increase in action potential firing frequency (AP FF) in leptin expressing POA neurons (POA^{LepR}) (Figure 2.4). The firing of POA^{LepR} turned out to be required for the development of heat endurance. I speculated that POA^{LepR} neurons have to change their molecular make-up during the heat acclimation to achieve the higher AP FF, potentially leading to improved heat endurance.

In this part of the thesis, I investigated the transcriptomic changes happening in POA^{LepR} by RNA sequencing approach after isolating neurons by fluorescence-activated cell sorting (FACS), from non-acclimated (NA), short-term acclimated (STA), and long—term acclimated (LTA) mice. Flow cytometry revealed interesting changes in POA^{LepR} cellular characteristics during heat acclimation. I found that POA^{LepR} cells increase in size and granularity during heat acclimation suggesting cellular and molecular changes induced by acclimation.

RNA sequencing revealed that substantial transcriptional changes happen in the POA^{LepR} neurons in the course of heat acclimation (Figure 2.9). The differential expression analysis has resulted in the detection of 386, 562, and 96 differentially expressed genes (DEGs) among NA and LTA, NA and STA, and between STA and LTA treatments, respectively. In addition, gene set enrichment analysis (GSEA) of DEGs suggests which molecular pathways or gene sets in the POA are changed with acclimation in mice (Figure 2.10.). These data jointly suggest the acclimation-induced transcriptional changes in POA^{LepR} neurons.

Focusing the attention on the molecules that might change the AP firing of POA^{LepR} neurons I have more closely investigated DEGs coding for ion channels and subunits known to regulate ion channel function. First, the *Kcnq2* gene, coding for Potassium Voltage-Gated Channel Subfamily Q Member 2 (K_v7.2) was found to be upregulated during the course of acclimation (Figure 2.11. A). Applying the antagonist of this ion channel *in vitro* on acute POA slices, interfered with organized AP firing of acclimated POA^{LepR} neurons, rendering it oscillating and bursty(Figure 2.13.). This finding indicated the potential role of K_v7.2 in the acclimation-induced increase of AP FF of these neurons. In addition, DE analysis revealed two other genes coding for ion channels to be borderline significantly up-and downregulated during heat

acclimation (Figure 2.11. B and C). These two were *Kcnn2* (Potassium Calcium-Activated Channel Subfamily N Member 2, $K_{Ca}2.2$) and *Kcnh2* (Potassium Voltage-Gated Channel Subfamily H Member 2, $K_v11.1$). Pharmacological manipulation of $K_{Ca}2.2$ via agonist resulted in a slight, but significant decrease of AP FF in POA^{LepR} neurons from LTA condition, which indicates the presence of this ion channel in the POA^{Lepr} neurons in a form of a functional protein (Figure 2.14. A). However, the application of its antagonist, apamin, exerted no effect (Figure 2.14. E). On the other hand, the application of the $K_v11.1$ antagonist increased the AP FF of POA^{LepR} neurons in the LTA condition, suggesting that this potassium channel might play a role in shaping the AP during the acclimation process (Figure 2.15.).

Moreover, in the RNA sequencing of POA^{LepR} cells, I found an increase in the expression of genetic markers of warmth-activated neurons (WANs) (Tan et al., 2016), *Pacap, and Bdnf*, with the course of heat acclimation (Figure 2.16. A). Indeed, acute warmth stimulation has resulted in augmented cFos expression in POA^{LepR} neurons, recapitulating the results of others (Yu et al., 2016) (Figure 2.16. B) This result suggests that LepR expressing neurons are part of the WANs population in the POA.

4.2. ANATOMICAL DISTRIBUTION OF LEPR NEURONS IN THE POA

I have analyzed the distribution of LepR expressing neurons in the POA in the LeprCreHTB mouse line where the Lepr Cre line is crossed by an HTB reporter line. I did immunohistochemistry in POA sections by staining against GFP and neuronal marker NeuN (Figure 2.6).

Previously, others have investigated the anatomical distribution of LepR in mouse and rat brains (Elmquist et al., 1998; Leshan et al., 2006; Scott et al., 2009). Although in those works POA has been proposed as one of the brain regions expressing a long-form of leptin receptor (LepRb) I wanted to further study the detailed distribution of Lepr expressing neurons in the mouse line we used for our experiments. I have found LepR neurons spreading almost throughout the whole POA starting at Bregma 0.38 to Bregma -0.10 with the highest number of GFP$^+$ found in the region of MPA and MnPOA. The overlap of the GFP (LepR) signal with NeuN varied from one POA section to another, and the average overlap of Lepr$^+$Neun$^+$ cells was 80%. Leptin receptor expression in MnPOA neurons was shown previously but in that work quantification of GFP (LepR) and NeuN overlap in the POA was not quantified (Y. Zhang et al., 2011). The goal of this experiment was also to compare the number of Lepr neurons in the POA between non-acclimated and long-term acclimated conditions. In the IHC analysis of the overlap of GFP (LepR) and NeuN, I did not find a significant difference in the number of double-positive cells between the two tested conditions (Figure 2.6. C). In addition, the anatomical distribution of these cells appeared the same in the POA tissue from non-acclimated and acclimated mice (Figure 2.6. B).

The other 20% of LepR/GFP signal, which did not overlap with NeuN, might be because of the low expression of NeuN in those cells. The analysis was done by the NIS-elements algorithm for cell counting (Nikon Instruments Inc) which entails subjective thresholding of a fluorescent signal which sometimes might miss put on faint signals.

Alternatively, it could be that this 20% of POA^{LepR} cells (or a fraction thereof) are not neurons but other cell types in the preoptic area. Single-cell RNA sequencing (scRNA-seq) of LepR expressing cells from the hypothalamus has shown that LepR neurons can be divided by their transcriptome into 8 neuronal and 17 non-neuronal clusters, mainly tanycytes and endothelial cells (Kakava-Georgiadou et al., 2020). Of all the sequenced cells about 45% were classified as neurons based on the expression of neuronal markers *Mapt* (Microtubule Associated Protein Tau) and *Tubb3* (Tubulin Beta 3 Class III) while the rest were assigned to non-neuronal cell types. It is worth noting that hypothalamic tissue used for sorting cells in that work also encompassed the POA (information obtained from the authors of the work). However, since the POA is a small portion of the whole hypothalamus it is hard to know how many cells, and therefore transcripts of LepR gene, are coming from POA in this data set.

The role of the preoptic area of the hypothalamus in thermoregulation was discovered a long time ago, and yet the molecular make-up of this region is unknown. Defining LepR neurons as part of the POA neuronal population has already been done by others (Yu et al., 2016; Y. Zhang et al., 2011) but here I provided a more detailed anatomical position of LepR neurons across the POA anterior-posterior axis.

4.3. FACS SORTING AND BULK RNA SEQUENCING OF POA^{LEPR} NEURONS FROM NON-ACCLIMATED, AND ACCLIMATED MICE

To collect as many as possible POA^{LepR} cells, I implemented a protocol of adult neuron dissociation (Moffitt et al., 2018) which resulted in an increase in cell survival after POA tissue dispersion. In the adult mouse brain tissue extracellular matrix is mainly consisted of chondroitin sulfate proteoglycans and it forms a structure called perineuronal nets which increase in abundance during mouse aging (Horii-Hayashi et al., 2015). Disturbing this extracellular matrix when triturating the brain tissue might cause damage to neurons and result in low neuronal survival. In all my FACS sorting experiments, the number of living cells as marked by propidium-iodide staining was consistent (60%-90%) among samples coming from different acclimation treatments suggesting that acclimation did not affect cell survival (Figure 2.7. B).

Interestingly, what was affected by acclimation treatment was the intensity of GFP fluorescence (Figure 2.7. D; left panel). The HTB line is constructed by cloning a tricistronic open reading frame containing Histone-2B-GFP, TVA, and B19 glycoprotein separated by 2A cleavage sequences into a Rosa26

targeting vector. The vector also contained a CAG promoter, cytomegalovirus (CMV) enhancer, fused to the chicken beta-actin promoter serving as an artificial way to increase levels of gene expression and a stop signal flanked by LoxP sites (Figure 2.3.; panel l) (Y. Li et al., 2013). It has been shown that GFP intensity can increase due to CAG promotor temperature sensitivity (Yuanyuan Doua, 2021). Nevertheless, it is hard to extrapolate this finding made on the HEK cell expression system to the whole mouse. In addition to that, temperature sensitivity in that work was not tested by increasing the temperature but by decreasing it. It would be interesting to know whether CAG promotor affects GFP expression due to temperature increase.

Further on, it has been shown that heat acclimation at 32 ˚C increases the proliferation of neuronal progenitor cells in the hypothalamus of rats (Matsuzaki et al., 2009). The number of bromodeoxyuridine (BrdU) positive cells was significantly increased in the hypothalamus of heat-exposed rats, and the number of BrdU+/NeuN+ cells increased at 43 days of heat exposure. Therefore, the increase of the GFP fluorescent intensity might be a sign of enhanced transcription following heat acclimation, or of the acclimation-induced proliferation of the stem cells present in the adult mouse hypothalamus.

In addition, I observed an increase in size (FSC) and granularity (SSC) of the POA^{LepR} cells dispersed from the POA tissue of the STA and LTA mice in comparison to cells from POA of NA mice (Figure 2.7. D; middle pannels). It was shown that some cells exposed to hyperthermia increase the cell size and granularity at the start of apoptosis (Lyon et al., 2021). The gene pathway analysis of POA^{LepR} cells has shown induction of apoptosis pathway after acclimation treatment. Therefore a plausible explanation for the increase in FSC and SSC of POA^{LepR} cells after acclimation might be the induction of apoptotic pathways due to potential DNA damage occurring during heat acclimation which as previously discussed by others (Horowitz et al., 2004).

Moreover, the number of surviving POA^{LepR} cells was the lowest in STA samples in comparison to both, NA and LTA (Figure 2.7. D; right panel). I hypothesize that the DNA damage is increased during the early acclimation period when animals are habituating to the novel environment and therefore it could be that the POA^{LepR} cells are also more sensitive to dissociation from the tissue. It has been found that STA is the important phase of heat acclimation as a period when an organism is experiencing the change for the first time and that genes related to DNA damage and cellular stress are higher in this phase of acclimation (Horowitz et al., 2004). In addition, it could be that the protocol I used for heat acclimation is quite harsh on the general health of animals as it entails an abrupt and drastic change of the environmental temperature of about 12 ˚C (change from standard housing room temperature of 23 ˚C to 36˚C). The STA phase may be a period when an animal goes through the process of extreme metabolic demands to adapt

to a novel environment and therefore the neurons' sensitivity to heat stress is also higher which changes once the acclimated phenotype is reached (as in the LTA).

In concordance with this, RNA quality from STA samples was compromised in comparison to the other two conditions (Figure 2.8. B). RIN numbers which represent the integrity of isolated RNA were low only in the RNA isolated from STA samples indicating that these samples were of lower quality than the others(Masotti & Preckel, 2006). Nevertheless, I still included these samples in the sequencing as the cDNA resulting from these was of good quality.

Next, to verify if FACS sorting of POA^{LepR} cells was specific enough to isolate POA^{LepR} neurons for RNA seq according to GFP fluorescence and PI staining, I checked for the expression of *Egfp* and *Lepr* transcripts in the GFP^{+} and GFP^{-} sample pairs sorted according to GFP fluorescence signal (Figure 2.8. E). It turned out that samples sorted as GFP^{-} had both *Egfp* and *Lepr* genes expressed, although by 6 and 22 fold higher in GFP^{+} samples than in the GFP^{-} ones. It was previously shown that the Lepr-Cre line we use in our experiments induces GFP expression in 81% of functional Lepr neurons in the lateral hypothalamus (Leinninger et al., 2009). Likely due to the Cre-recombination efficiency the other 19% of Lepr-Cre neurons fail to express GFP. Therefore, it might have been that some neurons in GFP^{-} samples still had Lepr transcript and therefore I found counts of Lepr transcript in those. Moreover, it might as well be that some GFP^{+} neurons were gated in FACS sorting falsely as GFP^{-} due to low expressing EGFP signal and this is why we see *Egfp* and *Lepr* transcripts in GFP^{-} samples.

In addition, dissociation of neurons from their native environment might have consequences on their health status and therefore on their transcriptome. Nevertheless, others have implemented brain tissue trituration to successfully isolate neuronal populations of interest to perform RNA sequencing (Ding et al., 2020; Saxena et al., 2012; Tasic et al., 2016). Here I showed that I was able to dissociate POA of adult mice and isolate a small cell population (<1% of total living cells) of POA^{Lepr} cells for RNA sequencing by using Cre dependent GFP reporter system.

4.3.1. Differential expression and gene set enrichment analysis of RNA-seq data

Principal component analysis (PCA) shows which are the variables in the data set carrying the most variance (Pearson, 1901). The PCA of the RNA-seq data I obtained suggests that the two principal components carrying the main variability of the RNA-seq data set are the GFP phenotype and the acclimation treatment (Figure 2.9. A). These are bringing 81% and 3% of the variance, respectively. PCA graph shows that samples are separated primarily according to GFP phenotype, and then GFP^{+} samples

are separated according to acclimation treatment. As expected, this suggests that the difference among the samples is due to the GFP phenotype being larger than the ones caused by acclimation treatment.

To find the genes that are coding for the differences among acclimated and non-acclimated POA^{LepR} neurons I performed a differential expression (DE) analysis of the genes in the RNA-seq data of the NA, STA, and LTA samples (Love et al., 2014). The statistics behind the DE analysis in DESeq2 were designed to look at the changes which are happening specifically in the GFP$^+$ samples during acclimation. Looking at the changes that happen in both GFP$^+$ and GFP$^-$ samples might show interesting things about how acclimation affects POA globally, but not in LepR expressing neurons specifically, and that is where we see the increase in AP FF. This type of DE analysis among GFP$^+$ samples revealed 386 significantly differentially expressed genes (DEGs) when comparing the NA and LTA conditions, 562 DEGs between NA and STA conditions, and 96 DEGs between STA and LTA. If the number of changed genes is taken into the account, it seems as if there is more of a change in the transcriptome level during the STA than during the LTA. This might again point out the fact that during the STA animals might be going through a more drastic change that helps to reach the acclimated phenotype in the LTA.

In addition, the heat map presenting the top 50 DEGs from each comparison (Figure 2.9. B) revealed that the main transcriptome differences in the obtained samples are coming from the GFP phenotype. Additionally, it showed that the transcriptome differences between GFP$^+$ samples are dependent on the acclimation treatment The same conclusion can be drawn if looking at the PCA analysis (Figure 2.9. A).

Further, I analyzed gene pathways activated or suppressed during heat acclimation by gene set enrichment analysis (GSEA) on DEGs (Figure 2.10.). Most of the pathways were common to both NA to STA and NA to LTA comparisons. One of these was the gene set defining the hypoxia pathway that showed to be upregulated. Genes connected to this pathway, such as HIF1-α (Hypoxia-inducible factor 1-alpha), were previously found to be increased in the hearts of heat acclimated rats (housed at 34 ˚C for 30 days) (Maloyan A et al. 2005). HIF1-α was suggested to play a role in acclimation-induced cross-tolerance to other novel stressors, in this particular work to ischemic heart injury. The hearts of heat acclimated rats showed higher levels of HIF1-α and less damage induced by ischemic injury.

On the other hand, one of the pathways specific to NA to STA comparison, and not found by analyzing DEGs from NA to LTA comparison was the protein secretion pathway (Figure 2.10.A). The increase in protein secretion might suggest higher neurotransmitter release since neurons follow the same mechanism of protein secretion as other eukaryotic membranes (Bajjalieh Sandra M. & Scheller Richard H., 1995). Moreover, these results agree with the data obtained by the cDNA array of rat hypothalamus

during STA and LTA, where upregulation of genes coding for neurotransmitter release and neuron excitability was observed (Horowitz, 2007; Schwimmer et al., 2004).

On the other hand, IL6 JAK/STAT signaling pathway, Interferon-α, and Interferon-γ signaling were upregulated specifically in DEGs set coming from NA to LTA comparison (Figure 2.10.B). An increase in interleukins and other cytokines was found in rats' hypothalamus after LTA, where 50% of upregulated genes were associated with immune response pathways (Schwimmer et al., 2006). These pathways might suggest that heat acclimation presents a strain on the organism which causes inflammatory and immune responses to rise (Boehm et al., 1997; Platanias, 2005; Schaper & Rose-John, 2015). In addition, an increase in the immune responses following heat acclimation has been correlated to neuroprotection mechanisms in traumatic brain injury (Shein et al., 2007). How exactly these immune pathways play a role in heat acclimation and perhaps as well in heat endurance of the mice following heat acclimation need to be further elucidated.

A Common downregulated pathway in both STA and LTA was oxidative phosphorylation (Figure 2.10.). Mitochondrial function was previously shown to change during heat acclimation by decreased oxygen consumption and oxidative complex activity (Assayag et al., 2012; Cassuto, 1968). The reduction of oxidative phosphorylation during heat acclimation goes hand in hand with reduced metabolic rates and the need of the organism to reduce any heat production (Sawka, Michael N. et al., 2011). On the other hand, due to the increase in AP FF, one would expect that POA^{LepR} neurons require higher ATP production and therefore higher rates of oxidative phosphorylation (Hall et al., 2012; Özugur et al., 2020).

RNA seq of POA^{LepR} neurons has discovered hundreds of DEGs among acclimation conditions. These genes provide insight into cellular and metabolic signaling pathways that are perturbed during heat acclimation and investigating these might bring novel findings on what facilitates heat acclimation. Moreover, they provide us a basis to investigate potential molecules mediating AP FF increase, which I believe is important for increased heat endurance of acclimated animals.

4.4. PHARMACOLOGY OF POTASSIUM ION CHANNELS IN LEPR POA NEURONS

While thinking about which proteins might induce AP FF to increase during heat acclimation or modulate heat acclimation phenotype, I hypothesized that proteins that play a role in that process should have something to do with the membrane properties of the neurons. Since my colleagues have demonstrated that the firing of the acclimated POA^{LepR} neurons is the intrinsic property of these neurons, not abolished by the application of synaptic blockers (Figure 2.4**.** E), it added another reason to believe that inherent change in the membrane of these neurons is modulating the increase in AP FF. Literature

provides several examples where ion channels are shown to be modulating long-lasting phenotypes such as the $Na_v1.7$ ion channel in integrating synaptic inputs in AGRP, POMC, and PVH neurons controlling the body weight homeostasis (Branco, 2016), which, interestingly, is a neighboring hypothalamic brain region interconnected with the POA. Therefore, I decided to focus on ion channel genes as potential molecules that mediate an increase in the firing frequency of POA^{LepR} neurons during heat acclimation and potentially play a role in achieving an acclimated phenotype. I checked the expression of all 180 genes coding for ion channels and found *Kcnq2* (Potassium Voltage-Gated Channel Subfamily Q Member 2, $K_v7.2$) ion channel to be significantly upregulated when comparing samples from NA to STA and NA to LTA (Figure 2.11. A). The other two ion channels I found to be borderline significant between non-acclimated and long-term acclimated conditions only were *Kcnn2* (Potassium Calcium-Activated Channel Subfamily N Member 2, KCa2.2) (downregulated)and *Kcnh2* (Potassium Voltage-Gated Channel Subfamily H Member 2, $K_v11.1$) (upregulated) (Figure 2.11. B and C).

Being that only one potassium channel (*Kcnq2*) was significantly increased during the heat acclimation, it made an obvious candidate to further test my hypothesis that it might play a role in AP FF of LepR neurons in the POA. As the power to detect molecules in RNA-seq depends on their abundance and their length, but also the achieved sequencing depth, RNA-seq can be a technique prone to zero reads for rare events (Sims et al., 2014). Therefore, I was keen on testing two additional potassium channels which did not significantly change their expression during heat acclimation but were borderline significant and followed the acclimation length with the change in their expression (*Kcnh2* and *Kcnn2*). Moreover, the trend of expression increase and decrease of Kcnh2 and Kcnn2, respectively, recapitulated the advancement of the acclimation process.

To test the function of the ion channel proteins that those three genes are coding for in AP firing of the POA^{LepR} neurons during heat acclimation, I used the whole-cell patch-clamp electrophysiology (Ephys) and different pharmacological agents to block or activate the ion channels. Before doing that, I first had to recapitulate the finding of my colleagues that POA^{LepR} neurons increase firing frequency during heat acclimation. In the whole-cell current-clamp measurements, I could recapitulate the finding of a significant increase in the firing frequency of POA^{LepR} neurons in STA and LTA conditions when compared to AP FF in NA conditions. On the other hand, I did not find a significant difference in POA^{LepR} AP FF between STA and LTA conditions. What could cause this discrepancy between the results of me and my colleagues is the day longer heat acclimation I used in STA. I recorded neurons on the 5th day of heat acclimation, the same as I did for the collection of the samples for FACS sorting and RNA sequencing, and my colleagues did the recording on the 4th day of heat acclimation. Since it seemed to me from their FF results that the

difference between NA and STA was not yet that large, I considered a day longer STA to be beneficial for capturing more robust transcriptomic differences between NA and STA conditions. As I did not perform heat endurance with 5 days acclimated animals I cannot say either if their heat acclimation was improved even more in comparison to 4 days acclimated animals, or if it was on the same level as the one from ≥4week acclimated animals. Additionally, although there is not much difference in AP FF of POA^{LepR} neurons from the STA and LTA conditions (Figure 2.12. A), RNAseq has detected transcriptomic differences between samples coming from these conditions. (Figure 2.9. B). It would be interesting to explore what these particular genes code for as that could give us a clue about the physiological processes happening to mice at the STA leading them to a full acclimated condition when the heat endurance is drastically improved. Perhaps these processes are equally important or additive to increased AP FF in POA^{LepR} neurons for achieving heat acclimation.

Next, I decided to test if ion channel candidates are present on the protein level in POA^{LepR} neurons and if these indeed have a function in AP FF during heat acclimation.

4.4.1. Kcnq2 (Kv7.2.)

The first candidate, the K_v7.2 channel is known to mediate M currents together with its counterpart K_v7.3 (H. Wang, 1998). M current mediates subthreshold excitability of neurons and regulates their firing properties and responsiveness to synaptic inputs (H. S. Wang & McKinnon, 1995). Activation of M current during the initial stage of an action potential suppresses propagation of consecutive action potentials and abbreviates the duration and frequency of the spike train induced by sustained depolarization (Brown & Passmore, 2009). It has also been shown that K_v7 channels play a role in neuronal firing by modulating several components of action potential; resting membrane potential through the opening at low subthreshold membrane voltages and mediating inactivating persistent current; interspike interval by increasing it in high-frequency firing neurons; and afterhyperpolarization by contributing to the medium afterhyperpolarization together with SK channels but potentially to slow afterhyperpolarization as well (Greene & Hoshi, 2017). In addition, it has been found that these channels contribute to increased Na_v channel availability in the nodes of Ranvier, enhance action potential conductance, and promote action potential spiking revealing the fact that the function of K_v7.2 and K_v7.3 heteromers can be context and location-dependent (Battefeld et al., 2014)

Loss of function mutations in K_v7 channels is involved in benign familial neonatal convulsion, and common idiopathic epilepsy (Charlier et al., 1998; Singh et al., 1998). However, a study using conditional knock-out mice has shown that abolished M current in Kv7.2 deficient neurons but not in K_v7.3, showing

that K_v7.2 might mediate M current without the K_v7.3 (Soh et al., 2014). In addition, increased Kcnq2 mRNA levels have been shown in pyramidal neurons after chemoconvulsant induction of seizures showing that Kcnq2 might be upregulated in the hyper-excited neurons (Carver et al., 2020).

Therefore, I hypothesize that the increase in expression of K_v7.2 mRNA levels during heat acclimation (Figure 2.11**.** A) helps to stabilize the already significantly increased firing frequency of POA^{LepR} neurons by counterbalancing the excitability of these neurons.

I have found that the application of ML252, an antagonist of K_v7.2, causes a dramatic and sudden shift from regular to the irregular firing of the neurons accompanied by oscillations in resting membrane potential (RMP) (Figure 2.13.). Blocking of Kv7.2 rendered POA neurons more depolarized by increasing the RMP (Figure 2.13. B) and it has increased the coefficient of variation of interspike interval (CV(ISI)) (Figure 2.13. C). This result is in concordance with the literature showing the role of the K_v7.2 in action potential firing regularity (Greene & Hoshi, 2017). Moreover, it has been shown that *Kcnq2* null mice show increased AP FF after the current injection (Niday et al., 2017). This finding suggests that the increase in mRNA levels we see during heat acclimation might serve as a protection mechanism for POA^{LepR} neurons not to go overboard with firing and to protect them from hyper-excitability. It was shown that the increase in *Kcnq2* mRNA expression levels caused by the hyper-excitability stimulus was transient and gone after the stimulus stops persisting (Carver et al., 2020). It would be interesting to see if the firing properties of the POA neurons followed by the application of the K_v7.2 blocker would be gone after the acclimated animal has been returned to a room temperature environment. This would potentially show that the increase in mRNA of K_v7.2 serves to shape and control AP firing during acclimation which without the increase in this channel might have become erratic and out of control.

The results I obtained by applying the K_v7.2 blocker, suggesting that it plays a role in shaping the action potential firing of POA^{LepR} neurons in long-term heat acclimation. However, to prove or disprove its role in heat endurance increased by heat acclimation one should knock out or knock down this gene in POA^{LepR} neurons specifically. In addition, although ML252 blocker application shows the effect on AP firing of POA^{LepR} neurons, and this blocker exhibits >40 fold selectivity for K_v7.2 over other K_v7 channels, it would be beneficial to also measure M currents during heat acclimation to prove that these are increased during the heat acclimation (Cheung et al., 2012). This would confirm the specificity of the expression increase found by RNA sequencing and the effect of the antagonist.

4.4.2. Kcnn2 ($K_{Ca}2.2$)

A member of the SK (slow-conductance calcium-activated) channel family, the $K_{Ca}2.2$ (SK2) channel, is known to participate in mediating medium afterhyperpolarization (mAHP) of an action potential (Bond, 2004). It has been shown in Purkinje cells that the application of SK channel blocker apamin mimicked an increase in cells' excitability by reducing the AHP amplitude (Belmeguenai et al., 2010). In RNA sequencing of the POA LepR neurons, we see a decrease of $K_{Ca}2.2$ mRNA with a $\log_2$-fold change of -2.03 between NA and LTA conditions (Figure 2.11. B) and we do see an increase in firing frequency with acclimation. If the expression of this channel plays a role in the firing properties of POA^{LepR} neurons it would most probably prolong the afterhyperpolarization phase and therefore slow down the firing of a neuron. In the whole-cell patch-clamp experiments I applied the SK2 channel activator CYPPA in the ACSF. CYPPA has significantly reduced the firing frequency of POA^{LepR} neurons in the LTA condition (Figure 2.14. A). Therefore, the reduction of AP FF after CYPPA application suggests that the $K_{Ca}2.2$ channel is present in the POA^{LepR} neurons as the functional protein. Importantly, CYPPA affects the SK3 channel as well so the effect observed might be due to the effect of CYPPA on SK2 and SK3 channels together (Hougaard et al., 2007). I did not observe hyperpolarization of POA^{LepR} neurons when applying the activator, which is expected to have happened if it increased AHP. Nevertheless, to see whether CYPPA exerted its effect through SK-mediated AHP I should measure AHP amplitude specifically.

Contrary to CYPPA, the application of general SK blocker apamin (Stocker et al., 1999) did not affect the firing frequency of POA^{LepR} neurons or any other measured parameter (Figure 2.14. E-G). This result might suggest that blocking SK channels, and by that mAHP, is not affecting the intrinsic firing of POA^{LepR} neurons. It could as well be that application of 300 nM apamin was too low a concentration to reach POA neurons in *ex vivo* slices to exert its action, and therefore I did not observe any effect on the AP firing.

Moreover, as the mRNA sequencing has shown, the levels of *Kcnn2* are higher in the non-acclimated condition. That is why I would expect also a larger effect of both drugs, CYPPA, and apamin, in the non-acclimated cells. However, the effect of the CYPPA was seen only in POA^{LepR} neurons after acclimation (LTA condition), and the apamin effect was absent in both NA and LTA conditions. To disprove or prove that SK2 is playing a role in the increase of the POA^{LepR} neurons AP FF I should measure the currents mediated by this channel, or mAHP while applying as specific blockers as possible.

4.4.3. Kcnh2 (K_v11.1)

The third ion channel gene found borderline significant in the RNA-seq of POA^{LepR} neurons was *Kcnh2* coding for K_v11.1 (Potassium Voltage-Gated Channel Subfamily H Member 2; Ether à go-go-related gene; *erg1*) (Figure 2.11. C). In neurons, erg channels mediate a small persistent current near the resting potential. Interestingly, dependent on the cell type, blocking erg channels results in different outcomes; in some neurons, such as vomeronasal neurons, the antagonist decreases firing frequency, and in others, such as mitral cells, it depolarizes cells and increases firing frequency (Hirdes et al., 2009; Niculescu et al., 2013). Consistent with the latter, the blocker of the K_v11.1 ion channel, E-4031, increased AP FF of POA^{LepR} neurons in LTA conditions, and it increased RMP of neurons in both NA and LTA conditions without affecting CV (ISI) (Figure 2.15.). This result suggests that the POA^{LepR} neurons express K_v11.1 on a protein level and that this ion channel might participate in shaping action potentials in the POA^{LepR} neurons potentially in a similar manner as the Kv7.2 ion channel by counteracting their hyperexcitability. It is however worth noting that although some papers present E-4031 as a K_v11.1 specific antagonist, others have found it equally potent in blocking the other members of its family as well (K_v11.2 and K_v11.3) (Shi et al., 1997) so the effect observed might be coming from this drug affecting other proteins as well.

The interesting finding is that E-4031 increased the RMP in both NA and LTA neurons, but the AP FF increased by blocking this channel only in the LTA condition. The reason for this might be the expression of other ion channels that changes after heat acclimation. Therefore, it may be that, apart from the potassium channels, which I found differentially expressed after heat acclimation, other ion channels are contributing to the modulation of heat-acclimation-induced increase of AP FF in POA^{LepR} neurons together with K_v11.1 and K_v7.2.

In addition, K_v11.1 activator NS-1643 did not affect AP FF, RMP, or CV (ISI) in POA^{LepR} neurons (Figure 2.15.). However, I could not find many papers that could serve as an example of applying this drug in acute brain slices or neurons in general as the majority of papers I found show application in heterologous expression systems (Dierich et al., 2018; Elmedyb et al., 2007, 2007). Therefore, it might be that the absence of the drug effect is technical and the concentration I used was too low to reach the cells in acute brain slices or that this drug is not suitable for this type of application. Besides that, it could be that activating K_v11.1 would not necessarily have the opposite effect as blocking it. Since it is a channel open almost constantly close to the resting membrane potential, perhaps augmenting its open state would be redundant for neuronal firing.

To conclude, all three ion channel candidates code for potassium channels playing role in neuronal afterhyperpolarization (*Kcnn2* and *Kcnq2* (Greene & Hoshi, 2017; Pedarzani et al., 2005),) or neuronal

excitability (*Kcnn2, Kcnq2,* and *Kcnh 2*(Carver et al., 2020; Cui & Strowbridge, 2018; Pedarzani et al., 2005)) by slowing down or abolishing the evoked neuronal AP firing. Therefore, at the first glance, one would expect these genes and their proteins to be down-regulated in POA^{LepR} neurons after heat acclimation for their AP FF to be increased. Only, *Kcnn2* (KCa2.2) has been found down-regulated by heat acclimation, whereas the other two ion channels *Kcnq2,* and *Kcnh2* are found up-regulated (Figure 2.11). The up-regulation of the other two is a bit surprising at first but on the other hand work of others has proven that in some contexts role of the potassium channels might be diverse and modulate neuronal firing in a manner opposite to the expected. For example, K_v7.2/7.3 channels increase sodium channel availability in the node of Ranvier and induce the amplitude of action potential (Battefeld et al., 2014). In addition, blocking the Kv11.1 channel in Purkinje cells reduces the RMP of a neuron and increases FF (Sacco et al., 2003). Overall, it will be interesting to further test the physiology of these ion channels in POA^{LepR} neurons during heat acclimation and to see how exactly they contribute to the AP of these neurons.

4.5. POA ^{LepR} NEURONS ARE A PART OF WARM-ACTIVATED POA NEURONS

Among other interesting genes that I found in the POA^{LepR} RNA sequencing, brain-derived neurotrophic factor (*Bdnf*) and pituitary adenylate cyclase polypeptide (*Adcyap1* or PACAP) genes were both significantly upregulated with the acclimation process (Figure 2.16).

These two genes are widely accepted in the field of thermoregulation to be markers of POA neurons acutely activated by peripheral warmth - warm-activated neurons (WANs) (Siemens & Kamm, 2018; Tan et al., 2016). Moreover, *in situ* hybridization combined with RNA sequencing has revealed 14 different clusters of *Adcyap1* and *Bdnf* neurons in POA, one of which was anatomically recapitulating the location of previously defined WANs and contains neurons expressing the LepR gene (Moffitt et al., 2018). Current literature suggests that *Pacap and Bdnf* are expressed more broadly in POA than the LepR and that POA^{LepR} is a subpopulation of WANs (Hrvatin et al., 2020; Moffitt et al., 2018; Upton et al., 2021). Moreover, Yu et al. showed that the number of POA^{LepR} neurons expressing cFos doubles upon peripheral warming (Yu et al., 2016).

To verify if POA^{LepR} neurons express immediate early gene cFos upon peripheral warming, I did the IHC on the POA tissue of LeprCreHTB mice challenged with peripheral heat for 4h at 36˚C. Overlap of GFP neurons and cFos expressing neurons in the POA tissue doubled from room temperature treated mice to peripherally warm (36˚C) -stimulated ones(Figure 2.16. B; right panel). Thus, POA^{LepR} neurons seem to receive input from the periphery and to be part of WANs labeled by genetic markers such as PACAP and *Bdnf*. It would be interesting to see how many POA^{LepR} which are activated by acute warmth (WANs)

increase their AP FF during heat acclimation and estimate if these physiological properties belong to the identical LepR neuronal population.

4.6. LIMITATIONS OF THIS STUDY

Together with FACS sorting and RNA sequencing I was able to explore the transcriptome of POA^{LepR} neurons and the transcriptomic differences they might exhibit during the heat acclimation process. Even though the crossing of the HTB reporter mouse line with the LeprCre line two mouse lines made it possible to visualize LepR cells in POA, we should not ignore the fact that labeling of Lepr cells in this way is not neuronal-specific. Cre recombinase is inserted into the 3'UTR region of the Leprb exon, and HTB in the Rosa26 locus (Leshan et al., 2006; Y. Li et al., 2013). The IHC staining in the POA tissue of LeprCre/GFP cells where I quantified GFP/NeuN overlap showed that on average 18% of cells did not express neuronal marker. In addition, it could be that the bulk of cells sorted for sequencing contained RNA from other cell types. On the other hand, in Ephys recordings of POA^{LepR} neurons in acute brain slices of LeprCre line, a large majority of the cells (exact proportion not calculated) fired action potentials showing that these indeed are neuronal cells. Furthermore, cell trituration from the native tissue and FACS sorting can cause changes in the transcriptome levels which then might cause confounding effects in the sequencing (van den Brink et al., 2017). On the contrary, other studies have shown that certain technical aspects of FACS machines, such as nozzle size and sample pressure, UV exposure, and instrument type, have minor effects on downstream applications such as RNA sequencing (Box et al., 2020). However, it is important to note that these studies have not tested their parameters on neurons and that it is very likely that these have different effects on different cell types. Nevertheless, the results obtained by differential gene expression analysis of POA^{LepR} neurons transcriptome in different acclimation conditions revealed specific changes in these cells due to the acclimation process. In addition, not only the transcriptome of POA^{LepR} neurons was obtained, but with this data set, we can further explore global changes that acclimation has on the POA of mice since we FACS sorted and sequenced bulks of GFP^{-} cells from the region which represent a mixture of neurons, glia, and other cell types in the POA.

Testing the role of ion channels in the POA^{LepR} neurons employing pharmacology can have disadvantages. Technically, constant drug' perfusion onto the brain slice containing POA should ensure that the drug reaches the neurons I record from and that it exerts its effect. However, the fairest way of recording neurons would be recording a neuron before and after a drug application. This is, in most cases, difficult as some of the drugs cannot be washed out of the slice, or these would accumulate over time. Therefore, paired recordings would entail recording from a very low number of cells in one brain slice,

which poses another layer of problems such as a larger number of animals needed in the experiment and a reduction of the throughput achieved. In addition, pharmacological agonists and antagonists sometimes affect other targets as well, therefore are not specific enough. For example, SK2 antagonist apamin blocks the other two channels in the family, its agonist CYPPA affects the SK3 channel as well, and Kv11.1 blocker E-4031 affects as well other members of its family (K_v11.2 and K_v11.3) (Grunnet et al., 2001; Hougaard et al., 2007; Shi et al., 1997). In addition, the experiments in which I tested the pharmacology of candidate ion channels cannot exclude the possibility that the observed effects on AP firing might be a consequence of drugs affecting local circuitry in the POA and not only POA^{LepR} neurons, as I did not use synaptic blockers in the ACSF while recording action potentials. Nevertheless, my colleagues in the lab have measured AP FF in the POA^{LepR} neurons after acclimation with synaptic blockers (Figure 2.4. E) and have found that the firing persists showing that the firing of these neurons, at least after the long-term acclimation, is autonomous and not driven by synaptic inputs.

In addition, some of the drugs did exhibit an effect on AP firing, RMP, and CV (ISI) of POA^{LepR} neurons, and that provides enough motivation to continue testing the role of these ion channels in heat acclimation via other means such as cell-specific knock-down or gene silencing.

In this study, I used mice approximately 11 weeks old and of both sexes. In this way, I used adult animals and I did not bias toward sex differences. However, the influence of heat acclimation, although not observed in our laboratory (no data shown), might have different effects on transcriptional changes in female and male mice. It has been shown that female mice have a different ambient temperature preference than male mice, and female mice were better at withstanding chronic heat exposure (Bridges et al., 2012; Kaikaew et al., 2017). In my work, however, I have looked specifically for heat acclimation-induced changes on the ion channel level, which might cause an increase in AP firing frequency. These ionic changes might not be sex-specific, nevertheless, due to the study design, these differences would not be captured since I pooled brain tissue from both sexes for obtaining cells for FACS sorting.

Additionally, an environmental temperature of 36˚C is considered to be a warm environment for a mouse (Škop et al., 2020; Tan et al., 2016). **A**lthough some places on Earth reach a daily temperature of 36˚C, it is unusual for the temperatures to stay that high over the whole day and night. Constant 36˚C environmental temperatures might present an unnatural environment for a mouse and could cause changes in circadian rhythm and metabolism (Eckel-Mahan & Sassone-Corsi, 2013). Therefore, in our future experiments, we should consider adopting the protocol of heat acclimation to include day-to-night temperature changes to achieve a more natural environment.

4.7. STUDY IMPLEMENTATION AND FUTURE RESEARCH

Isolating neurons from heat acclimated mice and performing RNA sequencing of these cells presents a way to detect molecules that change during heat acclimation in POA^{LepR} neurons and evaluate the role of those molecules in developing acclimation phenotype – the increased heat endurance. In the analysis of the RNA-seq data set, I primarily searched for changes happening on the level of POA^{LepR} neurons and genes coding for ion channel proteins. Further investigation should start by looking at differentially expressed genes coding for other types of proteins that might mediate the change happening in AP firing in these cells. These might reveal additional roles and mechanisms by which LepR neurons in POA play a role in heat acclimation. Moreover, looking into global transcriptomic changes that happen in heat-acclimated mice in comparison to short-term acclimated and non-acclimated mice could reveal modulations that happen in the POA, the thermoregulatory center, during the acclimation process.

However, on a more pressing note, I suggest several additional experiments that might improve the work presented in this thesis and address above discussed limitations. Our choice for gene candidates which might mediate action potential firing is based on differential expression analysis of RNA-seq data that, as discussed above, might be biased towards high expressing molecules shunting therefore detection of mRNA from low-expressing genes (Sims et al., 2014). In addition, the RNA-seq performed here was done by looking at all polyadenylated mRNA molecules by using oligodT primers (Picelli et al., 2014). It would be prudent to verify these RNA-seq data by using a more biased approach such as quantitative polymerase chain reaction (qPCR) with specific primers for each of the above-suggested potassium channel genes (*Kcnq2*, *Kcnn2*, and *Kcnh2*) and to see whether changes observed with RNA-seq hold in acclimation conditions.

Equally important would be to verify the observations made by Ephys recordings in POA^{LepR} neurons before and after acclimation:

- 1st to isolate currents mediated by each of the ion channels and see whether these are increased or decreased in POA^{LepR} neurons and at the same time apply channel agonists and agonists to see whether corresponding ionic currents can be modulated in POA^{LepR} neurons.
- 2nd to repeat some of the pharmacology experiments with the application of synaptic blockers. More specifically, to apply blockers of GABAergic and glutamatergic signaling to confirm that the effect of the drug on AP firing was due to a specific and direct effect on recorded POA^{LepR} neurons.
- 3rd to investigate the effect that genetic knockdown of most reliable channel candidates has in AP firing of POA^{LepR} neurons, heat acclimation process, and heat endurance.

Moreover, although we have evidence that POA^{LepR} neurons receive thermal input from the periphery (cFos induction during warmth challenge (Figure 2.16.)) it would be interesting to know how the POA^{LepR} neurons act on the thermoregulatory circuit level to exert their role in heat acclimation. It would be interesting to see if warm-activated POA^{LepR} neurons are the same population as the ones increasing AP FF during heat acclimation and necessary for heat endurance. Additionally, neuronal tracing of POA^{Lepr} neuron projections and investigations of their post-synaptic relays might help us learn more about the thermoregulatory circuit behind heat acclimation in mice.

5. MATERIALS AND METHODS

5.1. ANIMALS

The following mouse lines were used in this study: LepR-cre (B6.129-Leprtm3(cre)Mgmj/J; The Jackson Laboratory, 032457), Rosa26Lox-stop-LoxHTB (The Salk Institute for Biological Studies), Vglut2-cre (Slc17a6tm2(cre)Lowl/J; The Jackson Laboratory, 016963). All animal experiments were under the local ethics committee and governing body (Regierungspräsidium Karlsruhe, Germany) and were approved under protocol numbers: T-05/21, G-169/18, G-223/18, and G-181/21. Mice were housed at room temperature (23 ± 1°C; unless specified otherwise) with a standard 12-h light/dark cycle and with ad libitum access to food and water. All genetically modified mice in this part of the thesis were back-crossed onto the C57Bl/6N background. All studies employed a mixture of male and female mice.

5.2. HEAT ACCLIMATION PROTOCOL

Heat acclimation protocol consisted of continuous exposure of LeprCreHTB animals to 36 ± 0.5°C, 35 for 5 days (LTA), minimum 4 to maximum 5 weeks (LTA) at the climate chamber (Binder, KB720), with *ad libitum* access to food and water. All mice were kept at the standard 12-h light/dark cycle. Humidity (≈40%) and temperature in the climate chamber were monitored daily, cages were cleaned 1 time per week at random times in the day. Non-acclimated (NA) controls were similar as possible in age (approximately 11 weeks old) to the experimental animals on the day of processing for experiments (Ephys, cell isolation for FACS sorting, or IHC).

5.3. HEAT ENDURANCE ASSAY

At the end of the acclimation period, animals were evaluated in a heat endurance assay (Figure 2.4., and Figure 2.5.). The heat endurance assay took place in the same climate chamber as used for acclimation. The heat challenge was conducted for up to a maximum of 24 h and the mouse's body temperature was constantly monitored for the entire period. A body temperature of 41.5 °C was used as the cut-off criterion (Leon et al., 2005). At the end of the heat endurance test, animals were shortly placed back to 36 °C to avoid prolonged hypothermia and monitored until the sacrifice.

5.3.1. TETANUS TOXIN AND Gi-DREADDs SILENCING OF LEPR CELLS

For these experiments (Figure 2.5), stereotactic surgeries were performed in adult LepR^{Cre} mice as follows: The skin was sutured with sterile absorbable-needled sutures (Marlin 17241041; Catgut,

Germany) and mice were injected subcutaneously with Carprofen at 5 mg/Kg (Rimadyl; Zoetis, USA). Finally, anesthesia was antagonized using a subcutaneous injection of Atipamezole 2.5 mg/kg, Flumazenil 0.5 mg/kg, and Naloxone 1.2 mg/kg, and mice were transferred to their home cages. For postoperative care, the second dose of Carprofen was injected after 24 hours and mice cages were kept on a veterinary heating pad at 37°C for 12 hours and monitored closely. A minimum of 3 weeks of viral expression was allowed before any experiments were conducted.

Viruses used for the injection were 250 nl of rAAV encoding the Cre-dependent tetanus toxin light chain (TeTxLC) (ssAAV-5/2-hSyn1-chI-dlox-EGFP_2A_FLAG_TeTxLC(rev)-dlox-WPRE-SV40p(A)) or the inhibitory Gi-DREADDs (ssAAV-1/2-hEF1α-dlox-hM4D(Gi)_mCherry(rev)-dlox-WPRE-hGHp(A)) was injected bilaterally in MnPOA. AAVs encoding a Cre-dependent mCherry/EGFP were used as controls. Acute chemogenetic silencing of LepR cells was performed by injecting CNO (or saline) 0.3 mg/kg i.p. (Enzo, diluted in saline) 10 min before transferring the animals to the heat endurance assay. Body temperature was constantly monitored as mentioned above. To validate CNO effects on the firing frequency of acclimated LepR cells, a group of chemogenetically silenced animals was used for *in vitro* electrophysiological recordings. Slice preparation and electrophysiological recording procedure are described below.

5.4. IMMUNOHISTOCHEMISTRY

5.4.1. Anatomical position of LepR neurons within the POA

For the analysis number of POA^{LepR} neurons, I performed IHC on the free-floating brain sections of the LeprCreHTB animals. In brief, non-acclimated (NA) and long-term acclimated (LTA) animals were anesthetized with isoflurane and transcardially perfused with 1xPBS followed by 4% PFA. brains were dissected out and left overnight (O/N) in 4% PFA at 4 ˚C. On the following days, brains were kept in a sucrose gradient (24h in 10% followed by 30% sucrose solution (in 1xPBS), until completely sank). Brains were sectioned with microtome at 30 µm thickness and sections were further kept in cryo-protectant solution (250 ml glycerol, 250 ml ethylene glycol, 500 ml 1xPBS) at 4 ˚C until the immunohistochemistry. For the staining, sections were washed 1time in 1xPBS and left overnight at 4 ˚C in 0,2% TritonX-100 (PBX0.2). On the following day, sections were blocked with 5% goat serum in PBS containing 0,1% TritonX-100 (PBX0.1) for 2h at room temperature (RT). Sections were then incubated with chicken α-GFP (1:500; Novus Biotechne, NB100-1614) and rabbit α-NeuN (1:1000; D4G4O, Cell Signaling), diluted in 1% goat serum in PBS containing 0,1% TritonX-100 (PBX0.1) for 3 days at 4 ˚C. On the fifth day, sections were washed extensively with PBX0.2 and were then incubated with secondary antibodies and DAPI (Alexa488

α-chicken 1:750, Alexa555 α-rabbit 1:750) for 4 hours at RT. Finally, tissue was washed extensively with PBSX0.2 and 1 time with 1x PBS after which it was mounted using Immu-Mount (FisherScientific, UK).

5.4.2. c-Fos expression in POA^{LepR} neurons.

I investigated whether POA^{LepR} neurons are stimulated by acute warm (36 ˚C exposure. To do this, Lepr-CreHTB mice were placed to get accustomed to the refrigerated chamber at RT (25˚C) for 24 hours. On the 2nd-day, control animals were taken out of the chamber, anesthetized with isoflurane, and transcardially perfused with 1xPBS followed by 4% PFA. The binder temperature was switched to 36˚C and the experimental animals were kept at this temperature for 4h from the moment 36˚C was reached in the chamber. After that, the animals were removed from the chamber, anesthetized with isoflurane, and transcardially perfused with 1xPBS followed by 4% PFA. After the perfusion with 4 % PFA, brains were dissected out and left overnight (O/N) in 4% PFA at 4 ˚C. On the following days, brains were kept in a sucrose gradient (24h in 10% followed by 30% sucrose solution (in 1xPBS), until completely sank). Brains were sectioned with microtome at 30 µm thickness and sections were further kept in cryo-protectant solution (250 ml glycerol, 250 ml ethylene glycol, 500 ml 1xPBS) at 4 ˚C until the immunohistochemistry. For the staining, sections were washed 1time in 1xPBS and left overnight at 4 ˚C in 0,2% TritonX-100 (PBX0.2). On the following day, sections were blocked with 5% goat serum in PBS containing 0,1% TritonX-100 (PBX0.1) for 2h at room temperature (RT). Sections were then incubated with chicken α-GFP (1:500; Novus Biotechne, NB100-1614) and rabbit α-cFos (1:1000; SynapticSystems 226 003), diluted in 1% goat serum in PBS containing 0,1% TritonX-100 (PBX0.1) for 3 days at 4 ˚C. On the fifth day, sections were washed extensively with PBX0.2 and were then incubated with secondary antibodies and DAPI (Alexa488 α-chicken 1:750, Alexa555 α-rabbit 1:750) for 4 hours at RT. Finally, tissue was washed extensively with PBSX0.2 and 1 time with 1x PBS after which it was mounted using Immu-Mount (FisherScientific, UK).

Cell counting was done in NIS-Elements software (Nikon Instruments, Inc). Images were processed with Fiji(Schindelin et al., 2012). Statistical analysis was performed in GraphPad Prism (7.00), and plots were produced in R studio with R package *ggplot2* (*ggplot2: Elegant Graphics for Data Analysis*. Springer-Verlag New York. ISBN 978-3-319-24277-4).

5.5. RNA SEQUENCING OF POA^{LEPR} NEURONS

5.5.1. Cell isolation for FACS sorting

Individual adult mice LeprCreHTB, acclimated and non-acclimated, (P77 ± 5) were anesthetized with isoflurane and decapitated, the brain was immediately removed and submerged in ice-cold artificial

cerebrospinal fluid (ACSF). 3 brains were sectioned at the same time on a vibratome (Leica VT1200S) in a slicing chamber containing ice-cold ACSF (in Mm; 1.2 $NaH_2PO_4xH_2O$, 2.5 KCl, 20HEPES, 25 glucose; 30 $NaHCO_3$, 93 NMDG (n-methyl-glucamine), 5 Na-Ascorbate, 3 Na-pyruvate, 12 N-acetylcysteine, 10 $MgSO_4x7H_2O$, 0.5 $CaCl_2$), constantly bubbled with carbogen. Brain slices of 250 µm thickness, containing the OVLT and MnPOA, were transferred to a Petri dish containing ACSF. We implemented the neuron isolation protocol described in Moffit et al. 2018. The regions of interest were micro dissected under a dissecting microscope and transferred to a small Petri dish containing 3ml of Papain mix consisting of Hibernate mix (Hibernate A medium (Invitrogen A1247501), 1xGlutamax (Gibco 35050-038), 0.8mM Kynurenic acid (Sigma K3375-5G), 0.05 mM AP-V (HelloBio HB0225), 0.01 mM Rock inhibitor Y-27632 (HelloBio HB2297), 1 mM B27 (Invitrogen 17504001), 5% Trehalose (Sigma T9531-10G)) and 8U/ml papain (Sigma P4762), 100U/ml DNAseI (Worthington über Cell-Systems LK003172), 0.005U/ml Chondroitinase ABC (Sigma C3667-5UN), 0.07% Hyaluronidase (Sigma, H2126), 0.001 mM NaOH where the tissue was cut in smaller pieces. The dissected tissue pieces were transferred together with the Papain mix into a 2ml tube at 37˚C to incubate while gently shaking (700 rpm) for 2h. After incubation, with the tissue pieces sitting at the bottom of the tube, the papain solution was pipetted out of the tube and exchanged with the hibernate mix containing 0.1mg/ml ovalbumin and centrifuged for 1 min at 300 g. Supernatant was removed, and hibernate mix was added to the tissue pieces which were further dissociated into single cells by gentle trituration through Pasteur pipettes with fire-polished tip openings of 600-µm, 300-µm, and 150-µm diameter. The cell suspension was centrifuged at RT at 300 g, for 10 minutes, and the supernatant was removed and exchanged with 500mul of Hibernate A medium.

5.5.2. FACS sorting

Resuspended cell material was passed through a 20um filter. The cell suspension was stained with propidium iodide (PI BD Pharmingen, Cat 51 66211E, 2ml - 50ug/ml) to exclude the dead cells before the FACS analysis. FACS sorting was performed on BD FACS Aria II Flow Cytometry Cell Sorter using the “purity” sorting mode. FACS populations were arbitrarily chosen to select cells with low PI and high GFP fluorescence but the criteria were kept the same for each sorting round.

Cells were FACS sorted into bulks of GFP$^+$ and GFP directly into the RLT buffer (QIAGEN RNeasy Micro Kit 74004), immediately frozen on the dry ice, and stored at -80˚C. Samples were further processed in a maximum of 1 month from the isolation day, by using the column purification method with QIAGEN RNeasy Micro Kit according to the manufacturer’s instructions. Samples were stored at -80 ˚C until further processing.

5.5.3. cDNA library preparation and RNA sequencing

The same protocol was used as in section 5.4.1 (page 54) RNA integrity and concentration of each sample were assessed by Agilent Bioanalyzer Nano 6000 chip (Agilent technologies) and QUBIT2 fluorometer measurement (Thermofisher Scientific) by manufacturer's instruction. I used the Smart-Seq2 protocol for the cDNA library preparation (all processing performed at Gene Core EMBL, Heidelberg). 1ul of each bulk sample RNA was processed for the reverse transcription (Superscript IV, ThermoFisher Scientific, cat. no. 18090010) followed by 18 cycles of PCR amplification, library tagmentation via Tn5 transposase (Tn5 was produced in-house by Protein Expression and Purification *Core* Facility, EMBL Heidelberg), sample barcoding (Illumina primers) and final enrichment by 12 cycles of PCR. Samples were sequenced on Illumina NextSeq 500 High sequencer; single end with 75 base-pair long reads in two pools of 18 samples each (Genomic Core Facility EMBL, Heidelberg).

5.6. STATISTICAL DATA ANALYSIS

Statistical analysis of flow cytometry parameters was performed in GraphPad Prism (7.00), and plots were produced in R studio with R package *ggplot2* (*ggplot2: Elegant Graphics for Data Analysis*. Springer-Verlag New York. ISBN 978-3-319-24277-4).

The first steps of RNA sequencing data analysis were done by *fastp* (S. Chen et al., 2018), *fastqc* (Steven W. Wingett & Simon Andrews, 2018), and *Salmon* (Patro et al., 2017)tools (as described in 5.4.2 (page 55)). Further count matrix was created with the *tximport* package (Soneson et al., 2016), and was analyzed in R and R studio (version 4.0.3. (2020-10-10)). Differential expression analysis was performed using *DESeq2* (Love et al., 2014) package with Wald test for the significance testing of the p-value and Benjamini-Hochberg for calculating the false discovery rate (FDR, adjusted p-value). Comparisons modeled in the analysis were: NA:STA; NA:LTA, and STA:LTA extracting changes happening only in GFP^{+} samples among the conditions. Plots were made using R based *ggplot2* package. Gene set enrichment analysis was done using the *fgsea* package (Korotkevich et al., 2016). Figures were assembled in Adobe Illustrator (2022).

5.7. ELECTROPHYSIOLOGY AND PHARMACOLOGY

5.7.1. Acute brain slice preparation

For electrophysiology, 8 to 12-week-old $LepR^{Cre}$;HTB mice were anesthetized using a Ketamine/Xylazine cocktail (ketamine: 220 mg/kg, Ketavet; Zoetis, USA and Xylazine 16 mg/kg, Rompun; Bayer, Germany). Under the deep anesthesia validated by the non-responsive movement of limbs to the pinching of the skin, mice were quickly decapitated, and brains were dissected out to the ice-cold oxygenated (95% O2, 5% CO2) slicing artificial cerebrospinal fluid slicing ACSF (in Mm; 1.2 $NaH_2PO_4xH_2O$, 2.5 KCl, 20HEPES, 25 glucose; 30 $NaHCO_3$, 93 NMDG (n-methyl-glucamine), 5 Na-Ascorbate, 3 Na-pyruvate, 12 N-acetylcysteine, 10 $MgSO_4x7H_2O$, 0.5 $CaCl_2$). Coronal (250 µm thick) POA slices were sliced with a vibratome (Leica VT1200S, Germany) in the same slicing solution. Slices were then transferred to and incubated at 32 °C in a bath containing oxygenated holding ACSF (in mM; 118 NaCl, 2.5KCl, 7 glucose, 1.2 $NaH_2PO_4xH_2O$, 24 $NaHCO_3$, 5 HEPES, 7 Glucose, 4 Ascorbic acids (sodium-L-ascorbate), 2.4 Na-pyruvate, 2 N-acetylcysteine (NAC), 1 $MgSo_4*7H_2O$; 2 $CaCl_2$). After a recovery period of 30 minutes, individual slices were transferred to the recording chamber where they were continuously superfused with oxygenated recording ACSF (in mM; 125 NaCl, 2.5 KCl, 7 glucose, 1.2 $NaH_2PO_4xH_2O$, 24$NaHCO_3$, 5 HEPES, 8 Glucose, 1 $MgSO_4*7H_2O$, 2 $CaCl_2$) at ≈2 ml/min.

5.7.2. Ephys recordings in POA^{LepR} neurons

Electrophysiological recordings of POALepR cells were acquired using a MultiClamp 700B amplifier (Molecular Devices, USA), Axon Digidata 1550B digitizer (Molecular Devices, USA), and Clampex 11.0.3 software (Molecular Devices, USA). Cells were visualized using a SliceScope upright microscope (Scientifica, UK) equipped with a 40X water immersion objective (U-TV1X-2, Olympus, Japan). Images were acquired by a digital CCD camera (ORCA-R2 C10600-10B, Hamamatsu Photonics K.K., Japan) using MicroManager 1.4 software (Vale's lab, UCSF, USA). Borosilicate glass micropipettes (O.D. 1.5 mm, I.D. 0.86 mm, Sutter Instrument, BF150-86-7.5) were pulled with the micropipette puller (P-97, Sutter Instrument, USA). The open pipette resistance was between 4-8 MΩ.

All the POA^{LepR} cell AP firing rate recordings were performed at 33 (±1) °C where the temperature was controlled using a gravity-operated perfusion system including an in-line heater (CL-100, Warner Instruments, USA) combined with a temperature-controlled microscope stage (Badcontroller V, Luigs & Neumann, Germany). External ACSF in which APs were recorded in the recording ACSF. The recording

pipette was filled with an internal solution containing (in mM; 138 K-gluconate, 2 KCl; 5 NaCl, 10 HEPES, 10 EGTA, 1 $CaCl_2$, 1 Mg-ATP. Signals were sampled at 10 kHz and low pass filtered at 2 kHz.

5.7.3. Pharmacology agents

For all 3 ion channels tested blockers or the activators were diluted in recording ACSF:

a) K_v7.2 (Kcnq2) blocker ML252 ((*S*)-2-Phenyl-*N*-(2-(pyrrolidine-1-yl)phenyl) butanamide), 10 µM
b) K_{Ca}2.2 activator CYPPA (*N*-Cyclohexyl-*N*-[2-(3,5-dimethyl-pyrazole-1-yl)-6-methyl-4-pyrimidinamine), 10 µM
c) SK2 blocker-apamin, 300 nM
d) E4031 blocker of K_V11.1, 10 µM
e) NS-1643 (*N*,*N*'-*Bis*[2-hydroxy-5-(trifluoromethyl)phenyl]urea), a K_v11.1 opener, 10 µM.

5.7.4. Data and Statistical analysis of electrophysiological data

For AP frequency quantification, the first 1 minute of recordings was omitted. Basic cell membrane properties such as capacitance and input resistance were calculated based on a membrane test protocol (a brief step of -10 mV from a holding potential of -65 mV). Series resistance (Rs) was typically 10–25 MΩ across experiments. AP firing frequency (Hz) was counted in Clampfit 11.1 and divided by the duration (s) of the period in which APs were counted. The first minute of the recording was always ignored. AP traces were always recorded for a minimum of 3 minutes. The RMP was calculated in Clampfit 11.1 as an average membrane potential value during the same period from which AP FF was calculated. Interspike interval was calculated from the same period of recording as the FF and RMP as the time between each spike. The coefficient of variation of ISI was calculated by dividing the standard deviation of ISI by the mean of ISI.

Statistical tests were performed using R and R studio or GraphPad Prism (Version 7.00; GraphPad Software, USA). Results are presented as mean ± standard deviation of the mean (STD) unless indicated otherwise. The distribution of data was assayed using the Kolmogorov-Smirnov normality test, the D´agostino and Pearson omnibus normality test, and the Shapiro-Wilk normality test. Further statistical details are listed in the figure legends. Plots were produced in R studio using the *ggplot2* package, Clampfit 11.1 (example traces), and Microsoft Excel 2016 (pie chart in Figure 2.13.). Figures were assembled in Adobe Illustrator 2022.

5.8. GENOTYPING PCR PROTOCOLS

Lepr Cre; Forward lepr TCCAAGAAGCCTCAAGGTTCCA**;** Reverse Cre LRC: ACGCACACCGGCCTTATTCC**;** Reverse Wild-type LRC: TCGTGTTGAAATTTCTTCTTTCCAG. PCR cycler procedure: 94 ˚C 3 min; 35x: 94˚C 30 sec, 60 ˚C 30 sec, 72 ˚C 1min; 72 ˚C 10min, 12 ˚C hold. PCR reaction per 1 sample: 2xbuffer 10 µl (36.4% sucrose, 3.5mM MgCl2, 11mM (NH4)2SO4, 0.005% cresole red, 1:1000 β-mercaptoethanol), dNTPs 10mM, Fwd primer 10mM (1 µl), Rew primer Cre 10mM (1µl), Rew primer Wildtype 10mM (1µl), taq polymerase 5U/µl (0.125 µl), H_2O (4.875 µl), DNA sample (1µl).

Bibliography

Abbott, S. B. G., Machado, N. L. S., Geerling, J. C., & Saper, C. B. (2016). Reciprocal Control of Drinking Behavior by Median Preoptic Neurons in Mice. *Journal of Neuroscience*, *36*(31), 8228–8237. https://doi.org/10.1523/JNEUROSCI.1244-16.2016

Abbott, S. B. G., & Saper, C. B. (2017). Median preoptic glutamatergic neurons promote thermoregulatory heat loss and water consumption in mice: Median preoptic neurons promote heat loss and water consumption. *The Journal of Physiology*, *595*(20), 6569–6583. https://doi.org/10.1113/JP274667

Abe, J., Okazawa, M., Adachi, R., Matsumura, K., & Kobayashi, S. (2003). Primary cold-sensitive neurons in acutely dissociated cells of rat hypothalamus. *Neuroscience Letters*, *342*(1–2), 29–32. https://doi.org/10.1016/S0304-3940(03)00239-8

Agilent Technologies. (2009). *Performance-characteristics-high-sensitivity-dna-assay-agilent-2100-bioanalyzer.pdf*.

Ahima, R. S., Prabakaran, D., Mantzoros, C., Qu, D., Lowell, B., Maratos-Flier, E., & Flier, J. S. (1996). Role of leptin in the neuroendocrine response to fasting. *Nature*, *382*(6588), 250–252. https://doi.org/10.1038/382250a0

Ahima, R. S., Saper, C. B., Flier, J. S., & Elmquist, J. K. (2000). *Leptin Regulation of Neuroendocrine Systems*. 45.

Amorim, F. T., Fonseca, I. T., Machado-Moreira, C. A., & Magalhães, F. de C. (2015). Insights into the role of heat shock protein 72 to whole-body heat acclimation in humans. *Temperature*, *2*(4), 499–505. https://doi.org/10.1080/23328940.2015.1110655

Aronsohn, Ed., & Sachs, J. (1885). Die Beziehungen des Gehirns zur Körperwärme und zum Fieber: Experimentelle Untersuchungen. *Pflüger, Archiv für die Gesammte Physiologie des Menschen und der Thiere*, *37*(1), 232–301. https://doi.org/10.1007/BF01752423

Asarian, L., Gloy, V., & Geary, N. (2012). Homeostasis. In *Encyclopedia of Human Behavior* (pp. 324–333). Elsevier. https://doi.org/10.1016/B978-0-12-375000-6.00191-9

Assayag, M., Saada, A., Gerstenblith, G., Canaana, H., Shlomai, R., & Horowitz, M. (2012). Mitochondrial performance in heat acclimation—A lesson from ischemia/reperfusion and calcium overload insults in the heart. *American Journal of Physiology-Regulatory, Integrative and Comparative Physiology*, *303*(8), R870–R881. https://doi.org/10.1152/ajpregu.00155.2012

Bado, A., Levasseur, S., Attoub, S., Kermorgant, S., Laigneau, J.-P., Bortoluzzi, M.-N., Moizo, L., Lehy, T., Guerre-Millo, M., Le Marchand-Brustel, Y., & Lewin, Miguel. J. M. (1998). The stomach is a source of leptin. *Nature*, *394*(6695), 790–793. https://doi.org/10.1038/29547

Bajjalieh Sandra M. & Scheller Richard H. (1995). The Biochemistry of Neurotransmitter Secretion(∗). *Journal of Biological Chemistry*, *270*(5), 1971–1974. https://doi.org/10.1074/jbc.270.5.1971

Balthasar, N., Coppari, R., McMinn, J., Liu, S. M., Lee, C. E., Tang, V., Kenny, C. D., McGovern, R. A., Chua, S. C., Elmquist, J. K., & Lowell, B. B. (2004). Leptin Receptor Signaling in POMC Neurons Is Required for Normal Body Weight Homeostasis. *Neuron*, *42*(6), 983–991. https://doi.org/10.1016/j.neuron.2004.06.004

Barbour, H. G. (1912). Die Wirkung unmittelbarer Erwärmung und Abkühlung der Wärmezentra auf die Körpertemperatur. *Archiv für Experimentelle Pathologie und Pharmakologie*, *70*(1), 1–26. https://doi.org/10.1007/BF01865333

Barry, H., Chaseling, G. K., Moreault, S., Sauvageau, C., Behzadi, P., Gravel, H., Ravanelli, N., & Gagnon, D. (2020). Improved neural control of body temperature following heat acclimation in humans. *The Journal of Physiology*, *598*(6), 1223–1234. https://doi.org/10.1113/JP279266

Bates, S. H., Stearns, W. H., Dundon, T. A., Schubert, M., Tso, A. W. K., Wang, Y., Banks, A. S., Lavery, H. J., Haq, A. K., Maratos-Flier, E., Neel, B. G., Schwartz, M. W., & Myers, M. G. (2003). STAT3 signalling is required for leptin regulation of energy balance but not reproduction. *Nature*, *421*(6925), 856–859. https://doi.org/10.1038/nature01388

Battefeld, A., Tran, B. T., Gavrilis, J., Cooper, E. C., & Kole, M. H. P. (2014). Heteromeric Kv7.2/7.3 Channels Differentially Regulate Action Potential Initiation and Conduction in Neocortical Myelinated Axons. *Journal of Neuroscience*, *34*(10), 3719–3732. https://doi.org/10.1523/JNEUROSCI.4206-13.2014

Bauman, D. E., & Bruce Currie, W. (1980). Partitioning of Nutrients During Pregnancy and Lactation: A Review of Mechanisms Involving Homeostasis and Homeorhesis. *Journal of Dairy Science*, *63*(9), 1514–1529. https://doi.org/10.3168/jds.S0022-0302(80)83111-0

Baumann, H., Kim, H., Lai, C.-F., & TARTAGLIAt, L. A. (1996). The full-length leptin receptor has signaling capabilities of interleukin 6-type cytokine receptors. *Proc. Natl. Acad. Sci. USA*, 5.

Bazett, C., Alpers, B. J., & Erb, W.H. (1933). HYPOTHALAMUS AND TEMPERATURE CONTROL. *Journal of Mental Science*, *80*(328), 129.

Beaudoin, G. M. J., Lee, S.-H., Singh, D., Yuan, Y., Ng, Y.-G., Reichardt, L. F., & Arikkath, J. (2012). Culturing pyramidal neurons from the early postnatal mouse hippocampus and cortex. *Nature Protocols*, *7*(9), 1741–1754. https://doi.org/10.1038/nprot.2012.099

Belmeguenai, A., Hosy, E., Bengtsson, F., Pedroarena, C. M., Piochon, C., Teuling, E., He, Q., Ohtsuki, G., De Jeu, M. T. G., Elgersma, Y., De Zeeuw, C. I., Jorntell, H., & Hansel, C. (2010). Intrinsic Plasticity Complements Long-Term Potentiation in Parallel Fiber Input Gain Control in Cerebellar Purkinje Cells. *Journal of Neuroscience*, *30*(41), 13630–13643. https://doi.org/10.1523/JNEUROSCI.3226-10.2010

Blondin, D. P., Nielsen, S., Kuipers, E. N., Severinsen, M. C., Jensen, V. H., Miard, S., Jespersen, N. Z., Kooijman, S., Boon, M. R., Fortin, M., Phoenix, S., Frisch, F., Guérin, B., Turcotte, É. E., Haman, F., Richard, D., Picard, F., Rensen, P. C. N., Scheele, C., & Carpentier, A. C. (2020). Human Brown Adipocyte Thermogenesis Is Driven by β2-AR Stimulation. *Cell Metabolism*, *32*(2), 287-300.e7. https://doi.org/10.1016/j.cmet.2020.07.005

Boehm, U., Klamp, T., Groot, M., & Howard, J. C. (1997). CELLULAR RESPONSES TO INTERFERON-γ. *Annual Review of Immunology*, *15*(1), 749–795. https://doi.org/10.1146/annurev.immunol.15.1.749

Bond, C. T. (2004). Small Conductance Ca2+-Activated K+ Channel Knock-Out Mice Reveal the Identity of Calcium-Dependent Afterhyperpolarization Currents. *Journal of Neuroscience*, *24*(23), 5301–5306. https://doi.org/10.1523/JNEUROSCI.0182-04.2004

Boulant, J. A. (2000). Role of the Preoptic-Anterior Hypothalamus in Thermoregulation and Fever. *Clinical Infectious Diseases*, *31*(Supplement_5), S157–S161. https://doi.org/10.1086/317521

Boulant, J. A. (2006). Neuronal basis of Hammel's model for set-point thermoregulation. *Journal of Applied Physiology*, *100*(4), 1347–1354. https://doi.org/10.1152/japplphysiol.01064.2005

Boulant, J. A. (2011). Hypothalamic Neurons Regulating Body Temperature. In R. Terjung (Ed.), *Comprehensive Physiology*. John Wiley & Sons, Inc. https://doi.org/10.1002/cphy.cp040106

Boulant, J. A., & Dean, J. B. (1986). Temperature Receptors in the Central Nervous System. *Ann.Rev.Physiol*, 639–654.

Boulant, J. A., & Hardy, J. D. (1974). The effect of spinal and skin temperatures on the firing rate and thermosensitivity of preoptic neurones. *The Journal of Physiology*, *240*(3), 639–660. https://doi.org/10.1113/jphysiol.1974.sp010627

Box, A., DeLay, M., Tighe, S., Chittur, S. V., Bergeron, A., Cochran, M., Lopez, P., Meyer, E. M., Saluk, A., Thornton, S., & Brundage, K. (2020). *Evaluating the Effects of Cell Sorting on Gene Expression*. *31*(3), 12.

Branco, T. (2016). *Near-Perfect Synaptic Integration by Nav1.7 in Hypothalamic Neurons Regulates Body Weight*. 14.

Bridges, T. M., Tulapurkar, M. E., Shah, N. G., Singh, I. S., & Hasday, J. D. (2012). Tolerance for chronic heat exposure is greater in female than male mice. *International Journal of Hyperthermia*, *28*(8), 747–755. https://doi.org/10.3109/02656736.2012.734425

Brown, D. A., & Passmore, G. M. (2009). Neural KCNQ (Kv7) channels. *British Journal of Pharmacology*, 11.

Brück, K., & Zeisberger, E. (1987). Adaptive changes in thermoregulation and their neuropharmacological basis. *Pharmacology & Therapeutics*, *35*(1–2), 163–215. https://doi.org/10.1016/0163-7258(87)90106-9

Butler, A., Hoffman, P., Smibert, P., Papalexi, E., & Satija, R. (2018). Integrating single-cell transcriptomic data across different conditions, technologies, and species. *Nature Biotechnology*, *36*(5), 411–420. https://doi.org/10.1038/nbt.4096

Cadwell, C. R., Palasantza, A., Jiang, X., Berens, P., Deng, Q., Yilmaz, M., Reimer, J., Shen, S., Bethge, M., Tolias, K. F., Sandberg, R., & Tolias, A. S. (2016). Electrophysiological, transcriptomic and morphologic profiling of single neurons using Patch-seq. *Nature Biotechnology*, *34*(2), 199–203. https://doi.org/10.1038/nbt.3445

Cadwell, C. R., Scala, F., Fahey, P. G., Kobak, D., Mulherkar, S., Sinz, F. H., Papadopoulos, S., Tan, Z. H., Johnsson, P., Hartmanis, L., Li, S., Cotton, R. J., Tolias, K. F., Sandberg, R., Berens, P., Jiang, X., & Tolias, A. S. (2020). Cell type composition and circuit organization of clonally related excitatory neurons in the juvenile mouse neocortex. *ELife*, *9*, e52951. https://doi.org/10.7554/eLife.52951

Cadwell, C. R., Scala, F., Li, S., Livrizzi, G., Shen, S., Sandberg, R., Jiang, X., & Tolias, A. S. (2017). Multimodal profiling of single-cell morphology, electrophysiology, and gene expression using Patch-seq. *Nature Protocols*, *12*(12), 2531–2553. https://doi.org/10.1038/nprot.2017.120

Cai, C., Meng, X., He, J., Wu, H., & Zou, F. (2012). Effects of ZD7288 on firing pattern of thermosensitive neurons isolated from hypothalamus. *Neuroscience Letters*, *506*(2), 336–341. https://doi.org/10.1016/j.neulet.2011.11.041

Cannon, B., & Nedergaard, J. (2004). Brown Adipose Tissue: Function and Physiological Significance. *Physiological Reviews*, *84*(1), 277–359. https://doi.org/10.1152/physrev.00015.2003

Carlisle, H. J., & Dubuc, P. U. (1984). Temperature preference of genetically obese (ob/ob) mice. *Physiology & Behavior*, *33*(6), 899–902. https://doi.org/10.1016/0031-9384(84)90225-7

Carver, C. M., Hastings, S. D., Cook, M. E., & Shapiro, M. S. (2020). Functional responses of the hippocampus to hyperexcitability depend on directed, neuron-specific KCNQ2 K^+ channel plasticity. *Hippocampus*, *30*(5), 435–455. https://doi.org/10.1002/hipo.23163

Cassuto, Y. (1968). Metabolic adaptations to chronic heat exposure in the golden hamster. *American Journal of Physiology-Legacy Content*, *214*(5), 1147–1151. https://doi.org/10.1152/ajplegacy.1968.214.5.1147

Cavicchi, Sandro. (1995). CHROMOSOMAL ANALYSIS OF HEAT-SHOCK TOLERANCE IN DROSOPHILA MELANOGASTER EVOLVING AT DIFFERENT TEMOERATURES IN LABORATORY. *Evolution*, *49*(4), 676–684. https://doi.org/10.1111/j.1558-5646.1995.tb02304.x

Cechetto, D. F., Standaert, D. G., & Saper, C. B. (1985). Spinal and trigeminal dorsal horn projections to the parabrachial nucleus in the rat. *The Journal of Comparative Neurology*, *240*(2), 153–160. https://doi.org/10.1002/cne.902400205

Charlier, C., Singh, N. A., Ryan, S. G., Lewis, T. B., Reus, B. E., & Leppert, M. (1998). *A pore mutation in a novel KQT-like potassium channel gene in an idiopathic epilepsy family*. *18*, 3.

Chen, H., Charlat, O., Tartaglia, L. A., Woolf, E. A., Weng, X., Ellis, S. J., Lakey, N. D., Culpepper, J., More, K. J., Breitbart, R. E., Duyk, G. M., Tepper, R. I., & Morgenstern, J. P. (1996). Evidence That the Diabetes Gene Encodes the Leptin Receptor: Identification of a Mutation in the Leptin Receptor Gene in db/db Mice. *Cell*, *84*, 5.

Chen, S., Zhou, Y., Chen, Y., & Gu, J. (2018). fastp: An ultra-fast all-in-one FASTQ preprocessor. *Bioinformatics*, *34*(17), i884–i890. https://doi.org/10.1093/bioinformatics/bty560

Cheung, Y.-Y., Yu, H., Xu, K., Zou, B., Wu, M., McManus, O. B., Li, M., Lindsley, C. W., & Hopkins, C. R. (2012). Discovery of a Series of 2-Phenyl- *N* -(2-(pyrrolidin-1-yl)phenyl)acetamides as Novel Molecular Switches that Modulate Modes of K_v 7.2 (KCNQ2) Channel Pharmacology: Identification of (*S*)-2-Phenyl- *N* -(2-(pyrrolidin-1-yl)phenyl)butanamide (ML252) as a Potent, Brain Penetrant K_v 7.2 Channel Inhibitor. *Journal of Medicinal Chemistry*, *55*(15), 6975–6979. https://doi.org/10.1021/jm300700v

Coleman, D. L. (1978). *Obese and diabetes: Two mutant genes causing diabetes-obesity syndromes in mice*. 8.

Collier, R. J., Baumgard, L. H., Zimbelman, R. B., & Xiao, Y. (2019). Heat stress: Physiology of acclimation and adaptation. *Animal Frontiers*, *9*(1), 12–19. https://doi.org/10.1093/af/vfy031

Collier, R. J., & Gebremedhin, K. G. (2015). Thermal Biology of Domestic Animals. *Annual Review of Animal Biosciences*, *3*(1), 513–532. https://doi.org/10.1146/annurev-animal-022114-110659

Conceição, E. P. S., Madden, C. J., & Morrison, S. F. (2019). Neurons in the rat ventral lateral preoptic area are essential for the warm-evoked inhibition of brown adipose tissue and shivering thermogenesis. *Acta Physiologica*, *225*(4), e13213. https://doi.org/10.1111/apha.13213

Cui, E. D., & Strowbridge, B. W. (2018). *Modulation of Ether-a`-Go-Go Related Gene (ERG) Current Governs Intrinsic Persistent Activity in Rodent Neocortical Pyramidal Cells*. 18.

Curras, M. C., Kelso, S. R., & Boulant, J. A. (1991). Intracellular analysis of inherent and synaptic activity in hypothalamic thermosensitive neurones in the rat. *The Journal of Physiology*, *440*(1), 257–271. https://doi.org/10.1113/jphysiol.1991.sp018707

Cypess, A. M., Williams, G., Goldfine, A. B., Tseng, Y.-H., & Kolodny, G. M. (2009). Identification and Importance of Brown Adipose Tissue in Adult Humans. *The New England Journal of Medicine*, 9.

Davis, T. R. A., & Mayer, J. (1954). Imperfect Homeothermia in the Hereditary Obese-Hyperglycemic Syndrome of Mice. *American Journal of Physiology-Legacy Content*, *177*(2), 222–226. https://doi.org/10.1152/ajplegacy.1954.177.2.222

de Luca, C., Kowalski, T. J., Zhang, Y., Elmquist, J. K., Lee, C., Kilimann, M. W., Ludwig, T., Liu, S.-M., & Chua, S. C. (2005). Complete rescue of obesity, diabetes, and infertility in db/db mice by neuron-specific LEPR-B transgenes. *Journal of Clinical Investigation*, *115*(12), 3484–3493. https://doi.org/10.1172/JCI24059

Dean, J. B., & Boulant, J. A. (1989). In vitro localization of thermosensitive neurons in the rat diencephalon. *American Journal of Physiology-Regulatory, Integrative and Comparative Physiology*, *257*(1), R57–R64. https://doi.org/10.1152/ajpregu.1989.257.1.R57

Dehaye, J. P., Winand, J., & Christophe, J. (1977). Lipolysis and cyclic AMP levels in epididymal adipose tissue of obese-hyperglycaemic mice. *Diabetologia*, *13*(6), 553–561. https://doi.org/10.1007/BF01236307

Dierich, M., Evers, S., Wilke, B. U., & Leitner, M. G. (2018). Inverse Modulation of Neuronal Kv12.1 and Kv11.1 Channels by 4-Aminopyridine and NS1643. *Frontiers in Molecular Neuroscience*, *11*, 11. https://doi.org/10.3389/fnmol.2018.00011

Ding, S.-L., Yao, Z., Hirokawa, K. E., Nguyen, T. N., Graybuck, L. T., Fong, O., Bohn, P., Ngo, K., Smith, K. A., Koch, C., Phillips, J. W., Lein, E. S., Harris, J. A., Tasic, B., & Zeng, H. (2020). Distinct Transcriptomic Cell Types and Neural Circuits of the Subiculum and Prosubiculum along the Dorsal-Ventral Axis. *Cell Reports*, *31*(7), 107648. https://doi.org/10.1016/j.celrep.2020.107648

Dubbs, A., Guevara, J., & Yuste, R. (2016). moco: Fast Motion Correction for Calcium Imaging. *Frontiers in Neuroinformatics*, *10*. https://doi.org/10.3389/fninf.2016.00006

Duclaux, R., & Kenshalo DR, Sr. (1980). Response characteristics of cutaneous warm receptors in the monkey. *Journal of Neurophysiology*, *43*(1), 1–15. https://doi.org/10.1152/jn.1980.43.1.1

Eberwine, J., & Bartfai, T. (2011). Single cell transcriptomics of hypothalamic warm sensitive neurons that control core body temperature and fever response. *Pharmacology & Therapeutics*, *129*(3), 241–259. https://doi.org/10.1016/j.pharmthera.2010.09.010

Eckel-Mahan, K., & Sassone-Corsi, P. (2013). Metabolism and the Circadian Clock Converge. *Physiological Reviews*, *93*(1), 107–135. https://doi.org/10.1152/physrev.00016.2012

Elias, C. F., Aschkenasi, C., Lee, C., Kelly, J., Ahima, R. S., Bjorbæk, C., Flier, J. S., Saper, C. B., & Elmquist, J. K. (1999). Leptin Differentially Regulates NPY and POMC Neurons Projecting to the Lateral Hypothalamic Area. *Neuron*, *23*(4), 775–786. https://doi.org/10.1016/S0896-6273(01)80035-0

Elmedyb, P., Olesen, S.-P., & Grunnet, M. (2007). Activation of ERG2 potassium channels by the diphenylurea NS1643. *Neuropharmacology*, *53*(2), 283–294. https://doi.org/10.1016/j.neuropharm.2007.05.009

Elmquist, J. K., Bjorbaek, C., Ahima, R. S., Flier, J. S., & Saper, C. B. (1998). Distributions of leptin receptor mRNA isoforms in the rat brain. *The Journal of Comparative Neurology*, *395*(4), 535–547. https://doi.org/10.1002/(SICI)1096-9861(19980615)395:4<535::AID-CNE9>3.0.CO;2-2

Engblom, D., Saha, S., Engström, L., Westman, M., Audoly, L. P., Jakobsson, P.-J., & Blomqvist, A. (2003). Microsomal prostaglandin E synthase-1 is the central switch during immune-induced pyresis. *Nature Neuroscience*, *6*(11), 1137–1138. https://doi.org/10.1038/nn1137

Falconer, D. S., & Isaacson, J. H. (1959). ADIPOSE, A NEW INHERITED OBESITY OF THE MOUSE. *Journal of Heredity*, *50*(6), 290–292. https://doi.org/10.1093/oxfordjournals.jhered.a106929

Feketa, V. V., Nikolaev, Y. A., Merriman, D. K., Bagriantsev, S. N., & Gracheva, E. O. (2020). CNGA3 acts as a cold sensor in hypothalamic neurons. *ELife*, *9*, e55370. https://doi.org/10.7554/eLife.55370

Fischer, A. W., Cannon, B., & Nedergaard, J. (2020). Leptin: Is It Thermogenic? *Endocrine Reviews*, *41*(2), 232–260. https://doi.org/10.1210/endrev/bnz016

Fischer, A. W., Hoefig, C. S., Abreu-Vieira, G., de Jong, J. M. A., Petrovic, N., Mittag, J., Cannon, B., & Nedergaard, J. (2016). Leptin Raises Defended Body Temperature without Activating Thermogenesis. *Cell Reports*, *14*(7), 1621–1631. https://doi.org/10.1016/j.celrep.2016.01.041

Flier, J. S., Underhill, L. H., Saper, C. B., & Breder, C. D. (1994). The Neurologic Basis of Fever. *New England Journal of Medicine*, *330*(26), 1880–1886. https://doi.org/10.1056/NEJM199406303302609

Földy, C., Darmanis, S., Aoto, J., Malenka, R. C., Quake, S. R., & Südhof, T. C. (2016). Single-cell RNAseq reveals cell adhesion molecule profiles in electrophysiologically defined neurons. *Proceedings of the National Academy of Sciences*, *113*(35). https://doi.org/10.1073/pnas.1610155113

Fox, R. H., Goldsmith, R., Kidd, D. J., & Lewis, H. E. (1963). Acclimatization to heat in man by controlled elevation of body temperature. *The Journal of Physiology*, *166*(3), 530–547. https://doi.org/10.1113/jphysiol.1963.sp007121

Friedman, J. (2014). 20 YEARS OF LEPTIN: Leptin at 20: an overview. *Journal of Endocrinology*, *223*(1), T1–T8. https://doi.org/10.1530/JOE-14-0405

Friedman, J. M., Leibel, R. L., & Bahary, N. (1991). Molecular mapping of obesity genes. *Mammalian Genome*, *1*(3), 130–144. https://doi.org/10.1007/BF00351059

Friedman, J. M., Leibel, R. L., Siegel, D. S., Walsh, J., & Bahary, N. (1991). Molecular mapping of the mouse ob mutation. *Genomics*, *11*(4), 1054–1062. https://doi.org/10.1016/0888-7543(91)90032-A

Fuzik, J., Zeisel, A., Máté, Z., Calvigioni, D., Yanagawa, Y., Szabó, G., Linnarsson, S., & Harkany, T. (2016). Integration of electrophysiological recordings with single-cell RNA-seq data identifies neuronal subtypes. *Nature Biotechnology*, *34*(2), 175–183. https://doi.org/10.1038/nbt.3443

Garbuz, D., Evgenev, M. B., Feder, M. E., & Zatsepina, O. G. (2003). Evolution of thermotolerance and the heat-shock response: Evidence from inter/intraspecific comparison and interspecific hybridization in the *virilis* species group of *Drosophila* . I. Thermal phenotype. *Journal of Experimental Biology*, *206*(14), 2399–2408. https://doi.org/10.1242/jeb.00429

Geerling, J. C., Kim, M., Mahoney, C. E., Abbott, S. B. G., Agostinelli, L. J., Garfield, A. S., Krashes, M. J., Lowell, B. B., & Scammell, T. E. (2016). Genetic identity of thermosensory relay neurons in the lateral parabrachial nucleus. *American Journal of Physiology-Regulatory, Integrative and Comparative Physiology*, *310*(1), R41–R54. https://doi.org/10.1152/ajpregu.00094.2015

Geiser, F. (2020). Seasonal Expression of Avian and Mammalian Daily Torpor and Hibernation: Not a Simple Summer-Winter Affair. *Frontiers in Physiology*, *11*, 19.

Gordon, J., Amini, S., & White, M. K. (2013). General Overview of Neuronal Cell Culture. In S. Amini & M. K. White (Eds.), *Neuronal Cell Culture* (Vol. 1078, pp. 1–8). Humana Press. https://doi.org/10.1007/978-1-62703-640-5_1

Gouwens, N. W., Sorensen, S. A., Baftizadeh, F., Budzillo, A., Lee, B. R., Jarsky, T., Alfiler, L., Baker, K., Barkan, E., Berry, K., Bertagnolli, D., Bickley, K., Bomben, J., Braun, T., Brouner, K., Casper, T., Crichton, K., Daigle, T. L., Dalley, R., … Zeng, H. (2020). Integrated Morphoelectric and Transcriptomic Classification of Cortical GABAergic Cells. *Cell*, *183*(4), 935-953.e19. https://doi.org/10.1016/j.cell.2020.09.057

Greene, D. L., & Hoshi, N. (2017). Modulation of Kv7 channels and excitability in the brain. *Cellular and Molecular Life Sciences*, *74*(3), 495–508. https://doi.org/10.1007/s00018-016-2359-y

Griffin, J. D., & Boulant, J. A. (1995). Temperature effects on membrane potential and input resistance in rat hypothalamic neurones. *The Journal of Physiology*, *488*(2), 407–418. https://doi.org/10.1113/jphysiol.1995.sp020975

Griffin, J. D., Kaple, M. L., Chow, A. R., & Boulant, J. A. (1996). Cellular mechanisms for neuronal thermosensitivity in the rat hypothalamus. *The Journal of Physiology*, *492*(1), 231–242. https://doi.org/10.1113/jphysiol.1996.sp021304

Grunnet, M., Jensen, B. S., Olesen, S.-P., & Klaerke, D. A. (2001). Apamin interacts with all subtypes of cloned small-conductance Ca 2+ -activated K + channels. *Pflugers Archiv European Journal of Physiology*, *441*(4), 544–550. https://doi.org/10.1007/s004240000447

Guieu, J. D., & Hardy, J. D. (1970). Effects of heating and cooling of the spinal cord on preoptic unit activity. *Journal of Applied Physiology*, *29*(5), 675–683. https://doi.org/10.1152/jappl.1970.29.5.675

Haddad, W., & Horowitz, M. (1999). Heat acclimation alters nitric oxide response in the splanchnic circulation. *Journal of Thermal Biology*, *24*(5–6), 403–408. https://doi.org/10.1016/S0306-4565(99)00054-6

Hall, C. N., Klein-Flugge, M. C., Howarth, C., & Attwell, D. (2012). Oxidative Phosphorylation, Not Glycolysis, Powers Presynaptic and Postsynaptic Mechanisms Underlying Brain Information Processing. *Journal of Neuroscience*, *32*(26), 8940–8951. https://doi.org/10.1523/JNEUROSCI.0026-12.2012

Hamann, A., Anderson, S., Lollmann, B., & Lowell, B. B. (1995). Leptin levels reflect body lipid content in mice: Evidence for diet-induced resistance to leptin action. *NATURE MEDICINE*, *1*(12), 4.

Hammel, H. T., Hardy, J. D., & Fusco, M. M. (1960). Thermoregulatory responses to hypothalamic cooling in unanesthetized dogs. *American Journal of Physiology-Legacy Content*, *198*(3), 481–486. https://doi.org/10.1152/ajplegacy.1960.198.3.481

Hammel, H. T., Jackson, D. C., Stolwijk, J. A. J., Hardy, J. D., & Stromme, S. B. (1963). Temperature regulation by hypothalamic proportional control with an adjustable set point. *Journal of Applied Physiology*, *18*(6), 1146–1154. https://doi.org/10.1152/jappl.1963.18.6.1146

Haque, A., Engel, J., Teichmann, S. A., & Lönnberg, T. (2017). A practical guide to single-cell RNA-sequencing for biomedical research and clinical applications. *Genome Medicine*, *9*(1), 75. https://doi.org/10.1186/s13073-017-0467-4

Harding, E. C., Yu, X., Miao, A., Andrews, N., Ma, Y., Ye, Z., Lignos, L., Miracca, G., Ba, W., Yustos, R., Vyssotski, A. L., Wisden, W., & Franks, N. P. (2018). A Neuronal Hub Binding Sleep Initiation and Body Cooling in Response to a Warm External Stimulus. *Current Biology*, *28*(14), 2263-2273.e4. https://doi.org/10.1016/j.cub.2018.05.054

Hardy, J. D., Hellon, R. F., & Sutherland, K. (1964). Temperature-sensitive neurones in the dog's hypothalamus. *The Journal of Physiology*, *175*(2), 242–253. https://doi.org/10.1113/jphysiol.1964.sp007515

Harris, R. B. S., Zhou, J., Redmann, S. M., Smagin, G. N., Smith, S. R., Rodgers, E., & Zachwieja, J. J. (1998). *A Leptin Dose-Response Study in Obese (ob/ob) and Lean (□/?) Mice*. *139*(1), 12.

Hemingway, A., Rasmussen, T., Wikoff, H., & Rasmussen, A. T. (1940). Effects of heating hypothalamus of dogs by diathermy. *Journal of Neurophysiology*, *3*, 329-338. https://doi.org/10.1152/jn.1940.3.4.329

Hensel, H., & Iggo, A. (1971). Analysis of cutaneous warm and cold fibres in primates. *Pflugers Archiv European Journal of Physiology*, *329*(1), 1–8. https://doi.org/10.1007/BF00586896

Hicks, S. C., Townes, F. W., Teng, M., & Irizarry, R. A. (2018). Missing data and technical variability in single-cell RNA-sequencing experiments. *Biostatistics*, *19*(4), 562–578. https://doi.org/10.1093/biostatistics/kxx053

Hirdes, W., Napp, N., Wulfsen, I., Schweizer, M., Schwarz, J. R., & Bauer, C. K. (2009). Erg K+ currents modulate excitability in mouse mitral/tufted neurons. *Pflügers Archiv - European Journal of Physiology*, *459*(1), 55–70. https://doi.org/10.1007/s00424-009-0709-4

Hom, L. L., Lee, E. C.-H., Apicella, J. M., Wallace, S. D., Emmanuel, H., Klau, J. F., Poh, P. Y. S., Marzano, S., Armstrong, L. E., Casa, D. J., & Maresh, C. M. (2012). Eleven days of moderate exercise and heat exposure induces acclimation without significant HSP70 and apoptosis responses of lymphocytes in college-aged males. *Cell Stress and Chaperones*, *17*(1), 29–39. https://doi.org/10.1007/s12192-011-0283-5

Hori, A., Minato, K., & Kobayashi, S. (1999). Warming-activated channels of warm-sensitive neurons in rat hypothalamic slices. *Neuroscience Letters*, *275*(2), 93–96. https://doi.org/10.1016/S0304-3940(99)00732-6

Horii-Hayashi, N., Sasagawa, T., Matsunaga, W., & Nishi, M. (2015). Development and Structural Variety of the Chondroitin Sulfate Proteoglycans-Contained Extracellular Matrix in the Mouse Brain. *Neural Plasticity*, *2015*, 1–12. https://doi.org/10.1155/2015/256389

Horowitz, M. (2002). *From molecular and cellular to integrative heat defense during exposure to chronic heat*. 9.

Horowitz, M. (2007). Heat acclimation and cross-tolerance against novel stressors: Genomic–physiological linkage. In *Progress in Brain Research* (Vol. 162, pp. 373–392). Elsevier. https://doi.org/10.1016/S0079-6123(06)62018-9

Horowitz, M. (2014). Heat Acclimation, Epigenetics, and Cytoprotection Memory. In R. Terjung (Ed.), *Comprehensive Physiology* (1st ed., pp. 199–230). Wiley. https://doi.org/10.1002/cphy.c130025

Horowitz, M. (2016). Epigenetics and cytoprotection with heat acclimation. *Journal of Applied Physiology*, *120*(6), 702–710. https://doi.org/10.1152/japplphysiol.00552.2015

Horowitz, M., Eli-Berchoer, L., Wapinski, I., Friedman, N., & Kodesh, E. (2004). Stress-related genomic responses during the course of heat acclimation and its association with ischemic-reperfusion cross-tolerance. *Journal of Applied Physiology*, *97*(4), 1496–1507. https://doi.org/10.1152/japplphysiol.00306.2004

Horowitz, M., Kaspler, P., Simon, E., & Gerstberger, R. (1999). Heat acclimation and hypohydration: Involvement of central angiotensin II receptors in thermoregulation. *American Journal of Physiology-Regulatory, Integrative and Comparative Physiology*, *277*(1), R47–R55. https://doi.org/10.1152/ajpregu.1999.277.1.R47

Horowitz, M., Maloyan, A., & Shlaier, J. (1997). HSP 70 kDa Dynamics in Animals Undergoing Heat Stress Superimposed on Heat Acclimation. *Annals of the New York Academy of Sciences*, *813*(1 Thermoregulat), 617–619. https://doi.org/10.1111/j.1749-6632.1997.tb51755.x

Horowitz, M., & Meiri, U. (1985). Altered responsiveness to parasympathetic activation of submaxillary salivary gland in the heat-acclimated rat. *Comparative Biochemistry and Physiology Part A: Physiology*, *80*(1), 57–60. https://doi.org/10.1016/0300-9629(85)90678-4

Hougaard, C., Eriksen, B., Jørgensen, S., Johansen, T., Dyhring, T., Madsen, L., Strøb, D., & Christophersen, P. (2007). Selective positive modulation of the SK3 and SK2 subtypes of small conductance Ca2 þ -activated K þ channels. *British Journal of Pharmacology*, 11.

Hrvatin, S., Sun, S., Wilcox, O. F., Yao, H., Lavin-Peter, A. J., Cicconet, M., Assad, E. G., Palmer, M. E., Aronson, S., Banks, A. S., Griffith, E. C., & Greenberg, M. E. (2020). Neurons that regulate mouse torpor. *Nature*, *583*(7814), 115–121. https://doi.org/10.1038/s41586-020-2387-5

Hübschle, T., McKinley, M. J., & Oldfield, B. J. (1998). Efferent connections of the lamina terminalis, the preoptic area and the insular cortex to submandibular and sublingual gland of the rat traced with pseudorabies virus. *Brain Research*, *806*(2), 219–231. https://doi.org/10.1016/S0006-8993(98)00765-3

Hummel K.P., Dickie M.M., & Coleman D. (1966). Diabetes, a New Mutation in the Mouse. *Science*, *153*.

Hutchison, V. H., & Maness, J. D. (1979). The Role of Behavior in Temperature Acclimation and Tolerance in Ectotherms. *American Zoologist*, *19*(1), 367–384. https://doi.org/10.1093/icb/19.1.367

Hylden, J. L. K., Hayashi, D. R. H., Dubner, R., & Bennett, G. J. (1986). Physiology and morphology of the lamina i spinomesencephalic projection. *The Journal of Comparative Neurology*, *247*(4), 505–515. https://doi.org/10.1002/cne.902470410

Ilicic, T., Kim, J. K., Kolodziejczyk, A. A., Bagger, F. O., McCarthy, D. J., Marioni, J. C., & Teichmann, S. A. (2016). Classification of low quality cells from single-cell RNA-seq data. *Genome Biology*, *17*(1), 29. https://doi.org/10.1186/s13059-016-0888-1

Imai-Matsumura, K., Matsumura, K., & Nakayama, T. (1984). Involvement of ventromedial hypothalamus in brown adipose tissue thermogenesis induced by preoptic cooling in rats. *The Japanese Journal of Physiology*, *34*(5), 939–943. https://doi.org/10.2170/jjphysiol.34.939

Imbeaud, S. (2005). Towards standardization of RNA quality assessment using user-independent classifiers of microcapillary electrophoresis traces. *Nucleic Acids Research*, *33*(6), e56–e56. https://doi.org/10.1093/nar/gni054

Ingalls AM, Dickie MM, & Snell GD. (1950). OBESE, A NEW MUTATION IN THE HOUSE MOUSE. *J Hered.*

Iriuchijima, J., & Zotterman, Y. (1960). The Specificity of Afferent Cutaneous C Fibres in Mammals. *Acta Physiologica Scandinavica*, *49*(2–3), 267–278. https://doi.org/10.1111/j.1748-1716.1960.tb01952.x

Isaac Ott. (1887). THE_HEAT_CENTRE_IN_THE_BRAIN.2.pdf. *Journal of Nervous and Mental Diseases*, *14*(3), 152–162.

Jakovcevski, I. (2005). Olig Transcription Factors Are Expressed in Oligodendrocyte and Neuronal Cells in Human Fetal CNS. *Journal of Neuroscience*, *25*(44), 10064–10073. https://doi.org/10.1523/JNEUROSCI.2324-05.2005

J.L. Halaas. (1995). *Weight-Reducing Effects of the Plasma Protein Encoded by the obese Gene*. *269*.

Johansen, N., & Quon, G. (2022). *Projecting clumped transcriptomes onto single cell atlases to achieve single cell resolution* [Preprint]. Bioinformatics. https://doi.org/10.1101/2022.04.26.489628

Johnson, J. M., Minson, C. T., & Kellogg, D. L. (2014). Cutaneous Vasodilator and Vasoconstrictor Mechanisms in Temperature Regulation. *Comprehensive Physiology*, *4*, 57.

Kaech, S., Huang, C.-F., & Banker, G. (2012). General Considerations for Live Imaging of Developing Hippocampal Neurons in Culture. *Cold Spring Harbor Protocols*, *2012*(3), pdb.ip068221. https://doi.org/10.1101/pdb.ip068221

Kaikaew, K., Steenbergen, J., Themmen, A. P. N., Visser, J. A., & Grefhorst, A. (2017). Sex difference in thermal preference of adult mice does not depend on presence of the gonads. *Biology of Sex Differences*, *8*(1), 24. https://doi.org/10.1186/s13293-017-0145-7

Kakava-Georgiadou, N., Severens, J. F., Jørgensen, A. M., Stoltenborg, I., Garner, K. M., Luijendijk, M. C. M., Drkelic, V., van Dijk, R., Dickson, S. L., Pers, T. H., Basak, O., & Adan, R. A. H. (2020). *Single-cell analysis reveals cellular heterogeneity and molecular determinants of hypothalamic leptin-receptor cells* [Preprint]. Neuroscience. https://doi.org/10.1101/2020.07.23.217729

Kamm, G. B., Boffi, J. C., Zuza, K., Nencini, S., Campos, J., Schrenk-Siemens, K., Sonntag, I., Kabaoğlu, B., El Hay, M. Y. A., Schwarz, Y., Tappe-Theodor, A., Bruns, D., Acuna, C., Kuner, T., & Siemens, J. (2021). A synaptic temperature sensor for body cooling. *Neuron*, *109*(20), 3283-3297.e11. https://doi.org/10.1016/j.neuron.2021.10.001

Kanosue, K., Nakayama, T., Tanaka, H., Yanase, M., & Yasuda, H. (1990). Modes of action of local hypothalamic and skin thermal stimulation on salivary secretion in rats. *The Journal of Physiology*, *424*(1), 459–471. https://doi.org/10.1113/jphysiol.1990.sp018077

Kanosue, K., Yanase-Fujiwara, M., & Hosono, T. (1994). Hypothalamic network for thermoregulatory vasomotor control. *American Journal of Physiology-Regulatory, Integrative and Comparative Physiology*, *267*(1), R283–R288. https://doi.org/10.1152/ajpregu.1994.267.1.R283

Kanosue, K., Zhang, Y. H., Yanase-Fujiwara, M., & Hosono, T. (1994). Hypothalamic network for thermoregulatory shivering. *American Journal of Physiology-Regulatory, Integrative and Comparative Physiology*, *267*(1), R275–R282. https://doi.org/10.1152/ajpregu.1994.267.1.R275

Kataoka, N., Hioki, H., Kaneko, T., & Nakamura, K. (2014). Psychological Stress Activates a Dorsomedial Hypothalamus-Medullary Raphe Circuit Driving Brown Adipose Tissue Thermogenesis and Hyperthermia. *Cell Metabolism*, *20*(2), 346–358. https://doi.org/10.1016/j.cmet.2014.05.018

Kataoka, N., Shima, Y., Nakajima, K., & Nakamura, K. (2020). A central master driver of psychosocial stress responses in the rat. *Science*, *367*(6482), 1105–1112. https://doi.org/10.1126/science.aaz4639

Kelso, S. R., & Boulant, J. A. (1982). Effect of synaptic blockade on thermosensitive neurons in hypothalamic tissue slices. *American Journal of Physiology-Regulatory, Integrative and Comparative Physiology*, *243*(5), R480–R490. https://doi.org/10.1152/ajpregu.1982.243.5.R480

Kelso, S. R., Perlmutter, M. N., & Boulant, J. A. (1982). Thermosensitive single-unit activity of in vitro hypothalamic slices. *American Journal of Physiology-Regulatory, Integrative and Comparative Physiology*, *242*(1), R77–R84. https://doi.org/10.1152/ajpregu.1982.242.1.R77

King, D., Skehel, P. A., Dando, O., Emelianova, K., Barron, R., & Wishart, T. M. (2021). Microarray profiling emphasizes transcriptomic differences between hippocampal *in vivo* tissue and *in vitro* cultures. *Brain Communications*, *3*(3), fcab152. https://doi.org/10.1093/braincomms/fcab152

Kiyohara, T., Hirata, M., Hori, T., & Akaike, N. (1990). Hypothalamic warm-sensitive neurons possess a tetrodotoxin-sensitive sodium channel with a high Q10. *Neuroscience Research*, *8*(1), 48–53. https://doi.org/10.1016/0168-0102(90)90056-K

Kloog, Y., Horowitz, M., Meiri, U., Galron, R., & Avron, A. (1985). Regulation of submaxillary gland muscarinic receptors during heat acclimation. *Biochimica et Biophysica Acta (BBA) - Molecular Cell Research*, *845*(3), 428–435. https://doi.org/10.1016/0167-4889(85)90208-3

Kluger, M. J. (1991). Fever: Role of Pyrogens and Cryogens. *Physiological Reviews*, *71*(1), 93–127. https://doi.org/10.1152/physrev.1991.71.1.93

Kobayashi, S. (1989). Temperature-sensitive neurons in the hypothalamus: A new hypothesis that they act as thermostats, not as transducers. *Progress in Neurobiology*, *32*(2), 103–135. https://doi.org/10.1016/0301-0082(89)90012-9

Kobayashi, S., Hori, A., Matsumura, K., & Hosokawa, H. (2006). Point-Counterpoint: Heat-induced membrane depolarization of hypothalamic neurons: a putative/an unlikely mechanism of central thermosensitivity. *American Journal of Physiology-Regulatory, Integrative and Comparative Physiology*, *290*(5), R1479–R1484. https://doi.org/10.1152/ajpregu.00655.2005

Kobayashi & Takahashi. (1993). Whole-cell properties of temperature-sensitive neurons in rat hypothalamic slices. *Proceedings of the Royal Society of London. Series B: Biological Sciences*, *251*(1331), 89–94. https://doi.org/10.1098/rspb.1993.0013

Korotkevich, G., Sukhov, V., Budin, N., Shpak, B., Artyomov, M. N., & Sergushichev, A. (2016). *Fast gene set enrichment analysis* [Preprint]. Bioinformatics. https://doi.org/10.1101/060012

Kretz, A., Marticke, J. K., Happold, C. J., Schmeer, C., & Isenmann, S. (2007). A primary culture technique of adult retina for regeneration studies on adult CNS neurons. *Nature Protocols*, *2*(1), 131–140. https://doi.org/10.1038/nprot.2007.12

Kroeger, D., Absi, G., Gagliardi, C., Bandaru, S. S., Madara, J. C., Ferrari, L. L., Arrigoni, E., Münzberg, H., Scammell, T. E., Saper, C. B., & Vetrivelan, R. (2018). Galanin neurons in the ventrolateral preoptic area promote sleep and heat loss in mice. *Nature Communications*, *9*(1), 4129. https://doi.org/10.1038/s41467-018-06590-7

Lazarus, M., Yoshida, K., Coppari, R., Bass, C. E., Mochizuki, T., Lowell, B. B., & Saper, C. B. (2007). EP3 prostaglandin receptors in the median preoptic nucleus are critical for fever responses. *Nature Neuroscience*, *10*(9), 1131–1133. https://doi.org/10.1038/nn1949

Lee, B. R., Budzillo, A., Hadley, K., Miller, J. A., Jarsky, T., Baker, K., Hill, D., Kim, L., Mann, R., Ng, L., Oldre, A., Rajanbabu, R., Trinh, J., Vargas, S., Braun, T., Dalley, R. A., Gouwens, N. W., Kalmbach, B. E., Kim, T. K., … Berg, J. (2021). *Scaled, high fidelity electrophysiological, morphological, and transcriptomic cell characterization*. 30.

Lee, G.-H., Proenca, R., Montez, J. M., Carroll, K. M., Darvishzadeh, J. G., Lee, J. I., & Friedman, J. M. (1996). Abnormal splicing of the leptin receptor in diabetic mice. *Nature*, *379*(6566), 632–635. https://doi.org/10.1038/379632a0

Leinninger, G. M., Jo, Y.-H., Leshan, R. L., Louis, G. W., Yang, H., Barrera, J. G., Wilson, H., Opland, D. M., Faouzi, M. A., Gong, Y., Jones, J. C., Rhodes, C. J., Chua, S., Diano, S., Horvath, T. L., Seeley, R. J., Becker, J. B., Münzberg, H., & Myers, M. G. (2009). Leptin Acts via Leptin Receptor-Expressing Lateral Hypothalamic Neurons to Modulate the Mesolimbic Dopamine System and Suppress Feeding. *Cell Metabolism*, *10*(2), 89–98. https://doi.org/10.1016/j.cmet.2009.06.011

Leon, L. R., DuBose, D. A., & Mason, C. W. (2005). Heat stress induces a biphasic thermoregulatory response in mice. *American Journal of Physiology-Regulatory, Integrative and Comparative Physiology*, *288*(1), R197–R204. https://doi.org/10.1152/ajpregu.00046.2004

Leshan, R. L., Björnholm, M., Münzberg, H., & Myers, M. G. (2006). Leptin Receptor Signaling and Action in the Central Nervous System. *Obesity*, *14*, 208S-212S. https://doi.org/10.1038/oby.2006.310

Leshan, R. L., Greenwald-Yarnell, M., Patterson, C. M., & Jr, M. G. M. (2012). *Leptin action via hypothalamic nitric oxide synthase-1 neurons controls energy balance*. 13.

Levin, E., Diekmann, H., & Fischer, D. (2016). Highly efficient transduction of primary adult CNS and PNS neurons. *Scientific Reports*, *6*(1), 38928. https://doi.org/10.1038/srep38928

Li, G. H., Katakura, M., Maruyama, M., Enhkjargal, B., Matsuzaki, K., Hashimoto, M., & Shido, O. (2008). Changes of noradrenaline-induced contractility and gene expression in aorta of rats acclimated to heat in two different modes. *European Journal of Applied Physiology*, *104*(1), 29–40. https://doi.org/10.1007/s00421-008-0772-0

Li, J., Xiong, K., Pang, Y., Dong, Y., Kaneko, T., & Mizuno, N. (2006). Medullary dorsal horn neurons providing axons to both the parabrachial nucleus and thalamus. *The Journal of Comparative Neurology*, *498*(4), 539–551. https://doi.org/10.1002/cne.21068

Li, K., Abbott, S. B. G., Shi, Y., Eggan, P., Gonye, E. C., & Bayliss, D. A. (2021). TRPM4 mediates a subthreshold membrane potential oscillation in respiratory chemoreceptor neurons that drives pacemaker firing and breathing. *Cell Reports*, *34*(5), 108714. https://doi.org/10.1016/j.celrep.2021.108714

Li, S., Wang, Y., Matsumura, K., Ballou, L. R., Morham, S. G., & Blatteis, C. M. (1999). *The febrile response to lipopolysaccharide is blocked in cyclooxygenase-2yry, but not in cyclooxygenase-1yry mice*. 9.

Li, X.-H., Song, Q., Chen, Q.-Y., Lu, J.-S., Chen, T., & Zhuo, M. (2017). Characterization of excitatory synaptic transmission in the anterior cingulate cortex of adult tree shrew. *Molecular Brain*, *10*(1), 58. https://doi.org/10.1186/s13041-017-0336-5

Li, Y., Stam, F. J., Aimone, J. B., Goulding, M., Callaway, E. M., & Gage, F. H. (2013). Molecular layer perforant path-associated cells contribute to feed-forward inhibition in the adult dentate gyrus. *Proceedings of the National Academy of Sciences*, *110*(22), 9106–9111. https://doi.org/10.1073/pnas.1306912110

Liberzon, A., Birger, C., Thorvaldsdóttir, H., Ghandi, M., Mesirov, J. P., & Tamayo, P. (2015). The Molecular Signatures Database Hallmark Gene Set Collection. *Cell Systems*, *1*(6), 417–425. https://doi.org/10.1016/j.cels.2015.12.004

Lipovsek, M., Bardy, C., Cadwell, C. R., Hadley, K., Kobak, D., & Tripathy, S. J. (2021). Patch-seq: Past, Present, and Future. *The Journal of Neuroscience*, *41*(5), 937–946. https://doi.org/10.1523/JNEUROSCI.1653-20.2020

Liu, Q., & Markatou, M. (2016). *Evaluation of Methods in Removing Batch Effects on RNA-seq Data*. 7.

Lock, J. T., Parker, I., & Smith, I. F. (2015). A comparison of fluorescent Ca2+ indicators for imaging local Ca2+ signals in cultured cells. *Cell Calcium*, *58*(6), 638–648. https://doi.org/10.1016/j.ceca.2015.10.003

Love, M. I., Huber, W., & Anders, S. (2014). Moderated estimation of fold change and dispersion for RNA-seq data with DESeq2. *Genome Biology*, *15*(12), 550. https://doi.org/10.1186/s13059-014-0550-8

Lundius, E. G., Sanchez-Alavez, M., Ghochani, Y., Klaus, J., & Tabarean, I. V. (2010). Histamine Influences Body Temperature by Acting at H1and H3 Receptors on Distinct Populations of Preoptic Neurons. *Journal of Neuroscience*, *30*(12), 4369–4381. https://doi.org/10.1523/JNEUROSCI.0378-10.2010

Lyon, P. C., Suomi, V., Jakeman, P., Campo, L., Coussios, C., & Carlisle, R. (2021). Quantifying cell death induced by doxorubicin, hyperthermia or HIFU ablation with flow cytometry. *Scientific Reports*, *11*(1), 4404. https://doi.org/10.1038/s41598-021-83845-2

Machado, N. L. S., Bandaru, S. S., Abbott, S. B. G., & Saper, C. B. (2020). EP3R-Expressing Glutamatergic Preoptic Neurons Mediate Inflammatory Fever. *The Journal of Neuroscience*, *40*(12), 2573–2588. https://doi.org/10.1523/JNEUROSCI.2887-19.2020

Machado, N. L. S., & Saper, C. B. (2022). Genetic identification of preoptic neurons that regulate body temperature in mice. *Temperature*, 1–9. https://doi.org/10.1080/23328940.2021.1993734

Macosko, E. Z., Basu, A., Satija, R., Nemesh, J., Shekhar, K., Goldman, M., Tirosh, I., Bialas, A. R., Kamitaki, N., Martersteck, E. M., Trombetta, J. J., Weitz, D. A., Sanes, J. R., Shalek, A. K., Regev, A., & McCarroll, S. A. (2015). Highly Parallel Genome-wide Expression Profiling of Individual Cells Using Nanoliter Droplets. *Cell*, *161*(5), 1202–1214. https://doi.org/10.1016/j.cell.2015.05.002

Madden, C. J., & Morrison, S. F. (2010). Endogenous activation of spinal 5-hydroxytryptamine (5-HT) receptors contributes to the thermoregulatory activation of brown adipose tissue. *American Journal of Physiology-Regulatory, Integrative and Comparative Physiology*, *298*(3), R776–R783. https://doi.org/10.1152/ajpregu.00614.2009

Madden, C. J., & Morrison, S. F. (2019). Central nervous system circuits that control body temperature. *Neuroscience Letters*, *696*, 225–232. https://doi.org/10.1016/j.neulet.2018.11.027

Magoun, H. W., Harrison, F., Brobeck, J. R., & Ranson, S. W. (1938). Activation of heat loss mechanism by local heating of the brain. *Journal of Neurophysiology*, *1*, 101–114. https://doi.org/10.1152/jn.1938.1.2.101

Maloyan A, Eli-Berchoer L., Semenza G.L., & Michael D. Stern. (2005). *HIF-1α-targeted pathways are activated by heat acclimation and contribute to acclimation-ischemic cross-tolerance in the heart*. *23*(5), 79–88.

Maloyan, A., & Horowitz, M. (2002). β-Adrenergic signaling and thyroid hormones affect HSP72 expression during heat acclimation. *Journal of Applied Physiology*, *93*(1), 107–115. https://doi.org/10.1152/japplphysiol.01122.2001

Mao, L., & Wang, J. Q. (2001). Upregulation of preprodynorphin and preproenkephalin mRNA expression by selective activation of group I metabotropic glutamate receptors in characterized primary cultures of rat striatal neurons. *Molecular Brain Research*, *86*(1–2), 125–137. https://doi.org/10.1016/S0169-328X(00)00276-X

Masotti, A., & Preckel, T. (2006). *Using the Agilent 2100 Bioanalyzer for small RNA analysis*. 2.

Masuzaki M., Ogawa Y., & Sagawa N. (1997). Leptin as a novel placenta-derived hormone in humans. *Nature Medicine*, *3*, 1029–1033. https://doi.org/10.1038/nm0997-1029

Matsumura, K., Cao, C., Ozaki, M., Morii, H., Nakadate, K., & Watanabe, Y. (1998). Brain Endothelial Cells Express Cyclooxygenase-2 during Lipopolysaccharide-Induced Fever: Light and Electron Microscopic Immunocytochemical Studies. *The Journal of Neuroscience*, *18*(16), 6279–6289. https://doi.org/10.1523/JNEUROSCI.18-16-06279.1998

Matsuzaki, K., Katakura, M., Hara, T., Li, G., Hashimoto, M., & Shido, O. (2009). Proliferation of neuronal progenitor cells and neuronal differentiation in the hypothalamus are enhanced in heat-acclimated rats. *Pflügers Archiv - European Journal of Physiology*, *458*(4), 661–673. https://doi.org/10.1007/s00424-009-0654-2

Mayer J. & Barnett R.J. (1953). Sensitivity to cold in the hereditary obese-hyperglycemic syndrome of mice. *The Yale Journal of Biology and Medicine*, *26*(1), 38–45.

Mazuir, E., Richevaux, L., Nassar, M., Robil, N., de la Grange, P., Lubetzki, C., Fricker, D., & Sol-Foulon, N. (2021). Oligodendrocyte Secreted Factors Shape Hippocampal GABAergic Neuron Transcriptome and Physiology. *Cerebral Cortex*, *31*(11), 5024–5041. https://doi.org/10.1093/cercor/bhab139

McCarthy, J. J., & Intergovernmental Panel on Climate Change (Eds.). (2001). *Climate change 2001: Impacts, adaptation, and vulnerability: contribution of Working Group II to the third assessment report of the Intergovernmental Panel on Climate Change*. Cambridge University Press.

Miao, C., Cao, Q., Ito, H. T., Yamahachi, H., Witter, M. P., Moser, M.-B., & Moser, E. I. (2015). Hippocampal Remapping after Partial Inactivation of the Medial Entorhinal Cortex. *Neuron*, *88*(3), 590–603. https://doi.org/10.1016/j.neuron.2015.09.051

Middelkamp, H. H. T., Verboven, A. H. A., De Sá Vivas, A. G., Schoenmaker, C., Klein Gunnewiek, T. M., Passier, R., Albers, C. A., 't Hoen, P. A. C., Nadif Kasri, N., & van der Meer, A. D. (2021). Cell type-specific changes in transcriptomic profiles of endothelial cells, iPSC-derived neurons and astrocytes cultured on microfluidic chips. *Scientific Reports*, *11*(1), 2281. https://doi.org/10.1038/s41598-021-81933-x

Mishra, S. K., Tisel, S. M., Orestes, P., Bhangoo, S. K., & Hoon, M. A. (2011). TRPV1-lineage neurons are required for thermal sensation: TRPV1-lineage neurons. *The EMBO Journal*, *30*(3), 582–593. https://doi.org/10.1038/emboj.2010.325

Mistry, A. M., Swick, A. G., & Romsos, D. R. (1997). Leptin Rapidly Lowers Food Intake and Elevates Metabolic Rates in Lean and ob/ob Mice. *The Journal of Nutrition*, *127*(10), 2065–2072. https://doi.org/10.1093/jn/127.10.2065

Moffitt, J. R., Bambah-Mukku, D., Eichhorn, S. W., Vaughn, E., Shekhar, K., Perez, J. D., Rubinstein, N. D., Hao, J., Regev, A., Dulac, C., & Zhuang, X. (2018). Molecular, spatial, and functional single-cell profiling of the hypothalamic preoptic region. *Science*, *362*(6416), eaau5324. https://doi.org/10.1126/science.aau5324

Morgan, J. I., Cohen, D. R., Hempstead, J. L., & Curran, T. (1987). Mapping Patterns of c-*fos* Expression in the Central Nervous System After Seizure. *Science*, *237*(4811), 192–197. https://doi.org/10.1126/science.3037702

Morrison, S. F., & Madden, C. J. (2014). Central Nervous System Regulation of Brown Adipose Tissue. In R. Terjung (Ed.), *Comprehensive Physiology* (1st ed., pp. 1677–1713). Wiley. https://doi.org/10.1002/cphy.c140013

Morrison, S., F. & Nakamura, K. (2011). Central neural pathways for thermoregulation. *Frontiers in Bioscience*, *16*(1), 74. https://doi.org/10.2741/3677

Morrison, S. F., & Nakamura, K. (2019). Central Mechanisms for Thermoregulation. *Annual Review of Physiology*, *81*(1), 285–308. https://doi.org/10.1146/annurev-physiol-020518-114546

Mreisat, A., Kanaani, H., Saada, A., & Horowitz, M. (2020). Heat acclimation mediated cardioprotection is controlled by mitochondrial metabolic remodeling involving HIF-1α. *Journal of Thermal Biology*, *93*, 102691. https://doi.org/10.1016/j.jtherbio.2020.102691

Muñoz-Manchado, A. B., Bengtsson Gonzales, C., Zeisel, A., Munguba, H., Bekkouche, B., Skene, N. G., Lönnerberg, P., Ryge, J., Harris, K. D., Linnarsson, S., & Hjerling-Leffler, J. (2018). Diversity of Interneurons in the Dorsal Striatum Revealed by Single-Cell RNA Sequencing and PatchSeq. *Cell Reports*, *24*(8), 2179-2190.e7. https://doi.org/10.1016/j.celrep.2018.07.053

Myers MG, & Leibel RL. (2015). In *Lessons From Rodent Models of Obesity.* MDText.com, South Dartmouth (MA).

Nakamura, K. (2004). Identification of Sympathetic Premotor Neurons in Medullary Raphe Regions Mediating Fever and Other Thermoregulatory Functions. *Journal of Neuroscience*, *24*(23), 5370–5380. https://doi.org/10.1523/JNEUROSCI.1219-04.2004

Nakamura, K., & Morrison, S. F. (2008). A thermosensory pathway that controls body temperature. *Nature Neuroscience*, *11*(1), 62–71. https://doi.org/10.1038/nn2027

Nakamura, K., & Morrison, S. F. (2010). A thermosensory pathway mediating heat-defense responses. *Proceedings of the National Academy of Sciences*, *107*(19), 8848–8853. https://doi.org/10.1073/pnas.0913358107

Nakamura, K., & Morrison, S. F. (2011). Central efferent pathways for cold-defensive and febrile shivering: Brain circuitry for shivering. *The Journal of Physiology*, *589*(14), 3641–3658. https://doi.org/10.1113/jphysiol.2011.210047

Nakayama, T., Eisenman, J. S., & Hardy, J. D. (1961). Single Unit Activity of Anterior Hypothalamus during Local Heating. *Science*, *134*(3478), 560–561. https://doi.org/10.1126/science.134.3478.560

Nakayama, T., Hammel, H. T., Hardy, J. D., & Eisenman, J. S. (1963). Thermal stimulation of electrical activity of single units of the preoptic region. *American Journal of Physiology-Legacy Content*, *204*(6), 1122–1126. https://doi.org/10.1152/ajplegacy.1963.204.6.1122

Niculescu, D., Hirdes, W., Hornig, S., Pongs, O., & Schwarz, J. R. (2013). Erg Potassium Currents of Neonatal Mouse Purkinje Cells Exhibit Fast Gating Kinetics and Are Inhibited by mGluR1 Activation. *Journal of Neuroscience*, *33*(42), 16729–16740. https://doi.org/10.1523/JNEUROSCI.5523-12.2013

Niday, Z., Hawkins, V. E., Soh, H., Mulkey, D. K., & Tzingounis, A. V. (2017). Epilepsy-Associated KCNQ2 Channels Regulate Multiple Intrinsic Properties of Layer 2/3 Pyramidal Neurons. *The Journal of Neuroscience*, *37*(3), 576–586. https://doi.org/10.1523/JNEUROSCI.1425-16.2016

Ootsuka, Y., & Tanaka, M. (2015). Control of cutaneous blood flow by central nervous system. *Temperature*, *2*(3), 392–405. https://doi.org/10.1080/23328940.2015.1069437

Özugur, S., Kunz, L., & Straka, H. (2020). Relationship between oxygen consumption and neuronal activity in a defined neural circuit. *BMC Biology*, *18*(1), 76. https://doi.org/10.1186/s12915-020-00811-6

Padilla, S. L., Johnson, C. W., Barker, F. D., Patterson, M. A., & Palmiter, R. D. (2018). A Neural Circuit Underlying the Generation of Hot Flushes. *Cell Reports*, *24*(2), 271–277. https://doi.org/10.1016/j.celrep.2018.06.037

Park, H.-K., & Ahima, R. S. (2014). Leptin signaling. *F1000Prime Reports*, *6*. https://doi.org/10.12703/P6-73

Patro, R., Duggal, G., Love, M. I., Irizarry, R. A., & Kingsford, C. (2017). Salmon provides fast and bias-aware quantification of transcript expression. *Nature Methods*, *14*(4), 417–419. https://doi.org/10.1038/nmeth.4197

Patronas, P., Horowitz, M., Simon, E., & Gerstberger, R. (1998). Differential stimulation of c-fos expression in hypothalamic nuclei of the rat brain during short-term heat acclimation and mild dehydration. *Brain Research*, *798*(1–2), 127–139. https://doi.org/10.1016/S0006-8993(98)00405-3

Pearson, K. (1901). LIII. *On lines and planes of closest fit to systems of points in space*. *The London, Edinburgh, and Dublin Philosophical Magazine and Journal of Science*, *2*(11), 559–572. https://doi.org/10.1080/14786440109462720

Pedarzani, P., McCutcheon, J. E., Rogge, G., Jensen, B. S., Christophersen, P., Hougaard, C., Strøbæk, D., & Stocker, M. (2005). Specific Enhancement of SK Channel Activity Selectively Potentiates the Afterhyperpolarizing Current IAHP and Modulates the Firing Properties of Hippocampal Pyramidal Neurons. *Journal of Biological Chemistry*, *280*(50), 41404–41411. https://doi.org/10.1074/jbc.M509610200

Pedarzani, P., Mosbacher, J., Rivard, A., Cingolani, L. A., Oliver, D., Stocker, M., Adelman, J. P., & Fakler, B. (2001). Control of Electrical Activity in Central Neurons by Modulating the Gating of Small Conductance Ca2+-activated K+ Channels. *Journal of Biological Chemistry*, *276*(13), 9762–9769. https://doi.org/10.1074/jbc.M010001200

Périard, J. D., Racinais, S., & Sawka, M. N. (2015). Adaptations and mechanisms of human heat acclimation: Applications for competitive athletes and sports: Adaptations and mechanisms of heat acclimation. *Scandinavian Journal of Medicine & Science in Sports*, *25*, 20–38. https://doi.org/10.1111/sms.12408

Petrović, A., Ban, J., Tomljanović, I., Pongrac, M., Ivaničić, M., Mikašinović, S., & Mladinic, M. (2021). Establishment of Long-Term Primary Cortical Neuronal Cultures From Neonatal Opossum Monodelphis domestica. *Frontiers in Cellular Neuroscience*, *15*, 661492. https://doi.org/10.3389/fncel.2021.661492

Picelli, S., Faridani, O. R., Björklund, Å. K., Winberg, G., Sagasser, S., & Sandberg, R. (2014). Full-length RNA-seq from single cells using Smart-seq2. *Nature Protocols*, *9*(1), 171–181. https://doi.org/10.1038/nprot.2014.006

Pierau, F.-K., Sann, H., Yakimova, K. S., & Haug, P. (1998). Chapter 5 Plasticity of hypothalamic temperature-sensitive neurons. In *Progress in Brain Research* (Vol. 115, pp. 63–84). Elsevier. https://doi.org/10.1016/S0079-6123(08)62030-0

Piñol, R. A., Mogul, A. S., Hadley, C. K., Saha, A., Li, C., Škop, V., Province, H. S., Xiao, C., Gavrilova, O., Krashes, M. J., & Reitman, M. L. (2021). Preoptic BRS3 neurons increase body temperature and heart rate via multiple pathways. *Cell Metabolism*, *33*(7), 1389-1403.e6. https://doi.org/10.1016/j.cmet.2021.05.001

Piñol, R. A., Zahler, S. H., Li, C., Saha, A., Tan, B. K., Škop, V., Gavrilova, O., Xiao, C., Krashes, M. J., & Reitman, M. L. (2018). Brs3 neurons in the mouse dorsomedial hypothalamus regulate body temperature, energy expenditure, and heart rate, but not food intake. *Nature Neuroscience*, *21*(11), 1530–1540. https://doi.org/10.1038/s41593-018-0249-3

Platanias, L. C. (2005). Mechanisms of type-I- and type-II-interferon-mediated signalling. *Nature Reviews Immunology*, *5*(5), 375–386. https://doi.org/10.1038/nri1604

Pogorzala, L. A., Mishra, S. K., & Hoon, M. A. (2013). The Cellular Code for Mammalian Thermosensation. *Journal of Neuroscience*, *33*(13), 5533–5541. https://doi.org/10.1523/JNEUROSCI.5788-12.2013

Ran, C., Hoon, M. A., & Chen, X. (2016). The coding of cutaneous temperature in the spinal cord. *Nature Neuroscience*, *19*(9), 1201–1209. https://doi.org/10.1038/nn.4350

Ranels, H. J., & Griffin, J. D. (2003). The effects of prostaglandin E2 on the firing rate activity of thermosensitive and temperature insensitive neurons in the ventromedial preoptic area of the rat hypothalamus. *Brain Research*, *964*(1), 42–50. https://doi.org/10.1016/S0006-8993(02)04063-5

Riccardi, C., & Nicoletti, I. (2006). Analysis of apoptosis by propidium iodide staining and flow cytometry. *Nature Protocols*, *1*(3), 1458–1461. https://doi.org/10.1038/nprot.2006.238

Ring, L. E., & Zeltser, L. M. (2010). Disruption of hypothalamic leptin signaling in mice leads to early-onset obesity, but physiological adaptations in mature animals stabilize adiposity levels. *Journal of Clinical Investigation*, *120*(8), 2931–2941. https://doi.org/10.1172/JCI41985

Riquelme, D., Cerda, O., & Leiva-Salcedo, E. (2021). TRPM4 Expression During Postnatal Developmental of Mouse CA1 Pyramidal Neurons. *Frontiers in Neuroanatomy*, *15*, 643287. https://doi.org/10.3389/fnana.2021.643287

Rodríguez-Rodríguez, R., Miralpeix, C., Fosch, A., Pozo, M., Calderón-Domínguez, M., Perpinyà, X., Vellvehí, M., López, M., Herrero, L., Serra, D., & Casals, N. (2019). CPT1C in the ventromedial nucleus of the hypothalamus is necessary for brown fat thermogenesis activation in obesity. *Molecular Metabolism*, *19*, 75–85. https://doi.org/10.1016/j.molmet.2018.10.010

Romanovsky, A. A. (2004). Do fever and anapyrexia exist? Analysis of set point-based definitions. *American Journal of Physiology-Regulatory, Integrative and Comparative Physiology*, *287*(4), R992–R995. https://doi.org/10.1152/ajpregu.00068.2004

Romanovsky, A. A. (2007). Thermoregulation: Some concepts have changed. Functional architecture of the thermoregulatory system. *American Journal of Physiology-Regulatory, Integrative and Comparative Physiology*, *292*(1), R37–R46. https://doi.org/10.1152/ajpregu.00668.2006

Rubiolo, J. A., Vale, C., Martín, V., Mendez, A. G., Juncal, A. B., Vieytes, M. R., & Botana, L. (2016). Transcriptomic Profiling of Mice Primary Cortical Neurons in Response to Medium Change. *Transcriptomics: Open Access*, *04*(02). https://doi.org/10.4172/2329-8936.1000138

Sacco, T., Bruno, A., Wanke, E., & Tempia, F. (2003). Functional Roles of an ERG Current Isolated in Cerebellar Purkinje Neurons. *Journal of Neurophysiology*, *90*(3), 1817–1828. https://doi.org/10.1152/jn.00104.2003

Sawka, Michael N., Wenger, Brue C., & Pandolf, Kent B. (2011). Comprehensive Physiology—2011—Sawka—Thermoregulatory Responses to Acute Exercise-Heat Stress and Heat Acclimation.pdf. In *Supplement 14. Handbook of Physiology, Environmental Physiology: Vol. Volume 1. American Physiology Society* (pp. 157–187). Oxford University Press.

Saxena, A., Wagatsuma, A., Noro, Y., Kuji, T., Asaka-Oba, A., Watahiki, A., Gurnot, C., Fagiolini, M., Hensch, T. K., & Carninci, P. (2012). Trehalose-enhanced isolation of neuronal sub-types from adult mouse brain. *BioTechniques*, *52*(6), 381–385. https://doi.org/10.2144/0000113878

Scala, F., Kobak, D., Bernabucci, M., Bernaerts, Y., Cadwell, C. R., Castro, J. R., Hartmanis, L., Jiang, X., Laturnus, S., Miranda, E., Mulherkar, S., Tan, Z. H., Yao, Z., Zeng, H., Sandberg, R., Berens, P., & Tolias, A. S. (2021). Phenotypic variation of transcriptomic cell types in mouse motor cortex. *Nature*, *598*(7879), 144–150. https://doi.org/10.1038/s41586-020-2907-3

Scala, F., Kobak, D., Shan, S., Bernaerts, Y., Laturnus, S., Cadwell, C. R., Hartmanis, L., Froudarakis, E., Castro, J. R., Tan, Z. H., Papadopoulos, S., Patel, S. S., Sandberg, R., Berens, P., Jiang, X., & Tolias, A. S. (2019). Layer 4 of mouse neocortex differs in cell types and circuit organization between sensory areas. *Nature Communications*, *10*(1), 4174. https://doi.org/10.1038/s41467-019-12058-z

Scammell, T. E., Price, K. J., & Sagar, S. M. (1993). Hyperthermia induces c-fos expression in the preoptic area. *Brain Research*, *618*(2), 303–307. https://doi.org/10.1016/0006-8993(93)91280-6

Schaper, F., & Rose-John, S. (2015). Interleukin-6: Biology, signaling and strategies of blockade. *Cytokine & Growth Factor Reviews*, *26*(5), 475–487. https://doi.org/10.1016/j.cytogfr.2015.07.004

Schindelin, J., Arganda-Carreras, I., Frise, E., Kaynig, V., Longair, M., Pietzsch, T., Preibisch, S., Rueden, C., Saalfeld, S., Schmid, B., Tinevez, J.-Y., White, D. J., Hartenstein, V., Eliceiri, K., Tomancak, P., & Cardona, A. (2012). Fiji: An open-source platform for biological-image analysis. *Nature Methods*, *9*(7), 676–682. https://doi.org/10.1038/nmeth.2019

Schwimmer, H., Eli-Berchoer, L., & Horowitz, M. (2006). Acclimatory-phase specificity of gene expression during the course of heat acclimation and superimposed hypohydration in the rat hypothalamus. *Journal of Applied Physiology*, *100*(6), 1992–2003. https://doi.org/10.1152/japplphysiol.00850.2005

Schwimmer, H., Gerstberger, R., & Horowitz, M. (2004). Heat acclimation affects the neuromodulatory role of AngII and nitric oxide during combined heat and hypohydration stress. *Molecular Brain Research*, *130*(1–2), 95–108. https://doi.org/10.1016/j.molbrainres.2004.07.011

Scott, M. M., Lachey, J. L., Sternson, S. M., Lee, C. E., Elias, C. F., Friedman, J. M., & Elmquist, J. K. (2009). Leptin targets in the mouse brain. *The Journal of Comparative Neurology*, *514*(5), 518–532. https://doi.org/10.1002/cne.22025

Seibenhener, M. L., & Wooten, M. W. (2012). Isolation and Culture of Hippocampal Neurons from Prenatal Mice. *Journal of Visualized Experiments*, *65*, 3634. https://doi.org/10.3791/3634

Sergushichev, A. A. (2016). *An algorithm for fast preranked gene set enrichment analysis using cumulative statistic calculation*. 9.

Shabalina, I. G., Petrovic, N., de Jong, J. M. A., Kalinovich, A. V., Cannon, B., & Nedergaard, J. (2013). UCP1 in Brite/Beige Adipose Tissue Mitochondria Is Functionally Thermogenic. *Cell Reports*, *5*(5), 1196–1203. https://doi.org/10.1016/j.celrep.2013.10.044

Shein, N. A., Doron, H., Horowitz, M., Trembovler, V., Alexandrovich, A. G., & Shohami, E. (2007). Altered cytokine expression and sustained hypothermia following traumatic brain injury in heat acclimated mice. *Brain Research*, *1185*, 313–320. https://doi.org/10.1016/j.brainres.2007.09.024

Shi, W., Wymore, R. S., Wang, H.-S., Pan, Z., Cohen, I. S., McKinnon, D., & Dixon, J. E. (1997). Identification of Two Nervous System-Specific Members of the *erg* Potassium Channel Gene Family. *The Journal of Neuroscience*, *17*(24), 9423–9432. https://doi.org/10.1523/JNEUROSCI.17-24-09423.1997

Shibata, H., & Nagasaka, T. (1984). Role of sympathetic nervous system in immobilization- and cold-induced brown adipose tissue thermogenesis in rats. *The Japanese Journal of Physiology*, *34*(1), 103–111. https://doi.org/10.2170/jjphysiol.34.103

Sicherman, J., Newton, D. F., Pavlidis, P., Sibille, E., & Tripathy, S. J. (2021). Estimating and Correcting for Off-Target Cellular Contamination in Brain Cell Type Specific RNA-Seq Data. *Frontiers in Molecular Neuroscience*, *14*, 637143. https://doi.org/10.3389/fnmol.2021.637143

Siemens, J., & Kamm, G. B. (2018). Cellular populations and thermosensing mechanisms of the hypothalamic thermoregulatory center. *Pflügers Archiv - European Journal of Physiology*, *470*(5), 809–822. https://doi.org/10.1007/s00424-017-2101-0

Silva, N. L., & Boulant, J. A. (1986). Effects of testosterone, estradiol, and temperature on neurons in preoptic tissue slices. *American Journal of Physiology-Regulatory, Integrative and Comparative Physiology*, *250*(4), R625–R632. https://doi.org/10.1152/ajpregu.1986.250.4.R625

Sims, D., Sudbery, I., Ilott, N. E., Heger, A., & Ponting, C. P. (2014). Sequencing depth and coverage: Key considerations in genomic analyses. *Nature Reviews Genetics*, *15*(2), 121–132. https://doi.org/10.1038/nrg3642

Singh, N. A., Charlier, C., Stauffer, D., DuPont, B. R., Leach, R. J., Melis, R., Ronen, G. M., Bjerre, I., Quattlebaum, T., Murphy, J. V., McHarg, M. L., Gagnon, D., Rosales, T. O., Peiffer, A., Anderson, V. E., & Leppert, M. (1998). A novel potassium channel gene, KCNQ2, is mutated in an inherited epilepsy of newborns. *Nature Genetics*, *18*(1), 25–29. https://doi.org/10.1038/ng0198-25

Škop, V., Guo, J., Liu, N., Xiao, C., Hall, K. D., Gavrilova, O., & Reitman, M. L. (2020). Mouse Thermoregulation: Introducing the Concept of the Thermoneutral Point. *Cell Reports*, *31*(2), 107501. https://doi.org/10.1016/j.celrep.2020.03.065

Smith, J. E., Jansen, A. S. P., Gilbey, M. P., & Loewy, A. D. (1998). CNS cell groups projecting to sympathetic outflow of tail artery: Neural circuits involved in heat loss in the rat. *Brain Research*, *786*(1–2), 153–164. https://doi.org/10.1016/S0006-8993(97)01437-6

Soh, H., Pant, R., LoTurco, J. J., & Tzingounis, A. V. (2014). Conditional Deletions of Epilepsy-Associated KCNQ2 and KCNQ3 Channels from Cerebral Cortex Cause Differential Effects on Neuronal Excitability. *Journal of Neuroscience*, *34*(15), 5311–5321. https://doi.org/10.1523/JNEUROSCI.3919-13.2014

Soneson, C., Love, M. I., & Robinson, M. D. (2016). Differential analyses for RNA-seq: Transcript-level estimates improve gene-level inferences. *F1000Research*, *4*, 1521. https://doi.org/10.12688/f1000research.7563.2

Song, K., Wang, H., Kamm, G. B., Pohle, J., Reis, F. d. C., Heppenstall, P., Wende, H., & Siemens, J. (2016). The TRPM2 channel is a hypothalamic heat sensor that limits fever and can drive hypothermia. *Science*, *353*(6306), 1393–1398. https://doi.org/10.1126/science.aaf7537

Steiner, A. A., Ivanov, A. I., Serrats, J., Hosokawa, H., Phayre, A. N., Robbins, J. R., Roberts, J. L., Kobayashi, S., Matsumura, K., Sawchenko, P. E., & Romanovsky, A. A. (2006). Cellular and Molecular Bases of the Initiation of Fever. *PLoS Biology*, *4*(9), e284. https://doi.org/10.1371/journal.pbio.0040284

Steven W. Wingett & Simon Andrews. (2018). FastQ Screen: A tool for multi-genome mapping and quality control. *F1000Research*. https://doi.org/10.12688/f1000research.15931.2

Stocker, M., Krause, M., & Pedarzani, P. (1999). An apamin-sensitive Ca^{2+} -activated K^{+} current in hippocampal pyramidal neurons. *Proceedings of the National Academy of Sciences*, *96*(8), 4662–4667. https://doi.org/10.1073/pnas.96.8.4662

Storm, J. F. (1990). Chapter 12 Potassium currents in hippocampal pyramidal cells. In *Progress in Brain Research* (Vol. 83, pp. 161–187). Elsevier. https://doi.org/10.1016/S0079-6123(08)61248-0

Stuart, T., Butler, A., Hoffman, P., Hafemeister, C., Papalexi, E., Mauck, W. M., Hao, Y., Stoeckius, M., Smibert, P., & Satija, R. (2019). Comprehensive Integration of Single-Cell Data. *Cell*, *177*(7), 1888-1902.e21. https://doi.org/10.1016/j.cell.2019.05.031

Sweeney, S. T., Broadie, K., Keane, J., Niemann, H., & O'Kane, C. J. (1995). Targeted expression of tetanus toxin light chain in Drosophila specifically eliminates synaptic transmission and causes behavioral defects. *Neuron*, *14*(2), 341–351. https://doi.org/10.1016/0896-6273(95)90290-2

Szu, J., Wojcinski, A., Jiang, P., & Kesari, S. (2021). Impact of the Olig Family on Neurodevelopmental Disorders. *Frontiers in Neuroscience*, *15*, 659601. https://doi.org/10.3389/fnins.2021.659601

Tabarean, I. V., Conti, B., Behrens, M., Korn, H., & Bartfai, T. (2005). Electrophysiological properties and thermosensitivity of mouse preoptic and anterior hypothalamic neurons in culture. *Neuroscience*, *135*(2), 433–449. https://doi.org/10.1016/j.neuroscience.2005.06.053

Tada, M., Takeuchi, A., Hashizume, M., Kitamura, K., & Kano, M. (2014). A highly sensitive fluorescent indicator dye for calcium imaging of neural activity *in vitro* and *in vivo*. *European Journal of Neuroscience*, *39*(11), 1720–1728. https://doi.org/10.1111/ejn.12476

Takahashi, T. M., Sunagawa, G. A., Soya, S., Abe, M., Sakurai, K., Ishikawa, K., Yanagisawa, M., Hama, H., Hasegawa, E., Miyawaki, A., Sakimura, K., Takahashi, M., & Sakurai, T. (2020). A discrete neuronal circuit induces a hibernation-like state in rodents. *Nature*, *583*(7814), 109–114. https://doi.org/10.1038/s41586-020-2163-6

Takebayashi, H., Yoshida, S., Sugimori, M., Kosako, H., Kominami, R., Nakafuku, M., & Nabeshima, Y. (2000). Dynamic expression of basic helix-loop-helix Olig family members: Implication of Olig2 in neuron and oligodendrocyte differentiation and identi®cation of a new member, Olig3. *Mechanisms of Development*, 6.

Tan, C. L., Cooke, E. K., Leib, D. E., Lin, Y.-C., Daly, G. E., Zimmerman, C. A., & Knight, Z. A. (2016). Warm-Sensitive Neurons that Control Body Temperature. *Cell*, *167*(1), 47-59.e15. https://doi.org/10.1016/j.cell.2016.08.028

Tan, C. L., & Knight, Z. A. (2018). Regulation of Body Temperature by the Nervous System. *Neuron*, *98*(1), 31–48. https://doi.org/10.1016/j.neuron.2018.02.022

Tanaka, H., Kanosue, K., Nakayama, T., & Shen, Z. (1986). Grooming, body extension, and vasomotor responses induced by hypothalamic warming at different ambient temperatures in rats. *Physiology & Behavior*, *38*(1), 145–151. https://doi.org/10.1016/0031-9384(86)90145-9

Tanaka, M., McKinley, M. J., & McAllen, R. M. (2009). Roles of two preoptic cell groups in tonic and febrile control of rat tail sympathetic fibers. *American Journal of Physiology-Regulatory, Integrative and Comparative Physiology*, *296*(4), R1248–R1257. https://doi.org/10.1152/ajpregu.91010.2008

Tanaka, M., McKinley, M. J., & McAllen, R. M. (2011). Preoptic-Raphe Connections for Thermoregulatory Vasomotor Control. *Journal of Neuroscience*, *31*(13), 5078–5088. https://doi.org/10.1523/JNEUROSCI.6433-10.2011

Tanaka, M., Nagashima, K., McAllen, R. M., & Kanosue, K. (2002). Role of the medullary raphé in thermoregulatory vasomotor control in rats. *The Journal of Physiology*, *540*(2), 657–664. https://doi.org/10.1113/jphysiol.2001.012989

Tartaglia, L. A., Dembski, M., Weng, X., Deng, N., Culpepper, J., Devos, R., Richards, G. J., Campfield, L. A., Clark, F. T., Deeds, J., Muir, C., Sanker, S., Moriarty, A., Moore, K. J., Smutko, J. S., Mays, G. G., Wool, E. A., Monroe, C. A., & Tepper, R. I. (1995). Identification and expression cloning of a leptin receptor, OB-R. *Cell*, *83*(7), 1263–1271. https://doi.org/10.1016/0092-8674(95)90151-5

Tasic, B., Menon, V., Nguyen, T. N., Kim, T. K., Jarsky, T., Yao, Z., Levi, B., Gray, L. T., Sorensen, S. A., Dolbeare, T., Bertagnolli, D., Goldy, J., Shapovalova, N., Parry, S., Lee, C., Smith, K., Bernard, A., Madisen, L., Sunkin, S. M., … Zeng, H. (2016). Adult mouse cortical cell taxonomy revealed by single cell transcriptomics. *Nature Neuroscience*, *19*(2), 335–346. https://doi.org/10.1038/nn.4216

Taube, J. S. (2010). Interspike Interval Analyses Reveal Irregular Firing Patterns at Short, But Not Long, Intervals in Rat Head Direction Cells. *Journal of Neurophysiology*, *104*(3), 1635–1648. https://doi.org/10.1152/jn.00649.2009

Taylor, N. A. S. (2014). Human Heat Adaptation. In R. Terjung (Ed.), *Comprehensive Physiology* (1st ed., pp. 325–365). Wiley. https://doi.org/10.1002/cphy.c130022

Tetievsky, A., & Horowitz, M. (2010). Posttranslational modifications in histones underlie heat acclimation-mediated cytoprotective memory. *Journal of Applied Physiology*, *109*(5), 1552–1561. https://doi.org/10.1152/japplphysiol.00469.2010

Togashi, K., Inada, H., & Tominaga, M. (2008). Inhibition of the transient receptor potential cation channel TRPM2 by 2-aminoethoxydiphenyl borate (2-APB): TRPM2-inhibition by 2-APB. *British Journal of Pharmacology*, *153*(6), 1324–1330. https://doi.org/10.1038/sj.bjp.0707675

Tóth, I. E., Tóth, D. E., Boldogkoi, Z., Hornyák, Á., Palkovits, M., & Blessing, W. W. (2006). Serotonin-Synthesizing Neurons in the Rostral Medullary Raphé/Parapyramidal Region Transneuronally Labelled After Injection of Pseudorabies Virus into the Rat Tail. *Neurochemical Research*, *31*(2), 277–286. https://doi.org/10.1007/s11064-005-9018-2

Trayhurn, P. (1979). Thermoregulation in the diabetic-obese (db/db) mouse: The role of non-shivering thermogenesis in energy balance. *Pflugers Archiv European Journal of Physiology*, *380*(3), 227–232. https://doi.org/10.1007/BF00582901

Trayhurn, P., & James, W. P. T. (1978). Thermoregulation and non-shivering thermogenesis in the genetically obese (ob/ob) mouse. *Pflugers Archiv European Journal of Physiology*, *373*(2), 189–193. https://doi.org/10.1007/BF00584859

Tripathy, S. J., Toker, L., Bomkamp, C., Mancarci, B. O., Belmadani, M., & Pavlidis, P. (2018). Assessing Transcriptome Quality in Patch-Seq Datasets. *Frontiers in Molecular Neuroscience*, *11*. https://doi.org/10.3389/fnmol.2018.00363

Ueno, S., Bracamontes, J., Zorumski, C., Weiss, D. S., & Steinbach, J. H. (1997). Bicuculline and Gabazine Are Allosteric Inhibitors of Channel Opening of the GABA $_{A}$ Receptor. *The Journal of Neuroscience*, *17*(2), 625–634. https://doi.org/10.1523/JNEUROSCI.17-02-00625.1997

Upton, B. A., D'Souza, S. P., & Lang, R. A. (2021). QPLOT Neurons—Converging on a Thermoregulatory Preoptic Neuronal Population. *Frontiers in Neuroscience*, *15*, 665762. https://doi.org/10.3389/fnins.2021.665762

Valério-Gomes, B., Guimarães, D. M., Szczupak, D., & Lent, R. (2018). The Absolute Number of Oligodendrocytes in the Adult Mouse Brain. *Frontiers in Neuroanatomy*, *12*, 90. https://doi.org/10.3389/fnana.2018.00090

van de Wall, E., Leshan, R., Xu, A. W., Balthasar, N., Coppari, R., Liu, S. M., Jo, Y. H., MacKenzie, R. G., Allison, D. B., Dun, N. J., Elmquist, J., Lowell, B. B., Barsh, G. S., de Luca, C., Myers, M. G., Schwartz, G. J., & Chua, S. C. (2008). Collective and Individual Functions of Leptin Receptor Modulated Neurons Controlling Metabolism and Ingestion. *Endocrinology*, *149*(4), 1773–1785. https://doi.org/10.1210/en.2007-1132

van den Brink, S. C., Sage, F., Vértesy, Á., Spanjaard, B., Peterson-Maduro, J., Baron, C. S., Robin, C., & van Oudenaarden, A. (2017). Single-cell sequencing reveals dissociation-induced gene expression in tissue subpopulations. *Nature Methods*, *14*(10), 935–936. https://doi.org/10.1038/nmeth.4437

Vandewauw, I., De Clercq, K., Mulier, M., Held, K., Pinto, S., Van Ranst, N., Segal, A., Voet, T., Vennekens, R., Zimmermann, K., Vriens, J., & Voets, T. (2018). A TRP channel trio mediates acute noxious heat sensing. *Nature*, *555*(7698), 662–666. https://doi.org/10.1038/nature26137

Vasilyev, D. V., & Barish, M. E. (2002). Postnatal Development of the Hyperpolarization-Activated Excitatory Current I_{h} in Mouse Hippocampal Pyramidal Neurons. *The Journal of Neuroscience*, *22*(20), 8992–9004. https://doi.org/10.1523/JNEUROSCI.22-20-08992.2002

Vong, L., Ye, C., Yang, Z., Choi, B., Chua, S., & Lowell, B. B. (2011). Leptin Action on GABAergic Neurons Prevents Obesity and Reduces Inhibitory Tone to POMC Neurons. *Neuron*, *71*(1), 142–154. https://doi.org/10.1016/j.neuron.2011.05.028

Vriens, J., Nilius, B., & Voets, T. (2014). Peripheral thermosensation in mammals. *Nature Reviews Neuroscience*, *15*(9), 573–589. https://doi.org/10.1038/nrn3784

Wang, H. (1998). KCNQ2 and KCNQ3 Potassium Channel Subunits: Molecular Correlates of the M-Channel. *Science*, *282*(5395), 1890–1893. https://doi.org/10.1126/science.282.5395.1890

Wang, H. S., & McKinnon, D. (1995). Potassium currents in rat prevertebral and paravertebral sympathetic neurones: Control of firing properties. *The Journal of Physiology*, *485*(2), 319–335. https://doi.org/10.1113/jphysiol.1995.sp020732

Wang, T. A., Teo, C. F., Åkerblom, M., Chen, C., Tynan-La Fontaine, M., Greiner, V. J., Diaz, A., McManus, M. T., Jan, Y. N., & Jan, L. Y. (2019). Thermoregulation via Temperature-Dependent PGD2 Production in Mouse Preoptic Area. *Neuron*, *103*(2), 309-322.e7. https://doi.org/10.1016/j.neuron.2019.04.035

Weber, Y. G., Geiger, J., Kämpchen, K., Landwehrmeyer, B., Sommer, C., & Lerche, H. (2006). Immunohistochemical analysis of KCNQ2 potassium channels in adult and developing mouse brain. *Brain Research*, *1077*(1), 1–6. https://doi.org/10.1016/j.brainres.2006.01.023

Wechselberger, M., Wright, C. L., Bishop, G. A., & Boulant, J. A. (2006). Ionic channels and conductance-based models for hypothalamic neuronal thermosensitivity. *American Journal of Physiology-Regulatory, Integrative and Comparative Physiology*, *291*(3), R518–R529. https://doi.org/10.1152/ajpregu.00039.2006

Yahiro, T., Kataoka, N., Nakamura, Y., & Nakamura, K. (2017). The lateral parabrachial nucleus, but not the thalamus, mediates thermosensory pathways for behavioural thermoregulation. *Scientific Reports*, *7*(1), 5031. https://doi.org/10.1038/s41598-017-05327-8

Yoshida, K., Konishi, M., Nagashima, K., Saper, C. B., & Kanosue, K. (2005). Fos activation in hypothalamic neurons during cold or warm exposure: Projections to periaqueductal gray matter. *Neuroscience*, *133*(4), 1039–1046. https://doi.org/10.1016/j.neuroscience.2005.03.044

Yu, S., Cheng, H., François, M., Qualls-Creekmore, E., Huesing, C., He, Y., Jiang, Y., Gao, H., Xu, Y., Zsombok, A., Derbenev, A. V., Nillni, E. A., Burk, D. H., Morrison, C. D., Berthoud, H.-R., & Münzberg, H. (2018). Preoptic leptin signaling modulates energy balance independent of body temperature regulation. *ELife*, *7*, e33505. https://doi.org/10.7554/eLife.33505

Yu, S., Qualls-Creekmore, E., Rezai-Zadeh, K., Jiang, Y., Berthoud, H.-R., Morrison, C. D., Derbenev, A. V., Zsombok, A., & Münzberg, H. (2016). Glutamatergic Preoptic Area Neurons That Express Leptin Receptors Drive Temperature-Dependent Body Weight Homeostasis. *The Journal of Neuroscience*, *36*(18), 5034–5046. https://doi.org/10.1523/JNEUROSCI.0213-16.2016

Yuanyuan Doua. (2021). The CAG promoter maintains high-level transgene expression in HEK293 cells. *FEBS Open Bio.*, 95–104. https://doi.org/10.1002/2211-5463.13029

Zhang, K. X., D'Souza, S., Upton, B. A., Kernodle, S., Vemaraju, S., Nayak, G., Gaitonde, K. D., Holt, A. L., Linne, C. D., Smith, A. N., Petts, N. T., Batie, M., Mukherjee, R., Tiwari, D., Buhr, E. D., Van Gelder, R. N., Gross, C., Sweeney, A., Sanchez-Gurmaches, J., … Lang, R. A. (2020). Violet-light suppression of thermogenesis by opsin 5 hypothalamic neurons. *Nature*, *585*(7825), 420–425. https://doi.org/10.1038/s41586-020-2683-0

Zhang, Y., Kerman, I. A., Laque, A., Nguyen, P., Faouzi, M., Louis, G. W., Jones, J. C., Rhodes, C., & Munzberg, H. (2011). Leptin-Receptor-Expressing Neurons in the Dorsomedial Hypothalamus and Median Preoptic Area Regulate Sympathetic Brown Adipose Tissue Circuits. *Journal of Neuroscience*, *31*(5), 1873–1884. https://doi.org/10.1523/JNEUROSCI.3223-10.2011

Zhang, Y., Proenca, R., Maffei, M., Barone, M., & Leopold, L. (1994). *Positional cloning of the mouse obese gene and its human homologue*. 8.

Zhang, Z., Reis, F. M. C. V., He, Y., Park, J. W., DiVittorio, J. R., Sivakumar, N., van Veen, J. E., Maesta-Pereira, S., Shum, M., Nichols, I., Massa, M. G., Anderson, S., Paul, K., Liesa, M., Ajijola, O. A., Xu, Y., Adhikari, A., & Correa, S. M. (2020). Estrogen-sensitive medial preoptic area neurons coordinate torpor in mice. *Nature Communications*, *11*(1), 6378. https://doi.org/10.1038/s41467-020-20050-1

Zhao, Z.-D., Yang, W. Z., Gao, C., Fu, X., Zhang, W., Zhou, Q., Chen, W., Ni, X., Lin, J.-K., Yang, J., Xu, X.-H., & Shen, W. L. (2017). A hypothalamic circuit that controls body temperature. *Proceedings of the National Academy of Sciences*, *114*(8), 2042–2047. https://doi.org/10.1073/pnas.1616255114

Ziegenhain, C., Vieth, B., Parekh, S., Reinius, B., Guillaumet-Adkins, A., Smets, M., Leonhardt, H., Heyn, H., Hellmann, I., & Enard, W. (2017). Comparative Analysis of Single-Cell RNA Sequencing Methods. *Molecular Cell*, *65*(4), 631-643.e4. https://doi.org/10.1016/j.molcel.2017.01.023

Appendix

Table 1. POA neuron populations involved in thermoregulation

Genetic marker	**Cell type**	**POA nucleus**	***In vivo* stimulus used**	***In vivo* effect observed**	**Source**
TRPM2	Vglut2	POA	I. Chemogenetic activation(GqDREADD) II. Chemogenetic inhibition (GiDREADD) II. Knock out +PGE2 icv injection	I. Hypothermia II. Hyperthermia II. Higher fever developed, out of control	(Song et al., 2016)
Ptgds (PGD2)	?	POA	I.Chemogenetic activation(GqDREADD) II.Chemogenetic inhibition (GiDREADD) II.Knock down	I. Hypothermia early night time II. Hyperthermia early day time II. Circadian rhythm disrupted, lethal	(T. A. Wang et al., 2019)
Vglut2	VGLUT2	MnPO and OVLT	I. Optogenetic (Chr2) activation	I. Hypothermia II. Vasodilation II. Water consumption	(Abbott & Saper, 2017)
Adcyap1 (PACAP) and Bdnf	*Gad2*	VMPO (MnPO/MPO)	I. Warm ambient exposure (37 ˚C) II. Optogenetic (Chr2) activation II. Cold exposure + optogenetic (Chr2) activation	I. cFos expression II. a) Hypothermia b) tail vasodilation, and BAT temperature decrease (thermogenesis inhibition) c) inhibition of warm seeking	(Tan & Knight, 2018)
LepR	Vglut2	MnPO	I. Warm ambient exposure (30 ˚C) II. Chemogenetic activation(GqDREADD)	I. cFos expression II. a) Hypothermia b) Energy expenditure decreased	(Yu et al., 2016)

				c) BAT thermogesnesis inhibited	
GAD67 (GAD1)	GABA	VLPO	I. Warm ambient exposure (29-38 ˚C) II. Optogenetic activation (Chr2)	I. cFos expression II. hypothermia	(Zhao et al., 2017)
GAL	GABA	vLPO	I. Optogenetic activation (Chr2) II. Chemogenetic activation(GqDREADD)	I. NREM sleep II. NREM sleep and hypothermia	(Kroeger et al., 2018)
NOS1	Vglut2	MnPO and MPO	I. Warm ambient exposure (32 ˚C) II. Chemogenetic activation(GqDREADD)	I. cFos expression II. a)Hypothermia b)Sleep	(Harding et al., 2018)
BRS3	Vglut and Vgat	MnPO, VMPO, VLPO	I. Optogenetic activation (Chr2)	a) Hyperthermia b) Heart rate c) Blood pressure	(Piñol et al., 2021)
QRFP	Vgat and Vglut2	AVPe, MPA	I. Chemogenetic activation(GqDREADD)	a) Hypothermia b) Decreased O2 consumption c) Decrease in BAT temperature d) Decrease in heart rate e) A week lasting quiessence	(Takahashi et al., 2020)
Adcyap1 (PACAP)	Vglut2	avMLPA	I. Torpor (fasting induced) TRAPing II. Chemogenetic activation(GqDREADD) II. Tetanus toxin silencing	I. cFos and TRAP signal (mCherry from GqDREADD virus) II. Torpor induction (hypothermia, reduced locomotor activity) II. Torpor disrupted	(Hrvatin et al., 2020)
PTGER3	Vglut2	MnPO, OVLT	I. LPS injection II. Knock down in MnPO	I. Fever II. Failure to induce LPS fever	(Machado & Saper, 2022)

			II. Knock down in Vglut2^{+} neurons V. Hot (37˚ C) and cold (4˚C) stress in Vglut2 and Vgat ablated mice	II. Failure to induce LPS fever V. Failure to defend body temperature	
Opn5	Vglut2	MnPO, OVLT	I. Chemogenetic activation(GqDREADD) II. Chemogenetic inhibition (GiDREADD) II. Opn5 null mice V.Enucletion of mice V.Mouse growing in dark	I. Decreased Tcore and BAT temperature II. Increased Tcore and and BAT temperature II. Elevated and BAT activity thermogenesis V. BAT activity suppressed V. BAT activity enhanced	(K. X. Zhang et al., 2020)
ERα/Esr1	?	MPA	I. Chemogenetic activation (GqDREADD) II. Fasting induced torpor II. Ablation	I. a)Hypothermia, tail vasodilation b)Torpor-like state (lower energy expenditure and O_2 consumption) II. Activation of neurons II. a)Body temperature increase (F mice) b)Failure to enter fasting induced torpor	(Z. Zhang et al., 2020)
*Tacr3/*NK3R	?	Arcuate nucleus to POA projection (MnPO OVLT)	I. Optogenetic activation (Chr2) of fiber terminals in POA II. Antagonizing NK3R)	I.a) increase cFos in POA b) Hypothermia c) Increased tail vasodilation d) Decrease in locomotor activity II. All from I) prevented	(Padilla et al., 2018)

Table 2. Top 50 differentially expressed genes (padj <0.1) from 3 comparisons in RNAseq analysis of POA^{LepR} neurons corresponding to heatmap in Figure 2.9.

NHA vs. LTHA	NHA vs. STHA	STHA vs. LTHA
Thbd	Mfsd2a	Vav1
Mfsd2a	Pkd2l1	Pkd2l1
Anxa2	Vav1	Card11
Gm10925	Scg2	Gm10925
Scg2	Nptx1	Gm5931
Gm13991	Mfge8	Thbd.2
Prkcsh	Apold1	Slc6a5
Lat2	Lat2	Ifi47
Sil1	Lrig3	Gm43948
Apold1	Rcn2	Frem1
Hbb.bs	Prkcsh	Hpn
Mfge8	Thbd	Lrig3
Vgf	Anxa2	Gm43066
Creb3l2	Ptprn	Arhgap28
Cd68	Casp8	Gm8038
Atf3	Gm37675	Serpina3g
Creld2	Ifi47	Bbox1
Nptx1	Ddost	Gm36737
Bbox1	Havcr2	Erbb2
Hpcal1	Arhgap28	Gm26865
Tmed3	Lgmn	Rpl30.ps9
Ctsa	Saraf	Tnfrsf11b
Lgmn	Eps8	Tgm6
Eps8	Card11	A2m
Havcr2	X2410004I01Rik	Ripk3
Pdia6	Vgf	Gbp2
Npy	Gm26588	Gm37074
Saraf	Hbb.bs	Epcam
Rcn2	Cd68	Cxcr6
Fmod	Hmga1	Mab21l4
Ptprn	Tnfrsf11b	Capn12
Tspan13	Hpcal1	Nr0b1
Ddost	Rgs20	H3c14
Gimap6	Nbl1	Gm5086
Ahnak2	Rnf128	EGFP
Ext2	Ackr2	X2610028E06Rik
Frem1	Fam186a	Smim5
Cbln4	Hpn	Pld2
Nbl1	Slc3a2	Chrna10
Ecm1	Gm19114	Fmod
Asb4	Crhbp	Irgm2
Ctsb	Ect2	Myh11
Ect2	Cpe	Grap
Edem2	Gm3928	Gm8603

Adcyap1	Pltp	Prelp
Chst8	Mab21l4	Gm6565
Golga7	Cxcr6	X2410004I01Rik
Ctsd	Slc2a10	Chat
Erlec1	Pdia6	Hhip
Fxyd5	Ahnak2	Mctp2

Table 3. Hallmark GSEA gene sets enriched in DEGs from NHA to STHA differential expression analysis

	Gene set	Padj value	Genes from the gene set matching DEGs
Up-regulated	MTORC1 SIGNALING	5e-9	Lgmn, Map2k, Calr, Coro1a, Cdkn1a, Elovl5, Rpn1, Pgk1, Itgb2, Atp2a2
	PROTEIN SECRETION	0.0000158	Tmed2, Arf1, Tmed10, Pam, Ppt1
	CHOLESTEROL HOMEOSTASIS	0.0001683	Lgmn, Plaur, Gusb, Atf3, Clu, Tnfrsf12a, Fdft1, Mvd, Srebf2, Ctnnb1, Idi1, Ldlr, Hsd17b7, Cpeb2, Cxcl16, Pcyt2, Fasn, Sc5d
	ALLOGRAFT REJECTION	0.0000021	Prkcb, Nlrp3, Cartpt
	PI3K AKT MTOR SIGNALING	0.0000247	Map2k3, Calr, Cdkn1a, Akt1s1, Prkcb, Rptor, Arf1
	HEME METABOLISM	0.00000431	Map2k3, Osbp2, Ctsb, Bsg, Slc6a8
	COAGULATION	0.00041168	Thbd, Lgmn, Clu, Ctsb
	GLYCOLYSIS	0.0001804	Chpf, Ext2, Gusb, Tpst1, Pgk1, Pkm, Plod1, Tgfbi
	COMPLEMENT	0.00020564	Lgmn, Plaur, Clu, Ctsl, Ctsb
	APICAL SURFACE	0.01156334	Plaur
	APOPTOSIS	0.00041168	Casp8, Atf3, Cdkn1a, Clu, Tnfrsf12a, Erbb2
	UV RESPONSE UP	0.00127688	Atf3, Creg1, Rpn1, Bsg, Tacr3, Ago2, Slc6a8
	IL2 STAT5 SIGNALING	0.00189379	Ecm1, Syngr2, Snx14
	HYPOXIA	0.0026547	Anxa2, Hexa, Plaur, Atf3, Cdkn1a, Prkca, Pgk1, Tgfbi
	UNFOLDED PROTEIN RESPONSE	0.0071151	Pdia6, Calr, Atf3, Eef2
	ANGIOGENESIS	0.0483802	Thbd, Col5a2
	P53 PATHWAY	0.0057300	Slc3a2, Atf3, Ralgds, Cdkn1a, Prmt2, Slc35d1, Procr, Tm7sf3, Tsc22d1, Pidd1, Gls2, Tcn2
	UV RESPONSE DN	0.0082261	Anxa2, Col5a2, Bdnf, Prkca, Erbb2, Slc7a1
	INFLAMMATORY RESPONSE	0.4317077	Plaur, Cdkn1a, Pvr, Tacr3, Atp2a2, Slc7a1
	TNF-α SIGNALING VIA NFκB	0.0082262	Plaur, Map2k3, Atf3, Cdkn1a, Tsc22d1
	MITOTIC SPINDLE	0.0079977	Ect2, Anln, Septin9
	ANDROGEN RESPONSE	0.0378120	Elovl5, Tsc22d1
	KRAS SIGNALING UP	0.0107735	Lat2, Cpe, Plaur, Tspan13, Ly96,Itgb2
	EPITHELIAL-MESENCHYMAL TRANSITION	0.0115633	Scg2, Plaur, Col5a2, Ecm1, Bdnf,Tpm4, Pvr, Tnfrsf12a, Plod1, Cthrc1, Cthrc1, Slc6a8,Tgfb
	MYOGENESIS	0.0082261	Cdkn1a, Clu, Syngr2, Slc6a8
	ESTROGEN RESPONSE EARLY	0.0231010	Nbl1, Syngr1, Aldh3b1, Fdft1, Elovl5
	ESTROGEN RESPONSE LATE	0.0354157	Nbl1, Cpe, Aldh3b1, Chst8, Fdft, Tspan13, Elovl5
Down-regulated	OXIDATIVE PHOSPHORYLATION	0.0081160	NONE

Table 4. Hallmark GSEA gene sets enriched in DEGs from NHA to LTHA differential expression analysis

	Gene set	Padj value	Genes from the gene set matching DEGs
Up-regulated	MITOTIC SPINDLE	0.000002	Ect2, Clip1, Bcr
	INFLAMMATORY RESPONSE	0.000005	Plaur, Pvr
	MTORC1 SIGNALING	0.000027	Lgmn, Map2k3, Calr, Coro1a, Cdkn1a, Elovl5, Rpn1, Hspa5, Hspa
	HEME METABOLISM	0.000034	Map2k3, Osbp2, Ctsb, Bsg, Picalm
	APICAL JUNCTION	0.000134	Itgb1, Cldn6, Cercam
	COMPLEMENT	0.000239	Lgmn, Plaur, Clu, Ctsl, Ctsb, CtsD, Hspa5, Cpq
	INTERFERON-γ RESPONSE	0.000239	Casp8, St3gal5
	PI3K AKT MTOR SIGNALING	0.000974	Map2k3, Calr, Akt1s1, Prkcb, Rptor, Arf1
	UNFOLDED PROTEIN RESPONSE	0.001477	Pdia6, Calr, Atf3, Hspa5, Wipi1
	IL6 JAK STAT3 SIGNALING	0.002307	Stat3
	ALLOGRAFT REJECTION	0.000692	Prkcb, Cartpt, Nlrp3
	APOPTOSIS	0.001143	Casp8, Atf3, Clu, Ppt1, Cd14
	ANGIOGENESIS	0.021431	Thbd, Col5a2, Lrpap1
	IL2 STAT5 SIGNALING	0.001100	Ecm1, Ctsz
	P53 PATHWAY	0.001477	Slc3a2, Atf3, Ralgds, Prmt2, Procr, Tm7sf3, Tsc22d1, Tcn2, Ctsd, Plxnb2
	EPITHELIAL-MESENCHYMAL TRANSITION	0.001604	Scg2, Plaur, Col5a2, Ecm1, Bdnf,Tpm4 , Pvr, Cthrc1, Qsox1, Vim, Itgb1, Fuca1
	INTERFERON-α RESPONSE	0.010471	Casp8, Procr, Tent5a
	COAGULATION	0.006120	Thbd, Lgmn, Clu, Ctsb, Sirt2, Cpq
	HYPOXIA	0.003188	Anxa2, Hexa, Plaur, Atf3, Hspa5, Prkca, Pam, Tgfbi
	TNF-α SIGNALING VIA NFκB	0.001719	Plaur, Map2k3, Atf3, Tsc22d1
	GLYCOLYSIS	0.004048	Chpf, Ext2, Hspa5, Pam, Qsox1
	CHOLESTEROL HOMEOSTASIS	0.019905	Lgmn, Plaur, Gusb, Atf3, Clu
	APICAL SURFACE	0.033539	Plaur
	KRAS SIGNALING UP	0.006120	Lat2, Cpe, Plaur, Tspan13, Ly96,Fuca1
	UV RESPONSE UP	0.021400	Atf3, Rpn1, Bsg, Nptx2, Ppt1
	UV RESPONSE DN	0.024739	Anxa2, Col5a2, Bdnf, Prkca
	ESTROGEN RESPONSE EARLY	0.030794	Nbl1
Down-regulated	ADIPOGENESIS	0.025126	NONE
	FATTY ACID METABOLISM	0.014551	Bphl
	MYC TARGETS V1	0.006969	NONE
	DNA REPAIR	0.003108	Nme3
	OXIDATIVE PHOSPHORYLATION	0.000000005	Timm17a